THE UNIVERSITY OF TEXAS AT AUSTIN
CENTER FOR TRANSPORTATION RESEARCH

Designing for Deck Stress Over Precast Panels in Negative Moment Regions

Xiaomeng Ge
Keaton Munsterman
Xianjue Deng
Matt Reichenbach
Sunghyun Park
Todd Helwig
Michael D. Engelhardt
Eric Williamson
Oguzhan Bayrak

TECHNICAL REPORT DOCUMENTATION PAGE

1. Report No. FHWA/TX-21/0-6909-1/5-6909-01-1	2. Government Accession No.	3. Recipient's Catalog No.	
4. Title and Subtitle Designing for Deck Stress Over Precast Panels in Negative Moment Regions		5. Report Date August 28, 2021 Published December 2021	
		6. Performing Organization Code	
7. Author(s) Xiaomeng Ge, Keaton Munsterman, Xianjue Deng, Matt Reichenbach, Sunghyun Park, Todd Helwig, Michael D. Engelhardt, Eric Williamson, Oguzhan Bayrak		8. Performing Organization Report No. 0-6909-1/5-6909-01-1	
9. Performing Organization Name and Address Center for Transportation Research The University of Texas at Austin 3925 W. Braker Lane Austin, TX 78759		10. Work Unit No.	
		11. Contract or Grant No. 0-6909 and 5-6909-01	
12. Sponsoring Agency Name and Address Texas Department of Transportation Research and Technology Implementation Division 125 E. 11th Street Austin, TX 78701		13. Type of Report and Period Covered Technical Report (Jan 2016-Dec 2019)	
		14. Sponsoring Agency Code	
15. Supplementary Notes Project performed in cooperation with the Texas Department of Transportation and the Federal Highway Administration. Research Study Title: Designing for Deck Stress over Precast Panels in Negative Moment Regions Implementation Project Title: Implementation of Field Instrumentation Steel Girder Bridge with Partial Precast Concrete Deck Panels			

16. Abstract

With increases in the use of PCPs in Texas bridges, ensuring acceptable deck cracking behavior is of paramount importance to avoid long-term maintenance problems. The purpose of this study is to understand the cracking behavior of reinforced concrete bridge decks with precast concrete panels in the negative moment regions of continuous girders under service loading and to develop comprehensive guidelines for reinforcing steel details in the bridge decks in the negative moment regions of bridges utilizing PCPs. A major focus of the study is the influence of the reinforcing details on the control of deck crack width.

Four concrete bridges were monitored during the construction period. TxDOT Implementation Project 5-6909-01 is focused on the instrumentation and monitoring of the continuous steel bridge in Bastrop to further evaluate deck reinforcement requirements. Concrete early-age shrinkage is the dominant reason for deck cracking. Increasing reinforcement ratio and decreasing rebar spacing showed some benefits. Through large-scale laboratory testing on composite Tub girders, the surface crack widths generally matched the predictions from the AASHTO crack width equation correlating with the maximum rebar stress, and concrete tension stiffening effect was also observed in the concrete specimen direct tensile tests. The numerical parametric studies confirmed that the deck reinforcement ratio is the critical factor for the maximum rebar stress.

Finally, a design procedure is proposed for the longitudinal deck reinforcement in the negative moment regions. In most cases, using #4 bars spaced at 9-in. plus #5 bars spaced at 9-in. (ρ=1.1%) or #5 bars spaced at 6-in.(ρ=1.1%) reinforcing steel in the top mat, the maximum rebar stress can be limited to no more than 36-ksi under Service I load combination, and crack width can be limited to approximate 0.012 in.

| 17. Key Words
Deck Cracking, Negative Moment, Deck Reinforcing Detail, PCP, Field Instrumentation, Shrinkage | 18. Distribution Statement
No restrictions. This document is available to the public through the National Technical Information Service, Alexandria, Virginia 22312, https://www.ntis.gov/. | | |
| 19. Security Classif. (of this report)
Unclassified | 20. Security Classif. (of this page)
Unclassified | 21. No. of Pages
TBD | 22. Price |

Form DOT F 1700.7 (8-72)   Reproduction of completed page authorized

Designing for Deck Stress over Precast Panels
in Negative Moment Regions

Xiaomeng Ge
Keaton Munsterman
Xianjue Deng
Matt Reichenbach
Sunghyun Park
Todd Helwig
Michael D. Engelhardt
Eric Williamson
Oguzhan Bayrak

Disclaimers

Author's Disclaimer: The contents of this report reflect the views of the authors, who are responsible for the facts and the accuracy of the data presented herein. The contents do not necessarily reflect the official view or policies of the Federal Highway Administration or the Texas Department of Transportation (TxDOT). This report does not constitute a standard, specification, or regulation.

Patent Disclaimer: There was no invention or discovery conceived or first actually reduced to practice in the course of or under this contract, including any art, method, process, machine manufacture, design or composition of matter, or any new useful improvement thereof, or any variety of plant, which is or may be patentable under the patent laws of the United States of America or any foreign country.

Notice: The United States Government and the State of Texas do not endorse products or manufacturers. If trade or manufacturers' names appear herein, it is solely because they are considered essential to the object of this report.

Engineering Disclaimer

NOT INTENDED FOR CONSTRUCTION, BIDDING, OR PERMIT PURPOSES.

Project Engineer: Todd A. Helwig
Professional Engineer License State and Number: Texas No. 92480
P. E. Designation: Research Supervisor

Acknowledgments

Table of Contents

List of Figures

List of Tables

Chapter 1. Introduction

1.1 Introduction

A leading factor contributing to structural deficiencies in the US bridge inventory is related to deterioration and durability issues with concrete bridge decks (NCHRP, 2004). The federal classification, structural deficient, has been replaced with the designation, Poor Condition. Bridges is "Poor Condition" are ones exhibiting signs of advanced structural deterioration and are not unsafe. The long-term costs associated with maintenance issues on bridges can quickly exceed the initial cost of the bridge. The primary factor that can affect the durability of the concrete deck is cracking that provides a direct conduit for moisture and other corrosive agents to penetrate the concrete and attack the reinforcing steel. The area of the bridge where deck cracking is likely to be the most predominant is in the negative moment region where the deck is subjected to tensile stresses from girder bending behavior. Therefore, controlling the size and distribution of the cracks in this region is of paramount importance. The size and distribution of cracks in the deck are controlled by providing reinforcing steel. The purpose of this research is to find the minimum reinforcing steel required for the concrete bridge deck in negative moment regions.

1.2 Background

1.2.1 Bridge Deck Design in AASHTO LRFD

The design of concrete decks is covered in Chapter 9 of the American Association of State Highway and Transportation Officials (AASHTO) Load and Resistance Factor (LRFD) Bridge Design Specifications (2017), which includes two different methods of design. The two methods consist of a) the Empirical Design Method, and b) the Traditional Design Method.

The Empirical Design Method that is covered in AASHTO Section 9.7.2 is based upon research studies that have demonstrated the predominant load transfer mechanism for wheel loads in many typical bridge decks is actually through a combination of arching action and flexural behavior. The steel that is utilized in the deck provides both the required flexural resistance of the bridge slab as well as the necessary confinement for the arching component to resist the force effects resulting from the wheel loads. The controlling failure mechanism in the bridge deck is usually punching shear.

The Traditional Design Method that is covered in AASHTO Section 9.7.3 is based upon the conventional model for the force transfer mechanism of the deck through flexure. The method is based upon an assumption of four layers of reinforcing steel with two layers of steel in each direction (i.e., top and bottom steel in both the transverse and longitudinal direction of the bridge). Flexure analysis method specified in Section 4.6.2.1 or Section 4.6.3.2 can be used to design the transverse reinforcement for the positive moment under wheel loads.

Nevertheless, these two design methods primarily apply for the transverse moment of bridge deck under wheel loads. For the bridge deck in the negative moment region, due to the stress from girder flexure, the deck tensile stress in longitudinal direction could be more critical than that of the transverse direction. However, the requirements for the deck reinforcing steel are not clear in the negative moment region with inconsistent requirements for steel and concrete

girders provided in the AASHTO LRFD Specification Chapter 5 for reinforced concrete structures and Chapter 6 for steel structures.

According to Section 6.10.1.7 of AASHTO LRFD Specification, for bridge decks over steel girder systems, the minimum deck reinforcement in the negative moment region is 1% of the total cross-sectional area of the concrete. The reason provided for the 1.0% reinforcement ratio requirement is to make sure reinforcing steel does not yield under the service load combination (Haaijer et al., 1987). However, this conclusion is based upon the full depth cast-in-place concrete decks. The reinforcement requirement for the bridge decks with stay-in-place concrete forms as the bottom layer is questionable.

With respect to the decks over concrete girder systems, no specialized requirements for permitted stresses in deck reinforcing steel or acceptable crack widths can be founded in AASHTO LRFD. The general requirement for reinforced concrete structures under service load combination is specified in Section 5.6.7. The reinforcing steel stress should not exceed 60 percent of yield stress and crack widths not exceed 0.013 inches. However, the method to calculate stress in the deck reinforcing steel is not specified.

1.2.2 TxDOT Standard Deck Design with PCPs

Although AASHTO LRFD Section 9.7.2.6 precludes the use of the Empirical Design Method on bridge decks that utilize stay-in-place concrete formwork such as partial depth precast concrete panels (PCPs), the more recent TxDOT details that are based upon this method are recommended with PCPs. Figure 1-1 shows some typical PCPs in storage.

Figure 1- 1 Precast Concrete Panel (PCP) in Storage

Depending on the geometrical requirements, the forms can come in different spans/widths and even different thickness values as necessary; however, the forms need to satisfy the requirements outlined in Section 9.7.4. The ends of the panels with the protruding prestressing strands overlap the edges of the girders and are supported on a bedding strip inset from the edge of the panel so that wet concrete flows under the panel providing good vertical support in the finished bridge. When PCPs are utilized, the reinforcing in the panel can be treated as primary reinforcing in the deck slab. If bottom distribution reinforcement is used, AASHTO

allows that reinforcing to be placed directly on top of the panels with splices located way from the panel joints.

The current TxDOT bridge deck design practices are based upon the AASHTO Empirical Design procedure, the recommended reinforcement scheme for the top layer of steel is #4 bars spaced at 9 inches in both transverse and longitudinal directions. (Holt and Smith, 2014; TxDOT Bridge Design Manual, 2017). The current reinforcing details are depicted in Figure 1-2.
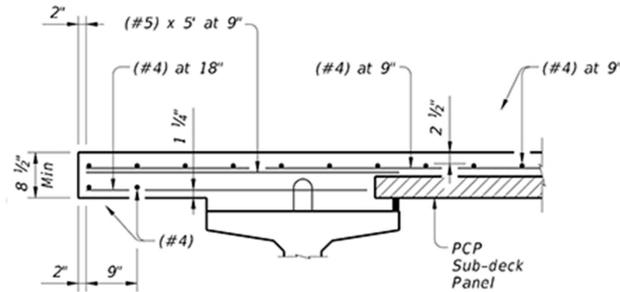
Figure 1- 2 TxDOT Deck Reinforcing Detail (Holt and Smith, 2014)

The rationale for the use of PCPs based upon the Empirical Design Method are based upon past TxDOT research from the 1980's that demonstrated that the use of PCPs with a similar amount of reinforcing steel provided a resilient deck that performed as well or better than conventional cast-in-place slabs (Fang et al., 1986; Kim et al., 1986; Tsui et al., 1988). In 2002, Merrill estimated that PCP's were used in approximately 85% of all Texas bridges. With wider usage on both steel and concrete girder systems, that number has likely grown and will continue to increase in the coming years. Figure 1-3 shows an example of top mat reinforcement over precast deck panels during concrete placement.

Figure 1- 3 Top Mat Reinforcement Over PCPs During Concrete Placement

The recent TxDOT deck reinforcing details are applied on simply supported bridges, where concrete decks are under compressive stress from the longitudinal flexure of girder

3

systems. Deck reinforcing details for the negative moment region continuous concrete bridge are not determined yet.

While TxDOT has significant experience in the use of PCPs on simply supported girder systems, very little data is available to substantiate the use of the PCPs for continuous girder systems. Most continuous girder systems have made use of steel girders since shorter segments can be shipped and bolted in the field. Continuous steel girders have historically utilized permanent deformed metal deck forms (PMDF), but many contractors would prefer to use PCPs due to improvements in economics and construction efficiency. Although there are extensive applications of PCPs as the stay-in-place deck form for concrete bridges in Texas, the overwhelming majority of them are simply supported girder systems. In recent years, TxDOT started using spliced precast concrete girders in practice, but the deck reinforcement requirements in the negative moment regions are unclear.

Although AASHTO does not preclude the use of PCPs as the stay-in-place form of bridge decks, there is currently a disconnect in the reinforcing steel detailing requirements in the AASHTO LRFD Specification for continuous steel and concrete girders that utilize PCPs.

1.3 Objective and Scope

The objectives of this research study were as follow:

- To understand the cracking behavior of reinforced concrete bridge decks with PCPs in the negative moment regions of continuous girders under service loading.
- To develop guidelines in designing deck reinforcing steel details in the negative moment regions over prestressed concrete girders or structural steel girders under service loading.

Two "poor-boy" continuous bridges and two three-span spliced continuous prestressed concrete bridges were monitored during the construction period. Deck strain distribution, reinforcing steel stress distribution, and surface crack widths were measured during construction and in service. Deck cracks at critical sections with four different reinforcing details were compared in this field study.

Large scale laboratory tests were also conducted to obtain supplementary measurements. Three composite continuous steel tub girders were tested to failure. These tests focused on the deck in the negative moment regions. Uni-axial tension tests on concrete specimens with different reinforcing details were also conducted to examine existed crack width equation and tension stiffening equation. Concrete cracking processes were recorded by Digital Image Correlation System (DIC). The size and distribution of deck cracking were presented and compared.

A sectional analytical program was developed to conduct the parametric study on the influence to the deck cracking behavior from numerous factors, such as bridge layout, girder stiffness, deck reinforcing ratio, and others. The results from this analytical program were verified by numerous finite element models of continuous bridges. Based upon the results from field tests, laboratory tests, and parametric studies, a design methodology was developed for the longitudinal deck reinforcement details in the negative moment region. Design examples were provided. A recommended reinforcement detail for the general cases of continuous bridges was also presented.

A continuous steel girder bridge with PCPs that was recently constructed on SH 21 over the Colorado River in Bastrop, Texas provided a unique opportunity to further evaluate deck reinforcement requirements. The instrumentation, monitoring, and live load testing of this bridge that was conducted as part of this implementation project, as documented in this report, provided further validation of the design recommendations developed in TxDOT Research Project 0-6909.

1.4 Project Outline

This dissertation is divided into eleven chapters, including this introduction:

Chapter 2 contains the literature review focusing on bridge deck cracking in the negative moment region of continuous bridges with or without PCPs. The essential tensile behaviors of reinforced concrete related to bridge deck cracking are summarized.

Chapter 3 contains the results from field instrumentation on two "Poor-boy" continuous bridges and two spliced continuous bridges. The influences from different deck reinforcement arrangements are examined.

Chapter 4 contains the results from field load testings on two "Poor-boy" continuous bridges and two spliced continuous bridges.

Chapter 5 contains the laboratory test results of three composite steel tub girders. The size and distribution of deck cracks with various reinforcing details are compared and discussed.

Chapter 6 contains the results of "tension stiffening" tests. The size and distribution of cracks in each specimen are presented. The relationship between crack widths and reinforcing steel stresses are also discussed.

Chapter 7 contains the deck reinforcing steel stresses from several finite element models and numerous analytical analyses. Significant factors affecting deck cracking are examined.

Chapter 8 contains a design procedure for deck reinforcing detail in the negative moment region, and design examples are presented in .

Chapter 9 contains a TxDOT Implementation Project 5-6909-01, which is focused on the instrumentation and monitoring of the continuous steel bridge in Bastrop to further evaluate deck reinforcement requirements.

Overall conclusions and deck reinforcement recommendations are provided in Chapter 10.

Chapter 2. Literature Review

2.1 Overview

Cracking of concrete in bridge decks continues to be a concern for bridge owners and structural engineers, particularly with bridge decks exposed to severe environments.

The major causes of cracking in bridge decks are concrete volume shrinkage, thermal deformation, and restraint effects (Brown et al. 2001).

There are two general structural approaches to control cracks in concrete structures. The first one is to prevent the cracks, by ensuring the tensile strain in concrete not beyond the cracking strain. This requirement might hardly be fulfilled for the non-prestressed concrete bridge decks. The second approach is to ensure that adequate reinforcing steel is present to control the possible crack widths not over the limitation to affect the serviceability and durability of concrete structures. The second approach is applied to Cast-in-Place (CIP) concrete decks with or without Precast Concrete Panels (PCPs) as the stay-in-place forms.

In this section, the leading causes of deck cracking are summarized, followed by the research on two kinds of widely used concrete deck systems. In the end, the crack width limitation and commonly used crack width equations are discussed.

2.2 Major Causes of Deck Cracking

2.2.1 Concrete Volume Shrinkage

Plastic shrinkage, autogenous shrinkage, and drying shrinkage are three primary components of concrete volume shrinkage.

Plastic shrinkage occurs near the surface of fresh concrete, whose mechanism is the moisture evaporates from the concrete surface in the hardening procedure. Severe plastic shrinkage commonly occurs under conditions that produce high evaporation rates, such as high temperature, low humidity, and high wind velocity over the concrete surface (Russell, H.G. 2017). Cover the concrete with a moisture-proof mat as soon as concrete finishing is complete and provide a high humidity environment during all the curing process are essential measures to minimize plastic shrinkage cracks on the deck surface.

Autogenous shrinkage, which also occurs during the hardening procedure, is caused by the chemical process of hydration of cement. It could be significant if concrete mixtures with a low water-cement ratio or with a superfine concrete mix like silica fume (Brown et al. 2001). As a result, higher strength concrete may have a more significant autogenous shrinkage.

Drying shrinkage is the dominant component of volume shrinkage for hardened concrete. It occurs by the loss of moisture from the cement paste unless kept underwater or in the air with 100% relative humanity. On the other hand, concrete can expand if wetted (ACI Committee 224, 2007).

The amount of concrete volume shrinkage briefly depends on the component and dimension of concrete, environmental humidity, and length of time the concrete is subjected to dry air. Referring to AASHTO LRFD Section 5.4.2.3, for concrete compressive strength up to

15.0 *ksi*, in the absence of more accurate information, the concrete shrinkage strain may be assumed to be 200 $\mu\varepsilon$ after 28 days and 500 $\mu\varepsilon$ after one year of drying, or the approximate concrete shrinkage strain at age t can be taken as:

$$\varepsilon_{sh} = -k_s k_{hs} k_f k_{td} \times 0.48 \times 10^{-3} \tag{2-1}$$

in which:

$$k_s = 1.45 - 0.13(V/S) \geq 1.0 \tag{2-2}$$
$$k_{hs} = 2 - 0.014H \tag{2-3}$$
$$k_f = \frac{5}{1 + f'_{ci}} \tag{2-4}$$
$$k_{td} = \frac{t}{12\left(\dfrac{100 - 4f'_{ci}}{f'_{ci} + 20}\right) + t} \tag{2-5}$$

where:

ε_{sh} = free shrinkage strain

k_s = factor for the effect of the volume-to-surface ratio of the component

k_{hs} = humanity factor for shrinkage

k_f = factor for the effect of concrete strength

k_{td} = time development factor

V/S = volume-to-surface ratio

H = average annual ambient relative humidity (percent)

f'_{ci} = design concrete compressive strength at time of prestressing for pre-tensioned members and at time of initial loading for non-prestressed members. If concrete age at time of initial loading is unknown at design time, f'_{ci} may be taken as 0.80 f'_c (*ksi*).

t = maturity of concrete (day), defined as age of concrete between the end of curing and time being considered for analysis of shrinkage effects.

Because various factors can influence the magnitude of shrinkage strain, ACI Committee 209 (2008) report that "it would be unrealistic to expect results from prediction models to be within plus or minus 20% of the test data for shrinkage."

2.2.2 Thermal Deformation

The coefficient of thermal expansion for plain concrete can vary from 3×10^{-6} to 8×10^{-6} /°F, depending on the material component. AASHTO LRFD (2017) specifies the coefficient of thermal expansion as 6×10^{-6}/°F for concrete and 6.5×10^{-6}/°F for steel. The insignificant difference between the thermal deformation of concrete and steel may be neglected. CEB-FIP (1990) and Fib (2010) specify that for the purpose of structural analysis, the coefficient of thermal expansion for normal weight concrete and reinforcing steel can be taken as 10×10^{-6}/°C (5.5×10^{-6}/°F). Collins and Mitchell also indicated that "while the coefficient of thermal

expansion for steel is actually about 11.5×10^{-6} /°C (6.5×10^{-6}/°F), it is conventional to use a value of 10×10^{-6} /°C (5.5×10^{-6}/°F) for both the concrete and the reinforcement." For the purpose of structural analysis of concrete bridge deck, it is reasonable to take the coefficient of thermal expansion for the integral component of reinforced concrete as 6×10^{-6}/°F.

The temperature change in concrete decks can be characterized into two reasons: uniform temperature change and temperature gradient effect. Both resources of temperature change are dependent on the location of bridges.

Uniform temperature change is mostly caused by the seasonal temperature variation. A historical method from AASHTO LRFD (2017) Section 3.12.2 indicates that the range of uniform temperature changes can be taken as -30 to 120 °F in steel bridges or 0 to 80 °F in concrete bridges. The uniform temperature will cause ends movement for concrete deck with concrete girder systems. Conservatively, due to the difference of thermal coefficients for concrete and structural steel, restraint stress between concrete deck and steel girder system should be included.

The vertical temperature gradient in concrete and steel girders with concrete deck can be found in AASHTO LRFD (2017) Section 3.12.3. The temperature gradient effect is taken for bridge decks will heat more quickly from sunshine than the supporting girders, which will cause positive moment on the superstructures. In other words, the concrete deck will be under compression. Consequently, the temperature gradient effect is a favorable effect to reduce the likelihood of deck cracking. However, AASHTO LRFD (2017) also specifies a negative temperature gradient effect equal to -0.3 times the "positive" temperature gradient effect. As a result, this negative temperature gradient will induce tensile stress in bridge decks and should be included in the evaluation of deck cracking.

2.2.3 Restraint Effect

If concrete specimens can move totally freely, volume shrinkage or uniform thermal change will induce zero stress, but only free-body volume change, which is named as concrete strain offset, ε_{offset}, in which

$$\varepsilon_{apparent} = \varepsilon_{offset} + \varepsilon_c \qquad (2\text{-}6)$$
$$\varepsilon_c = 0 \qquad (2\text{-}7)$$
$$\varepsilon_{offset} = \varepsilon_{sh} + \alpha_c \times \Delta T \qquad (2\text{-}8)$$
where

$\varepsilon_{apparent}$ = apparent strain or total strain in concrete

ε_c = mechanical strain or strain due to stress in concrete

ε_{sh} = concrete free shrinkage strain, $\varepsilon_{sh} < 0$ for shrinkage

α_c = the coefficient of thermal expansion for concrete (in./in./°F)

ΔT = temperature change in concrete (°F)

However, in another extreme case, if the concrete specimen is fully restrained by boundaries, volume shrinkage or uniform temperature change will induce stresses in the concrete, but not any deformation or apparent strain. Equation (2-6) still works, but in this case:

$$\mathcal{E}_{apparent} = \mathcal{E}_{offset} + \mathcal{E}_c = 0 \qquad\qquad (2\text{-}9)$$
$$\mathcal{E}_c = - \mathcal{E}_{offset} = - \mathcal{E}_{sh} - \alpha_c \times \Delta T \qquad\qquad (2\text{-}10)$$

Concrete will crack if it is under tension and the magnitude of mechanical strain larger than the concrete cracking strain ($\mathcal{E}_{ct}$). Usually, concrete will be restrained in some way. For concrete bridge decks, the restraint effects can be characterized into two types:

- Restrained by the supporting girders.
- Restrained by the boundary conditions.

The first type, named as internal restraint effect, is for the concrete decks over steel girder or precast concrete girders in simply supported bridges. Figure 2-1 (Hadidi & Saadeghvaziri 2005) depictures the mechanism of internal restraint effect caused by deck shrinkage. In this case, although the apparent strains in bridge deck are compressive, due to the restraint effect from the girder, the magnitude of apparent deck strains will be larger than the free shrinkage strains in concrete deck, which results in tensile stresses for the deck and compressive stresses for the girder. This internal restraint effect is caused by the different strain offset in each component of the whole bridge section. For example, the uniform temperature change will not cause significant restraint strain or stress in the concrete deck over concrete girder, due to the similar coefficient of thermal expansion factors and the same temperature changes in deck and girder concrete. For determinate structural systems, like simply supported bridges, this kind of internal restraint effect will not cause any load change in boundary conditions.
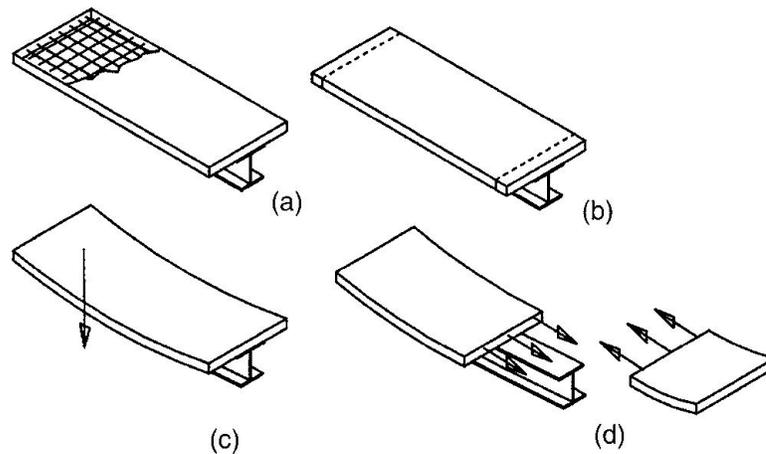
Figure 2- 1 Mechanism of Internal Restraint: (a) Concrete Deck Is Poured; (b) Concrete Deck Tends to Shrink; (c) Restraint Effect of Girder Causes Downward Deflection and Positive Moment; (d) Tensile Stresses and Possible Transverse Deck Cracking (Hadidi & Saadeghvaziri 2005)

However, for indeterminate structural systems, such as continuous bridges, the girder deflection caused by internal restraint effects induces a redistribution of vertical load in supporters. This redistribution of vertical reactions will result in a moment along with girder systems in the longitudinal direction. This mechanism is named as secondary restraint effect or external restraint effect. For example, for a two-span continuous bridge with CIP deck over steel girders, the secondary restraint effect due to deck shrinkage will increase the vertical load in the internal support, and reduce the vertical load in the end supports. This support reaction

redistribution will induce a negative moment over internal support. In other words, at this region, the apparent strain in concrete is in tension and the tensile stress in deck concrete, which depends on the superposition of apparent strain and the free shrinkage strain (Equation 2-9), will be probably beyond the tensile strength of concrete and cause transverse deck cracks. Temperature gradient effect can also cause secondary bending moment in continuous bridge systems.

2.3 Research on Full-Depth, Cast-in-Place Concrete Bridge Decks

Deck cracking is a historical issue of Cast-in-Place deck as the most broadly used bridge deck. PCA (1979) started a research project on concrete bridge deck durability in the 1960s. From a survey of 1,000 bridges randomly selected from eight states, transverse cracking was identified as the dominant type of deck cracks. In more recent years, H.G.Russell (2004,2013,2017) conducted three surveys of state departments of transportation for NCHRP Synthesis of Highway Practices. More than one-half of the agencies reported that deck cracks over frequently. Agencies reported that "the use of Hight-Performance Concrete (HPC) had not eliminate the concern about deck cracking." Drying shrinkage cracking was identified as the dominant issue in the use of HPC in CIP bridge deck. High strength concrete, especially the high early-age strength concrete, was also reported as the main reason contributed to increasing deck cracking. The strategy to minimize bridge deck cracking cited most by agencies was to apply wet curing early and provide a minimum curing period for deck concrete, followed by to specify maximum water-cementitious material ratio and to specify the maximum concrete temperature at placement. The construction practices and concrete material design were highlighted as critical strategies to control cracking in CIP bridge deck.

In addition to the surveys, numerous studies show that the primary causes of bridge deck cracking are shrinkage and temperature gradient effects.

Frosh et al. (2003) investigated bridge deck cracking in various bridge superstructure systems in Indiana. It was found that transverse deck cracking was caused by restrained shrinkage of the concrete deck. Restraint was primarily provided by composite attachment to the girders. The negative impacts from higher compressive strength concrete on deck cracking were revealed as follow:

- Additional cement for higher compressive strength concrete can produce more shrinkage strain.
- Higher tensile strength and higher modulus of elasticity of higher compressive strength concrete increase the likelihood of reinforcing bar yielding occurs at cracks.
- The compressive strength of deck concrete was recommended to be minimized from 6000 psi to 4000 psi, followed by a minimum reinforcement area requirement as 0.63% of the gross deck area.

Phares et al. (2015) conducted research on the negative moment reinforcing requirements for bridge decks. The study focused on CIP decks over multi-span bridges composed of simple-span precast girders with continuity diaphragms cast between ends of girders. The study included field monitoring as well as finite element analyses. The field monitoring consisted of live load tests that were carried out on 5 bridges. The research concluded as follow:

- The transverse field cracks over the pier and at 1/8 of the span length are mainly due to deck shrinkage.

10

- Bridges with larger skew angles have lower strains over the intermediate supports.
- Secondary moments affect the behavior in the negative moment region.

Xie et al. (2016) conducted a study on the early-age cracking in high-performance concrete decks of a two-span curved steel girder bridge in New Jersey. The deck crack map was obtained by visual inspection, as shown in Figure 2-2. The transverse cracks distributed at the whole region of two spans with crack spacing at approximate four inches. However, the deck cracks in the negative moment region showed a spider-like pattern with larger spacing. The crack widths were not reported. Various structural responses were collected during controlled filed load testing, including deck strain and girder deflections. 3D Finite Element Model of this bridge was developed to identify factors that affect early-age deck cracking. The early-age transverse deck cracking was attributed to the thermal gradient and restrained effects from bearings.
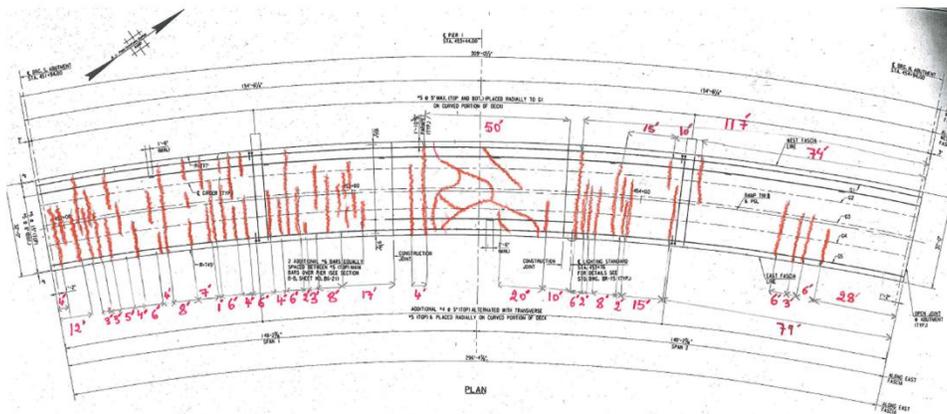
Figure 2- 2 Deck Crack Map of a Two-span Steel Composite Bridge (Xie et al., 2016)

2.4 Research on CIP-PCP Bridge Decks

The CIP-PCP bridge decks have Precast, prestressed concrete panels (PCPs) as the stay-in-place form at the bottom for Cast-in-Place concrete decks, as This kind of deck system was first introduced in a tollway bridge project in Illinois since 1961 (Barker 1975), and then have been widely used in over ten states (Sneedet al. 2010). Merrill (2002) estimated that the Texas Department of Transportation (TxDOT) used CIP-PCP bridge decks for approximately 85% of the bridges in Texas. The configuration of CIP-PC bridge decks is shown in Figure 2-3. The PCPs are prestressed in the transverse direction and initially supported on bearing strips over girder flanges. The TxDOT standard details and specifications explicitly require PCPs to be supported at least 1/4-inch above girders, and the panels overhang the bedding strips by a minimum of 1.5-inch, as indicated in Figure 2-4. After that, top-mat reinforcement is placed over PCPs. Before casting CIP topping, the PCPs should be fully cleaned by compressed air and saturated with water.
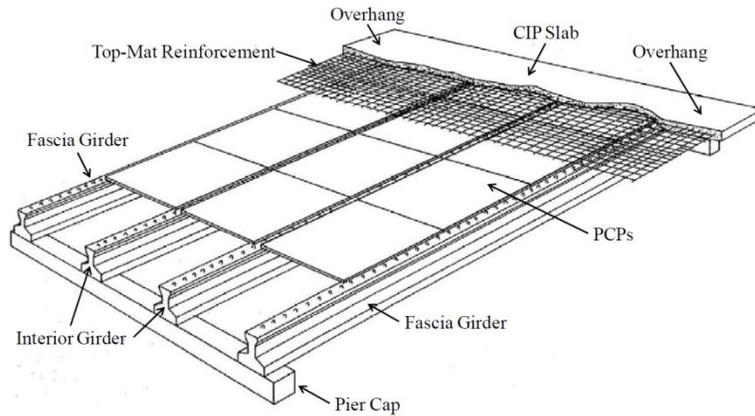
Figure 2- 3 CIP-PCP Bridge Deck (Buth et al. 1972)
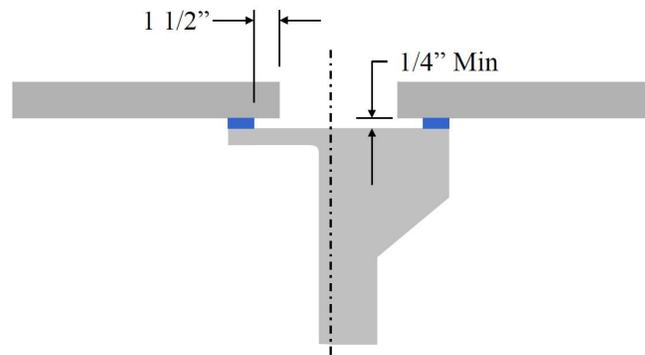
Figure 2- 4 Typical Installation of PCP on Steel or Precast Concrete Girders (Merrill 2002)

2.4.1 Advantages of CIP-PCP Decks

The advantages of CIP-PCP bridge decks are list as follow (Merrill, 2002):

- Fast construction: The time required to set and grade panels is much less than that required for plywood or permanent metal deck forms (PMDFs). The time required to tie the reinforcing steel is also reduced approximately in half because only one mat of reinforcement is required in CIP topping while two mats are needed for full-depth CIP decks. The use of PCPs also allows for larger bridge decks to be placed in one pouring operation, which can save time for the entire project.
- Safety: PCPs provide a stable and safe working platform for contractors placing reinforcing steel and pouring CIP concrete. High-speed winds, which may blow plywood forms or PMDFs off girder systems, can not be an issue for PCPs due to the self-weight. The risks from form removal are also eliminated by using PCPs as the stay-in-place forms, especially for the bridge projects over traffic.
- Cost savings: Compared with other types of deck form, fast construction and excellent safety from the use of PCPs result in reduced labor, equipment rental costs, and even insurance costs for contractors and bridge owners.

2.4.2 Composite Between CIP and PCP Layers

There has been a large amount of research carried out on the deck panels used in Texas since their introduction in 1963. One of the first major studies carried out on PCPs was reported by Buth et al. in 1972. The investigation included laboratory testing on the panels subjected to 2 million cyclic applications of a simulated design axle load to a bridge deck as well as static loads to failure. While some cracking was noted on the surface of the deck during the tests, no distress was observed at the interface between the PCP and CIP concrete. Following the tests in Texas, the Illinois department of transportation considered PCPs, permanent metal deck forms (PMDF), and wood forms (Barker 1975). With regard to PCPs, he studied the impact of different surface finishes as well as some panels with shear reinforcing bars extending into the topping slab. He found that no shear reinforcement was necessary at the panel-to-topping slab interface to achieve good bond.

Delamination between the PCP and the topping slab may be a concern with regard to the durability of the bridge decks. However, one early research conducted by Jones and Furr (1970) concluded that the full composite between CIP and PCP could be achieved under service load combination and CIP-PCP decks were stronger and stiffer than full-depth CIP decks. Composite action between the panels and the topping concrete was possible without the use of horizontal shear reinforcement. No evidence of any significant delamination or cracking between CIP and PCP was found from field load testing or cores taken from bridge decks in service. Dowell and Smith (2006) carried out tests on panels with a variety of finishes and found no problems with delamination occurring.

2.4.3 Cracks in CIP-PCP Decks

Because of the significant restraint provided by PCPs to the CIP decks, both longitudinal cracks and transverse cracks are observed on the surface of CIP-PCP decks. Folliard et al. (2003) conducted field evaluations of two CIP-PCP bridge decks that were experienced deck cracking. The general cracking pattern is pictured in Figure 2-5, which is often referred to as "reflective cracking" because the cracks in the CIP deck surface reflect the PCP edge. Merrill (2002) concluded that "reflective cracking" was mainly caused by the insufficient supporting to the PCPs. If the bedding strips were placed at the panel edge, no concrete could flow under the panel and support it well under live load. As indicated in Figure 2.3, the TxDOT standard details require PCPs to be supported at least 1/4-inch above the girder, and the panels overhang the bedding strips by a minimum of 1.5-inch to ensure sufficient CIP concrete supporting the edges of PCPs. Furthermore, if the bedding strips were placed too far in advance of pouring CIP deck, large deformation probably occurs to the bedding strips. This problem could be avoided by using high-density foam strip and gluing it to the girder flange.
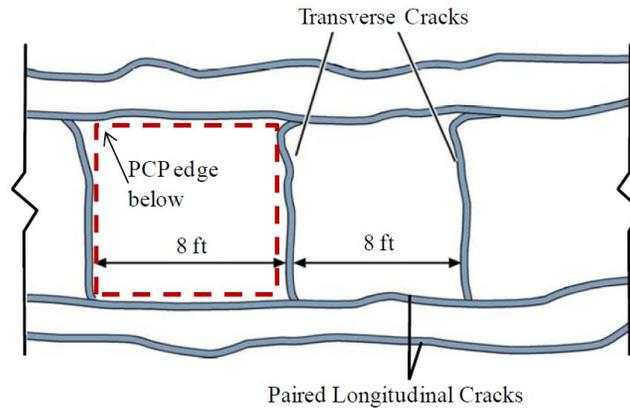
Figure 2- 5 Typical cracking pattern for CIP-PCP decks (Folliard et al. 2003)

The transverse cracking is another concern in CIP-PCP decks. Because of the difficulties simulating the constraint and boundary conditions between CIP-PCP deck and supporting girders in the laboratory, Foster (2010) did negative bending and uni-axial tension tests on CIP-PCP deck members, as depictured in Figure 2-6. The first transverse crack in CIP layer occurred near the joint between PCPs, and no transverse crack through PCPs was observed. Foster also concluded that the tensile strength of the CIP slab is critical to controlling transverse crack widths and higher strength concrete in CIP will cause wider crack widths for a given reinforcing arrangement.
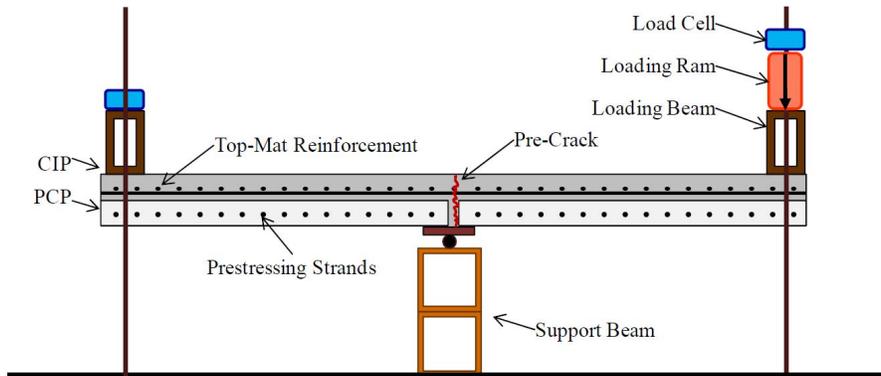
(a) Negative moment bending test
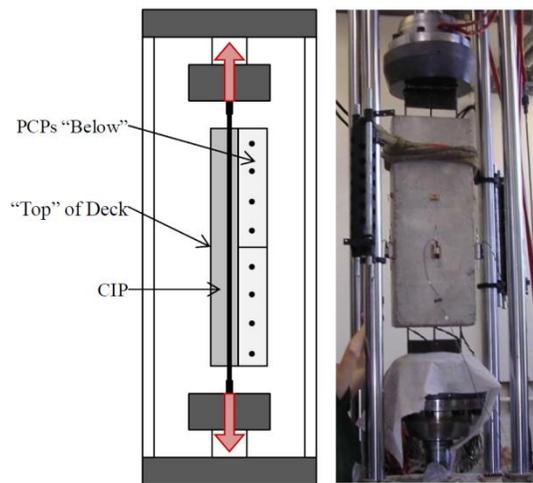
(b) Uniaxial tension test

Figure 2- 6 CIP-PCP laboratory test setup (Foster 2010)

2.4.4 CIP-PCP Decks in Negative Moment Regions

While TxDOT has significant experience in the use of PCPs on simply supported girder systems, very little data is available to substantiate the use of the CIP-PCP decks for continuous girder systems. Available research regarding the CIP-PCP deck behavior at bridge ends and "Poor boy" continuous bridge joints could provide some reference for decks in the negative moment region with transverse cracking.

One of the first studies utilizing PCPs in the negative moment region was carried out and reported by Tsui et al. (1986). The study included full-scale experiments on a composite steel girder system with 7.5-inch concrete deck and three 36-inch depth, W-shape steel girders, spaced at seven feet, where half the deck was constructed with PCPs and the other half had a cast-in-place (CIP) deck. The girder specimen was supported at a 40-ft span with both ends tied down to the lab floor, as shown in Figure 2-7. The experimental program included service-level negative moment test and 500 million cycles fatigue loading test, followed by an ultimate capacity loading test. For both the full-depth CIP and CIP-PCP deck regions, punching-shear was the critical failure model for CIP-PCP decks under live load, and the ultimate deck capacity under

tandem load was approximate 2.5 times the AASHTO design level. By the comparison between the deck regions with or without PCPs, Tsui et al. concluded that "The deck cast with PCPs was stronger, stiffer, and more crack resistant than the full-depth CIP deck."
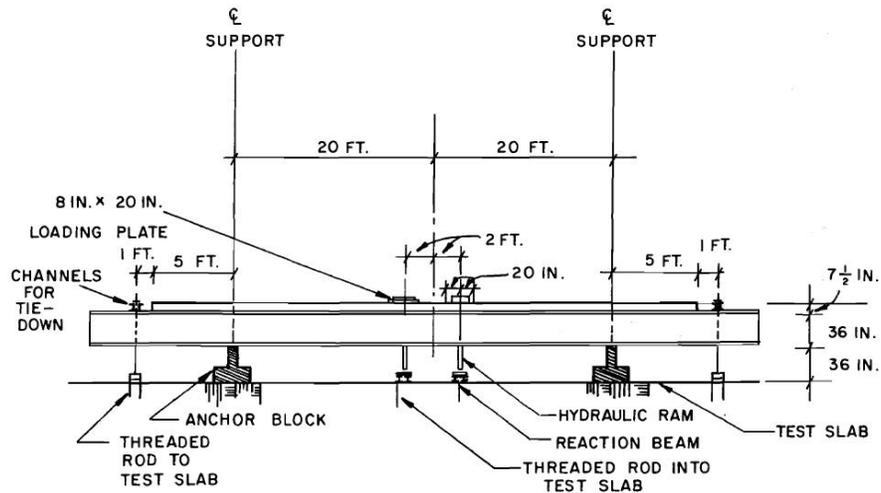
Figure 2- 7 *Elevation view of negative moment test setup (Tsui et al. 1986)*

Coselli (2004) conducted research looking at the behavior of systems where the panels were extended to the expansion joint and found good behavior was achieved without the thickened end regions. However, one concern with extending the panels to the end of the bridge was the long-term fatigue behavior of the deck panels. Agnew (2007) conducted fatigue tests on PCP panels and considered the impact of both positive and negative moments. Similar to the early versions of the PCPs that were studied and reported on by Buth et al. (1972), Agnew found that the panels did not have a problem with fatigue or delamination between the panel and the topping slab under cyclic loads. Although many of the previous studies focused on the use of PCP for bridges with normal supports, Boswell (2008) considered the impact of support skew on the behavior of the panels. He considered the use of trapezoidal shaped panels subjected to both static and cyclic fatigue loads. He found that the panels provided sufficient strength and stiffness to support the current design truck loads.

Bayrak et al.(2009) conducted a field study on the performance of "Poor boy" continuous deck detail. Dead load and long term effects, such as concrete creep and shrinkage, are identified as the dominant effects for the performance of "Poor boy" joints. It was also observed that the deck strain at "Poor boy" joints is not sensitive to live load effect, and the deck surface crack width is reduced from 0.013-inch to 0.008-inch by increasing reinforcement ratio from 0.6% to 1.8%.

2.5 Crack Width Limitation

Cracks in concrete structures may affect appearance only, or they may indicate significant structural distress or a lack of durability (ACI Committee 224, 2007). In many cases, the cracking in the tensile sides of non-prestressed concrete structures is inevitable. The control

of crack width is one of the critical criteria in the concrete structural design for the service limit state, especially for concrete bridge decks.

The permissible crack widths are not explicitly specified in AASHTO LRFD (2017). Referring to the commentary of Section 5.6.7 Control of Cracking by Distribution Reinforcement, the maximum reinforcing spacing design depends on crack widths of either 0.017 or 0.013-inch, according to the exposure conditions. "Class 1 exposure condition applies when cracks can be tolerated due to reduced concerns of appearance, corrosion, or both. Class 2 exposure condition applies to the transverse design of segmental concrete box girders for any loads applied prior to attaining full design concrete compressive strength or when there is increased concern of appearance, corrosion, or both." Conservatively, according to AASHTO LRFD, the limit of crack width in bridge decks could be taken as 0.013-inch.

Table 2- 1 Reasonable Crack widths (ACI Committee 224, 2008)

Exposure condition	Crack widths	
	inch	mm
Dry air or protective membrane	0.016	0.41
Humanity, moist, soil	0.012	0.30
Deicing chemicals	0.007	0.18
Seawater and seawater spray, wetting, and drying	0.006	0.15
Water-reataining structures	0.004	0.10

ACI Committee 224 (2008) provides a "Guide for reasonable crack widths" in reinforced concrete under service load, as shown in Tab 2-1. The report also notes that "It should be expected that a portion of the cracks in the structure will exceed these values. With time, a significant portion can exceed these values. These are general guidelines for design to be used in conjunction with sound engineering judgment." For bridge deck out of regions where deicing chemicals are utilized, 0.012-inch is a reasonable crack width limitations. Otherwise, stricter crack width requirement should be taken in practice.

ACI Committee 222 (2001), "Protection of Metals in Concrete Against Corrosion," discussed the relationship between concrete cracking and reinforcement corrosion. The depth of concrete cover to the reinforcing steel and the permeability of concrete are identified as two critical factors against corrosion in reinforcing steel. Although deeper concrete cover might induce wider cracking in concrete, it is still desired to protect reinforcing steel from the corrosive damaging. Cracks that followed the line of reinforcing bars can be more damaging than cracks perpendicular to reinforcing bar because of the longer corroded length of the bar. Where cracks are perpendicular to reinforcing bar, the relationship between crack widths and reinforcing steel corrosion is unclear, as summarized by ACI Committee 222. Some studies (Tremper 1947; Martin & Schiessl 1969; Raphael & Shalon, 1971) conclude that there is no relationship between surface widths and reinforcing steel corrosion, and another study (Atimtay & Ferguson 1974) shows that cracks less than approximate 0.012-inch have little influence on reinforcing bar corrosion. Even so, ACI Committee 222 highlights that uncontrolled cracks can usually cause concerns. It is suggested that sufficient crack control reinforcement should be placed so that it remains elastic after concrete cracking.

According to CEB-FIP (1990) and FIB (2010), the limitation of crack widths in reinforced concrete under service load is 0.3-mm (0.012-inch) if the environmental condition is exposure to air or moisture. The limitation of crack widths is 0.2-mm (0.008-inch) if the environmental condition is exposure to de-icing agents or airborne chlorides. The crack width limitation from CEB-FIP (1990) and FIB (2010) is similar to that from ACI Committee 224 (2008.

Based upon all statements above, the limitation of crack widths in bridge decks is dependent on the environmental condition of each individual project, and there is no universal conclusion on crack widths limitation from different design codes. Engineering experience on bridge deck cracking from bridges located in the adjacent area will be quite valuable. If there is no detailed information, the limitation of deck crack widths can be taken as 0.012-inch for bridges out of the regions where deicing chemicals are utilized. Otherwise, 0.08-inch is a reasonable limitation.

2.6 Calculation of Crack Widths

A number of equations have been developed to predict crack widths in reinforced concrete under flexure or tension. As a fundamental consideration of structural compatibility between concrete and steel, the average crack width is given by the average crack spacing multiplied by the strain difference between reinforcing steel and concrete, as shown follow (Beeby 1979):

$$w_m = S_m \times (\varepsilon_{sm} - \varepsilon_{cm}) \tag{2-11}$$

where

w_m = average crack width (inch)

S_m = average crack spacing (inch)

ε_{sm} = average reinforcing bar strain

ε_{cm} = average concrete strain

Because maximum crack width, rather than average crack width, is more critical to the appearance and durability of reinforced concrete. The previous equations can be transferred to:

$$w_{max} = S_{max} \times (\varepsilon_{sm} - \varepsilon_{cm}) \tag{2-12}$$

where

w_{max} = maximum crack width (inch)

S_{max} = maximum crack spacing (inch)

Normally the concrete strain between cracks will not larger than 150 με, thus ε_{cm} in Equation 2-11 can be neglected. This assumption results in:

$$w_{max} = S_{max} \times \varepsilon_{sm} \tag{2-13}$$

$$w_{max} = S_{max} \times \frac{f_{sm}}{E_s}$$ (2-14)

where

E_s = Young's modulus of reinforcing steel (ksi)

f_{sm} = average reinforcing bar stress (ksi)

Theoretically, the problem on the prediction of maximum crack width can be transferred to positions of maximum crack spacing and average reinforcing bar stress. However, either of them can be accurately calculated in practice. Crack width equations described in this section are partially based upon empirical assumptions or statistical analysis.

2.6.1 Kaar-Mattock Equation

Kaar and Mattock (1963) conducted a series of bending tests on reinforced concrete specimens, including three bridge-type girders, nine building-type rectangular or Tee-shape beams, and four eight-inch-depth slabs. They found crack widths due to loads was essentially proportional to reinforcing bar stress, and reinforcing bar stress under service load can be calculated by using elastic theory and assuming concrete has no tensile strength, also named as "elastic cracked section theory" in reinforced concrete design. Kaar and Mattock developed a crack width equation from a curve fit of test data:

$$w_{max} = 0.115 f_s \sqrt[4]{A} \times 10^{-3}$$ (2-15)

where

f_s = reinforcing bar stress calculated by "cracked elastic section method" (ksi)

A = area of concrete surrounding one bar (in.^{2}), $3 \leqslant A \leqslant 40$

The authors also reported some observed cracks 40% wider than predictions.

2.6.2 Gergely-Lutz Equation

Gergely and Lutz conducted a statistical analysis of laboratory test data. The data used in this analysis included test results from Clark (1956), Hognestad (1962), Kaar and Mattock (1963), Rüsch, H., and Rehm, G. (1963), and Kaar and Hognestad (1965). The following conclusions are reached regarding factors affecting crack widths:

- The stress in the reinforcing steel is the most important factor
- The cover thickness is an important variable
- The area of concrete symmetric to each bar is another important variable
- The reinforcing bar diameter is not a major variable
- The bottom crack width increase with strain gradient

Two equations were developed to best predict possible maximum flexure crack width on the bottom face and side face:

$$w_b = 0.091 \sqrt[3]{t_b A} \beta (f_s - 5) \times 10^{-3}$$ (2-16)

19

$$w_s = \frac{0.091\sqrt[3]{t_b A}\beta(f_s - 5) \times 10^{-3}}{1 + t_s/h_1}$$ (2-17)

where

w_b = most probable maximum crack width at bottom of beam (inch)

w_s = most probable maximum crack width at the level of reinforcement (inch)

f_s = reinforcing bar stress calculated by "cracked elastic section method" (ksi)

A = area of concrete symmetric to reinforcing steel divided by number of bars (in.^{2})

t_b = bottom cover to center of bar (inch)

t_s = side cover to center of bar (inch)

β = ratio of h and h_1

h = distance between the neutral axis and the tension face (inch)

h_1 = distance between the neutral axis and the center of bar (inch)

There is another simpler function for the maximum crack width at the tension side of concrete beams:

$$w = 0.076\sqrt[3]{d_c A}\beta f_s \times 10^{-3}$$ (2-18)

where

w = most probable maximum crack width (inch)

d_c = thickness of cover from extream tension fiber to the closed bar center (inch)

This simplified equation (2-18) was adopted by ACI 318-95 (1995).

2.6.3 Frosch Equation

Frosch (1999) reviewed the experimental test results used in Gergely and Lutz's analysis and proposed a new equation to predict flexure crack width. Frosch concluded that "the minimum theoretical crack spacing should be equal to the distance from the point at which the crack spacing is considered to the center of the reinforcing bar located closest to that point," as depicted in Figure 2.6. According to equation 2-14, maximum crack widths is proportion to maximum crack spacing and reinforcing bar stresses. Frosch proposed an equation to calculate cracking spacing:

$$S_c = \psi_s d^*$$ (2-19)

$$d^* = \sqrt{d_c^2 + (\frac{s}{2})^2}$$ (2-20)

where

S_c = crack spacing (inch)

d^* = controlling cover distance (inch)

d_c = thickness of cover from extream tension fiber to the closed bar center (inch)

s = bar spacing (inch)

ψ_s = crack spacing factor: 1.0 for minimum crack spacing; 1.5 for average crack spacing; and 2.0 for maximum crack spacing

Based upon equation 2-14, the maximum crack width is correlated with maximum crack spacing. As a result, the equation for maximum crack width is as follow:

$$w = 2\frac{f_s}{E_s}\beta\sqrt{d_c^2 + (\frac{s}{2})^2} \qquad (2\text{-}21)$$

where

$\beta = 1.0 + 0.08d_c$

f_s = reinforcing bar stress under service loading (ksi)

E_s = elastic modulus of reinforcing bar (ksi)

The equation 2-21 can be rewritten to find the permissible bar spacing

$$s = 2\sqrt{(\frac{w_c E_s}{2f_s\beta})^2 - d_c^2} \qquad (2\text{-}22)$$

where

s = permissible bar spacing (inch)

w_c = permissible crack width (inch)

The stress in reinforcing steel (f_s) is not entirely clear here, which could be either average reinforcing bar stress through the cracked region or maximum reinforcing bar stress at cracks. Frosch (1999) proposed a reinforcement stress of 60 percent of yield to account for the service stress corresponding to that recommended by ACI 318-95 (1995).

The current ACI 318 (2014) design code adopted a simplified version of permissible bar spacing equation based on Frosch crack width equation. As shown in Section 24.3.2, the maximum spacing of bonded reinforcement should be the lesser of

$$s = 15\left(\frac{40}{f_s}\right) - 2.5C_c \qquad (2\text{-}23)$$

$$s = 12\left(\frac{40}{f_s}\right) \qquad (2\text{-}24)$$

where

f_s = calculated reinforcing bar stress under unfactored moment, or it shall be permitted to take f_s as $(2/3)f_y$ (ksi)

f_y = yield stress of reinforcing steel (ksi)

C_c = least distance from the surface of reinforcing steel to tension face (ksi)

The current AASHTO LRFD design specification adopted another simplified version of permissible bar spacing equation based on Frosch crack width equation. As shown in Section 5.6.7, the maximum spacing of reinforcing steel closed to the tension surface is:

$$s = 700 \left(\frac{\gamma_e}{\beta_s f_{ss}} \right) - 2d_c \tag{2-25}$$

in which:

$$\beta_s = 1 + \frac{d_c}{0.7(h - d_c)} \tag{2-26}$$

where

β_s = ratio of flexural strain at the extreme tension face to the strain at the centroid of the reinforcement layer nearest the tension face

γ_e = exposure factor

= 1.00 for Class 1 exposure condition

= 0.75 for Class 2 exposure condition

d_c = thickness of concrete cover measured from extreme tension fiber to center of the flexural reinforcement located closest thereto (inch)

f_{ss} = calculated tensile stress in reinforcement at the service limit state not to exceed 0.60 f_y (ksi)

h = overall thickness or depth of the component (inch)

As referred in the previous section, Class 1 exposure condition is equivalent to the permissible crack widths as 0.017-inch, and Class 2 exposure condition is equivalent to the permissible crack widths as 0.013-inch. The exposure factor can be adjusted if the individual owner desires an alternative crack width limitation.

2.6.4 CEB-FIP Equation

The crack width equation in CEB-FIP(1990) follows the basic compatibility rule between concrete and reinforcing steel, as discussed previously in Equation 2-11, but considering concrete shrinkage strain in it. The equation in Section 7.4.3.1 is provided as follow:

$$w = l_{s,max} \times (\varepsilon_{sm} - \varepsilon_{cm} - \varepsilon_{cs}) \tag{2-27}$$

where

$l_{s,max}$ = the length over which the slip between steel and concrete occurs (inch)

ε_{sm} = average reinforcing bar strain within $l_{s,max}$

ε_{cm} = average concrete strain within $l_{s,max}$

ε_{cs} = the strain of concrete due to shrinkage

The $l_{s,max}$ utilized here is similar to the concept of maximum crack spacing utilized in Frosch Equation. However, the estimation of $l_{s,max}$ is based upon bond stress between steel and concrete, but not concrete clear cover depth or bar spacings. $l_{s,max}$ can be taken as:

$$l_{s,max} = \frac{f_{s,max}}{2\tau_{bk}} \times \phi_s \qquad (2\text{-}28)$$

where

$f_{s,max}$ = maximum reinforcing bar stress at crack (ksi)

ϕ_s = diameter of steel bar (inch)

τ_{bk} = average bond stress, and may be taken as $1.8f_{ctm}$

f_{ctm} = concrete tensile strength (ksi)

This crack width equation is fully based upon compatibility theory and reveals the relationship between concrete cracking and bond stress-slip. However, neither the average concrete strain nor average steel strain around cracks can be calculated accurately. The crack width equation in CEB-FIP appears not user-friendly enough.

The same crack width equation is adopted in fib (2010).

2.7 Summary

This chapter gives an overview of several key issues about the cracking in concrete bridge decks, such as the leading causes of deck cracking, research conclusions about full-depth CIP deck and CIP-PCP deck, and the calculation and limitation of crack width. These viewpoints can be summarized from the literature review:

- The major causes of cracking in bridge decks are concrete volume shrinkage, thermal deformation, and restraint effects.
- Higher compressive strength concrete used in the CIP concrete deck increasing the likelihood of deck cracking.
- Fully-composite behavior can be expected between CIP deck and PCPs as the bottom form. The deck cast with PCPs was stronger, stiffer, and more crack resistant than the full-depth CIP deck.
- Generally, the limitation of deck crack widths can be taken as 0.012-inch for bridges out of the regions where deicing chemicals are utilized. Otherwise, 0.08-inch is a reasonable limitation.
- Since the Frosch Equation has been adopted by AASHTO LRFD and ACI 318, it will be taken as the primary choice to predict crack width in the concrete deck.

Chapter 3. Field Instrumentation

3.1 Overview

Field measurements were made in four bridges included a bridge on SH 123 bridge in San Marcos, a bridge on SH72 in Bastrop, and two spliced concrete girder bridges near the intersection of Toll Road 45 and IH 35 in Round Rock, Texas. This chapter introduces the equipment used for instrumentation and outlines the process of assessing, installing sensors, and monitoring the selected parts of bridges during construction and in the service. Vibrating wire gages (VWGs), foil strain gages, and data logging equipment, as shown in Figure 3-1 (a to c), were the primary tools used for data measurements and collection. The length of time for monitoring was selected to ensure adequate and representative data can be collected to characterize Crack Width Limitation

(a) VWG   (b) Foil strain gauge   (c) Data logging equipment
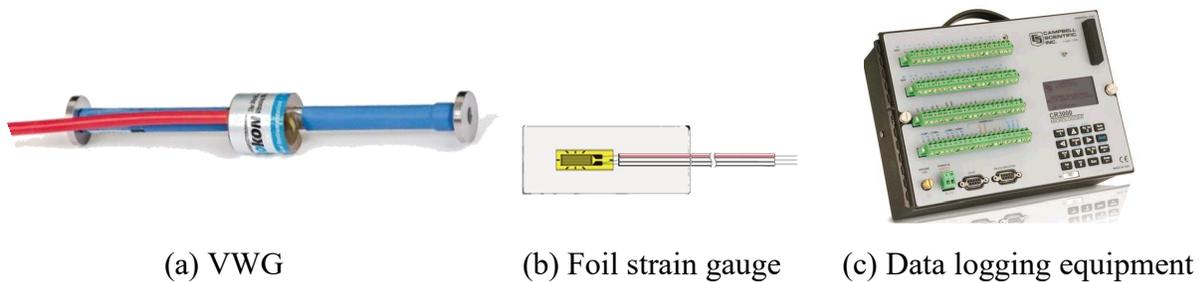
Figure 3- 1 Field Instrumentation Equipment

3.2 Instrumentation Plan

The primary objective of the instrumentation was to capture the cracking behavior of the bridge deck above interior supports. For the monitored bridges, a standard procedure for instrumentation and construction was developed and is described below. Specific descriptions and procedures for each bridge are detailed in the subsequent sections. The instrumentation was intended to give an indication of the benefits of variations in the deck reinforcing steel on the deck behavior in regions where the deck is subjected to tensile stresses. A reduction in the concrete strain and crack width was expected to correlate with the area and of steel provided and the reinforcing bar spacing. To obtain data on the effects of changes in reinforcing steel details, the deck strain of different composite girder sections, with variations in the top-mat longitudinal reinforcement details, were measured in each bridge using VWGs. Besides, in the bridge deck of Round Rock Bridges, the stress of longitudinal reinforcing bars were also measured by foil strain gages.

The first step for instrumentation was to examine drawings of the bridges, provided by TxDOT, to determine the ideal cross-sections for monitoring. A number of factors were considered to select the instrumentation locations, including the bridge cross-section, span length, safety, and accessibility. Once the gage locations were decided, a lead wire layout through the deck to the data logger was configured. The gages were ordered using the necessary length of lead wires. An additional length of 10 ft. was added to each lead wire to ensure its ability to reach the data logger.

Becoming familiar with the bridge through the drawings as well as visits to the site was important for developing the instrumentation plan. Visiting the site before the instrumentation helped to address complexities in the site that were not clear in the drawings. Installation of the instrumentation began after the contractor had finished placing the reinforcement for the bridge. The research team was generally granted approsimately 2 days to install gages and other intstrumantion and ensure that the system was functioning properly prior to concrete placement.

As part of the instrumentation scheme, the research team obtained approval of TxDOT and the contractor, to vary the deck reinforcing steel at interior supports. In some cases, this involved adding additional steel to the original details, while in others, the original steel from the design was reduced. During the instrumentation process, following the instrumentation scheme, bars were added and properly secured to the original steel. VWGs were also positioned and secured to the deck reinforcing bars using plastic spacers and zip-ties. The VWGs shown in Figure 1.1 consist of the VWGs as well as an electronic "plucker" and thermistor. The plucker/thermistor is contained in a plastic piece that slides on to the VWG and excites the internal taut wire to vibrate. The plucker, thermistor, and lead wire, were attached and secured using a hose clamp around the gage. In addition to VWGs, foil strain gages were used to monitor the stress in the deck reinforcing steel. The foil gages were installed to the reinforcing steel using adhesive. The gages were attached to the Reinforcing bar and covered by protection tape. Care was taken during all instrumentation installation to ensure proper alignment of the gages.

The wiring for all gages is generally the most vulnerable portion of the gage and must be protected from damage or shorting the gage. Cuts or breaks in the wires often render the gage useless. Figure 3-2 shows the means used to secure the wires and gages. The plucker housing was oriented for the wires to be on the underside of the reinforcement so as to minimize the likelihood of damage to the wiring from the vibrators used to consolidate the concrete during placement. As the wires extended from the gage toward the data logger, loops were made and loosely secured near the underside of the gage to provide strain relief and avoid damage throughout construction and subsequent monitoring. The wires were secured to the bottom of the reinforcement using zip-ties along a prescribed path to the surface of the deck. The path of the wiring was chosen to minimize the likelihood of damaging the wires during construction of the bridge deck. The strain relief provided in the wires lessened the likelihood of damage during construction.

Figure 3- 2 VWGs secured to the reinforcement

PCPs are generally supported on dense, foam, gedding strips near the edge of the girders. The foam-bedding strip was ideal for creating a hole to route the sensor wires to the underside of the bridge. Silicon caulk was used to secure the wires from movement and to close the hole created through the deck to minimize the seepage of the fresh concrete during the cast. The wires were routed through the hole until all excess wire was through the deck.

The data acquisition equipment was assembled in the laboratory to save time and keep the equipment organized and safe. The data acquisition system consisted of a Campbell Scientific (CS) CR3000 data logger, CS multiplexor (to extend the number of channels), and 12V auto-marine batteries to power the system. Electrical boxes were used to provide protection to the various components of the data acquisition system. The box housing the data acquisition system was transported to the construction site and positioned near the center of the bent to avoid interfering with construction and from falling off the edge. The battery housing was placed next to the housing for the data logger. Once the housing boxes were in place, the gage wires were routed through an opening in the box and connected to the data acquisition equipment. Identification tags were placed on the gage wires prior to installation to ensure each gage location matched the recording channel. Tags were marked at the beginning of the wire near the gage and at the end connections to the multiplexers. Once all of the gages were attached to the multiplexer, the wires were coiled and placed as neatly as possible in the housing box, as shown in Figures 3-3.

(a) Wires in the housing box   (b) Housing boxes between girders

Figure 3- 3 Equipment protection in field instrumentation

An antenna connected to the mobile internet station was placed outside of the housing box to allow remote communication with the data logger using a modem with a cellular link. The batteries were connected in parallel to the data logger to provide power for the system. After all of the wires from the gages and batteries were inside the data logging box, the hole the wires came through was sealed with the silicone caulk to minimize water, debris, or insects entering the box. Lime desiccant was provided to minimize the impact of humidity and unintentional moisture collection that might inhibit the function of the data acquisition system.

A mobile internet station was utilized to systematically evaluate the signals from the sensors to ensure that the gages and monitoring system was properly configured. The system allowed access to the data logger via a remote computer to check if all of the gages were functioning properly. Baseline readings were recorded for each gage to be used as a reference point for subsequent changes in strain. A sampling rate of 15 minutes was established to measure the concrete strains and temperatures measured by VWGs and the Reinforcing bar stresses measured by foil strain gages.

3.3 Field Instrumentation of "Poor-boy" Continuous Bridges

The research team started the field instrumentation with two simply supported bridges with "Poor-boy" continuous deck. Although the girders are simply supported, the bridge deck is continuous over internal piers. One of the bridges was in San Marcos while the other was in Bastrop. The San Marcos SH123 bridge was monitored for over 150 days, and the Bastrop SH71 bridge was monitored for over 60 days during construction. The detailed field instrumentation results are described below.

3.3.1 San Marcos SH123 Bridge

The first instrumentation for the study was on a bridge located on SH 123 bridge in San Marcos. The bridge was constructed in 2016 and 2017. The three-span bridge made use of PCPs to form the deck as well as metal deck forms near the interior supports. The bridge supports included a 45° skew and was oriented in the North-South direction, as shown in Figures 3-4 and 3-5. The North and Southbound sides of the bridge are independent of each other with a small

separation between the two and guard rails on the exterior. Due to the significant skew, the forming system that was used near the supports consisted of stay-in-place (SIP) metal deck forms. PCPs were used up to approximately 10 ft. from the support, and the metal SIP forms were then used. Therefore, the deck detail at the supports consisted of a fully cast-in-place deck. The two sides of the bridge are identical with five Tx54 prestressed concrete girders that use the "Poor-boy" continuous joint. The reinforcement in the cast-in-place (CIP) portion of the deck consists of #4 bars spaced at 9-in. longitudinally and #5 bars spaced at 6-in. transversely. The area of focus for the instrumentation encompassed the area over the first interior bent of the North-East section.
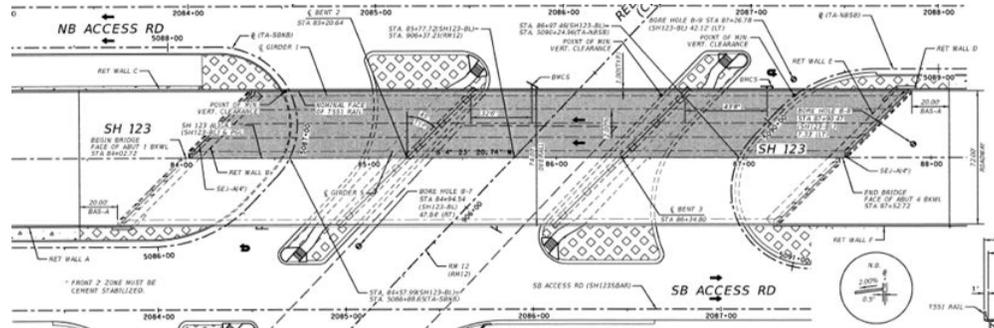
Figure 3- 4 San Marcos SH123 Bridge Plan View Drawing (TxDOT)
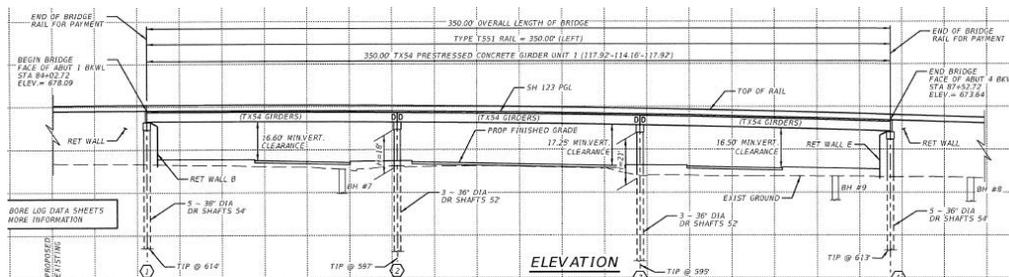
Figure 3- 5 San Marcos SH123 Bridge Elevation View Drawing (TxDOT)

Three interior girders were selected to be instrumented with varying reinforcement details. The standard TxDOT reinforcing consisted of #4 bars spaced 9 inches on center in each direction and served as the baseline reinforcing detail for the purposes of comparison. The other two sections had larger amounts of steel that were achieved by bundling additional reinforcement, either #4 or #6 bars, to the existing reinforcing. The different reinforcement ratios over the interior girders consisted of 0.5% (baseline),1.0%,and 1.6% of 4.5-inch-depth CIP concrete area.

Each monitored section had four vibrating wire gages strategically placed across the centerline of the bent. Three gages were attached to the top mat reinforcement, placed at the midpoint between girders over the PCP, at the edge of the PCP, and the centerline of the girder as shown in Figure 3-6. The fourth gage was located directly below the third gage at the centerline of the girder to capture the strain gradient through the deck. Gages 1-4 monitored the first section containing one additional #4 bar bundled to the existing longitudinal steel. Gages 5-8 monitored the second section containing the standard reinforcing. Gages 9-12 monitored the third section containing one additional #6 bar bundled to the existing longitudinal steel.
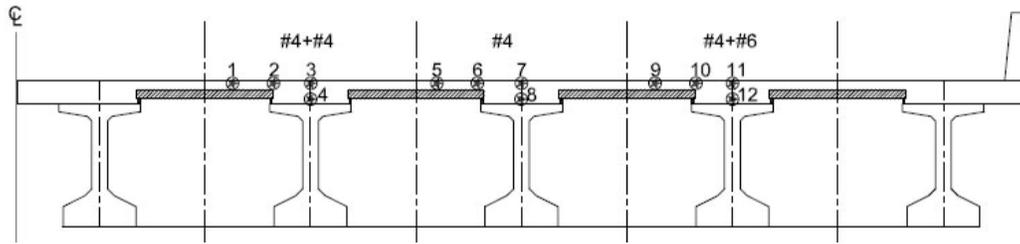
(a) Elevation view

(b) Plan view

Figure 3- 6 Gage Layout

For the San Marcos SH123 bridge, crack formers were used to initiate and control cracking in the "Poor-boy" continuous joints. Prior to placement of the concrete, , a two-inch steel angle was placed as a crack initiator from the bottom of the deck. This angle was positioned directly over the gap between the simply supported girders and ran along the centerline of the bent. The positioning of the crack-initiating angle introduced complexity since the ideal location for gages was directly over the middle of the support. Since the angle was at the bottom of the deck and at the center of the bent, it interfered with where the gage was intended to be placed. To be able to capture a strain gradient through the depth of the deck, the gages were placed immediately next to the angle, as shown in Figure 3-7. Because of the shift in the bottom gage location, the gage for the top of the deck was shifted to match the location. In addition to the crack initiator at the bottom of the bridge deck, a "zip strip" was inserted into the fresh concrete at the top to initiate cracking at the top of the slab.

(a) Top and bottom VWGs over a bridge line   (b) VWG at the edge of a bridge line

Figure 3- 7 Photo of VWGs in The Field

As described in the previous sections, the additional steel was bundled to the existing reinforcement (#4 bars spaced at 9 in. each direction). Once bundled, the gages and wires were secured using zip ties, as shown in Figure 3-2. When exiting the bottom of the deck, the wires were protected from the sharp edges of the permanent metal deck form (PMDF) to avoid shorting of the electrical wires. A silicone sealant was used to secure the wires from movement and avoid being cut by the metal, shown in Figure 3-8.

Figure 3- 8 Wires Passing Through The Deck

The data logging equipment was set up and placed between the girders as described in the previous section. The casting of the deck occurred on October 15, 2016 at 2 am with the use of a pump truck shown in Figure 3-9. Before casting began, the gages were checked to ensure proper functioning, as well as to secure any gages or wires that had become loose, as shown in Figure 3-10. No obstructions or interference with the gages were noticed during the cast.

Figure 3- 9 Concrete trucks　　　　　　　*Figure 3- 10 Securing VWGs*

As the concrete was poured over the instrumentation area, concrete cylinders were cast for testing. A slump test showed the concrete to have a slump of 7 inches which is within the allowable limit. After the concrete was approved, twelve 4-inch cylinders were collected. Details of the concrete mix design are provided in Table 3-1.

Table 3- 1 Concrete Mix Design

f'c (psi)	w/c Ratio	Fly Ash	Hydraulic Cement	Coarse Aggregate	Fine Aggregate
4000	0.45	67%	33%	58%	42%

Compression cylinder tests were conducted to measure the strength of the concrete in the bridge deck. In addition to obtaining the strength, the modulus of elasticity (E_c) was determined for the initial loading portion of the curves when the concrete stress-strain relationship is relatively linear. Cylinder splitting tests were conducted to measure the tensile strength of the concrete, as shown in Table 3-2. Figure 3-11 shows one of the specimens following the test. The fracture in some of the aggregate indicates a high strength concrete was used for the deck. This also shows what type of aggregate was used.

Figure 3- 11 Cylinder After Splitting Tensile Test

31

Table 3- 2 Material Strengths

Compression Strength f'$_c$	Elastic Modulus E$_c$	Splitting Tensile Strength f$_t$
7500 psi	5220 ksi	560 psi

The tensile tests provided the estimated tensile capacity of the bridge deck. Using the direct tensile strength of $f_t = 4 * \sqrt{f'_c}$, the cracking stress was estimated to be 350 psi. The test results correlated to the concrete cracking strain of 66 με.

Some issues occurred at some of the instrumentation locations as some of the gages did not capture the cracking strain across the crack due to the gage placement location as well as the placement of the crack former. VWGs over the girder were placed at the top and bottom reinforcement layers to capture the strain gradient through the depth of the slab, gages. Due to the presence of a steel angle at the center of the bent at the bottom of the deck, the gages were offset from the angle. As a result, this offset caused gages 4, 7, 8, 11, and 12 to be next to the crack, rather than centered across it. Gage 10 also missed the crack. This is believed to be either from the misplacement of the gage or from the location of the zip strip placed at the top of the deck. Figure 3-12 shows which gages did not capture the strains across a crack.
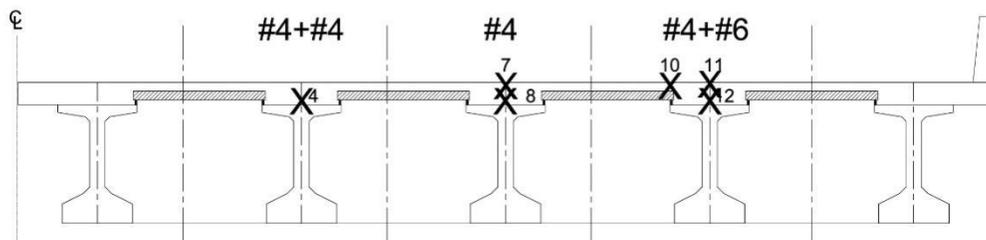
Figure 3- 12 VWGs Not Across Cracks

The gages centered over the panel (#1, #5, and #9) were the only gage locations to capture the crack in each case. Hence, this gage location was deemed the best indicator for the performance of the effectiveness of the reinforcement details.

The data initially collected from the gages was raw data and required processing. Figure 3-13 shows the raw data collected from the gages #1-4. As shown in the plot, the strain from gage #4 was very close to zero, indicating the gage was not across the crack. Gages #1-3 showed trends similar to each other that fluctuate along with the average temperature in the deck. There is also a distribution of strain between the middle of the panel to the girder due to the difference in stiffness and shear lag effect. The gages over the girder attract more strain than the others between girders.
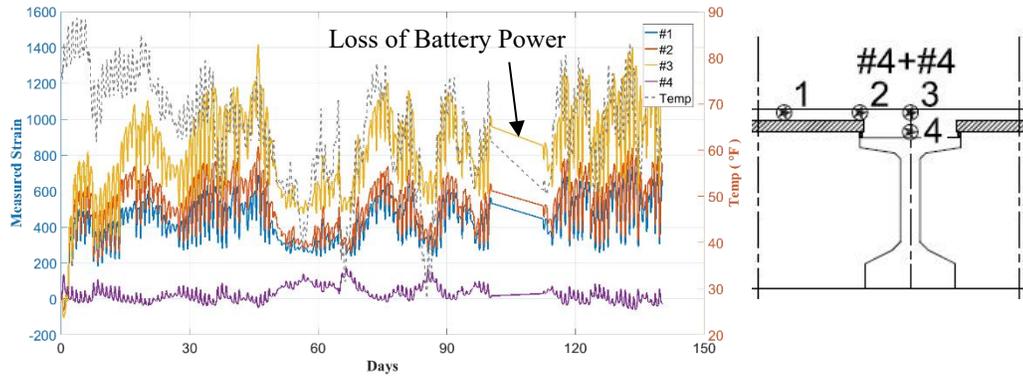
Figure 3- 13 Raw Data of Concrete Strains

Figure 3-13 also shows a loss of data when the data logger lost battery power. The data needed to be retrieved every few days to avoid the loss of stored data when the scanning frequency was relatively high.

As stated before, temperature fluctuations needed to be accounted for to identify the changes in strain due to shrinkage. Reducing the temperature influence by taking daily readings at 4 am, when the bridge is considered at a temperature equilibrium, resulted in more stable strain readings. Figure 3-14 shows the strain readings from each section. The low strain values for some of the gages (i.e., gages #4, 7, 8, 10, 11, 12) clearly indicate the gages did not cross a crack.

Gages were positioned over the girder as well as over the "panel" or formwork between adjacent girders. The gages over the panels were the most consistent gage in each section and the best indication of the effects of the reinforcement, as well. Figure 3-15 shows a graph of the strain values over the panel for each section. From this graph, the section with the current design consistently had the highest strain, the section with added #4 Reinforcing bar had the lowest strain, and the section with added #6 was between the other two. There was a trend in the reduction of strain due to the presence of steel, but it did not correlate with what was expected. There appeared to be an inconsistent relationship between the area of steel and strain in the concrete. The inconsistency was likely affected by the use of bundled bars instead of individual Reinforcing bars spaced across the width of the deck. Increasing the deck steel by using larger diameter Reinforcing bar or reducing the bar spacing is generally more effective compared to bundling bars. Based upon the experience with the San Marcos bridge, subsequent instrumentation schemes did not bundle the bars, but instead introduced new bars spaced between the "as-designed" reinforcing steel (Bastrop), or totally changing the bar sizes (Round Rock).
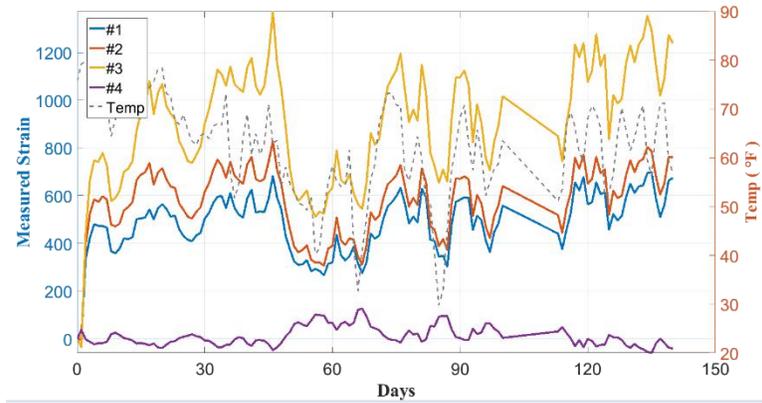
(a) VWG #1 to 4 in the section of 2#4 bars spaced at 9-in. reinforcement
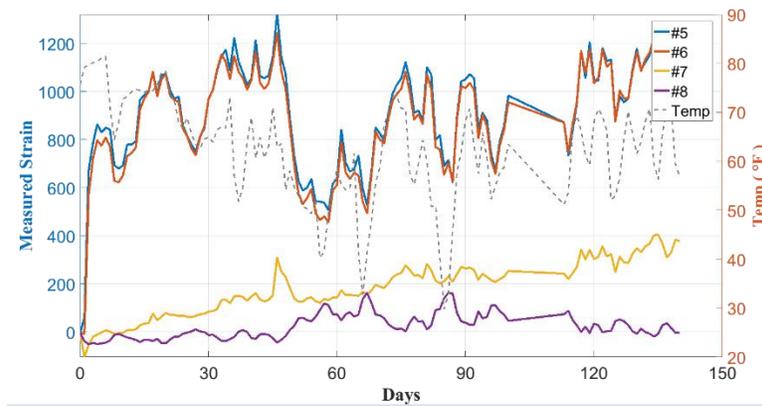
(b) VWG #5 to 8 in the section of #4 bars spaced at 9" reinforcement
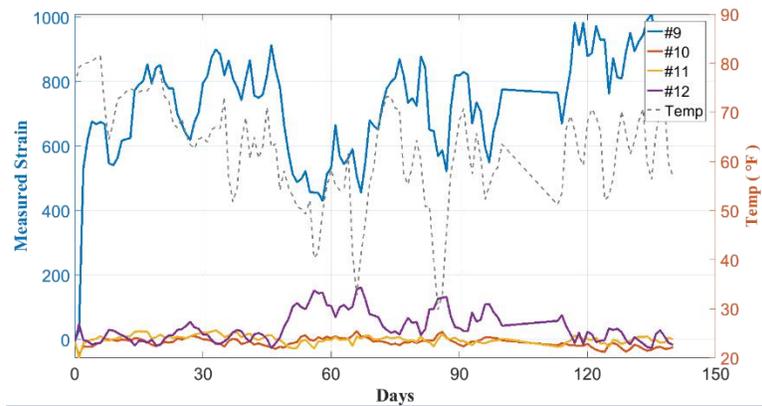
(c) VWG #9 to 12 in the section of #4+#6 bars spaced at 9" reinforcement

Figure 3- 14 Concrete Strains in San Marcos SH123 bridge
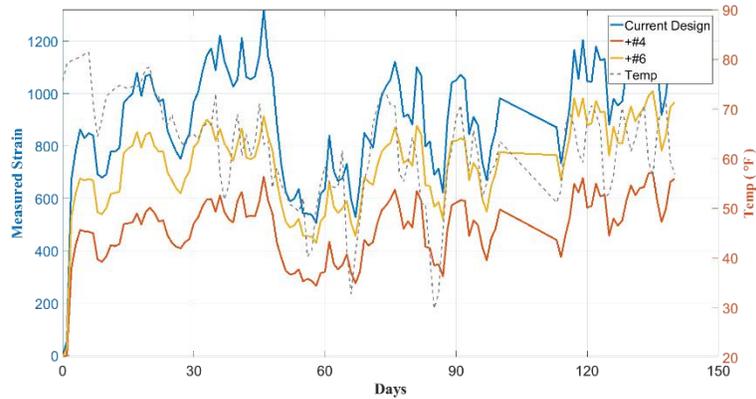
Figure 3- 15 Concrete Strains in San Marcos SH123 bridge

3.3.2 Bastrop SH71 Bridge

The second bridge instrumented was located in Bastrop, TX, and was also constructed in 2016 and 2017. This bridge was an entrance ramp onto SH71 from the frontage road, as shown in Fig 3-16. The bridge consisted of four beamlines of simply-supported girders with five total spans. The reinforcement in the CIP portion of the deck consisted of #4 bars spaced at 9-inch in each direction, with the transverse steel on the top. The reinforcement remained constant over the entire bridge other than over the bents, where one additional 5 ft-long #4 bars had been placed between every standard bars spacing at 9 inches, as part of the TxDOT detail of reinforcing for bridges with PCPs. The decision to place additional bars between the original steel instead of bundling was made following inconsistencies observed in the San Marcos instrumentation.
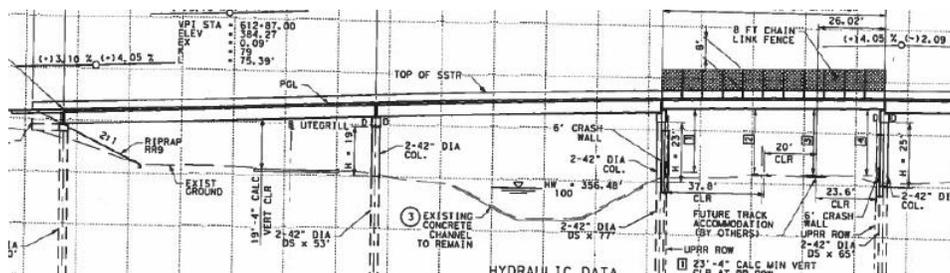
Figure 3- 16 Bastrop SH71 Bridge Elevation View Drawing (TxDOT)

The selected "Poor-boy" joint of SH71 between the first and second span, where the CIP portion routed a drainage pipe along the deck and required a thicker full-depth slab. This issue was deemed to be inconsequential as the CIP portion was limited to only one of the exterior girders. The other three girders used the PCP system. However, this did eliminate the possibility of having a fourth girder to measure.

The reinforcement remained constant over the entire bridge other than over the bents where intermediate 5 ft. #4 bars were added at 4.5" spacing between the standard bars, as shown in Figure 3-17, which were placed in accordance with TxDOT's details for PCP over bents, in anticipation of controlling cracks forming at that location.

35

Figure 3- 17 Deck Reinforcing Bars in Bastrop SH71 Bridge

Adding reinforcement to the existing steel would make the concrete too congested to be able to get the desired relationship between the area of steel and measured strain. To achieve three kinds of reinforcement detail in the section, the placement of the existing steel was adjusted. Figure 3-18 shows the steel layouts with the gages. Starting from the south side, the intermediate steel was removed over the exterior girder to reduce the steel down to the standard reinforcing of #4 bars spaced at 9-in. The steel over the first interior girder was not adjusted and remained #4 bars spacing in 4.5-inch. The steel over the second interior girder had one additional #4 bar added to the primary longitudinal bars to provide the same area of the bundled #6 used in the San Marcos Bridge.
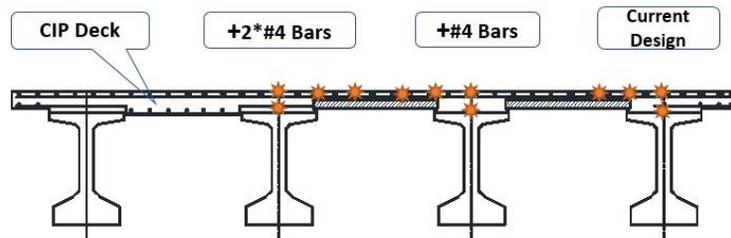
Figure 3- 18 Gage Layout in Elevation View

The crack former in this bridge differed from the San Marcos since the PCPs were continuous across the length of the bridge. Over the center of the bent, a 3/4 inch timber board was secured between two panels as shown in Figure 3-19. The wood extended from the top of the girders to one inch above the panels and was continuous across the width of the deck. This strip created a weak joint in the deck for a crack to form. The VWGs were placed over the wood crack former to ensure the gages obtain the concrete strains across the crack.

Figure 3- 19 Wood Crack Former

The top layer gages had no interference with the crack former as the longitudinal reinforcement remained above the strip. The gages were carefully placed directly over the crack former to ensure the gages captured the strain across the crack as shown in Figure 3-20. For the strain gradient, the bottom layer gages had to pass through the timber board, as shown in Figure 3-21. With permission of the contractor, holes were drilled in the wood to allow enough clearance for the gage and the attached reinforcement bar to fit through the wood strip.

Figure 3- 20 Top Layer Gages over the Crack Former

Figure 3- 21 Gage through the Crack Former

Figure 3-22 shows the gage layout in plan and section views. Gages #1-4 monitor the one additional #4 reinforcing bar added to the current design, gages #5-8 monitor the current design, and gages #9-12 monitor the two additional #4 reinforcing bar added to the current design. The reinforcement ratios of each region were 1.0%, 0.5%, and 1.6%, respectively.
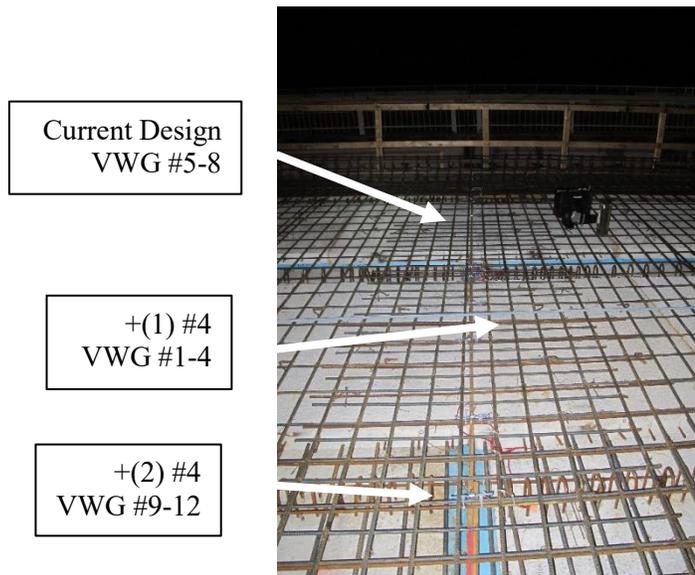
Figure 3- 22 Gage Layout in Plan View

The concrete deck for the instrumented span was cast on March 13, 2017, beginning at 2 am, as shown in Fig 3-23. The contractor for the bridges in Bastrop and San Marcos were the same, and therefore, similar procedures were used for the deck casting. The mix design for the CIP layer is listed in Table 2.3 below, with a slump of 4.5 inches. Concrete material testing samples were also fabricated in the Bastrop bridge. In addition to the twelve 4-inch concrete cylinders, modulus of rupture beam samples were cast to get more samples for tension testing.

38

Figure 3- 23 Screed Bridge During Concrete Deck Cast

Table 3- 3 Concrete Mix Design

f'c (psi)	w/c Ratio	Fly Ash	Hydraulic Cement	Coarse Aggregate	Fine Aggregate
4000	0.45	67%	33%	58%	42%

Figure 3- 24 Modulus of Rupture Test

Table 3- 4 Material Strengths

Compression Strength f'$_c$	Elastic Modulus E$_c$	Splitting Tensile Strength f$_t$	Modulus of Rupture f$_r$
5100 psi	5120 ksi	630 psi	560 psi

Material tests were conducted to get the strength of deck concrete. Modulus of rupture (MOR) beam test, shown in Figure 3-24, was conducted for flexural tensile capacities. The strength test values shown in Table 3-4 provided the estimated tensile capacity of the bridge deck. Using the direct tensile strength of $f_t = 4 * \sqrt{f'_c}$, the cracking stress was estimated to be 285 psi correlating to a strain of 55 με.

From the data collected, it was apparent that all VWGs were located across a crack. Figure 3-25 (a to c) shows the temperature compensated strain results of the four gages from

each section. In each section, readings from the top layer gages show positive strains, and the readings from the bottom layer gages typically show compressive strains, which indicates bending behavior at "Poor-boy" joints. The section with standard deck reinforcement was at an exterior girder, resulting in a difference in stiffness and load when compared to the interior girders. After the guard rail was constructed over the exterior girder on approximately day 35, VWGs #5-8 showed some additional strains from the weight of the barrier.

Like the procedures outlined for the San Marcos Bridge, large fluctuations due to temperature effects were minimized by taking the daily gage readings at 4 am. Some variations in the strain were due to additional loads on the bridge deck during construction that may change daily and could not be quantified. The significant additional load on the exterior girder was the guard rail construction around day 35. This additional load was supported almost entirely by the exterior girder, causing an increase in strain. During a portion of the construction of the guard rail, the batteries lost power, and some data was lost. Shifts in the strain only affected the exterior girder, while the two interior girders remained unaffected. The shift caused by the guard rail casting was about a difference of approximately 240με, which should be considered when comparing each of the three sections.

There was a distribution of strain across the width of the deck caused by shear lag, similar to observations in the San Marcos SH123 bridge. This consistent trend provided some confidence in the evaluations of the strain distributions.
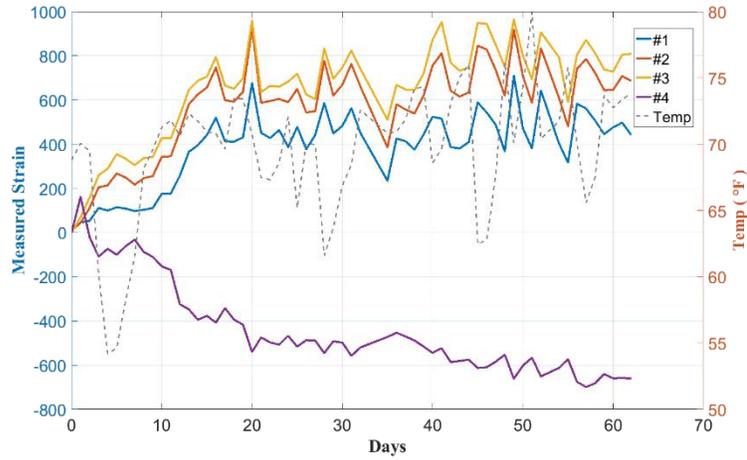
(a) Gage 1-4 (current design+#4 bars spaced at 9", 1.0%)
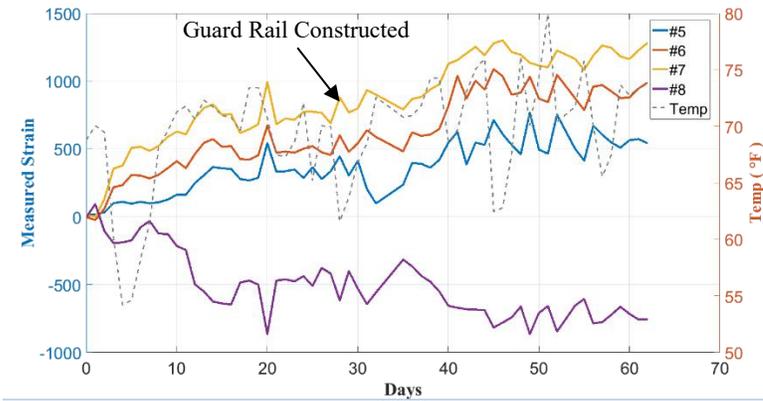
(b) Gage 5-8 (current design, 0.5%)
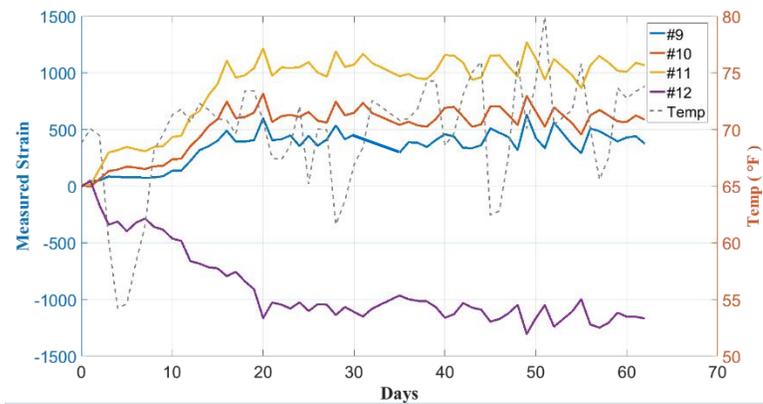
(c) Gage 9-12 (current design+2#4 bars spaced at 9", 1.6%)

Figure 3- 25 Concrete Strains in Bastrop SH71 Bridge
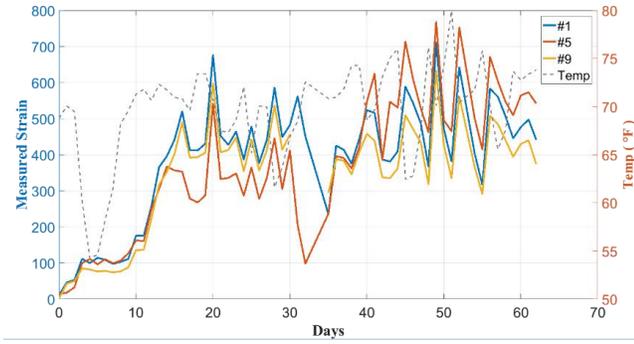
(a) Gages #1, 5, and 9 over the panels
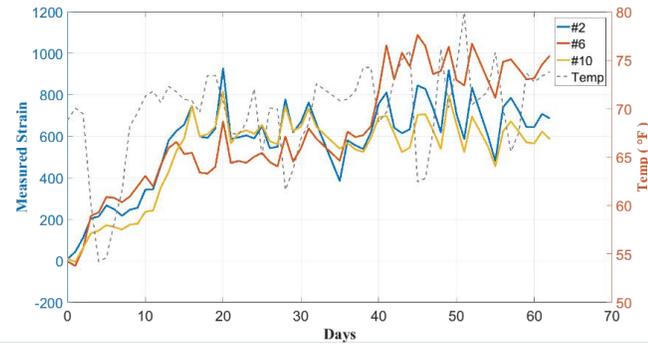
(b) Gages #2, 6, 10 at the edge of the panels
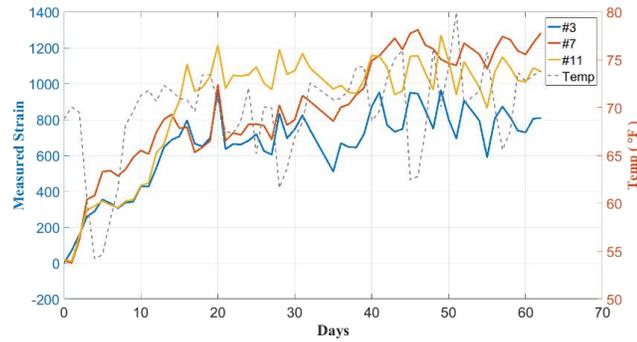
(c) Gages #3, 7, 11, top layer gages over girders
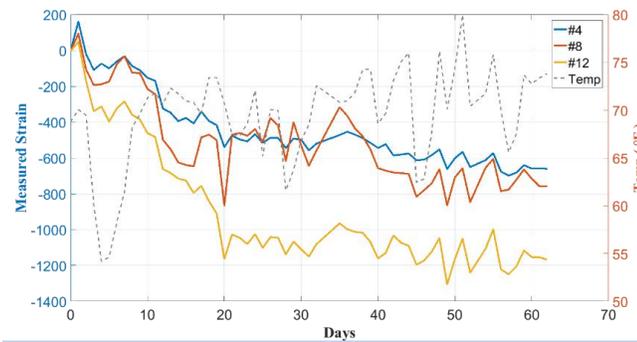
(d) Gages 4, 8, 12, bottom layer gages over girders

Figure 3- 26 Comparison of Concrete Strains Measured at the Same Locations

A comparison between similar gage locations for each section showed the influence of the amount of steel on the measured strains. Despite the changes in the deck reinforcement area, most of the strain values were relatively similar. There was not a consistent trend between the amount of steel at the section and the measured strain in the concrete. In an attempt for direct comparison, gages from similar locations were plotted together in Figure 3-26 (a to d). Gages over the panel show the highest strains correlating to the reinforcement section with one additional #4 bar followed by the section with two #4 bars. The section with the standard reinforcing shows the lowest strain. Gages over the girders show a different trend where the highest to lowest strains are two additional #4's, standard reinforcement, and one additional #4, respectively. The standard reinforcement and one additional #4 have similar values.

3.3.3 Summary of "Poor-boy" Continuous Deck Instrumentation

The results from the strain measurements during the early stages after bridge deck casting show the influences of additional reinforcement in the CIP portion of the "Poor-boy" continuous deck joints. Probably due to the crack formers, only minor benefits on reducing deck strain were measured by using more reinforcing steel or reducing reinforcing bar spacing on "Poor-boy" joints, and in some cases. Besides, the transverse distribution of concrete deck strain was measured at "Poor-boy" joints, as the concrete strain over bridge lines were always more significant than that measured over PCPs. From the field instrumentation and long-term monitoring of these two bridges, the research team got valuable experience on field instrumentation procedure and deck cracking behavior. More meaningful data can be measured on the bridge deck over the spliced continuous girder systems in the next chapter.

3.4 Field Instrumentation of Continuous Bridges

3.4.1 Overview

In 2018, the research team applied field measurements on two continuous concrete bridges at Round Rock, TX. This chapter introduces the equipment used for instrumentation and outlines the process of assessing, instrumenting, and monitoring the critical sections during construction and after service. The instrumentation was similar to that used on the San Marcos and Bastrop instrumentations outlined in the last chapter. The instrumentation included Vibrating Wire Gages (VWGs) and Foil Strain Gages with data logging equipment. The data presented in this section was taken from deck regions over four interior bents of two continuous bridge, which had the same geometries, but with different reinforcement details at the critical region of the bridge deck.

The primary objective of the instrumentation was to capture the behavior of the bridge deck cracking at a specific location. To study the global behaviors and deck cracking at the critical section, both precast girder and CIP deck in negative moment region were instrumented for Round Rock Bridges. Vibration Wire Gages (VWGs) were mounted on the girder surface and embedded in CIP concrete deck to measure the concrete deformation, and foil strain gages were also placed along with the longitudinal reinforcement in CIP concrete deck over interior bents to measure the reinforcing bar stress distribution around deck cracking. In addition to monitoring the girders and deck throughout the construction period, that instrumentation was monitored for approximately 100 days after bridges were open to traffic.

3.4.2 General Information of Round Rock Bridges

These two identical continuous bridges were a part of the overpass Ramp 20 and Ramp 21 of IH35 across McNeil Road, at the south side of Round Rock, TX. Each bridge consisted of four beamlines of three-span continuous girders with spans of 180 ft., 250 ft., 180 ft. Each beamline consisted of five segments of precast, prestressed concrete spliced, as shown in Figures 3-27 and 3-28, including two end girders, two haunched girders, and one drop-in girder. The depth of end girders and drop-in girders were 80 inches, and that of haunched girders varied from 80 inches at spliced joints to 130 inches over interior supports. The spacing between each beamline was 80 inches. Three tendons were post-tensioned when four bridge lines were connected by eight cast-in-place concrete diaphragms at bridge ends, over interior supports, and at splice-locations.

(a) Aerial view from "Google Maps"　　　(b) Elevation view of drop-in girder
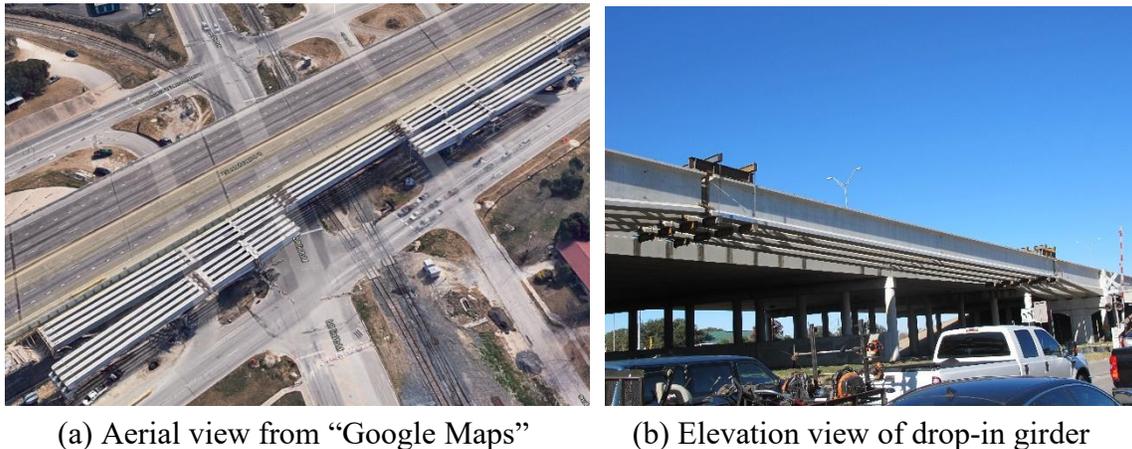
Figure 3- 27 Global Views of Round Rock Bridges

The bridge deck contained 4-inch deep prestressed precast concrete panels (PCPs) as the bottom layer and 4.5-inch depth cast-in-place concrete as the top layer. The original reinforcement design for the deck is #5 bars spaced at 9" over the positive moment region and #6 bars spaced at 4.5" over the negative moment region in the longitudinal direction, with #5 bars spaced at 9" transverse steel on top. For research purposes, after communicating with the engineer of record, TxDOT engineers, and the contractor, changes were made in the deck reinforcing details in the negative moment region. The four different longitudinal reinforcement details consisted of, #6 bars spaced at 4.5" (2.2%, as original design) over south interior support of Ramp 21, #6 bars spaced at 9" (1.1%) over north interior support of Ramp 21, #5 bars spaced at 6" (1.1%) over north interior support of Ramp 20, and #5 bars spaced at 9" (0.8%) over south interior support of Ramp 20, respectively. The reinforcement ratios listed here were based upon the reinforcing bar area divided by the cast-in-place concrete area.
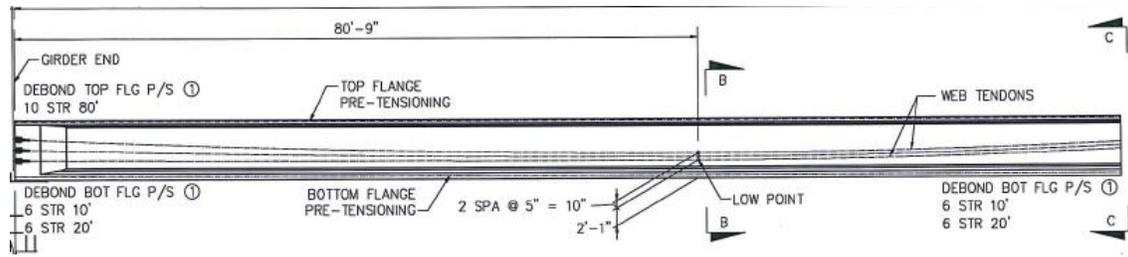
(a) End girder
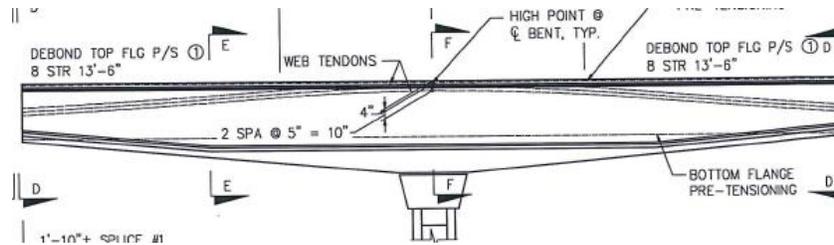
(b) Haunched girder
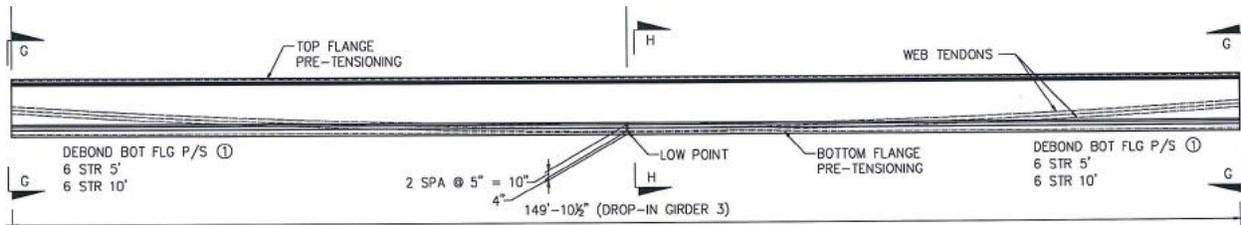
(c) Drop-in girder

Figure 3- 28 Round Rock Beamlines Elevation View Drawing (TxDOT)

3.4.3 Field Instrumentation on Girder Stressing

The research team worked on Round Rock Bridge Ramp 21 on January 5th, 2018 to install twelve total VWGs on the side surfaces of two interior haunched girders over the south interior bent of Ramp 21 to obtain the girder flexure profile under post-stressing and future construction process. The specific gage locations were shown in Figure 3-29. All gages worked properly until three out of four gages at top flanges were disturbed when contractors removed the bottom deck form at the end of March 2018.
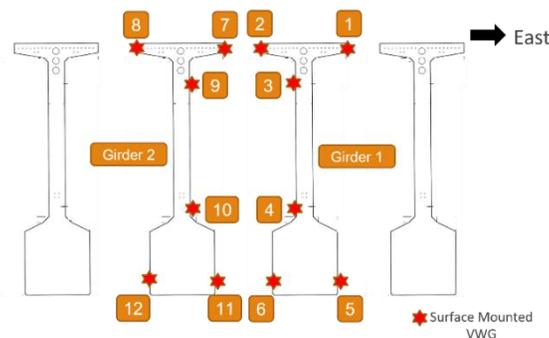
Figure 3- 29 Surface Mounted VWGs on Precast Girders

45
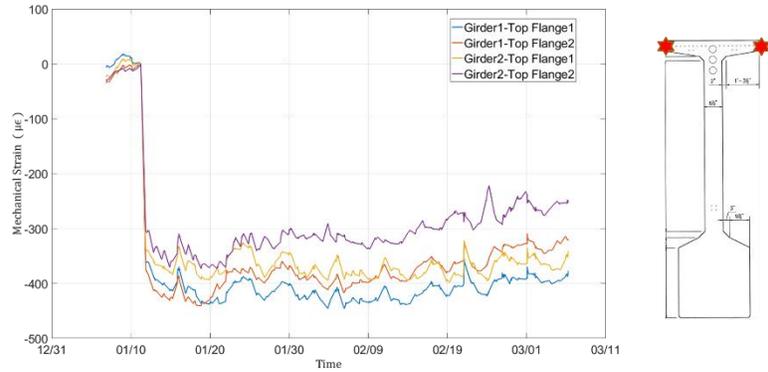
(a) Girder strains at top flanges
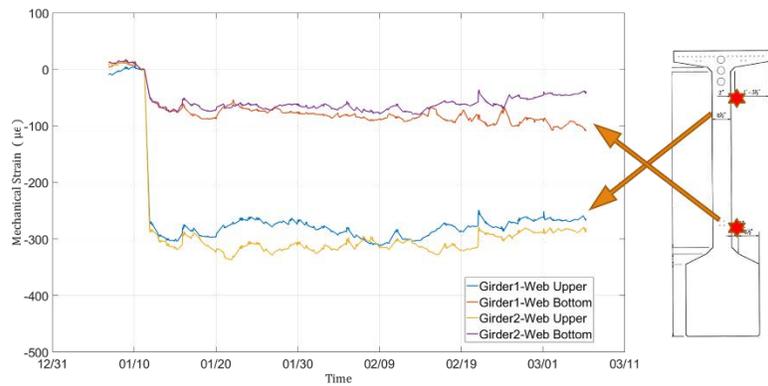
(b) Girder strains at webs
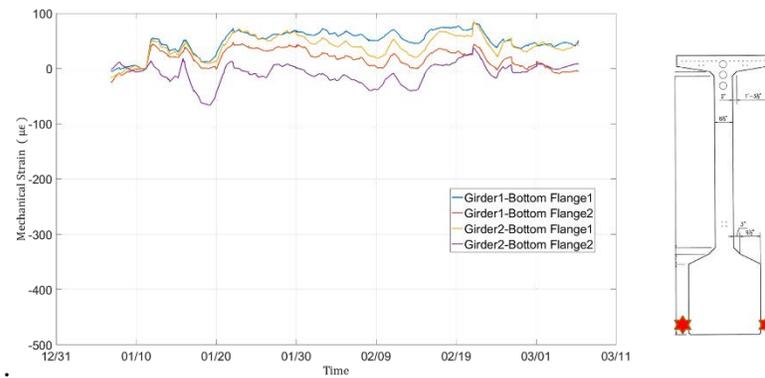
(c) Girder strains at bottom flanges

Figure 3- 30 Girder Strain Before and After Stressing

One week after girder instrumentation, the Ramp 21 girder system was stressed by the post-tensioning tendons. The concrete girder surface strain measured by VWGs are shown in Figure 3-30. Because the post-tensioning tendons were quite close to the top flanges over the interior supports, measurements of strains in the top flanges were approximately 300 to 400 με compression. The corresponding strain measured in the bottom flange was approximately 50 με tensile strain.

46

3.4.4 Field Instrumentation for Deck Cracking

Similar to the previous works at the bridges in San Marcos and Bastrop, the objective of the field instrumentation at the Round Rock Bridges was to indicate the benefits of variations in the deck reinforcing steel at the critical sections of the concrete deck above the interior supports. A reduction in the concrete strain and crack width was expected to correlate with increasing the amount of steel. To obtain the effects of changes in reinforcing steel, the research team monitored four different longitudinal reinforcement details over the interior supports of two bridges. As a plan, all field instrumentation at the Round Rock Bridges included a 15-minute frequency of data sampling.

(a) VWGs   (b) Foil Strain Gages
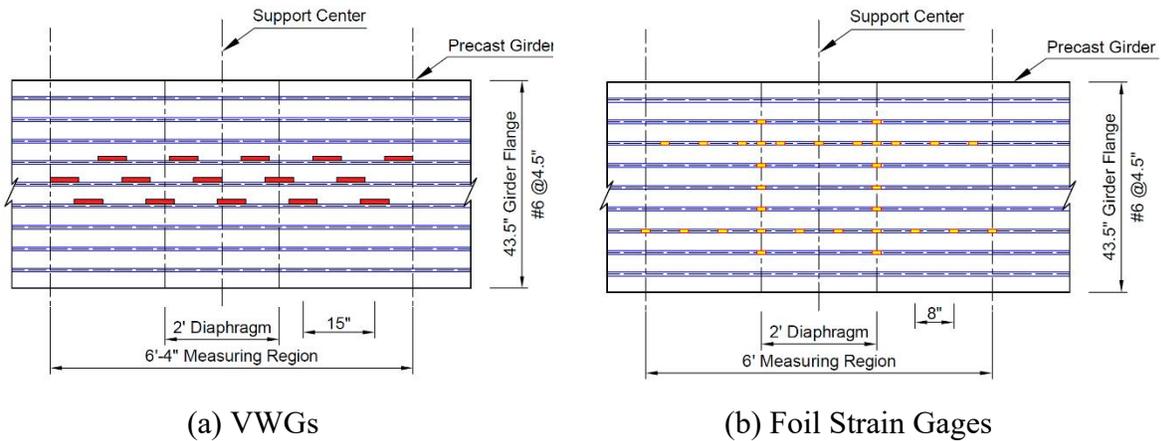
Figure 3- 31 Plan Views of Instrumentations in #6 bars spaced at 4.5" Region

(a) VWGs   *(b) Foil Strain Gages*
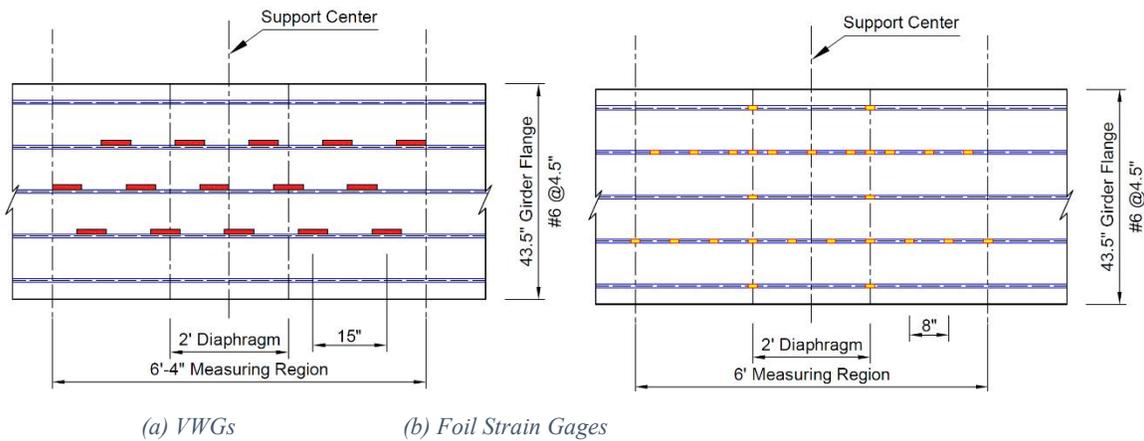
Figure 3- 32 Plan Views of Instrumentations in #6 bars spaced at 9" Region

The original design as #6 bars spaced at 4.5" (2.2% of CIP area) was kept over the south interior bent of Ramp 21. 15 VWGs and 31 foil strain gages were placed along reinforcing bars over one interior girder line, as shown in Figure 3-31. To avoid ruining the connection between concrete and reinforcing steel, research team placed VWGs and foil strain gages on several reinforcing bars over beamlines. The net spacing between each VWG and foil gage was around 8 inches. A reduced design as #6 bars spaced at 9" (1.1% of CIP area)was used over the north

interior bent of Ramp 21. 15 VWGs and 27 foil strain gages were placed along reinforcing bars over one interior girder line, as shown in Figure 3-32. The monitoring of Ramp 21 started from deck casting on March 30th, 2018 till March 10th, 2019, over 300 days. A similar detail as #5bars spaced at 6" (1.1% of CIP area)was used at the north interior bent of Ramp 20. 15 VWGs and 27 foil strain gages were placed along reinforcing bars over one interior girder line, as shown in Figure 3-33 (a). A reduced reinforcement detail with #5 bars spaced at 9" (0.8% of CIP area)was used at the south interior bent of Ramp 20, as shown in Figure 3-33 (b). 15 VWGs and 27 foil strain gages were placed along reinforcing bars over one interior beamline. The monitoring of Ramp 20 was started from casting concrete deck on July 5th, 2018 till March 10th, 2019, over 200 days.

(a) #5bars spaced at 6" region   (b) #5bars spaced at 9" region

Figure 3- 33 Instrumentation on Deck in Ramp 20

3.4.5 Material Testing

The compressive strength and modulus of elasticity (MOE) of the CIP concrete deck were obtained by concrete cylinder tests. Split cylinder tests and Modulus of Rupture (MOR) tests were conducted to determine the tensile strength of the concrete, as shown in Figure 3-34. The material properties of the CIP concrete decks of Ramp 20&21 bridges are shown in Table 3-5. Using the direct tensile strength of $f_t = 4 * \sqrt{f'_c}$, the cracking stress of the deck concrete was estimated as approximately 285-psi, correlating to a tensile strain of 50 με.

(a) MOE test	(b) Splitting test	(c) MOR test

Figure 3- 34 Concrete Material Property Tests for Round Rock Bridge Deck

Table 3- 5 Material Strengths Material Property of CIP deck

	Compression Strength f'_c	Elastic Modulus E_c	Split Cylinder f_{sp}	Modulus of Rupture
Ramp 21	5400 psi	5600 ksi	700 psi	710 psi
Ramp 20	4800 psi	6050 ksi	530 psi	800 psi

The impact-echo test, as a nondestructive detection method, was conducted to obtain the modulus of elasticity of the precast girder. The research team tested the wave speed through the 8.5" thickness girder webs, depending on the concrete material property, as shown in Equation 3-1 (Sansalone, 1997).

$$v = \sqrt{\frac{E_c\,(1-v)}{\rho(1+v)(1-2v)}} \tag{3-1}$$

Where v is wave speed obtained in impact-echo tests, Ec is the modulus of elasticity (MOE) of concrete; v is the Poisson's ratio of concrete, assuming as 0.18; and ρ is the density of concrete, assuming 150-pcf. From a total of 40 test locations, the average MOE of the precast girder was 5950 ksi. This MOE of precast girder is being used in the finite element modeling and further parametric study.

3.4.6 Deck Cracking Examination

For Ramp 20 and Ramp 21, the surface deck cracks were inspected before and after the live load testing on August 10th, 2018. For each concrete deck region over interior support, with different reinforcement detail, two cracks could be observed, whose width was around 0.005 to 0.007-inch (0.12 to 0.16 mm), as shown in Figure 3-35. Besides that, for Ramp 21, several transverse deck cracks were also observed around the middle of mid-span. The crack spacing was around four to five ft., with crack width around 0.005-inch (0.12mm), as shown in figure 3-36.
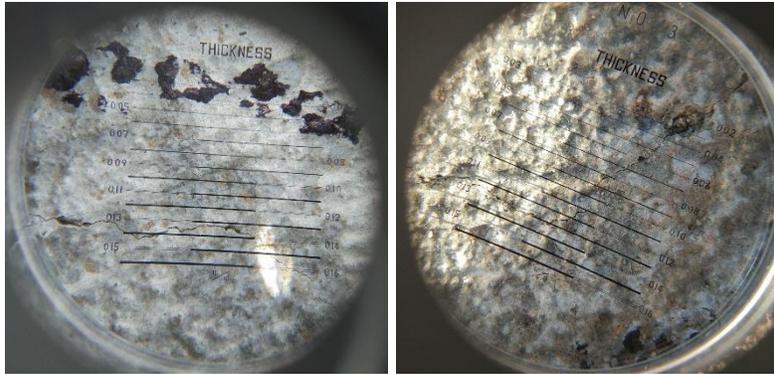
(a) #6 bars spaced at 4.5" (b) #6 bars spaced at 9"
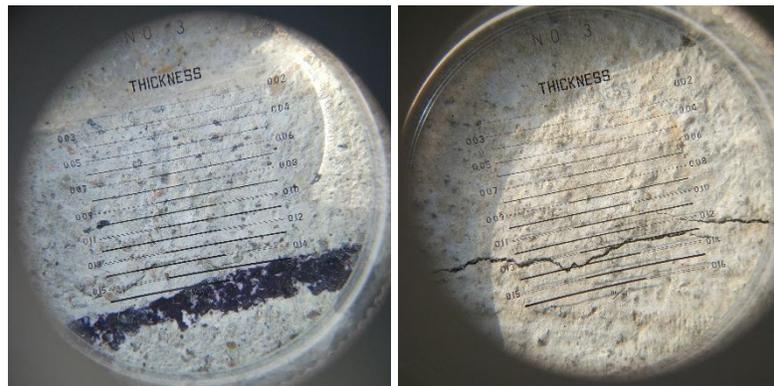
(c) #5 bars spaced at 6" (d) #5 bars spaced at 9"

Figure 3- 35 Photos of Surface Deck Cracks Over Interior Supports
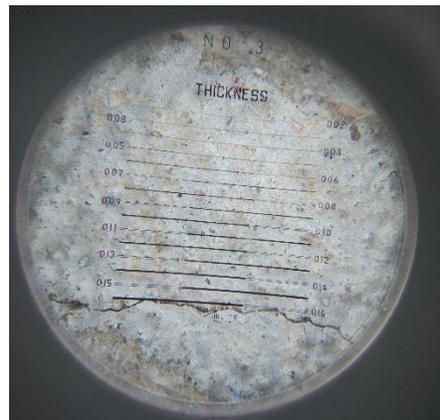
Figure 3- 36 Transverse Deck Crack at the Middle of Mid-span, Ramp 21

Generally, all observed deck surface cracks are around half of the 0.012 inches crack width limit recommended by ACI 224R08, and the research team did not observe any significant increases in crack width after the live load tests.

3.4.7 Long-Term Monitoring Data

All VWGs and foil gages were sampled every 15 minutes. However, to minimize the influence from thermal effects, only data between 2 AM and 4 AM was shown in the bellowed figures. For all four the region with different longitudinal reinforcing bar detail, deck cracking occurred after the concrete curing period. After that, those readings from VWGs across cracks increased intensely in a short time, and with reinforcing bar stress increasing simultaneously. In each region, three or four VWGs were across the concrete cracks, and all the others not. The measured concrete strains of four regions with different reinforcement detail results were shown in Figure 3-37, with colorful lines as cracked concrete strains and gray shades as uncracked concrete strains. Measured reinforcing bar stress results were shown in Figure 3-38, with colorful lines as measured at reinforcing bar closed to where concrete cracked and gray shades as reinforcing bar embedded in the uncracked concrete.

(a) #6 bars spaced at 4.5" (b) #6 bars spaced at 9"

(c) #5 bars spaced at 6" (d) #5 bars spaced at 9"
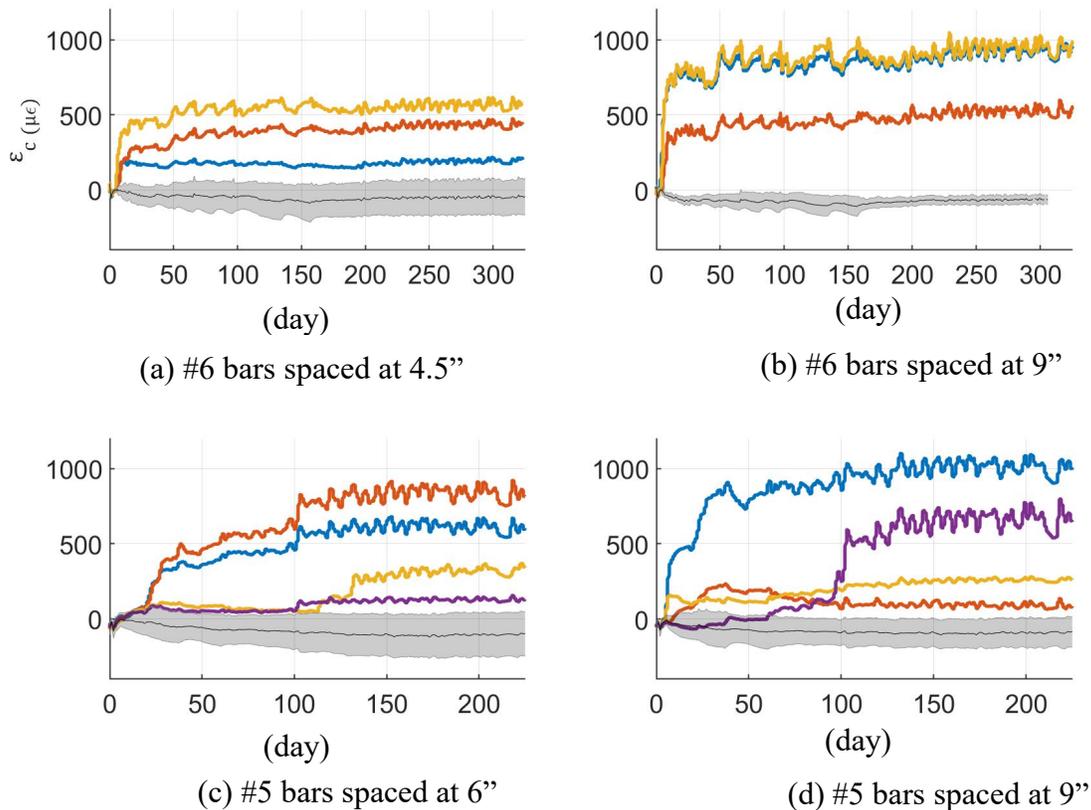
Figure 3- 37 Concrete Strain Long-Term Monitoring Data

Caused by concrete volume shrinkage, deck cracking occurred several days after casting, and the measured concrete strain increased suddenly to 500 to 800 µε, depending on reinforcement ratio. After this significant crack initiations, both the concrete strains and reinforcing bar stresses would grow a little over time. With more reinforcing steel in this region, like #6 bars spaced at 4.5-in. (2.2%) in one of the monitored cases, lower concrete cracking strains could be expected. Otherwise, with less reinforcing steel, like #5 bars spaced at 9-in. (0.8%), the concrete strain jumped to around 800 µε after crack initiation and gradually grew to 1000 µε. A similar trend was measured from the reinforcing bar stress data, as well. When the

51

concrete cracked, the maximum stress in the longitudinal reinforcing bar increased to around 10 ksi in several days and then grew to approximate 20 ksi if the reinforcement ratio was lower than 1.0%.

(a) #6 bars spaced at 4.5"

(b) #6 bars spaced at 9"

(c) #5 bars spaced at 6"

(d) #5bars spaced at 9"
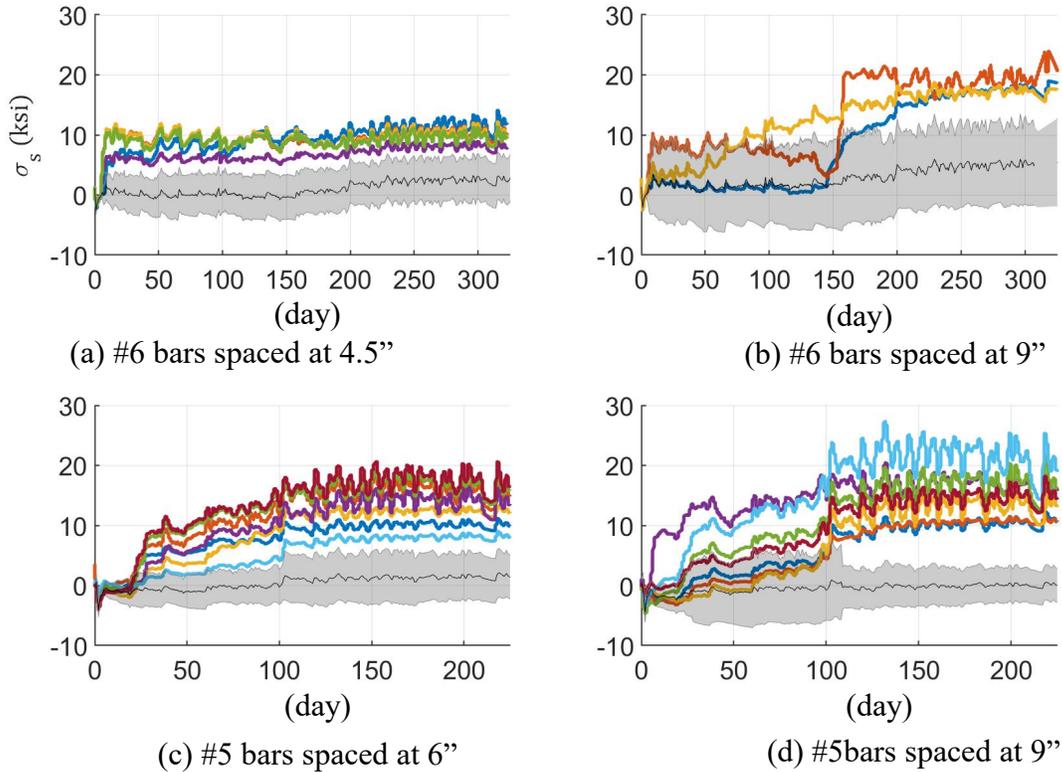
Figure 3- 38 Reinforcing bar Stress Long-Term Monitoring Data

Furthermore, when bridges were open to traffic, as after 200-day monitoring in Ramp 21 and 100-day monitoring in Ramp 20, some concrete cracking growth were measured. Generally, the concrete strains or reinforcing bar stresses caused by live load were always smaller than those occurred at early age.

3.4.8 Deck Strain and Reinforcing Bar Stress Spatial Distribution

The spatial distribution of concrete strains and reinforcing bar stresses of four different kinds of reinforcement detail are shown in Figure 3-39. Generally, for all four cases, the concrete strain distribution patterns matched well with those of reinforcing bar stresses: the concrete cracks occurred near the edges of interior bents over each supports, and the crack spacings were around 30-inch. Maximum reinforcing bar stresses were produced in the same regions as concrete cracking. For the bridge deck between cracks, the concrete strains and reinforcing bar stresses were both quite small. The spatial distributions showed a significant difference between deck reinforcing bar averaged stress and maximum stress after concrete cracking.
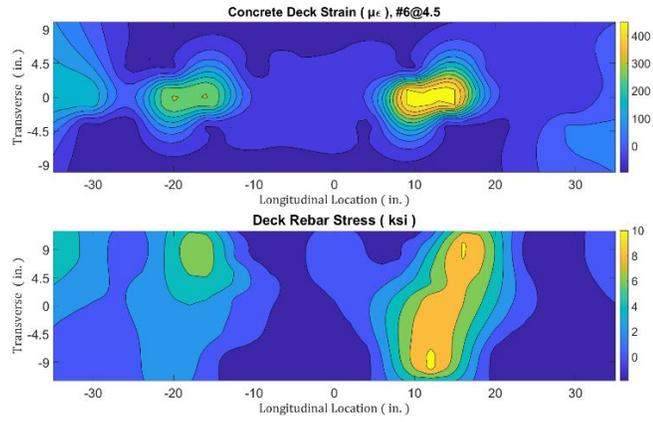
(a) #6 bars spaced at 4.5" (2.2%)
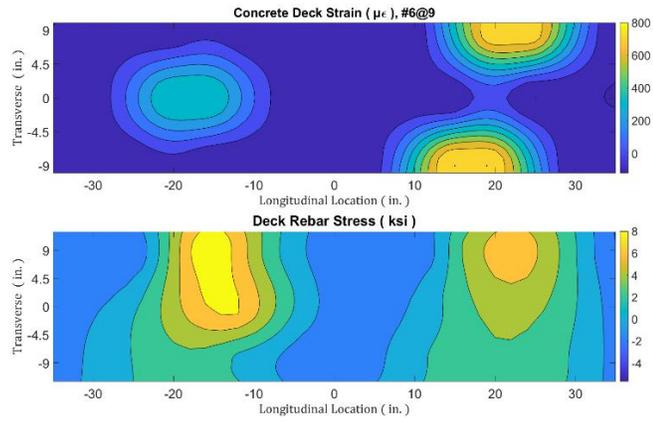
(b) #6 bars spaced at 9" (1.1%)
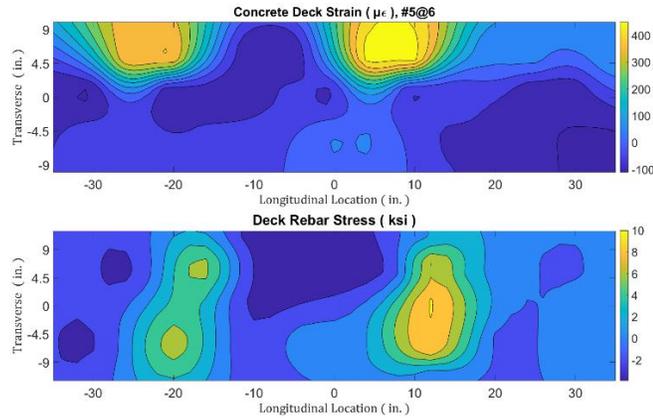
(c) #5 bars spaced at 6" (1.1%)
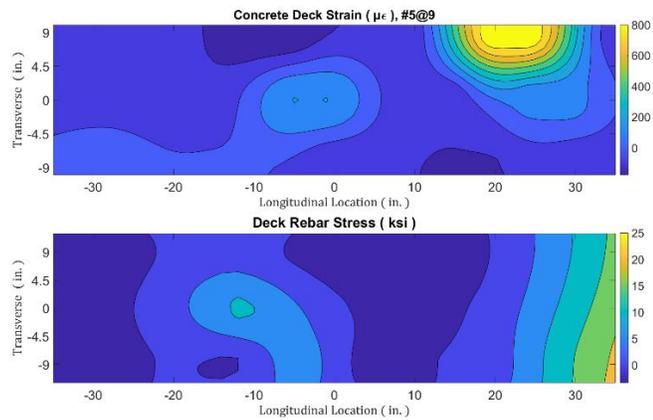
(d) #5 bars spaced at 9" (0.8%)

Figure 3- 39 Concrete Strain and reinforcing bar Stress Distribution

3.4.9 Cable Protection at Round Rock Bridges

Over 100 days after these Round Rock bridges were open to traffic, and both concrete strains and reinforcing bar stresses measurement showed a steady trend, the research team finished the field instrumentation work. The field monitoring continued over 300 days for Ramp 21, and over 200 days for Ramp 20. On March 10th, 2019, the data loggers, antennas, and batteries were brought back to the laboratory, but the cables of embedded VWGs and foil strain gages were protected in the housing boxes on each interior bent, as shown in Figure 3-40. Therefore, all the VWGs embedded in the concrete deck and foil strain gages on the longitudinal deck reinforcement could continue working in future research.

Figure 3- 40 Cables Protection After Field Instrumentation

3.5 Summary

Four total bridges were instrumented between 2016 and 2018 to study the cracking behavior of concrete deck in the negative moment regions. Two of them were "Poor-boy" continuous deck over simply support bridges, and the other two were over interior supports of spliced concrete continuous bridges. Different reinforcement details were compared, with reinforcement ratio from 0.5% to 2.2%, to cracking widths control under service loading conditions. Based upon the field instrumentation and field examination results, for the concrete deck in the negative moment region of continuous bridges, the following conclusions can be made:

- With each reinforcement detail, observed surface cracks were less than 0.006-inch.
- Increasing reinforcement ratio and decreasing reinforcing bar spacing showed some benefits.
- The deck cracking process includes two steps: early-age initiation and small long-term growth.
- Restrained shrinkage was the dominant factor for deck crack initiation with concrete strains in the range of 500 to 1000 $\mu\varepsilon$ and maximum reinforcing bar stresses of 12 to 20 ksi.
- Minor cracking occurred following bridges opening to traffic.

Chapter 4. Field Load Testing

4.1 Overview

Field load tests were conducted on four bridges. These included a bridge on SH 123 in San Marcos, a bridge on SH72 in Bastrop, and two spliced concrete girder bridges near the intersection of Toll Road 45 and IH 35 in Round Rock, Texas. Load tests were conducted soon before bridges opened to traffic. The goal of the field load testing was to measure the response of the bridges, especially the decks in the critical regions, under controlled live load conditions.

Vibrating Wire Gages (VWGs) and foil strain gages installed for the long-term field instrumentation, described in the previous section, were the primary sensors for the field load tests. In addition, crack width gages and laser rangefinders were also utilized to measure surface deck crack widths and girder deflection during the load tests. These sensors are depicted in Figure 4-1.

(a) VWG
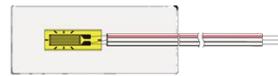
(b) Foil strain gage

(d) Crack width gage

(d) Laser rangefinder

Figure 4- 1 Field Instrumentation Equipment

4.2 Loading Truck Details

Field load tests on each bridge included several truck configurations using tandem-axle dump trucks filled with sand, provided by TxDOT. Examples of trucks are shown in Figure 4-2. Two trucks were utilized on each "Poor-boy" continuous bridge, and four trucks were utilized on each spliced concrete continuous bridge. Each truck had a total weight of approximately 52-kips with an axle spacing from front to back of approximately 18-feet. Nominal truck dimensions and axle weights are given in Figure 4-3.

Figure 4- 2 Trucks Utilized in Field Load Tests
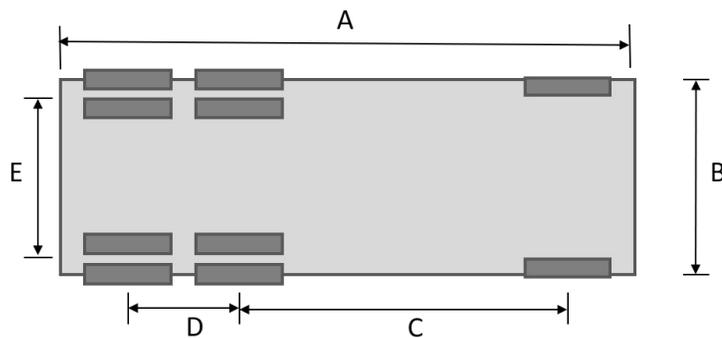
A (inch)	B (inch)	C (inch)	D (inch)	E (inch)	Rear Axle (kip)	Front Axle (kip)	Total Weight (kip)
300	83	170	54	72	39	13	52

Figure 4- 3 Truck Dimensions and Axle Weights

Selected bridges were marked for the truck locations the day before testing. To obtain a static measurement, the trucks were positioned at desired locations, and after waiting for approximately 30-second, the measurements were made. For each test, the actual dimensions and weights were measured prior to testing.

4.3 Field Load Testing of "Poor-boy" Continuous Bridges

4.3.1 San Marcos SH123 Bridge

Field load testing for the SH123 Bridge located in San Marcos was conducted on February 8, 2017. The test included five truck configurations discussed below using two tandem-axle dump trucks filled with sand provided by TxDOT. Vibration Wire Gages embedded in the

"Poor-boy" continuous joint were the primary instrumentation, and girder deflections at the mid-span were also measured. The layout of the VWGs is shown in Figure 4-4, and detailed information about this bridge can be found in the previous chapter.
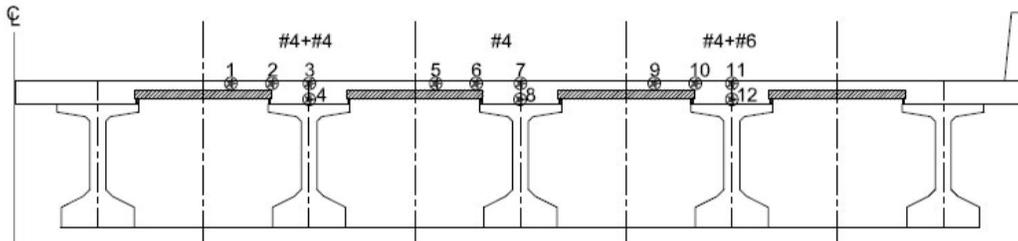
Figure 4- 4 Elevation View of VWG Layout

Truck locations used for the live load test are shown in Figures 4-5 (a)-(e). Load Case 1 is critical to the "Poor-boy" continuous deck over girder 2, measured by VWGs #1 to #4. The longitudinal reinforcement detail in this region is #4 bars plus one additional #4 bar, spaced at 9-inch. Load Case 2 is critical to the "poor-boy" continuous deck over girder 3, measured by VWGs #5 to #8. The longitudinal reinforcement detail in this region is #4 bars spaced at 9-in. (current design). Load Case 3 is critical to the "poor-boy" continuous deck over girder 4, measured by VWGs #9 to #12. The longitudinal reinforcement detail in this region is #4 bars plus one additional #5 bar, spaced at 9-inch. Load Cases 4 and 5 are two trucks side-by-side positioned in the middle of either span. Since the bridge is at a 45-degree skew, the mid-span of the girders are not side-by-side. The truck locations matched the skew angle in Load Cases 4 and 5. More detailed descriptions of the deck reinforcing steel layout at each monitored location is provided in Technical Memorandum No. 5.
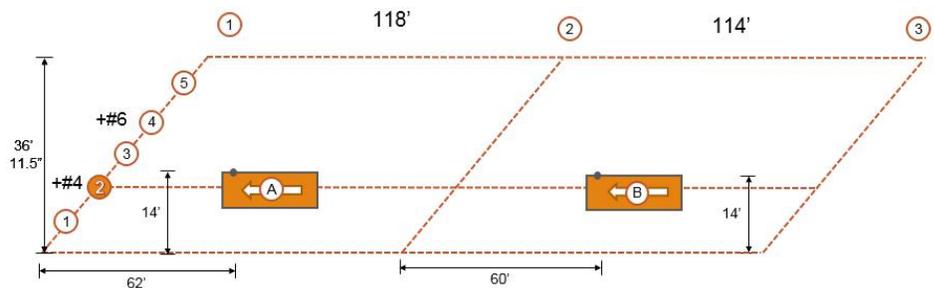
(a) Load Case 1
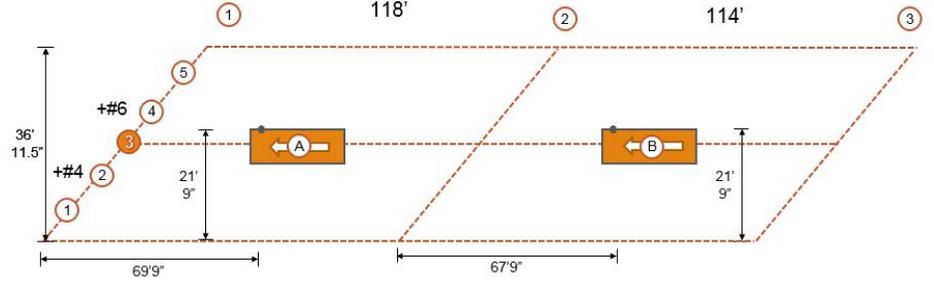
(b) Load Case 2
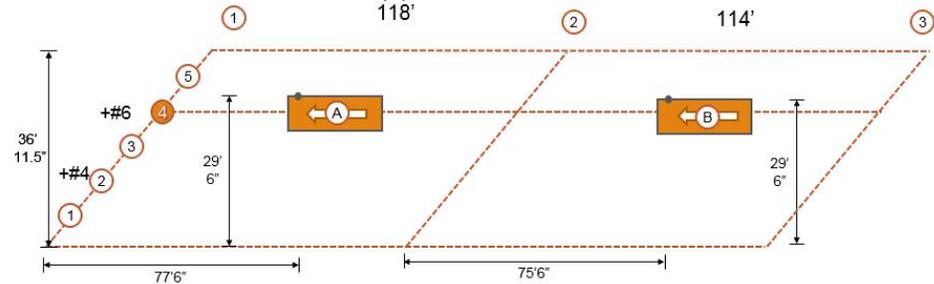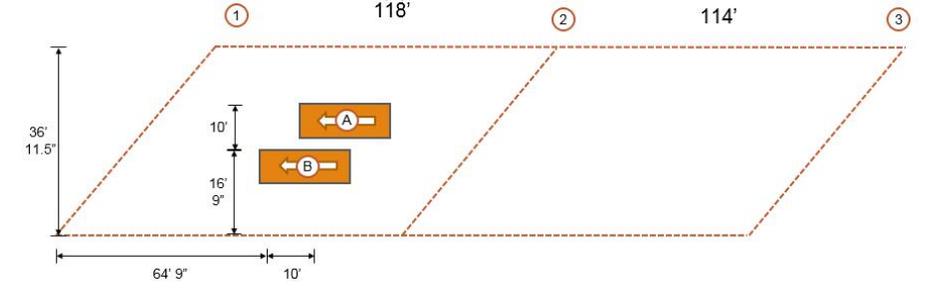
(c) Load Case 3
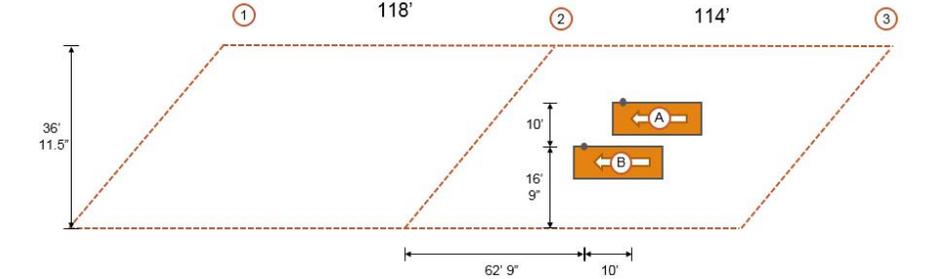
(d) Load Case 4

(e) Load Case 5

Figure 4- 5 Truck Locations for the San Marcos SH 123 Bridge Live Load Test

Figure 4-6 shows the measured deck strains for Load Cases 1 to 3 for the truck positioned over the respective VWGs. As indicated by this data, deck strains under the load tests were not larger than 200 με, which is less than half of the measured deck strains under shrinkage effects. Due to the zip strip embedded in the instrumented region, VWGs #1 to #3, #5, #6, and #9 located across the transverse deck crack, whose strain values are significantly higher than the other VWGs which are not located across a deck crack. From these values, based on the most comparable strain values over the panels (VWG #1, #5, and #9), there is a trend of reduction of strain due to the increase in the deck steel reinforcing area. The current design reinforcement had the highest strains, while the section with additional #6 bars had the lowest strain as expected. The strains from the additional #6 (85 με) and the additional #4 (78 με) had a respective reduction of 40% and 48% in maximum strain, relative to the existing detail which had a strain of 127 με.
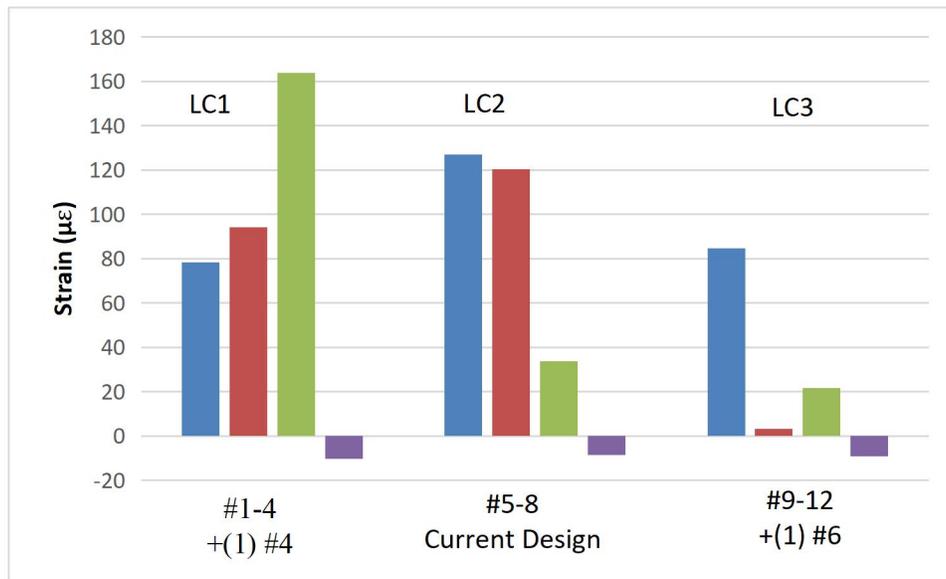
Figure 4- 6 Deck Strains under Load Cases 1 to 3

All the bottom layer gages (VWG #4, #8, and #12) showed compression values from the load test. These strains are small, but give an indication that there could be some bending within the "poor-boy" joints.
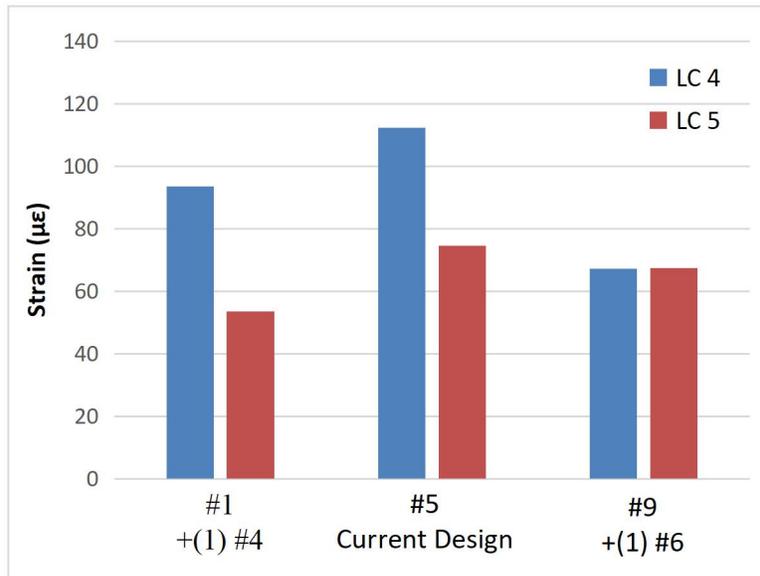
Figure 4- 7 Deck Strains (Over Panels) under Load Cases 4 and 5

Load Case 4 showed similar trends to those in the first three tests. However, Load Case 5 did not show a clear trend, as shown in Figure 4-7. Hence Load Case 4 will be used as the primary results for the side-by-side data. The sections with additional reinforcement show strains lower than the current design section. The difference between the current design (112 με) and both the additional #6 (67 με) and the additional #4 (93 με) is a reduction of 50% and 19%.

Between each load case, cracks in the top of the deck were observed and recorded. Before the test started, some cracks had already propagated from the zip strip embedded in the top of the deck. Figure 4-8 shows the extent of each crack marked with a number in the sequential order and which load case under which it occurred. Multiple cracks elongated during a subsequent load case. Most crack origins started at the bent cap centerline where the girders met. From there, the cracks typically propagated at a diagonal to the adjacent girder. The diagonal cracking pattern is believed to be due to the skew of the bridge.
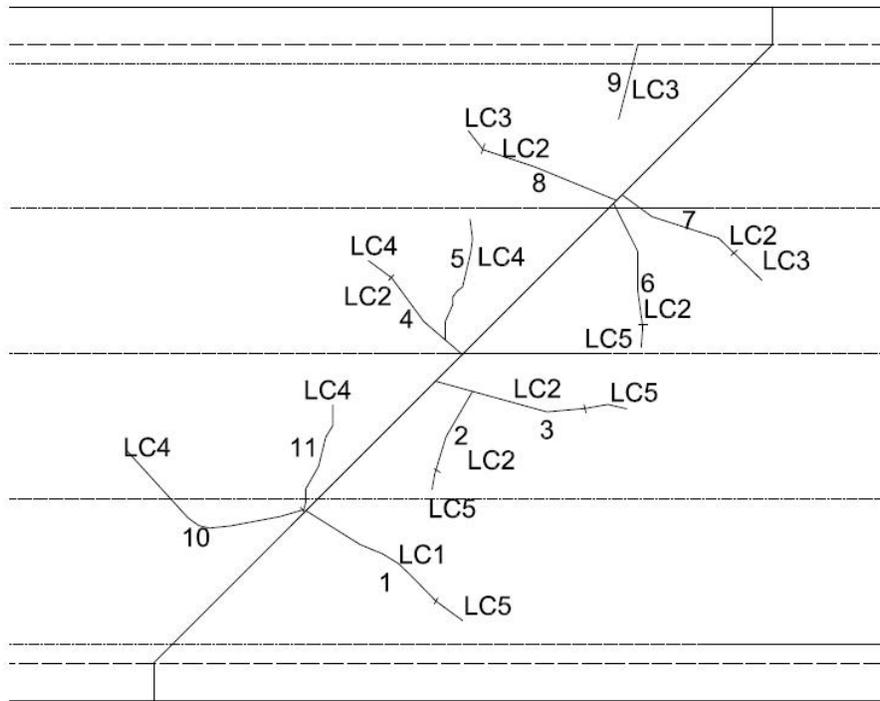
Figure 4- 8 Crack Diagram

Most cracks formed with both trucks centered over a single girder. Attempts were made to measure the crack widths using a crack gauge indicator. However, the cracks were too small to be able to read with the crack width indicator. All cracks closed after the trucks were removed.

Girder deflection readings were taken from the underside of the north span. A Laser Rangefinder was used to measure the initial and loaded height of the girder. Because the road under the second span was open to traffic during tests, girder deflections were only measured in the middle of the first span. Three readings were taken per test. The difference between the initial and loaded heights was averaged to determine the deflection.

As shown in Table 4-1, the deflections of the girders ranged from 1/16 to 1/8-inch for most of the tests. The tolerance of the laser rangefinder is 1/16-inch. Although the deflection readings are not significant enough and too close to the tolerance to accurately determine deflections, the maximum measured deflection of 3/16-inch is approximately 1/7500 of the span length, which is insignificant compared with the defection limitation as 1/800 of the span length required by AASHTO LRFD.

Table 4- 1 Live Load Deflections

Load Case	Girder	Average Deflection
1	2	1/8-inch
2	3	1/16-inch
3	4	1/16-inch
4	2	3/16-inch
	3	1/16-inch
	4	1/16-inch

4.3.2 Bastrop SH71 Bridge

Field load testing of the SH71 Bridge located in Bastrop was conducted on May 12, 2017. The test included five truck configurations using two tandem-axle dump trucks filled with sand provided by TxDOT. Vibration Wire Gages (VWGs) embedded in the "Poor-boy" continuous joint were the primary instrumentation, and girder deflections in the mid-span were also measured during the tests. The layout of VWGs is shown in Figure 4-9. Detailed information about this bridge can be found in the previous section.
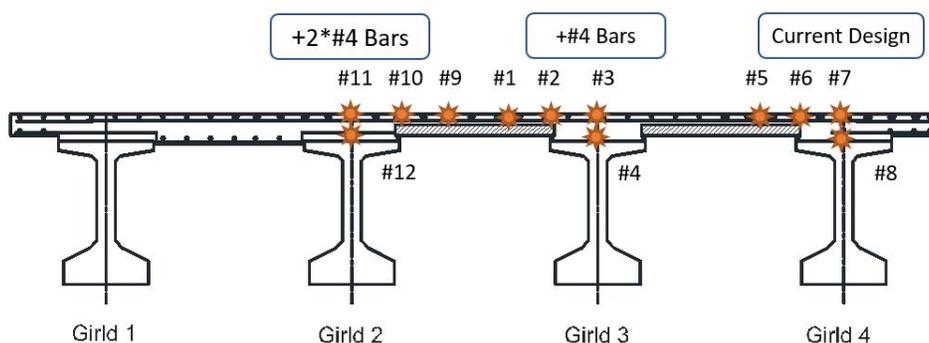
Figure 4- 9 Elevation View of VWG Layout

Field load testing in Bastrop followed the same procedure as in San Marcos using five truck configurations, as shown below in Figure 4-10 (a to e). The first three load cases positioned both trucks over one girder center-line with one truck at mid-span of the girder on either side of the pier, as shown in Figure 4-11 (a). The last two load cases positioned both trucks side-by-side at the mid-span of either span, as shown in Figure 4-11 (b).
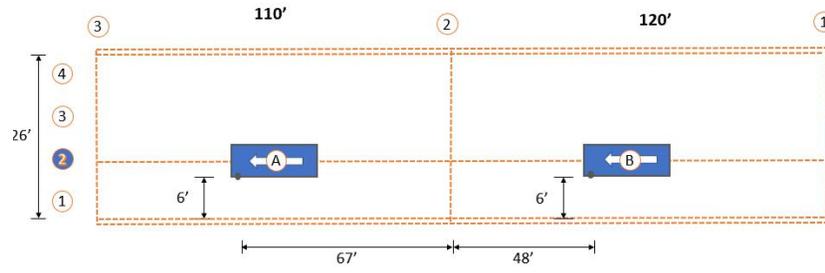
(a) Load Case 1
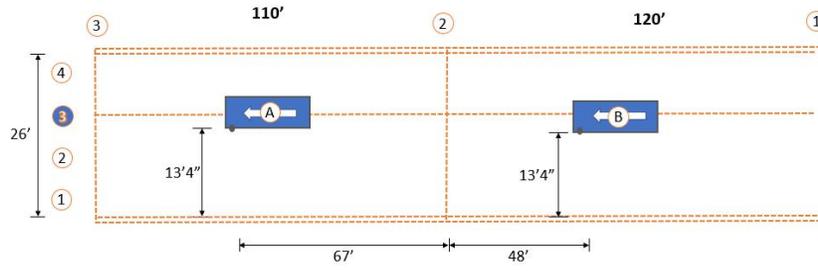
(b) Load Case 2
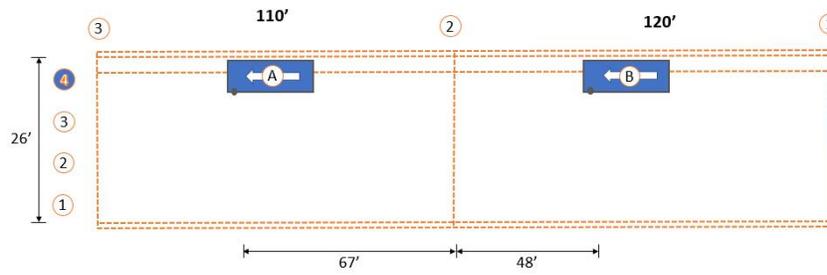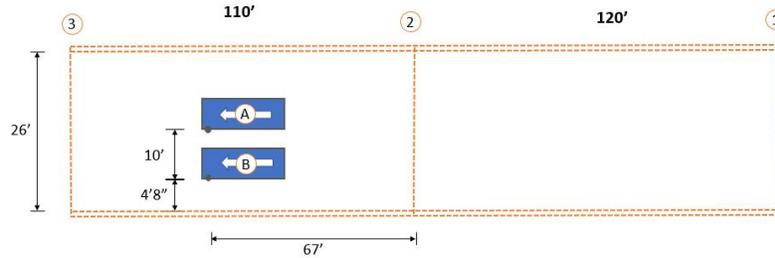
(c) Load Case 3
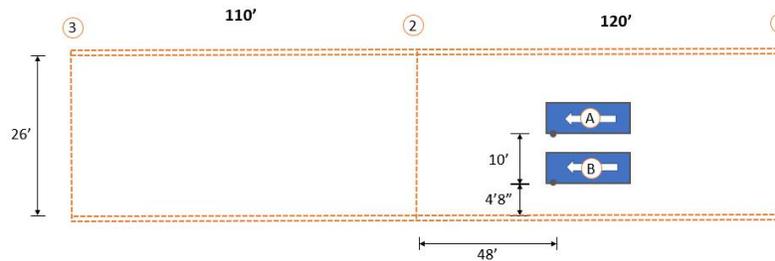
(d) Load Case 4

(e) Load Case 5

Figure 4- 10 Truck Configurations

| (a) Truck on each span | (b) Trucks positioned Side-by-Side |

Figure 4- 11 Photo of Trucks during Load Testing

Similar to the strain measurements at the San Marcos SH123 Bridge, the deck strain measurements during the field load testing of the Bastrop SH71 Bridge were half or less of the deck strains measured in the long-term field monitoring. All the VWGs in the top layer at "Poor-boy" deck joints (#1 to 3, #5 to 7, and #9 to11) are placed across the transverse deck cracks. The values of deck strains from the top layer of VWGs share the same trend, as shown in Figure 4-12. Independent on the reinforcement details, the deck strains from VWGs over girder centerlines (#3, #7, and #11) are larger than those at the overlaps between girder flanges and PCPs (#2, #6, and #10), which are larger than those from VWGs over PCPs ((#1, #5, and #9). This distinct deck strain distribution in the transverse direction shows the influence of a shear-lag effect.

The compression strains measured by the bottom layer VWGs (#4, #8, and #12) indicate larger amounts of bending occurring within the "Poor-boy" deck joint, compared with those measured in the San Marcos SH123 Bridge. These significant compression strains are probably due to the 3/4-inch timber board placed there as a deck cracking former.

65
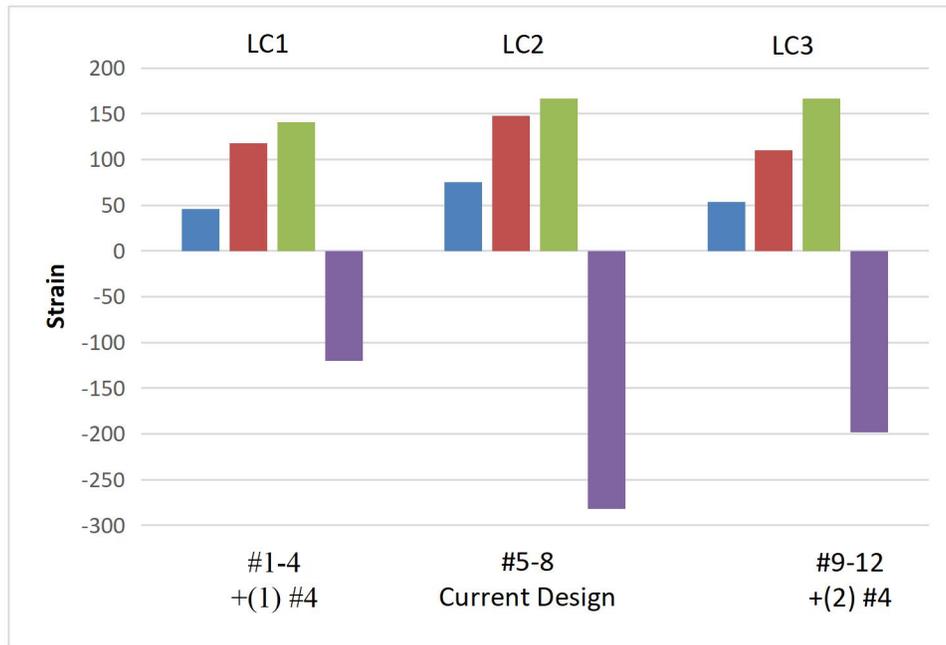
Figure 4- 12 Measured Deck Strains under Load Cases 1 to 3

There is not a consistent trend between the amount of steel at the section and the deck strain measured in the field load testing. The strain measurements from Load Cases 1 to 3 in Figure 4-12 shows the highest to lowest strains are the sections with standard reinforcing (#4 bars spaced at 9-inches), with two additional #4 bars, and with one additional #4 bars respectively. However, the differences in deck strains from deck regions with different longitudinal reinforcement details are insignificant. The average strains from top-layer VWGs from Load Cases 4 and 5 also do not show significant benefits from adding reinforcing steel, as shown in Figure 4-13. Besides, the strain values measured in Load Case 5 are approximately half of those in Load Case 4, which means the deck strains in the "Poor-boy" joints can be more sensitive to one span than the other. The reasons for this phenomenon are unclear.
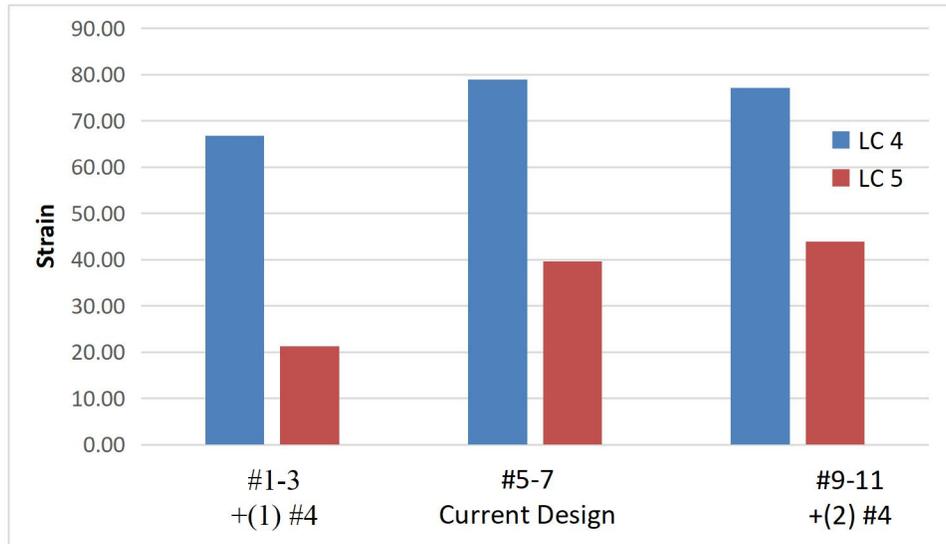
Figure 4- 13 Average Strains in Top Layer VWGs under Load Cases 4 to 5

The surface of the deck in this bridge had already been textured by saw-cut grooves before the load tests, which made the visibility of cracks difficult. However, careful observation identified any cracks in the deck surface before and during the live load tests. A single continuous crack propagated across the centerline of the bent before the tests started. Similar to the San Marcos bridge, the hairline crack was hardly measurable, as shown in Figure 4-14. This line was traced to highlight the crack. No additional crack were observed during load testing.
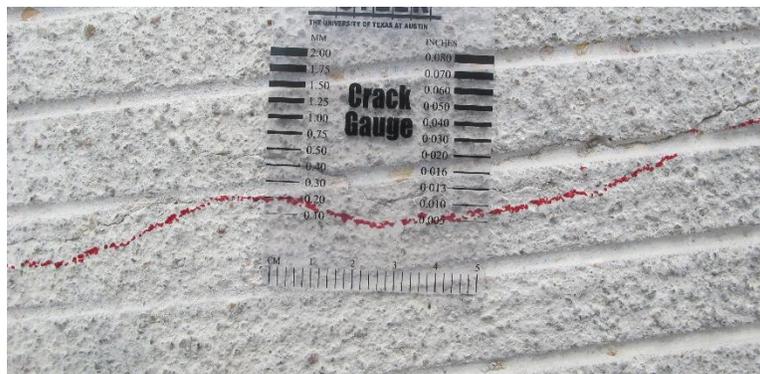
Figure 4- 14 Deck Surface Crack in Bastrop Bridge

Table 4-2 shows the average deflections from the tests. The maximum measured girder deflection is 1/4-inch, which is approximately 1/5000 of the bridge span length and insignificant compared with the deflection limitation as 1/800 of span length required by AASHTO LRFD.

Table 4- 2 Live Load Deflections

Load Case	Girder	Average Deflection
1	2	3/16-inch
2	3	3/16-inch
3	4	1/4-inch
4	2	1/4-inch
	3	3/16-inch
	4	3/16-inch

4.3.3 Summary

For these two "Poor-boy" continuous bridges, the measured deck strains under field load testing were much smaller than those measured due to shrinkage effects. From the measured data of the field load tests, increasing the reinforcement ratio did not show a direct correlation to the reduction in concrete strains. The deck behavior varies due to the different types of crack formation in the "Poor boy" joints. In addition, the effects of shear-lag on the deck strain distribution were also apparent from the strain measurements.

4.4 FIELD LOAD TESTING OF CONTINUOUS BRIDGES

4.4.1 Overview

The field load testing on two spliced concrete continuous bridges was conducted on the night of August 16th, 2018, one week before the bridges were open to traffic. Similar to the field instrumentation, the bridge decks over four interior supports were the primary test regions for field load testing. Four fully loaded dump trucks were provided by TxDOT for the testing, as shown in Figure 4-15. Five loading configurations were tested with trucks positioned at different locations.
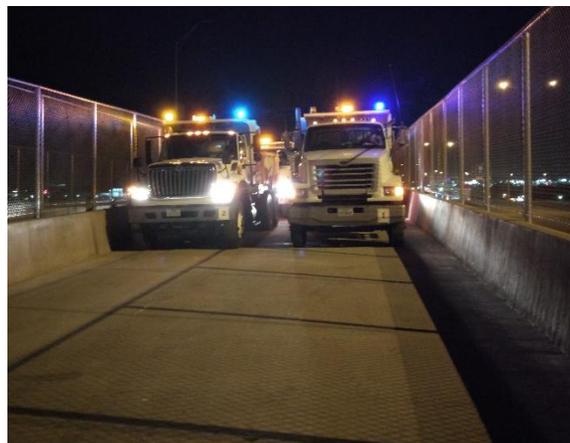
Figure 4- 15 Trucks Positioned During the Load Test

Sensors used for the field load testing included VWGs embedded in the deck, foil strain gages attached to the reinforcing steel surface, crack width gages (Pi-gages) installed on the deck surface, and laser rangefinders positioned under the middle of the middle-span and the side-span of each bridge. Because crack width gages can only measure the changes in deck surface crack

widths but not the absolute value of the existing crack widths, deck surface crack widths mentioned in this report are the crack openings under each load case, but not the total crack widths including deck shrinkage effects. Overall, deck strains, reinforcing bar stresses, surface crack openings, and girder deflections were recorded under each load case.

4.4.2 General Information on Round Rock Bridges

These two identical continuous bridges were a part of the overpass Ramp 20 and Ramp 21 of IH35 across McNeil Road, at the south of Round Rock, TX. Each bridge consisted of four beamlines of three-span continuous girders with spans of 180 ft., 250 ft., 180 ft. Each beamline was spliced by five pieces of precast, prestressed concrete segment, as shown in Figures 4-16 and 4-17, including two end girders, two haunched girders, and one drop-in girder. The depth of end girders and drop-in girders were 80 inches, and that of haunched girders varied from 80 inches at spliced joints to 130 inches over interior supports. The spacing between each beamline was 80 inches. Three tendons were post-tensioned when four bridge lines were connected by eight cast-in-place concrete diaphragms at bridge ends, over interior supports, and at splice-locations.

(a) Aerial view from "Google Maps"   (b) Elevation view of drop-in girder

Figure 4- 16 Global Views of Round Rock Bridges

The bridge deck contained 4-inch deep prestressed precast concrete panels (PCPs) as the bottom layer and 4.5-inch depth cast-in-place concrete as the top layer. The original reinforcement design for the deck is #5 bars spaced at 9" over the positive moment region and #6 bars spaced at 4.5" over the negative moment region in the longitudinal direction, with #5 bars spaced at 9" transverse steel on top. For research purposes, after communicating with the engineer of record, TxDOT engineers, and the contractor, changes were made in the deck reinforcing details in the negative moment region. The four different longitudinal reinforcement details consisted of, #6 bars spaced at 4.5" (2.2%, as original design) over south interior support of Ramp 21, #6 bars spaced at 9" (1.1%) over north interior support of Ramp 21, #5 spaced at 6" (1.1%) over north interior support of Ramp 20, and #5 bars spaced at 9" (0.8%) over south interior support of Ramp 20, respectively. The reinforcement ratios listed here were based upon the reinforcing bar area divided by the cast-in-place concrete area.
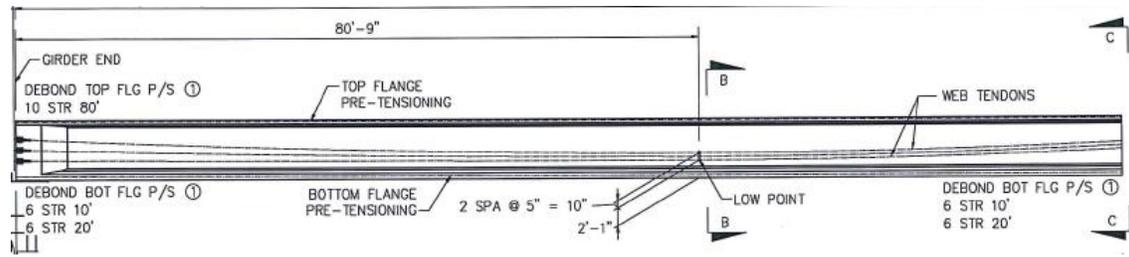
(a) End girder
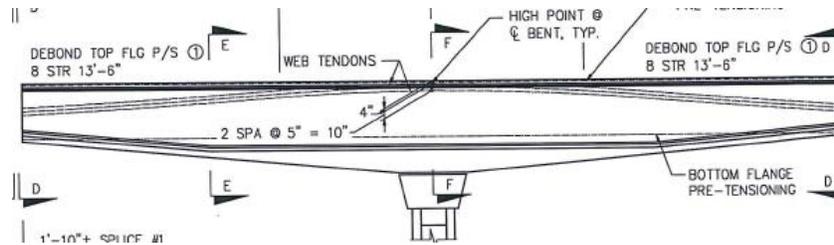
(b) Haunched girder
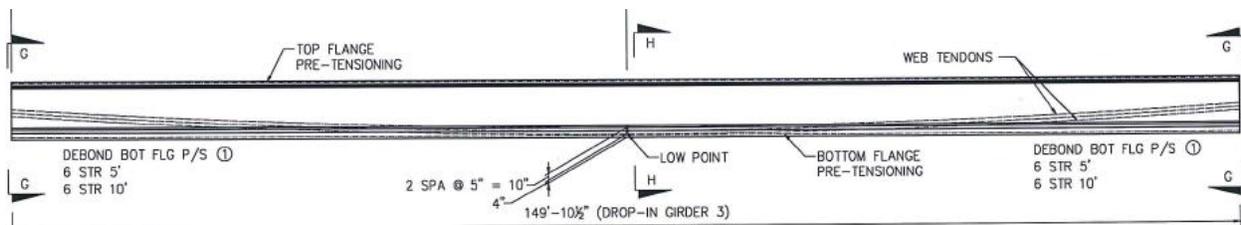
(c) Drop-in girder

Figure 4- 17 Round Rock Beamlines Elevation View Drawing (TxDOT)

4.4.3 Loading Configurations

Five loading configurations were used on each bridge. Because there are four critical deck regions over the south and north interior supports, trucks positioned at one specific location may cause different effects on each deck region. For example, when four trucks are positioned on the south side-span, the negative bending moment would be generated in the bridge section over the south interior support but the positive bending moment would be generated over the north interior support. To simplify load testing procedures, trucks only moved forward from south to north during the tests. The measured data were then rearranged in post-processing to make sure the instrumented deck regions were under the same loading conditions in each load case. The sequence of load cases described below does not reflect the actual testing sequence used in the field, but the sequence in the data analysis.

(a) Load Case 1

(b) Load Case 2

(c) Load Case 3

(d) Load Case 4
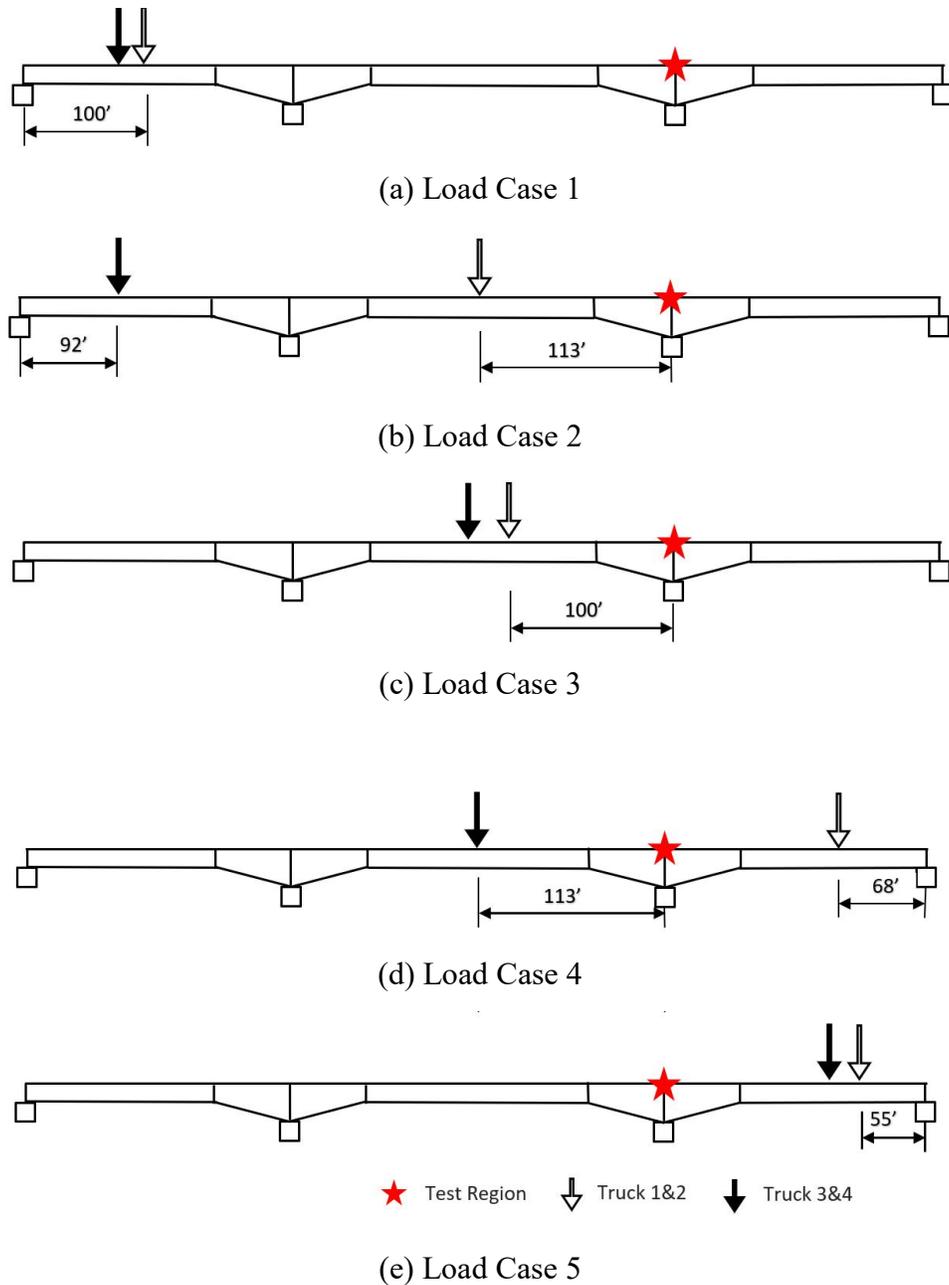
(e) Load Case 5

Figure 4- 18 Truck Locations for the Round Rock Bridges Load Test

The locations of loading trucks in each load case are shown in Figures 4-18. The red star shows the location of the instrumented deck regions with different reinforcement details. Each arrow represents two dump trucks, at the location of the truck front axle. Load Case 1 consisted of four trucks all positioned at one side-span away from the instrumented deck region. Load Case 2 consisted of two trucks remaining at the previous side-span and the other two positioned at the middle of mid-span. Load Case 3 consisted of four trucks all positioned at mid-span. Load Case 4 consisted of two trucks remaining at mid-span and the other two positioned at the side-span near the test region. Finally, Load Case 5 consisted of four trucks all positioned at the side-span

near the test region. Under each load case, two trucks were positioned side-by-side, with tires over the beamlines.
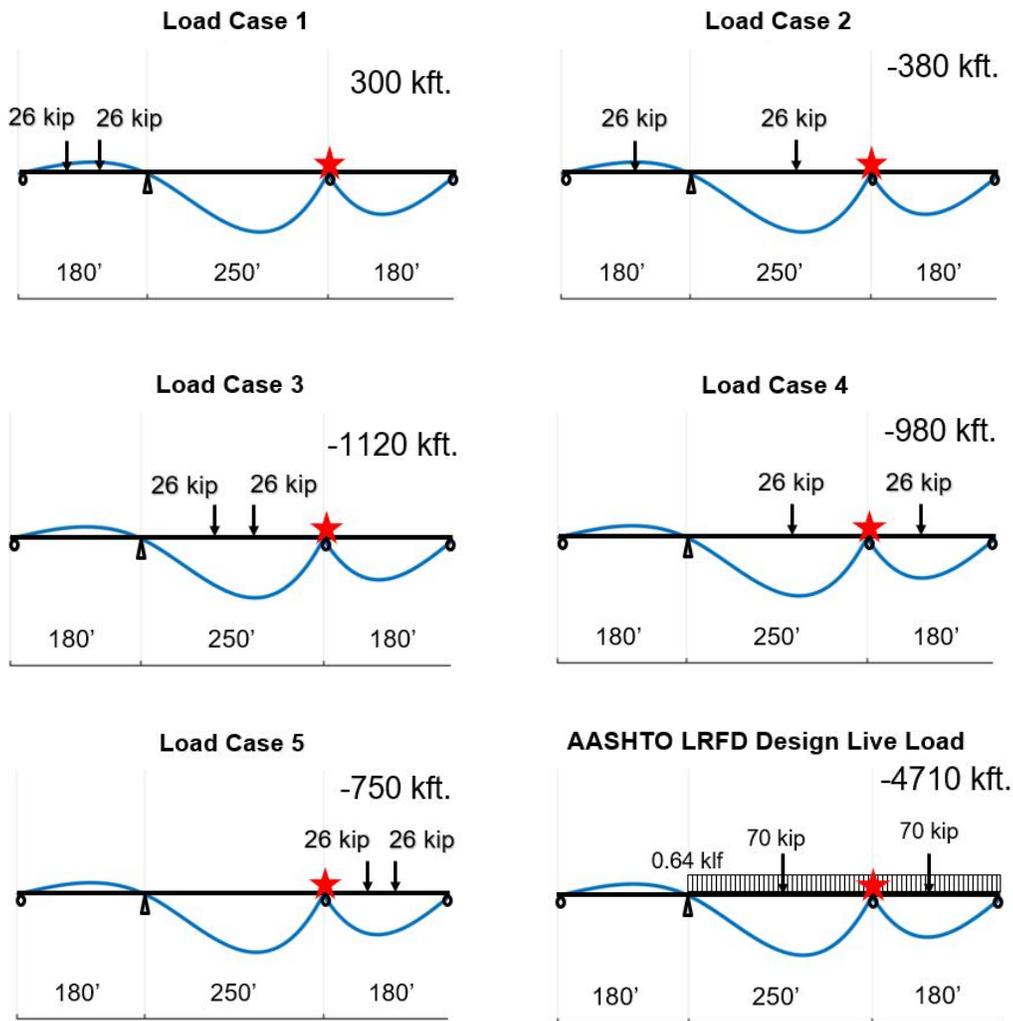
Figure 4- 19 Bending Moment Influence Lines for Each Load Case and
for the AASHTO design live load

As shown in Figure 4-19, the blue line is the influence line of the bending moment in the tested section marked by the red star. The black arrows represent the truck loading on each beamline. Because trucks were positioned with tires over each beamline, the transverse distribution factor is 0.5 and truck loading on each beamline was 26-kips. The bridge sections of the instrumented deck regions are under positive bending moment in Load Case 1, but under negative bending moment in the other four load cases. The critical negative moment for the test region is -1120-Kft. under Load Case 3, with four trucks all at the middle of mid-span, slightly worse than Load Case 4. However, according to AASHTO LRFD, the critical negative moment caused by HL-93 live load effects is 4710-Kft. Therefore, the negative bending moment on the test section in the field load testing was approximately 25% of the bending moment caused by the design live load. However, four fully loaded dump trucks on the bridge simultaneously is nonetheless a severe loading condition.

72

4.4.4 Girder Deflections

Girder deflection readings were taken from the underside of the mid-span and the north side-span of both Ramp 20 and Ramp 21. Two Laser Rangefinders placed on tripods were used to measure distances between the girder bottom surfaces and the ground in the loaded and unloaded conditions, as shown in Figure 4-20. Three readings were taken per test. The difference between the unloaded and loaded distances was averaged to determine the deflection. Because of railroad tracks under the center of mid-span, measurements were taken 10 feet south from the middle. Based on the calculation result of the finite element model, the deflections of south side-span were taken at 80 feet south from the interior support.

(a) mid-span   (b) side-span
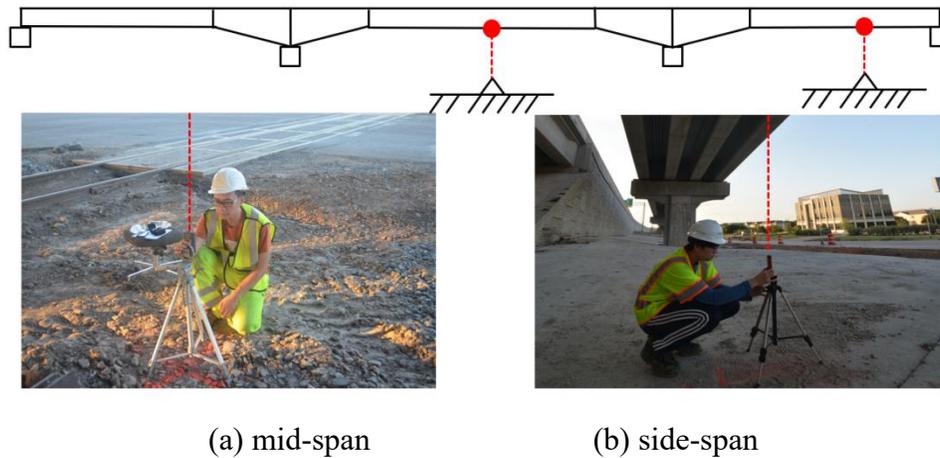
Figure 4- 20 Measuring Deflections under Girders

As shown in Figure 4-21, the deflections of Ramp 20 and Ramp 21 are similar to each other under each load case. The measurement tolerance of the laser rangefinder is 1/24-inch, as depicted in the error bars. The maximum deflections of the mid-span ranged from 0.6 to 0.7 inch, when four dump trucks were located in the middle of mid-span. The maximum deflection of the side-span was 0.43-inch when four loaded dump trucks were located on the side-span.
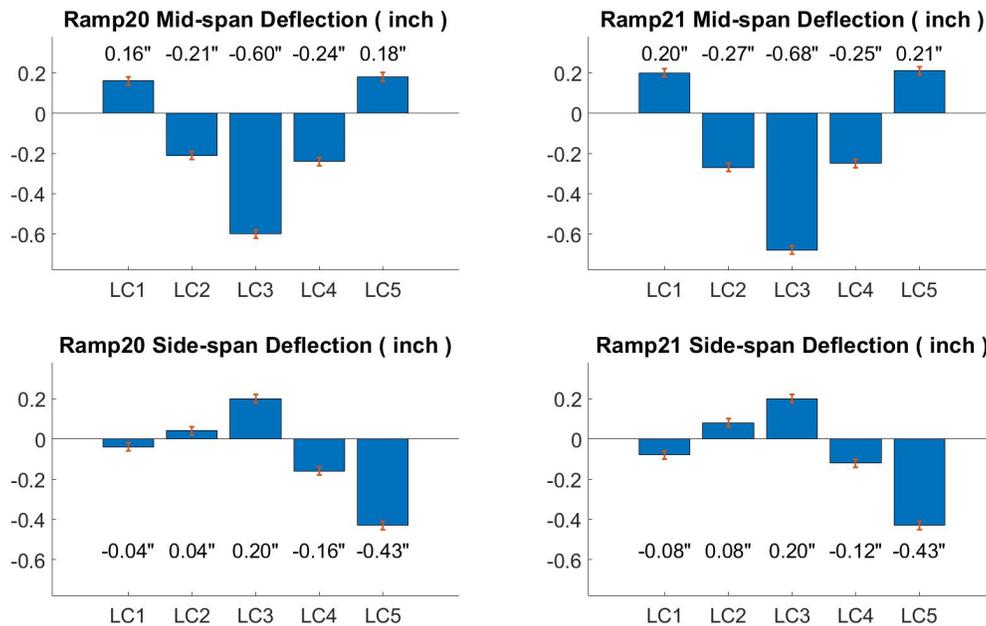
Figure 4- 21 Girder Deflection during the Load Test

4.4.5 Deck Surface Cracking

Surface crack width gages (PI-gages) were used to measure bridge deck crack opening displacements during the field loa tests. The PI-gage is a strain-based sensor attached to an arch-shaped spring plate, as shown in Figure 4-22.
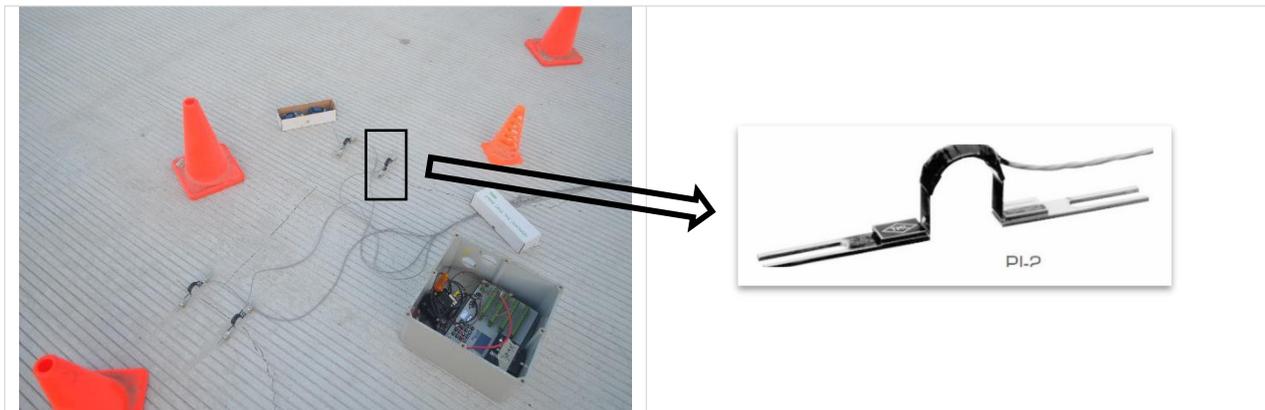
Figure 4- 22 PI-Gages on the Deck Surface

Prior to conducting the field load tests, there were two visible deck surface cracks over each interior bent, likely due to concrete shrinkage. Two PI-gages were installed over each transverse deck crack and data recorded by one Campbell Scientific datalogger every 20 seconds. In total, eight PI-gages were used on each continuous bridge to measure the crack widths during the field load tests. The PI-gages measured the change in crack opening during the field load tests.

74

In each deck region with different reinforcement details, the four PI-gages showed similar reading for all five load cases. Therefore, the maximum absolute value readings from those four PI-gages are shown in Figure 4-23. For all four longitudinal reinforcement details in the bridge deck in the negative moment regions, the crack opening widths during the live load testing were very small, around 10% to 20% of the crack opening widths caused by concrete volume shrinkage measured before the field load test. The maximum crack opening was less than 1/1000-inch, which occurred in the region with #5 bars spaced at 9-inch reinforcing. For each load case, the crack opening at the #6 bars spaced at 9-inches (1.1%) deck region was quite close to that of #5 bars spaced at 9-inches (0.8%) region, and around twice as crack opening widths measures at the #6 bars spaced at 4.5-inches (2.2%) and #5 bars spaced at 6-inches (1.1%) regions. Furthermore, due to the positive bending moment caused by Load Case 1, the tested deck regions were under compression. Therefore, PI-gages recorded negative crack opening readings, which meant deck cracks closed slightly under compression.
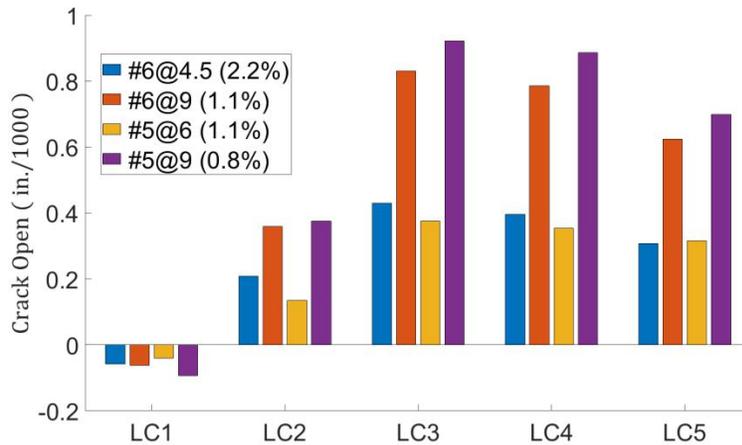
Figure 4- 23 Concrete Deck Crack Opening During the Load Test

Because the field load tests were conducted at night, it was too dark to observe deck surface cracking during the tests. The research team returned to the bridges the next morning but did not observe any significant changes in deck cracking at critical deck regions over interior supports, compared to what was observed prior to the field load tests, After the field load tests, the deck crack widths remained at approximately 0.006 to 0.008-inch, similar to the crack widths before the load tests.

4.4.6 Deck Strain and Reinforcing Bar Stress

Vibration Wire Gages (VWGs) embedded in the deck concrete and foil strain gages installed on longitudinal reinforcing steel surfaces were utilized to evaluate the concrete strains and reinforcing bar stresses during the field load tests. There were 15 VWGs and 27 foil strain gages installed in each test region. Detailed information about the field instrumentation can be found in the previous section.

The concrete strains obtained by the 15 total VWGs embedded in each region and a spline interpolation function were utilized to estimate concrete strains between the measured points. A similar method was utilized to obtain reinforcing bar stress distributions. Using LC 3 as

an example, the distribution of concrete tension strains and reinforcing bar stresses in four regions with different reinforcing details are shown in Figure 4-24. Generally, the locations of maximum concrete strains matched well with the locations of maximum reinforcing bar stresses. Furthermore, compared with those distributions measured from long-term field monitoring, as reported in the previous section, no new deck cracking caused by the field load test was measured by sensors embedded in these critical deck regions.
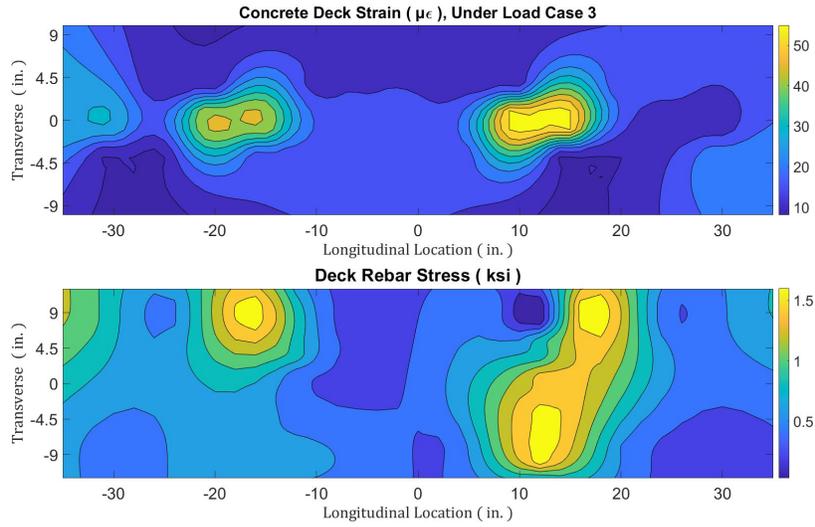
(a) #6 bars spaced at 4.5-inches (2.2%)
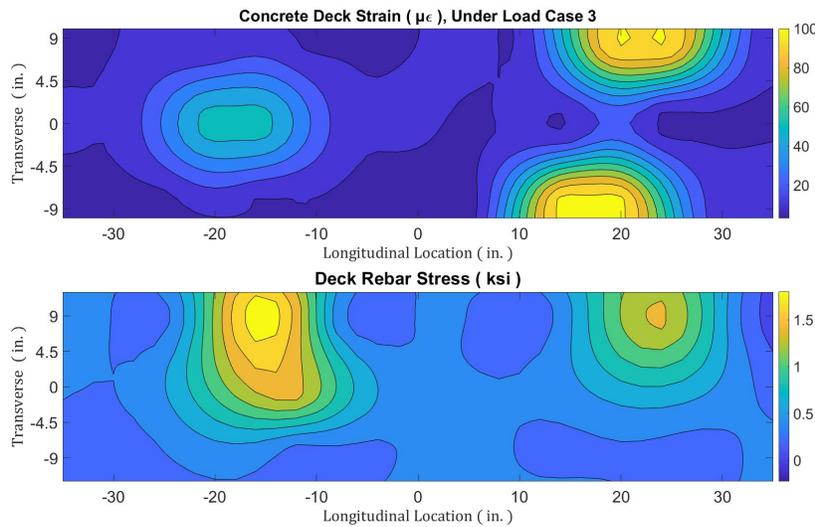
(b) #6 bars spaced at 9-inches (1.1%)
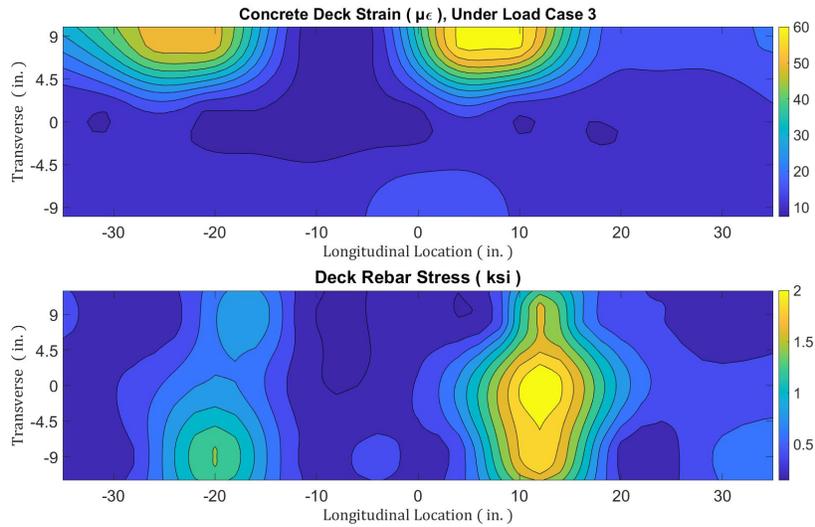
(c) #5 bars spaced at 6-inches (1.1%)
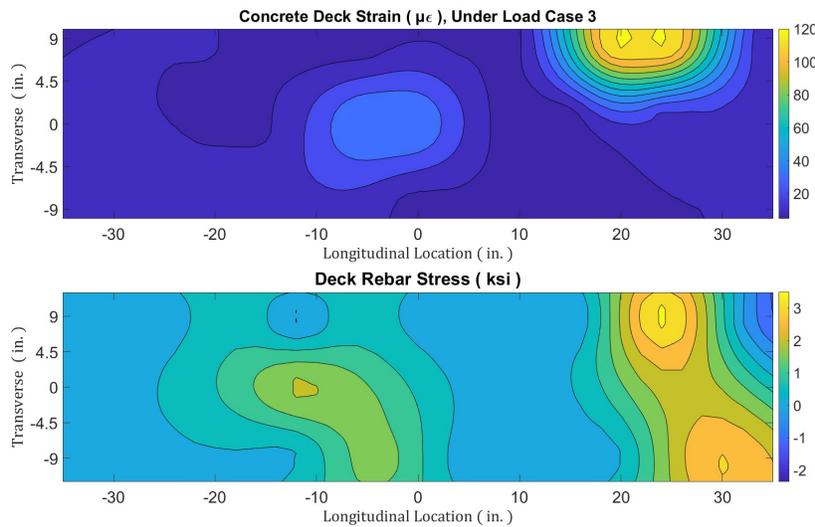
(d) #5 bars spaced at 9-inches (0.8%)

Figure 4- 24 Spatial Distribution of Concrete Strain and Reinforcing Bar Stress under Load Case 3

The average and maximum concrete strains obtained from each region with different reinforcing details are shown in Figure 4-25. For each load case, the average concrete strains from different deck regions are closed to each other and no larger than 30 $\mu\varepsilon$. Therefore, the average concrete strain under the live load was insensitive to reinforcing details. However, the maximum measured concrete strains from different deck regions were quite different. The values of concrete strain from deck regions with #6 bars spaced at 9-inches (1.1%) and #5 bars spaced at 9-inches (0.8%) reinforcing steel are approximately twice as those from deck regions with #6

bars spaced at 4.5-inches (2.2%) and #5 bars spaced at 6-inches (1.1%). Increasing the amount of steel and reducing the spacing between longitudinal reinforcing bars showed benefits in reducing maximum deck strains under truck loading.

(a) Average concrete strain   (b) Maximum concrete strain
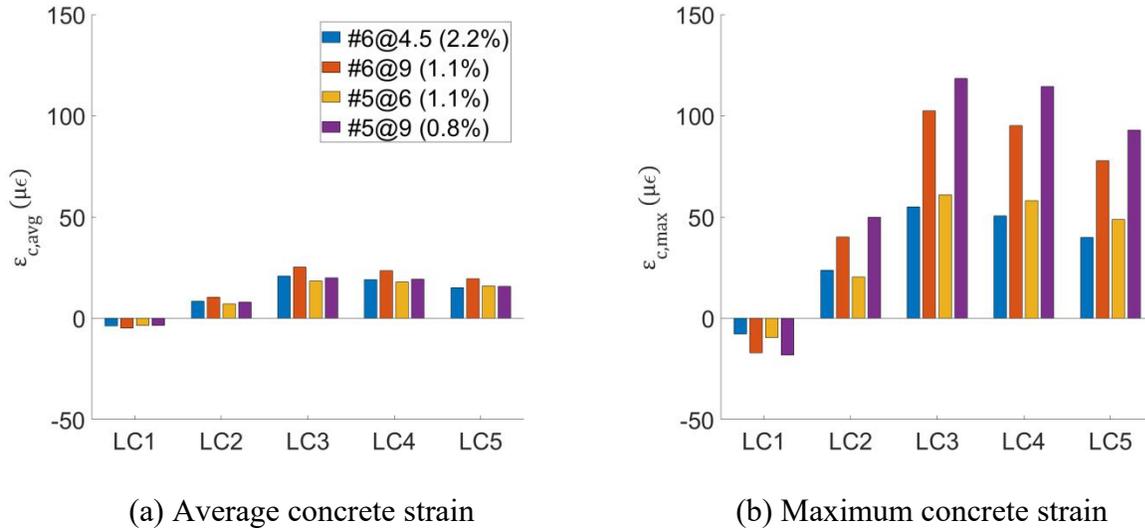
Figure 4- 25 Measured Concrete Strains for Each Load Case

Similarly, the average and maximum stresses in the longitudinal reinforcing steel obtained from each region are shown in Figure 4-26. For each load case, the average reinforcing bar stresses from the different deck regions are very similar and no larger than 1 ksi. Therefore, the average stress in the reinforcing steel under live load was insensitive to reinforcing details. However, the maximum reinforcing bar stresses from different deck regions showed significant differences. The values of maximum reinforcing bar stress from deck regions with #5 bars spaced at 9-inches (0.8%) reinforcing steel were up to 4.0-ksi. The maximum reinforcing bar stresses were approximately 2.0-ksi in the deck regions with #6 bars spaced at 4.5-inches (2.2%), #6 bars spaced at 9-inches (1.1%), and #5 bars spaced at 6-inches (1.1%).

(a) Average stress in reinforcing steel   (b) Maximum stress in reinforcing steel
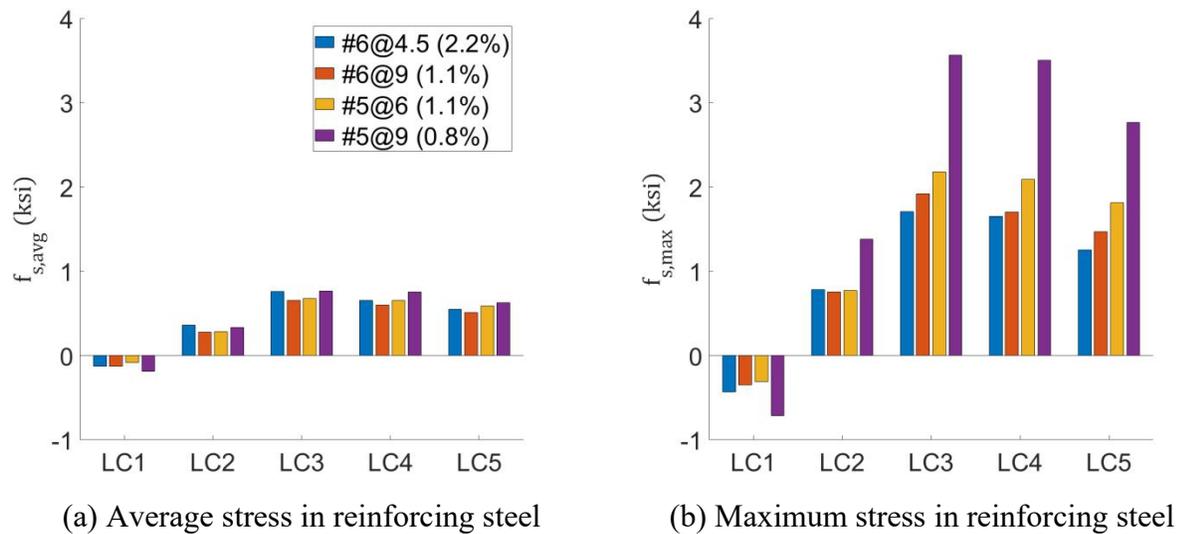
Figure 4- 26 Measured Reinforcing Bar Stress for Each Load Case

4.4.7 Discussion on Crack Width, Concrete Strain, and Reinforcing Bar Stress

The measured deck surface crack opening widths as shown in Figure 4-25 and the maximum concrete strains as shown in Figure 4-26 show similar trends in each deck region with different reinforcing details. The relationship between the measured surface crack widths and the measured maximum concrete strains is shown in Figure 4-27. This shows a very linear relationship that is independent of reinforcing details.
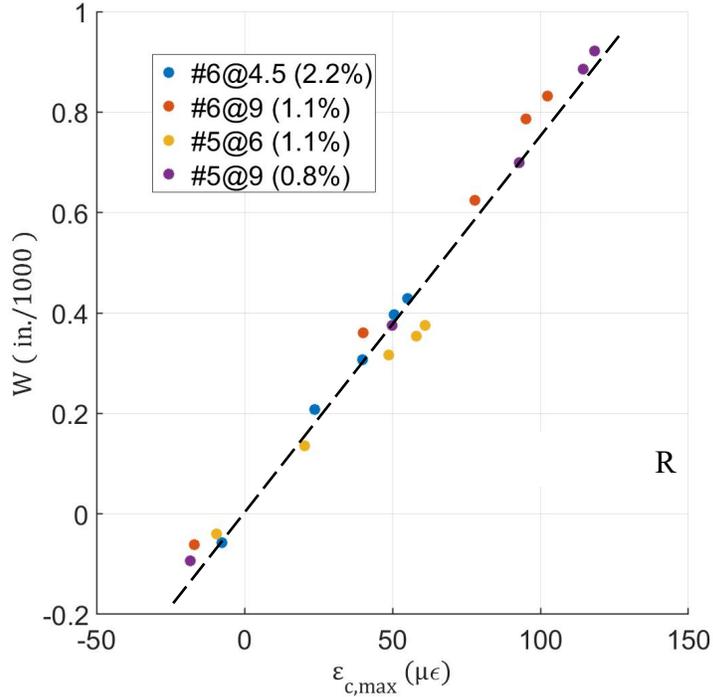
Figure 4- 27 Relationship Between Surface Crack Widths and Maximum Concrete Strains

This relationship can be expressed as below:

$$W = 1.3 \times l_{vwg} \times \varepsilon_c$$

where:

W = surface crack width (inch)

l_{vwg} = length of vibration wire gage, which is 6-inches in this case

ε_c = concrete strain measured by VWG across a crack

This linear relationship also indicates that the value of concrete strains measured by VWGs embedded in the concrete deck at the location of a crack during long-term field monitoring can also be used to estimate crack widths.

The relationship between surface crack widths and maximum reinforcing bar stress was also examined. As shown in Figure 4-28, a linear relationship is evident, but the slope depends on the arrangement of longitudinal reinforcing steel. The #6 bars spaced at 9-inches (1.1%) reinforcement shows the largest slope, followed by #6 bars spaced at 4.5-inches (2.2%) and #5

bars spaced at 9-inches (0.8%). The #5 bars spaced at 6-inches (1.1%) reinforcing steel shows the smallest slope. The trend for the value of slope correlatives neither with the reinforcement ratio nor the spacing between reinforcing bars. The reason for this lack of correlation is unclear.
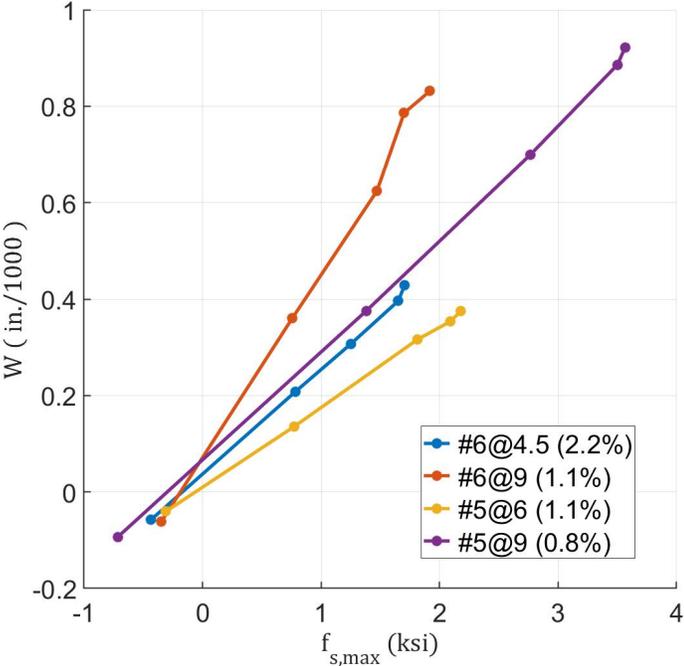
Figure 4- 28 Relationship Between Surface Crack Widths and Maximum Reinforcing Bar Stresses

4.5 Summary

Field static load tests were conducted on four bridges. Two of the bridges had simply supported spans with "Poor-boy" continuous decks, and the other two were spliced concrete continuous bridges. Although no direct correlation between increasing reinforcing steel and reduction in deck strain was observed in the "Poor boy" deck joints, the research team gained valuable experience from those two field load tests.

On the two spliced concrete continuous bridges, the concrete strains, longitudinal reinforcing bar stresses, and deck surface crack widths were examined for bridge deck regions with different reinforcement details. The maximum crack opening widths measured during the field load tests were under 0.001 inch, and no new cracking was observed during the load tests. The maximum reinforcing bar stress measured was less than 4 ksi. The following observations can be made for the concrete deck in the negative moment region of spliced concrete bridges :

- Deck strains, stresses in longitudinal reinforcing steel, and deck surface crack widths under controlled live loading were insignificant compared with those due to concrete shrinkage effects.
- Increasing the area of longitudinal reinforcing steel and decreasing bar spacing showed some benefits in reducing deck strains.
- Deck surface crack width is proportional to concrete strain measured by VWG crossing cracks, independent of reinforcement details.
- Similar trends could also be observed between reinforcing bar stresses and crack widths, but the slopes from various reinforcement details differed.

Chapter 5. Large Scale Laboratory Testing

5.1 Overview

As noted in the previous chapter, the data from the field tests were extremely unique and provided clear insight into the cracking behavior of the concrete bridge decks during construction and in service. However, throughout the instrumentation period, the bridges were subjected to a complex range of strains from numerous sources, including concrete shrinkage, temperature changing, and construction loading. The research team desired to gain additional data on the cracking behavior of the deck under controlled settings. Therefore, carrying out large-scale testing in a laboratory setting was desirable. Laboratory tests allowed the team to gain data in a controlled environment and to obtain clear cracking behavior under known loads.

The purpose of these negative moment bending tests was to investigate the impact of the longitudinal reinforcing details on deck cracking control in the negative moment regions of continuous supported composite girders. This chapter provides details on the configuration of the test setup, the description of the three specimens, testing procedure and results of the negative moment tests.

5.2 Description of Specimens

The research team was able to combine efforts with TxDOT study 0-6862 (Improved Tub Girder Details) that included tests of a 2 span girder. Therefore the team provided instrumentation in the concrete deck in the negative moment region. Tests were carried out on three steel tub girders that were designed to be fully composite with the 6.5-inch Cast-In-Place concrete deck. Each composite tub girder was tested as a two-span continuous bridge with a 28-foot span and a 56-foot span, as shown in Figure 5-1. These three composite tub girders share similar configurations and materials in the cross-section but have different longitudinal deck reinforcing details in the negative moment regions. The steel flanges and webs of the three specimens were fabricated with AASHTO M270 (ASTM A709), grade 50W. The nominal design compressive strength for the concrete was 4 ksi. Reinforcing bars with a nominal yield stress of 60 ksi were used in the concrete deck. A description of the design of the specimens is provided in subsequent subsections.
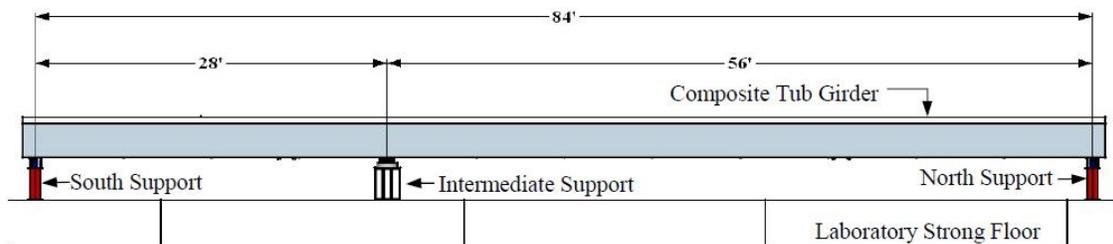
Figure 5- 1 Continuous Girder Configuration

5.2.1 Composite Tub Girder 1 (Tub 1)

As shown in Figure 5-2, the steel tub girder of the first specimen is 3-foot deep, with the distance of the top of the two sloping webs as 5.3-foot. The sloping ratio of webs is 4.27:1. The

width of each top flange is 12-inch, and the width of the bottom flange is 4-foot. The thickness of the flanges and webs is equal to 7/16-inch. A solid steel plate diaphragm was added to the tub girders at the location of the intermediate support to stiffen the bottom flange to withstand the reaction forces at the interior support.
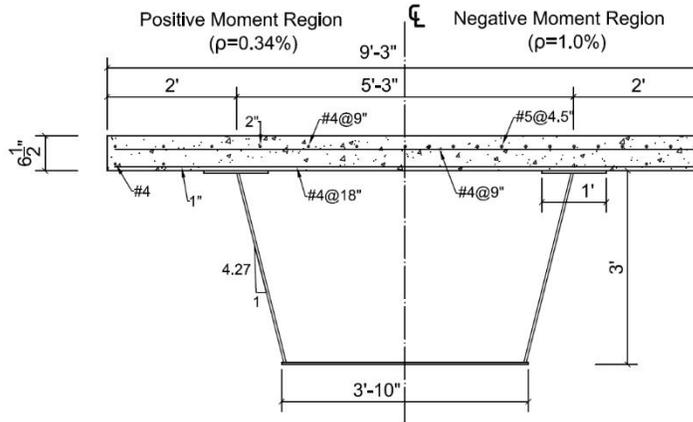
Figure 5- 2 Cross-section of Composite Tub Girder 1

The geometry of the concrete deck was 111-inch wide and 6.5-inch thick along the entire length of the girders. Reinforcement was provided in two layers for the concrete deck. The bottom mat included #4 bars at a spacing of 18-inch in the transverse direction and two #4 bars spaced at 9-inches longitudinally within each overhang only. The top mat included #4 bar spaced at 9-inches in the transverse and longitudinal directions   For the deck region in the negative bending moment the longitudinal reinforcement in the top mat was increased to #5 bars spaced at 4.5-inch, which resulted in an area of 1.0% of the total area of the concrete deck. The negative moment reinforcing was provided in the region 10 feet on either side (20 ft. total) of the interior support. The plan view of the deck reinforcing steel in Tub 1 is shown in Figure 5-3.
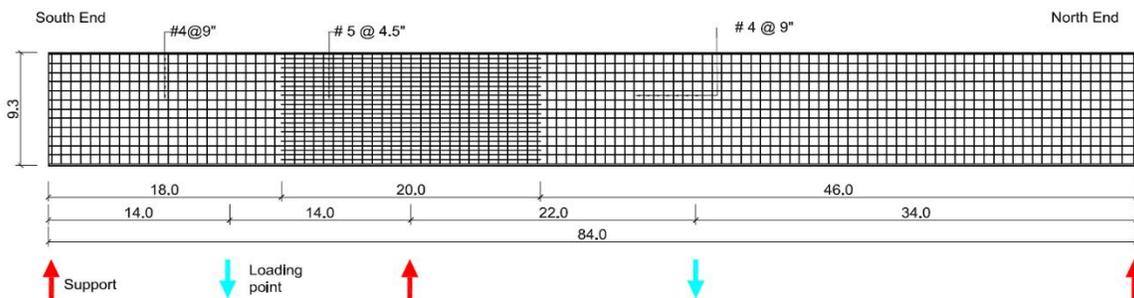
Figure 5- 3 Deck Reinforcing Steel Layout in Tub 1

The solid diaphragm of Tub #1 was fabricated from a W30x90 wide flange section. Four half-inch thick vertical stiffeners were added on both sides of the diaphragm to withstand the reaction force from the mediate support. Additionally, the bottom flange of Tub 1 was reinforced with a longitudinal stiffener consisting of a 7-foot long L5x5x1/2 on each side of the solid diaphragm, as depicted in Figure 5-4.
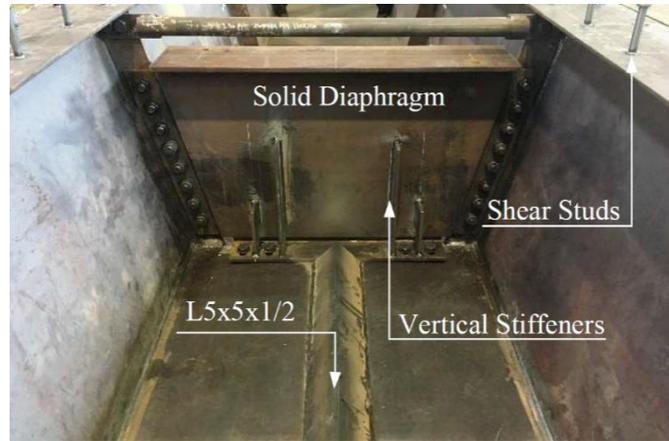
Figure 5- 4 Solid Diaphragm and Bottom Flange Reinforcement in Tub 1
(Photography Taken by Stalin Armijos)

5.2.2 Composite Tub Girder 2 (Tub 2)

As shown in Figure 5-5, the difference in the cross-section of the steel girders between the second and first specimens is the location of the top flanges. In the second specimen, the web and bottom flange of Tub 2 were the same as those of Tub 1. The top flanges were offset inward to the web. The width of the top flange was increased to 13-inch, instead of 12-inch. The thickness of the bottom flange and webs were equal to 7/16-inch, while the thickness of the top flange was equal to 9/16-inch.
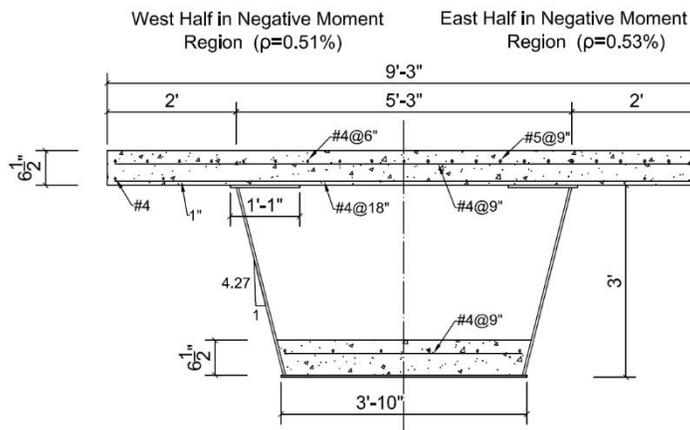
Figure 5- 5 Cross-section of Composite Tub Girder 2

The geometry of the reinforced concrete deck in the second specimen was also similar to specimen 1. However the longitudinal reinforcing steel in the negative moment region was different. The reinforcement in this region differed on the east and west sides. On the east side, #5 bar spaced at 9-inch (0.53%) was utilized, while on the west side, #4 bars spaced at 6-inch (0.51%) was utilized, as shown in Figure 5-5 and Figure 5-6.

84
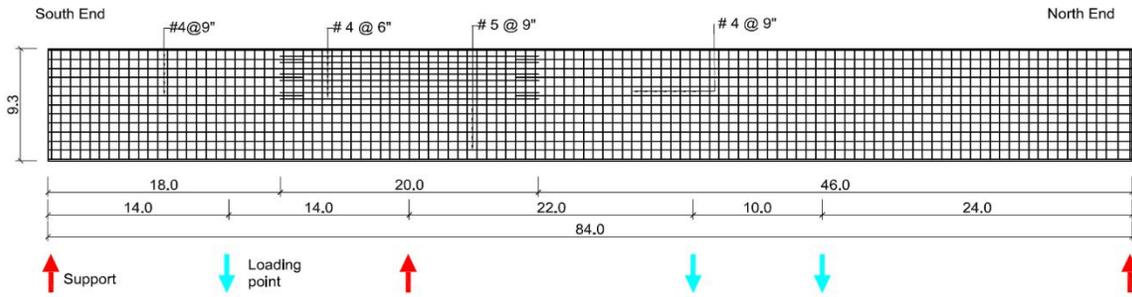
Figure 5- 6 Deck Reinforcing Steel Layout in Tub 2

The solid diaphragm of Tub #2 was fabricated from a W24x250 wide flange section, as shown in Figure 5-7. Three half-inch thick full vertical stiffeners are added on each side of the diaphragm. To avoid local buckling, the bottom flange of Tub #2 was reinforced by a 14-foot long, 6.5-inch thick concrete slab symmetric to the intermediate support. Shear studs were welded to the bottom flange to provide fully composite action between the bottom flange and the concrete slab. The reinforcement steel in the concrete deck consisted of #4 bar spaced at 9-inches in both directions.
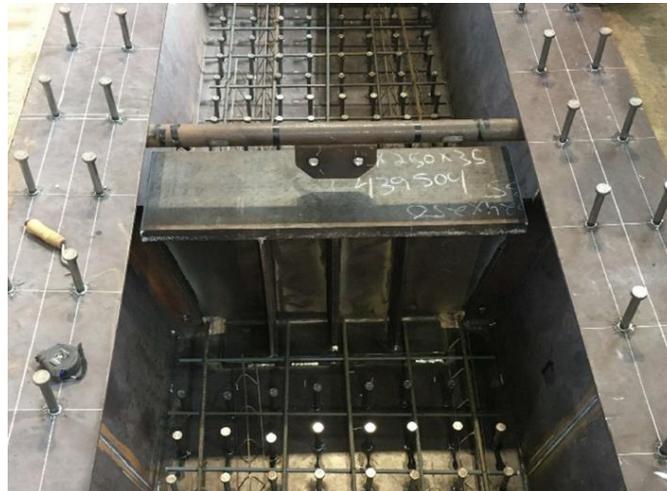
Figure 5- 7 Solid Diaphragm and Bottom Flange Reinforcement (Before Casting) in Tub 2
(Photography taken by Stalin Armijos)

5.2.3 Composite Tub Girder 3 (Tub 3)

The difference in the cross-section between the third and first specimen is the slope of the web. As shown in Figure -8, the slope ratio of the third specimen is 2.6:1, instead of 4.27:1 in the previous specimens. The distance between the upper of webs was the same as the first two specimens, which was 5.3-ft. With the decrease in web slope, the width of the bottom flange was reduced from 4-feet to approximately 3-ft. The thickness of the flanges and webs was equal to 7/16-inch.

85
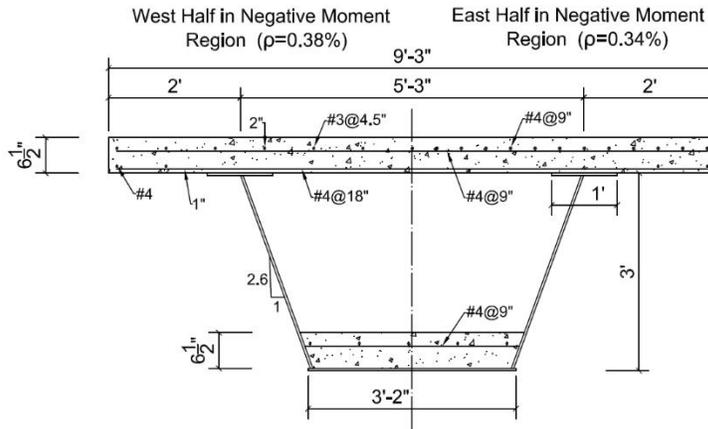
Figure 5- 8 Cross-section of Composite Tub Girder 2

In Tub 3, the longitudinal deck reinforcement in the negative moment region was reduced relative to the first two specimens to obtain the influence of reinforcement area on deck cracking. As shown in Figure 5-9, the reinforcement in this region varied between the east and the west sides of the girder. On the east side, #4 bar were spaced at 9-inch (0.36%), while on the west side, #3 bar were spaced at 4.5-inch (0.36%) is utilized in the west side. All other reinforcing steel in the other region were the same as the previous two specimens.
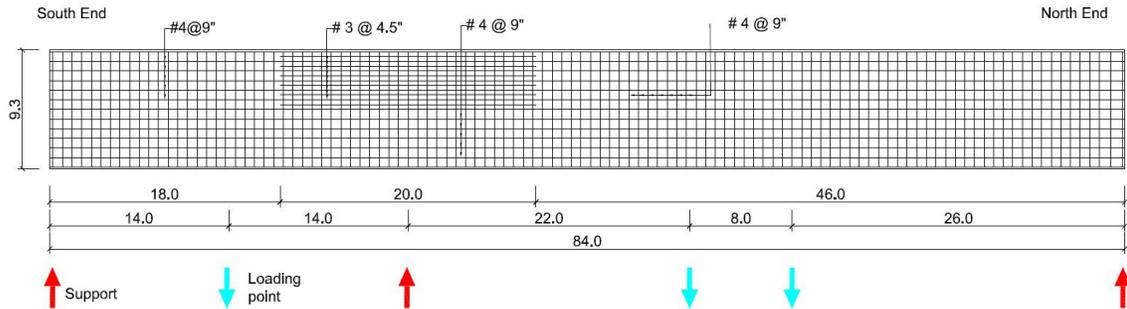
Figure 5- 9 Deck Reinforcing Steel Layout in Tub 3

The solid diaphragm of Tub 3 was fabricated with a 1.5-inch thick steel plate, as shown in Figure 5-10. The vertical stiffener was unnecessary due to the larger thickness of the plate. Similar to Tub 2, the bottom flange of Tub 3 was reinforced by casting a 14-foot long, 6.5-inch thick concrete slab symmetric to the intermediate support. Shear studs were welded to the bottom flange to provide full-composite action between the bottom flange and the concrete slab, and #4 reinforcing steel bars spaced at 9-inches in both directions for the concrete slab.

86

*Figure 5- 10 Solid Diaphragm and Bottom Flange Reinforcement (After Casting) in Tub 3
(Photography taken by Stalin Armijos)*

5.3 Material Testing

To obtain the material characteristics of the different components of the composite girders, material tests were performed on the steel plates of the tub girders, the reinforcing steel, and concrete from the slab.

5.3.1 Steel Coupon Testing

The material properties of the steel plates of the tub girders were obtained by conducting tension tests on coupons that were cut from the top flange plates, bottom flange plates, and from the web plates. The length of the tub girders necessitated the use of a splice in the flanges and webs along the girder length. The longitudinal axis of the girder was oriented in the north-south direction. Coupons from the south side and the north side of these spliced plates were fabricated and tested. Table 5-1 to 5-3 report the properties of the stress-strain curve corresponding to the plates on each component of the tub girders. No considerable difference in the material characteristics of the steel plate was found from the tension coupon tests.

Table 5- 1 Steel Plate Properties: Tub 1

Location	Plate Element	Upper Yield Point (ksi)	Dynamic Yield Stress (ksi)	Static Yield Stress (ksi)	Strain at Onset of Hardening	Ultimate Tensile Stress (ksi)	Strain at Development of Tensile Strength	Elongation (Strain at Fracture)
North Side	West Top Flange	63.1	60.9	57.5	1.7%	83.3	14.%	34.4%
	East Top Flange	62.3	60.7	57.3	1.6%	83.7	14.70%	33.6%
	Bottom Flange	65.6	61.7	58.3	1.8%	83.9	15.5%	32.2%
	West Web	64.1	61.7	58	1.9%	82.7	16.1%	32.3%
	East Web	61.8	61.3	58.2	1.6%	84	14.9%	29.4%
South Side	West Top Flange	63.8	61.5	58.6	1.7%	84	14.%	34.6%
	East Top Flange	63.9	61.5	58.7	1.6%	83.8	14.80%	34.7%
	Bottom Flange	64.8	61.4	58.3	1.7%	84.1	16.1%	31.3%
	West Web	64.6	62.95	59.5	2.2%	77.2	16.0%	36.5%
	East Web	65.5	61.97	58.4	2.4%	76	14.9%	35.2%

Table 5- 2 Steel Plate Properties: Tub 2

Location	Plate Element	Upper Yield Point (ksi)	Dynamic Yield Stress (ksi)	Static Yield Stress (ksi)	Strain at Onset of Hardening	Ultimate Tensile Stress (ksi)	Strain at Development of Tensile Strength	Elongation (Strain at Fracture)
North Side	West Top Flange	62.2	61.5	59.1	1.7%	83.8	20.1%	36.1%
	East Top Flange	61.4	60.4	58	1.6%	82.7	20.0%	33.4%
	Bottom Flange	65.9	60.6	58	1.6%	84.4	15.5%	33.6%
	West Web	64.4	59.8	58.1	2.0%	83.1	15.0%	31.2%
	East Web	63.1	59.8	58.1	1.7%	83.3	16.5%	31.2%
South Side	West Top Flange	62.5	60.8	58	1.6%	82.6	20.0%	35.0%
	East Top Flange	63.4	62.6	60.1	1.7%	84	20.0%	35.3%
	Bottom Flange	64.9	61.6	59.4	1.6%	85.1	17.5%	32.6%
	West Web	64	61.5	58.9	2.4%	76.6	15.5%	34.4%
	East Web	64.9	60.6	58.5	2.4%	76.7	16.4%	33.7%

Table 5- 3 Steel Plate Properties: Tub 3

Location	Plate Element	Upper Yield Point (ksi)	Dynamic Yield Stress (ksi)	Static Yield Stress (ksi)	Strain at Onset of Hardening	Ultimate Tensile Stress (ksi)	Strain at Development of Tensile Strength	Elongation (Strain at Fracture)
North Side	West Top Flange	62.9	58.4	56.4	1.6%	83	16.5%	33.3%
	East Top Flange	61	60	58	1.0%	82.9	10.8%	29.5%
	Bottom Flange	64.8	59.8	57.7	1.7%	83.5	15.1%	32.3%
	West Web	65.5	61.4	59.7	2.0%	83.4	15.5%	32.0%
	East tension Web	64.4	62	59.7	2.0%	83.9	14.9%	29.4%
South Side	West Top Flange	60.7	59.8	57	1.5%	84.2	15.1%	29.0%
	East Top Flange	66.3	61.9	60.1	1.5%	84.7	15.3%	33.5%
	Bottom Flange	65.7	60.7	58.5	1.7%	83.8	16.2%	31.1%
	West Web	60.2	57.9	56	1.9%	80.8	18.0%	32.0%
	East Web	60	56	54.6	1.6%	81.8	15.8%	33.2%

5.3.2 Reinforcing Bar Testing

Similar to the steel plates, uniaxial tension testing was conducted on short samples of reinforcing bars that were used in the concrete deck of each specimen. Table 5-4 presents the measured yield stress and ultimate strength values from the deck reinforcing steel. The yield stresses from #4 and #5 bars are close to 60-ksi, but that from #3 bars are slightly larger than 70-ksi.

Table 5- 4 Reinforcing Bar Material Properties

Bar Diameter	Yield Stress (ksi)	Yield Strain (1×10-3)	Ultimate Strength (ksi)	Ultimate Strain (1×10-3)	Specimen
#3	71.4	2.57	117.4	93.4	Tub 3
#3	72.4	2.63	117.7	105.9	Tub 3
#4	61.3	2.17	99.4	134.2	Tub 1
#4	64.0	2.25	104.3	133.1	Tub 2
#4	59.2	2.09	93.5	132.5	Tub 3
#5	63.5	2.28	102.9	134.7	Tub 1
#5	63.7	2.24	103.3	134.4	Tub 2

5.3.3 Concrete Material Testing

The concrete material properties were measured on the day of the ultimate strength test on the girders as well as 28days after casting. The concrete compressive strength, modulus of elasticity, and splitting tensile strength tests were conducted on 4-inch diameter concrete cylinders. The concrete modulus of rupture was obtained by third-point loading tests on specimens that were 24-inch long, 6-inch wide, and 6-inch thick. All results were averaged from three replicate tests. No significant variations in concrete strength were observed between the 14-day and 28-day tests. The concrete material properties at the testing day and 28-day are provided in Table 5-5.

Table 5- 5 Concrete Material Properties

Specimen	Top Flange				Bottom Flange		Concrete Age (day)	Remark
	f'_c (psi)	E_c (ksi)	f_{sp} (psi)	f_r (psi)	f'_c (psi)	E_c (ksi)		
Tub 1	5950	5180	580	810	-	-	21	Testing
	6150	4900	-	-	-	-	28	-
Tub 2	5400	6400	630	650	5950	4450	14	Testing
	5900	6050	600	-	6000	5300	28	-
Tub 3	4850	5025	550	650	5800	5550	28	Testing

f'_c : Compressive Strength (psi) E_c: Modulus of Elasticity (ksi)

f_{sp} : Splitting Tensile Strength (psi) f_r : Modulus of Rupture (psi)

5.4 Description of Test Setup

A test setup was designed and constructed in the Ferguson Structural Engineering Laboratory to conduct the negative moment bending test on three composite specimens loaded to failure. Elevation views of the test setup for each specimen are shown in Figure 5-11. The test setup consisted of three girder supports and two or three loading frames that were anchored to the strong floor in the laboratory.
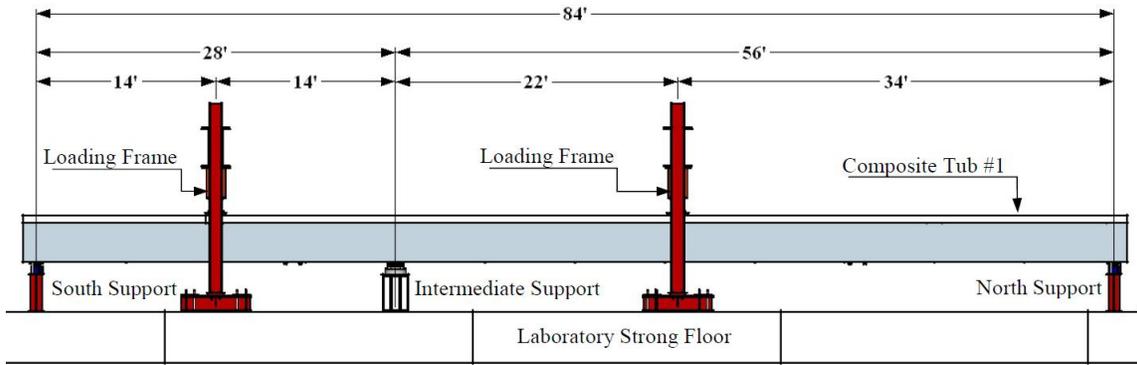
(a) Tub 1
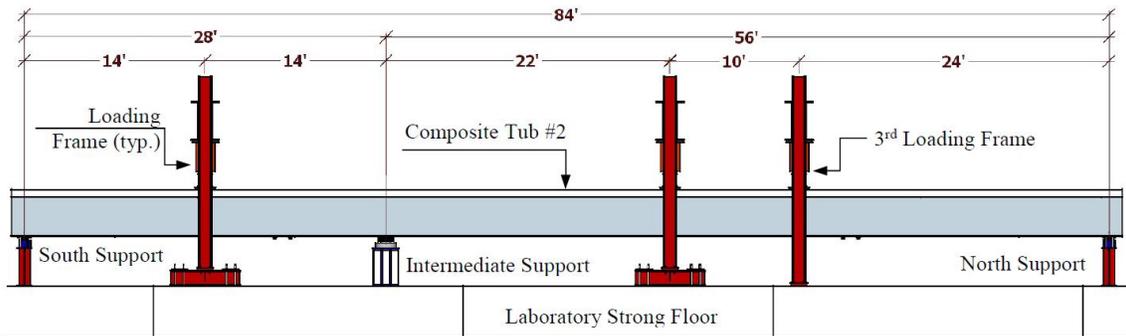
(b) Tub 2
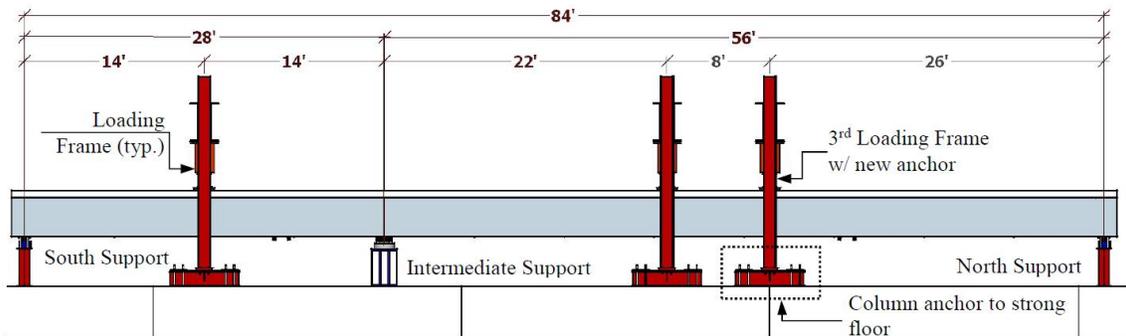
(c) Tub 3

Figure 5- 11 Elevation View of Test Setup on Each Specimen

Each specimen was supported as a two-span continuous girder, with a south span length of 28-foot and a north span length of 56-foot. The support setup consisted of tilt saddles over each of the supports at the north, south, and intermediate reaction points. Two tilt saddles were used at the two exterior supports and a single tilt saddle was used at the intermediate support. The tilt saddles allow rotations of the specimen on each support. The intermediate support was designed to behave as a pin support by allowing rotation and restricting translation. The north and south supports allow both rotational and lateral flexibility due to the web flexibility of the W36x135 wide flange sections that served as supports. Load cells with a 200-kip capacity were placed under the two tilt saddles on each end support. A load cell with a 1000 kip capacity was placed under the larger tilt saddle on the intermediate support as shown in Figure 5-12.

90
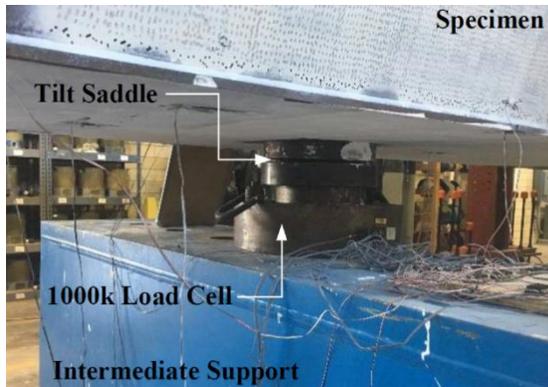
(a) Intermediate support	*(b) End support*

Figure 5- 12 Support Setup
(Photography taken by Stalin Armijos)

In order to apply the loads, a hydraulic actuator with 1000-kip capacity was mounted on each loading frame. The load was applied to the composite girders through steel loading beams placed over two 18″ long × 9″ wide × 1.75″ thick bearing elastomeric pads, which were located over the steel tub girder top flanges (5.3-foot distance). A tilt saddle was placed below the hydraulic actuator on top of the load cell over the loading beam. The purpose of the tile saddle was to accommodate rotations in the specimen during the test. Figure 5-13 shows the loading setup on each loading frame.

Figure 5- 13 Loading Frame Setup
(Photography taken by Stalin Armijos)

For Tub 1, two loading frames were placed 14-foot and 22-foot away from the intermediate support, respectively. As noted earlier, a significant difference between Tubs 1 and 2 was the use of a composite bottom flange concrete deck in Tub 2. Because of the concrete deck in the bottom flange in the negative moment region of Tub 2, the ultimate capacity of Tub 2 was higher than Tub 1. Thus, the previous loading setup could not test the specimen up to failure over the intermediate support. As a result, a third loading frame was erected 10-foot away from the existing loading frame in the north span of Tub 2. The anchorage capacity of the third frame was not as strong as that used for the other two due to the difference in the connection to the strong

floor. For the Tub 2 test, the two original frames were loaded close to their maximum capacities and the load level was maintained while the additional load was added to the added frame. The loading to the added frame led to failure in the girder. This loading process was deemed cumbersome for testing and also led to difficulties in processing the data. Thus, the loading setup was modified for the third specimen. The additional loading frame was moved two-feet north and connected to the strong floor in a similar way as the other two frames (straddling two anchorages – leading to increased frame capacity). As a result, all three frames shared the same load capacity. For the Tub 3 test, equal loads were applied simultaneously at all three loading frames. Pictures of negative moment bending tests on three composite girders are shown in Figures 5-14.

(a) Tub 1

(b) Tub 2
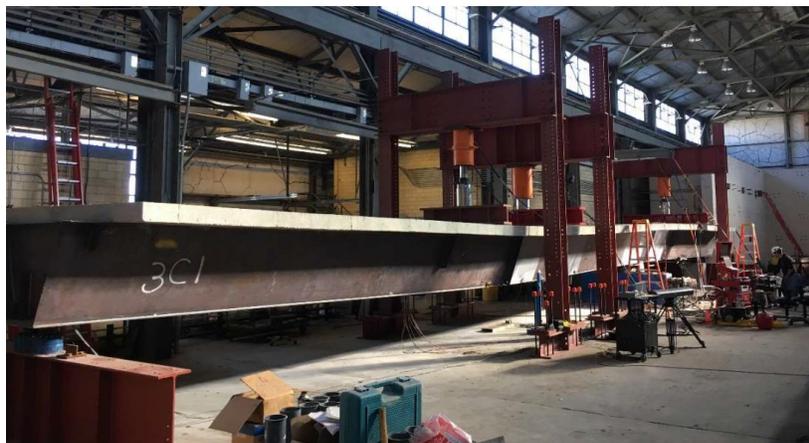
(c) Tub 3

Figure 5- 14 Negative Moment Bending Tests on Three Composite Girders
(Photography taken by Stalin Armijos)

5.5 Instrumentation

The behavior of the composite tub girders during testing was recorded by instruments installed on the specimen, which measured the loading and reaction forces, longitudinal strains, and deck cracking behavior. Four 200-kip and one 1000-kip load cells were utilized to record reaction loads. Two 1000-kip load cells were utilized to record loads applied at loading frames. The calibration of all load cells was validated prior to testing. The force in the third loading frame can be determined by the equilibrium. In addition, vertical deflections were measured with string potentiometers connected to the bottom flange at the loading point locations.
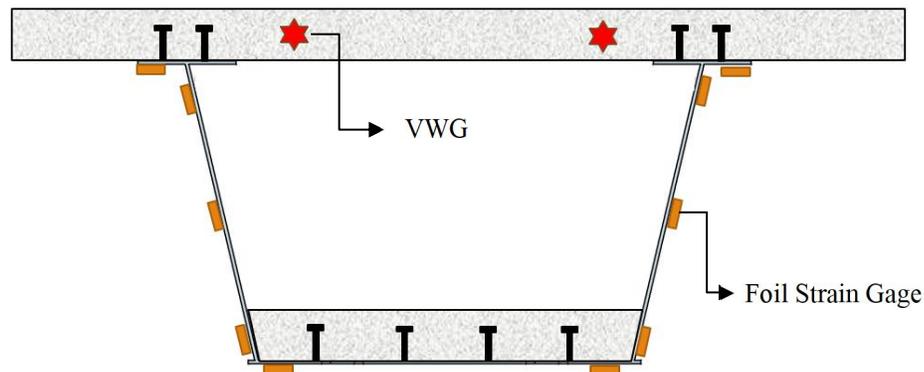
Figure 5- 15 Sectional View of Instrumentation Locations

Girder Strain profile over the intermediate support was measured with foil strain gauges installed on the steel tub girder and Vibration Wire Gages (VWGs) embedded in the concrete deck. Figure 5-15 shows a sectional view of instrumentation locations. Furthermore, the cracking behavior in the top flange concrete deck in the negative moment region was measured simultaneously using surface crack width gages (PI-gages) and Digital Image Correlation (DIC) system. PI-gages can measure the deck surface crack opening at a specific location. Since the location of deck cracking cannot be identified before testing, PI-gages were placed one after the other in a row spaced at 6-inches. Thus, the widths of the transverse deck crack occurring in this region could be measured.

The DIC system is a non-contact measurement solution for measuring field distribution of displacements and strains using a pair of stereo-mounted digital cameras. The measuring system requires a random speckle pattern to be painted onto the target surface before testing. In addition, artificial illumination is necessary to take clear photos. As shown in Figure 5-16, two 12.3 MegaPixel digital cameras were placed over the concrete deck in the negative moment region. The cameras should remain stationary during testing. For the purposes of the testing discussed herein, the cameras were mounted to a wall-bracket cantilever crane beam, to avoid contact with the test setup.
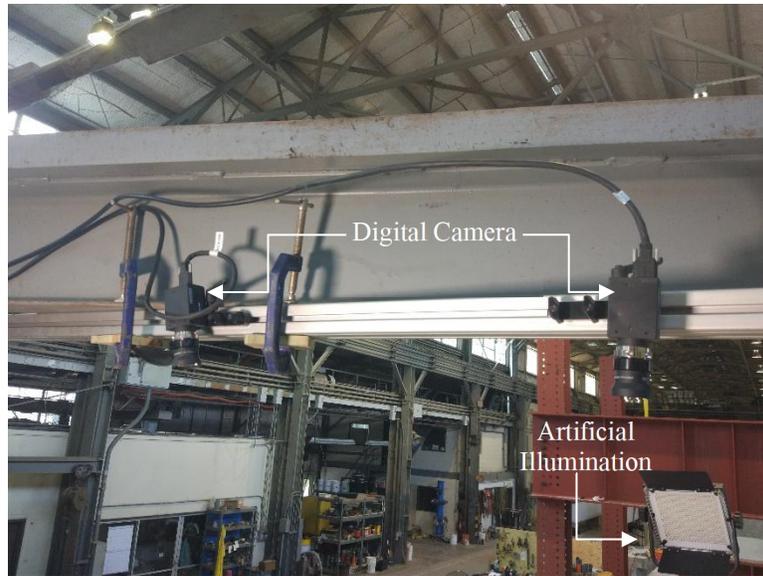
Figure 5- 16 DIC System over the Bridge Deck

As shown in Figure 5-17, twelve PI-gages were placed in a row at the west side on the concrete deck in the negative moment region of Tub 1, and the DIC system targeted the east half of the deck region. Because different longitudinal deck reinforcing details were applied in the east and west half on concrete decks in Tubs 2 and 3, six PI-gages were placed in a row at both east and west sides on the concrete deck, and the DIC system targeted the middle part of the concrete deck in this region. Therefore, exhaustive deck cracking behavior with various reinforcing details could be obtained simultaneously by the DIC system and PI-gages.

| *(a) Tub 1* | *(b) Tub 2&3* |
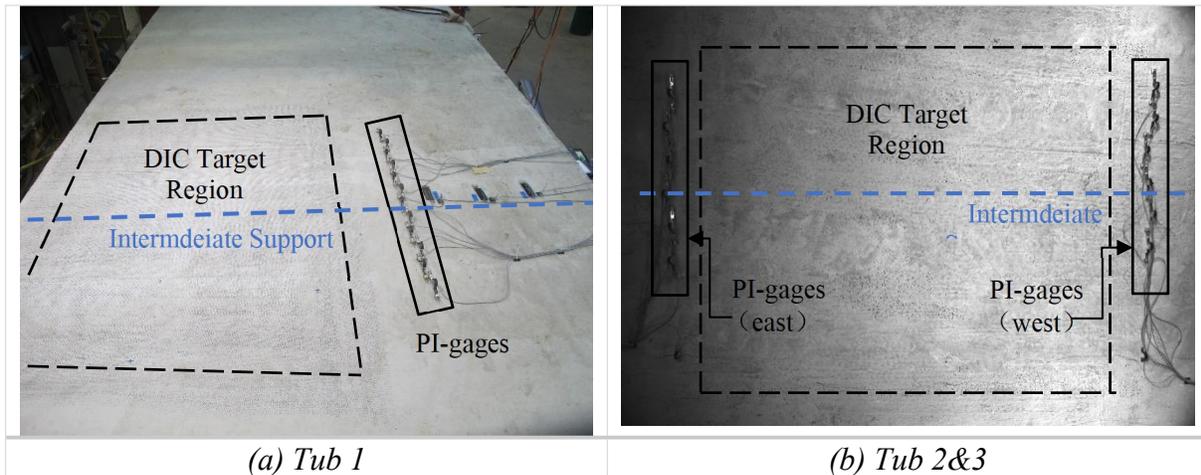
Figure 5- 17 Deck Cracking Instrumentation

5.6 Testing Procedure

Before the negative moment bending test on each specimen, the concrete decks over intermediate support were examined. No transverse deck cracking was observed in the concrete deck of Tub 1 and Tub 3, while one transverse deck crack was observed in Tub 2, most likely due to deck concrete shrinkage. The crack width was approximate 0.005-inch.

For Tub 1, two equal loads were applied simultaneously at both loading frames 14-foot and 22-foot from the intermediate support, respectively. Each specimen was loaded as a continuous girder configuration until significant yielding was observed in the cross-section over the intermediate support. Tub 1 was loaded with two loading frames, as shown in Figure 5-11(a), simultaneously with equal loads. Tub 2 was first loaded with the two initial loading frames till 525-kip on each frame, and then the third frame was loaded while maintaining a constant load in the initial two loading frames, as shown in Figure 5-11(b). Tub 3 was loaded with three loading frames simultaneously with equal loads, as shown in Figure 5-11(c). The applied loads were under manual control, using a pneumatically driven hydraulic pump. Data were recorded continuously during the entire tests. Strain measurements from vibrating wire gages (VWGs) were recorded by a Campbell Scientific Data-logger. The deck strain distribution was recorded by the DIC system, and other instrumentation (load cells, string potentiometers foil strain gages, PI-gages) were recorded by an Agilent data acquisition system. All data acquisition was synchronized to record data at 20-second intervals. Visual evaluation was performed for every 25-kip load increment in total load in the elastic range, and every half-inch increment in deflection once significant yielding was observed.

5.7 Experimental Results

5.7.1 Composite Tub Girder 1

Figure 5-18 presents the moment-curvature behavior of Tub 1 during the negative moment bending test. This plot corresponds to the curvature at the intermediate support location versus the negative moment in the same section. The negative moment is calculated by the load cell readings at the loading frames and supports, while the curvature is computed by the foil strain gages on the girders.
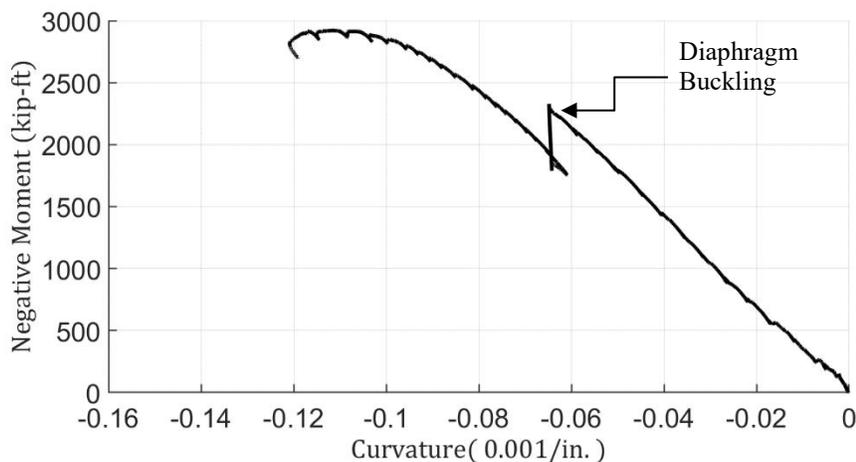
Figure 5- 18 Moment-Curvature of Tub 1

At approximate 2200 kip-ft of total bending moment, the load dropped approximatley 500 kip-ft accompanied by a load noise. After the system stabilized, the loading was continued on the girder. The test was stopped at a negative bending moment of 2920 kip-ft when the moment-curvature curve started to flatten. After the composite girder system was dissected, it was observed that the internal diaphragm over the intermediate support buckled, as shown in Figure 5-19. The local buckling of the internal diaphragm was the apparent cause for the load drop observed during the negative moment bending test.
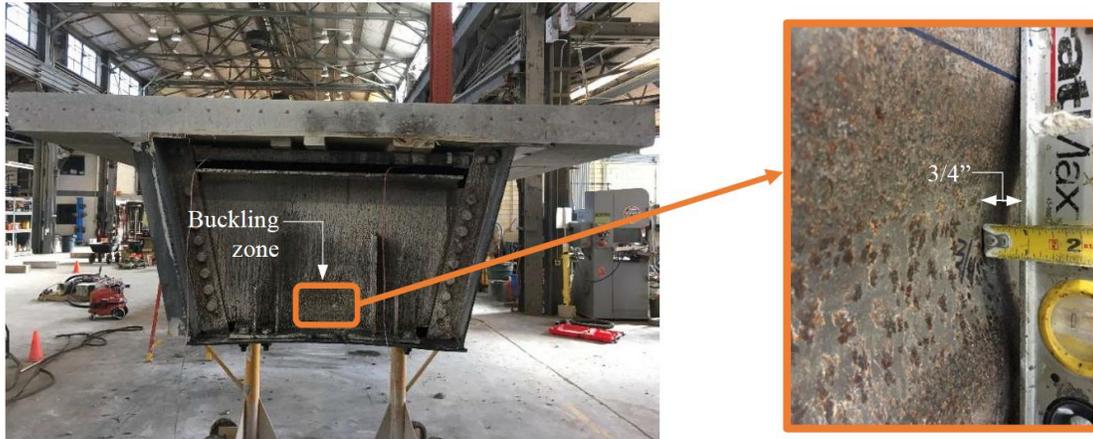
Figure 5- 19 Local Buckling at Internal Diaphragm
(Photography taken by Stalin Armijos)

The strain in the concrete deck over the intermediate support was measured using a combination of the VWGs embedded in the concrete deck and the DIC system focusing on the critical deck region. The deck strain obtained by the DIC system was the average longitudinal strain in the target region. As shown in Figure 5-20, strain readings in the VWGs were close to zero until a negative bending moment of approximately 500 kip-ft. Strain readings in the VWGs increased significantly to approximate 300 με, likely caused by a transverse deck cracking that occurred at the VWG location. If the bending moment was over 500 kip-ft , strain readings from the VWGs and DIC system were close to each other.
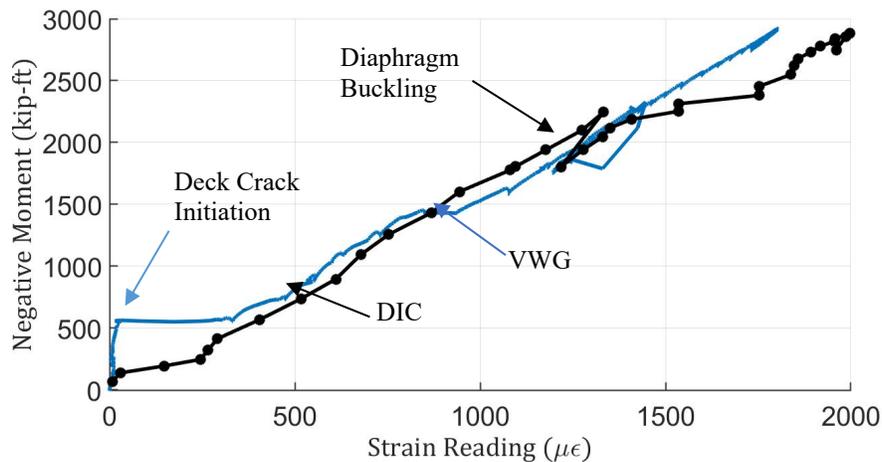
Figure 5- 20 Deck strains over the intermediate support

The deck cracking spatial distribution and crack widths can be derived from the DIC measurement. The deck cracking distribution under 1700 kip-ft negative bending moment (Curvature as $\phi = -4 \times 10^{-5}$ $in.^{-1}$) is shown in Figure 5-21(a) as an example. Eight transverse cracks were observed in this condition, and the crack spacing was approximate eight inches. Figure 5-21(b) shows the crack width probability density in this condition. The widths at most identified crack opening locations were less than 0.01-inch.

(a) Deck cracking spatial distribution　　　　(b) Crack width probability density
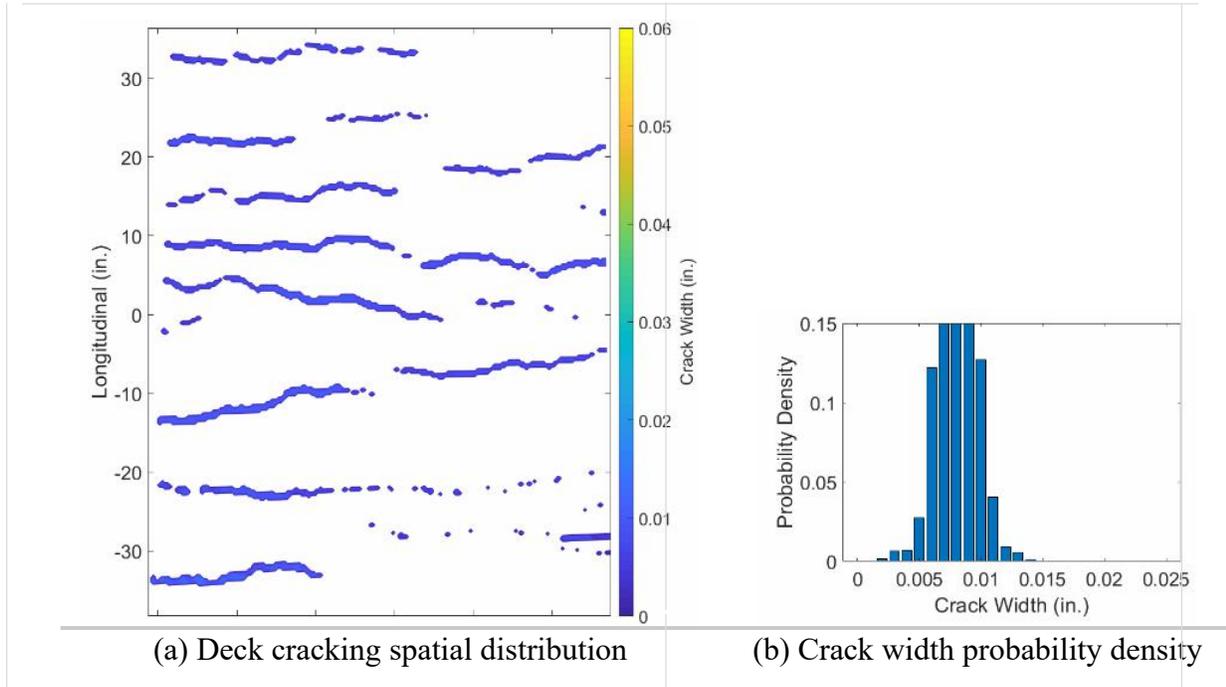
Figure 5- 21 Deck Cracking Behavior Measured by the DIC System (Tub 1)

Five out of twelve PI-gages in this region were positioned across transverse cracks. Figure 5-22 corresponds to the average crack widths measured by PI-gages to the negative bending moment. This figure shows experimental results until the diaphragm buckling occurred.
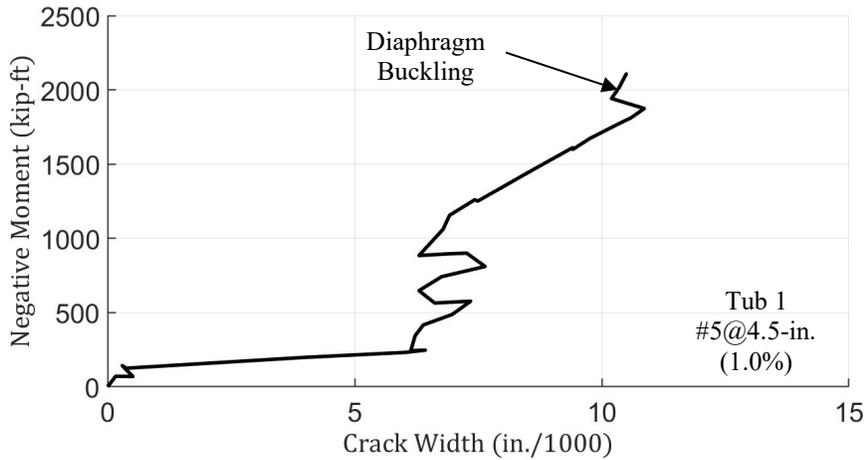
Figure 5- 22 Deck cracking measured by PI-gages (Tub 1)

5.7.2 Composite Tub Girder 2

Figure 5-23 presents the moment-curvature response of Tub 2 during the negative moment bending test. This plot corresponds to the curvature at the intermediate support location versus the negative moment in the same section. The negative moment is calculated by the load cell readings at the loading frames and supports, while the curvature is computed by the foil strain gages on the girder surface. The test was stopped at a negative bending moment of approximate 4920 kip-ft when the moment-curvature curve started to flatten significantly.
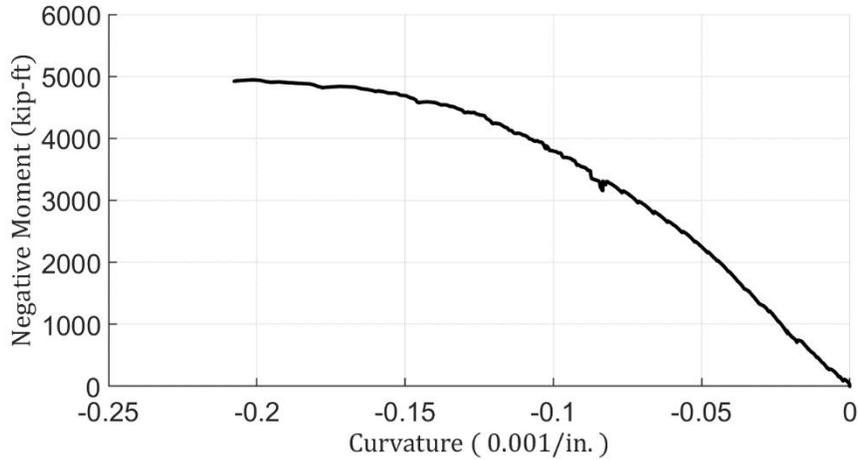
Figure 5- 23 Moment-Curvature of Tub 2

The deck cracking spatial distribution and crack widths can be derived from the DIC measurement. The deck cracking distribution under 2000 kip-ft negative bending moment (Curvature as $\phi = -4\times10^{-5}$ in.$^{-1}$) is shown in Figure 5-24(a) as an example. Six transverse cracks were observed in this condition, and the crack spacing was approximately ten inches. No significant differences in the crack widths or crack spacing were observed from each half of deck regions with different longitudinal reinforcing details, as #5 spaced at 9-inches and #4 spaced at 6-inches, respectively. Figure 5-24(b) shows the crack width probability density in this condition. The widths at most identified crack opening locations were less than 0.02-inch.

(a) Deck cracking spatial distribution   (b) Crack width probability density
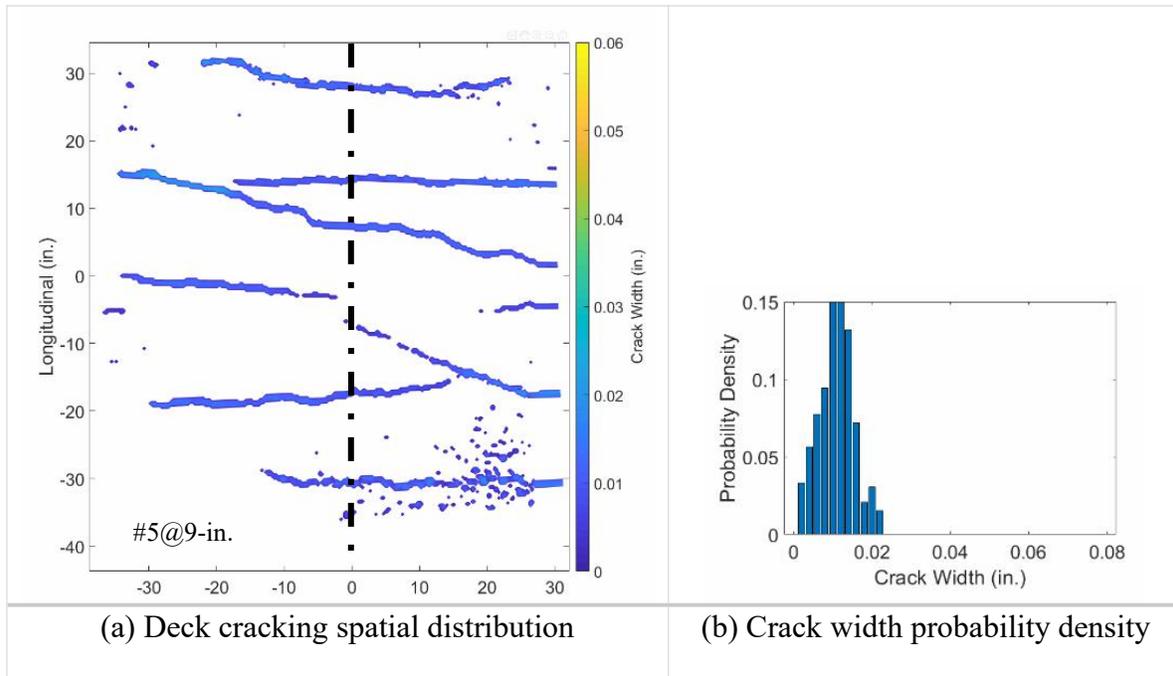
Figure 5- 24 Deck Cracking Behavior Measured by the DIC System (Tub 2)

Three out of six PI-gages in the east half of the concrete deck with #5 spaced at 9-inches reinforcing bar (0.5%) were positioned across transverse cracks, while four out of six PI-gages on the other deck region (#4 spaced at 6-inches, 0.5%) were positioned across transverse cracks. Figure 5-25 corresponds to the average crack widths measured by PI-gages in each region to the negative bending moment. Measured crack widths show some difference while the bending moment less than 2000 kip-ft but share similar cracking behavior in the higher bending moment. Staying the same reinforcement ratio (0.5%) but reducing bar spacing from 9-inch to 6-inch shows some benefits on reducing crack opening widths.
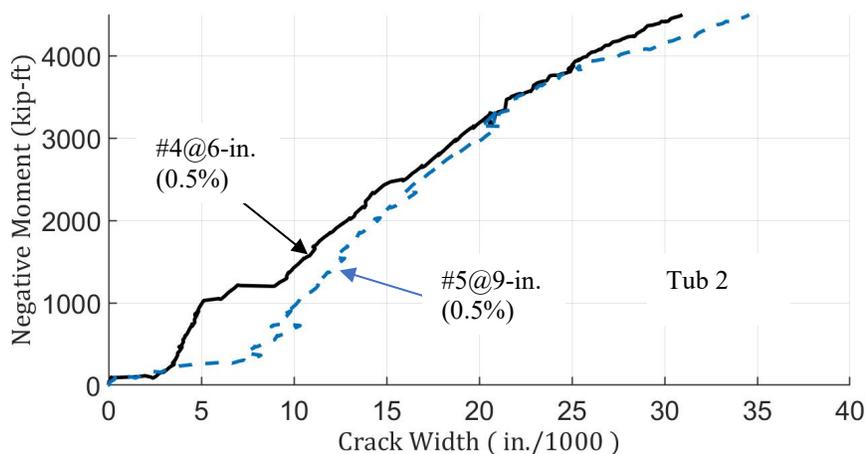
Figure 5- 25 Deck Cracking Measured by the PI-gages (Tub 2)

5.7.3 Composite Tub Girder 3

Figure 5-26 presents the moment-curvature response of Tub 3 during the negative moment bending test. This plot corresponds to the curvature at the intermediate support location versus the negative moment in the same section. The negative moment is calculated by the load cell readings at loading frames and supports, while the curvature is computed by the foil strain gages on the girder surface. The test was stopped at a negative bending moment of 4590 kip-ft when the moment-curvature curve started to flatten significantly.
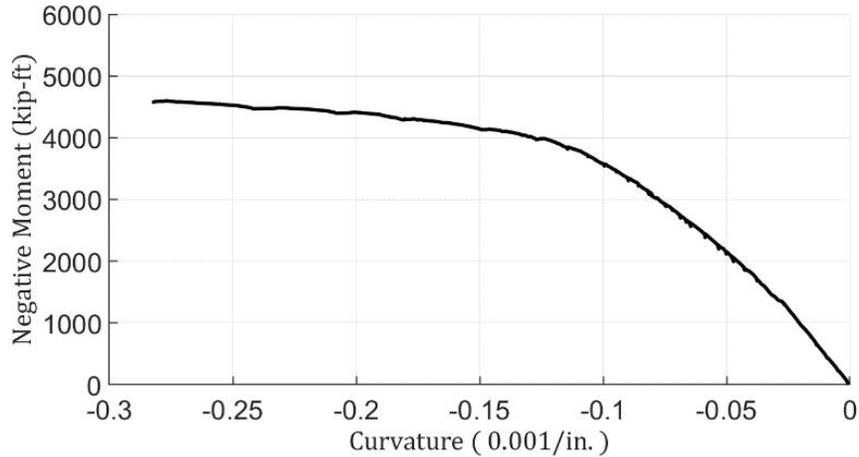
Figure 5- 26 Moment-Curvature of Tub 3

Deck cracking spatial distributions and crack widths can be derived from the DIC measurement. The deck cracking distribution under 2000 kip-ft negative bending moment (Curvature as $\phi = -4 \times 10^{-5}$ *in.$^{-1}$*) is shown in Figure 5-27(a) as an example. Although not very clear measurement obtained by the DIC system in this case, five transverse cracks could be identified, and the crack spacing was approximate twelve-inch. No significant differences in the crack widths or crack spacing were observed from each half of deck regions with different longitudinal reinforcing details, as #4 bars spaced at 9-inch and #3 bars spaced at 4.5-inch, respectively. Figure 5-27(b) shows the crack width probability density in this condition. The widths at most identified crack opening locations were less than 0.02-inch.

(a) Deck cracking spatial distribution

(b) Crack width probability density
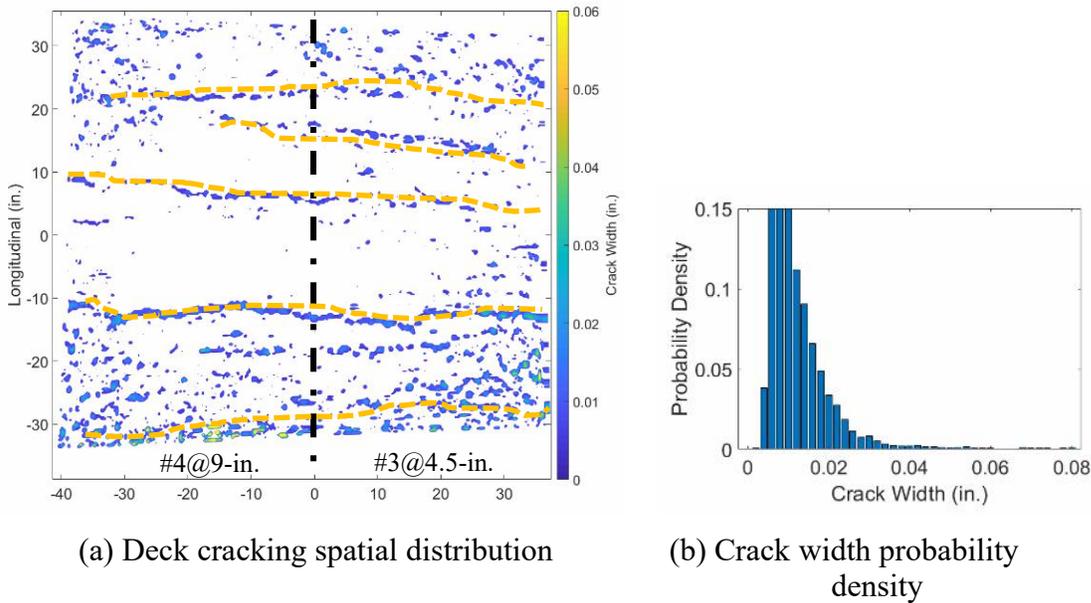
Figure 5- 27 Deck cracking behavior measured by the DIC system (Tub 3)

In the east (#4 spaced at 9-inch, 0.34%) and west (#3 spaced at 4.5-inch, 0.38%) half of the concrete deck over the intermediate support, three out of six PI-gages were positioned across the transverse deck cracks, respectively. Figure 5-28 corresponds to the average crack widths measured by PI-gages in each region to the negative bending moment. Reducing the bar spacing from 9-inches to 4.5-inches shows some benefits on reducing crack opening widths.
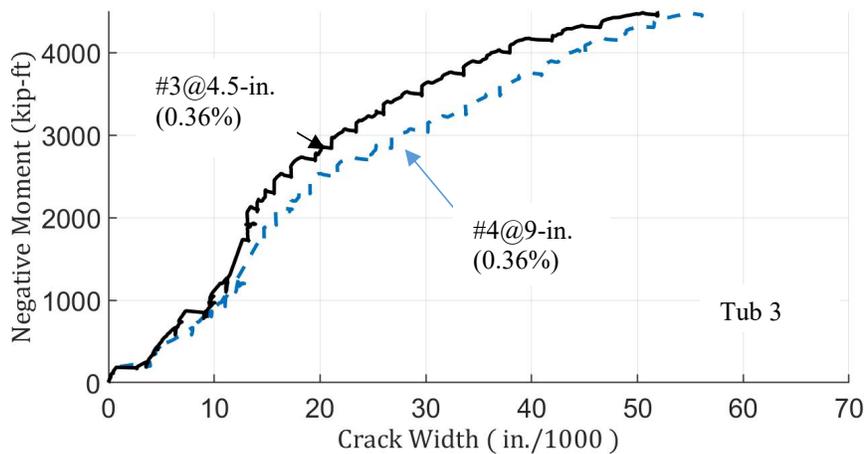
Figure 5- 28 Deck cracking measured by the PI-gages (Tub 3)

5.7.4 Comparison of Results

Figure 5-29 shows the negative moment-curvature curves of three specimens. Because Tub 1 is the only specimen without the bottom flange concrete slab over the intermediate support, its ultimate capacity of negative bending is significantly lower than that of the other two

specimens. Also caused by the difference in cross-sectional geometric, the negative bending moment-deck crack width relationships of each test are not easily comparable. As a result, the relationship between reinforcing bar stress and crack width was utilized to compare the influence from different reinforcing steel layouts to the deck cracking behaviors.
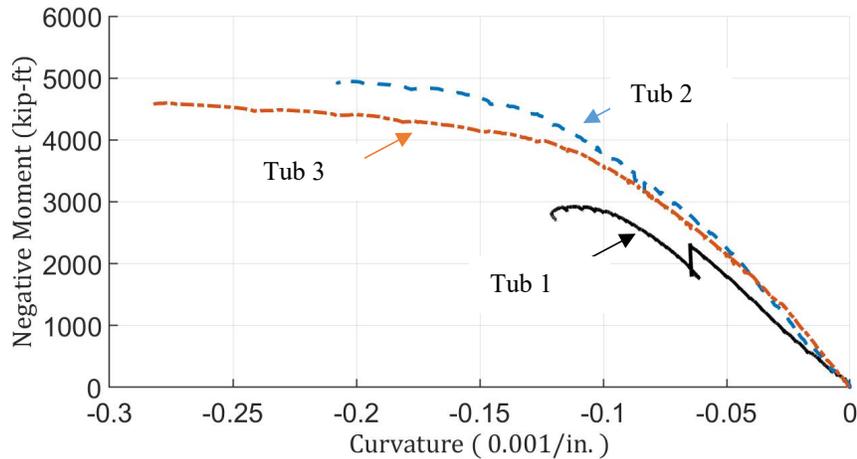
Figure 5- 29 Negative Moment verse Curvature of three specimens

The relationship between crack widths and the average reinforcing bar stress at crack was presented in Figure 5-30. The average reinforcing bar stresses are computed by the average concrete strains in the negative moment region measured by the DIC system, and the crack widths are the maximum crack width measured by the PI-gages in each test. The test result from Tub 1 was shown until the local buckling occurred at the internal diaphragm. Although the relationship between average reinforcing bar stress and crack width is not straightforward in all these three tests with various reinforcing details, increasing reinforcing steel to 1.0% of the deck area shows the benefits in reducing deck cracking widths. For the concrete decks in Tub 2 and Tub 3, while the reinforcement ratio is 0.5% and approximate 0.36%, respectively, the deck crack widths are all beyond 0.01-inch soon after cracking initiation. While for the concrete deck in Tub 1, whose reinforcement ratio is 1.0%, the crack width soon after cracking initiation can be controlled to not beyond 0.006-inch.

Besides, for the deck cracking in the Tub 2 (ρ=0.5%) and Tub 3 (ρ=0.36%), reducing the spacing between reinforcing bars does not show significant benefits in deck cracking control. Furthermore, since several crack width equations present a linear relationship between crack width and reinforcing bar stress but not clear on whether it should be the average reinforcing bar stress or the maximum reinforcing bar stress to be used to predict the crack width. This plot shows that the deck cracking widths may vary significantly, even with the similar average stresses in the reinforcing steel. The reinforcement ratio also shows some influence on the opening widths of the deck cracks.
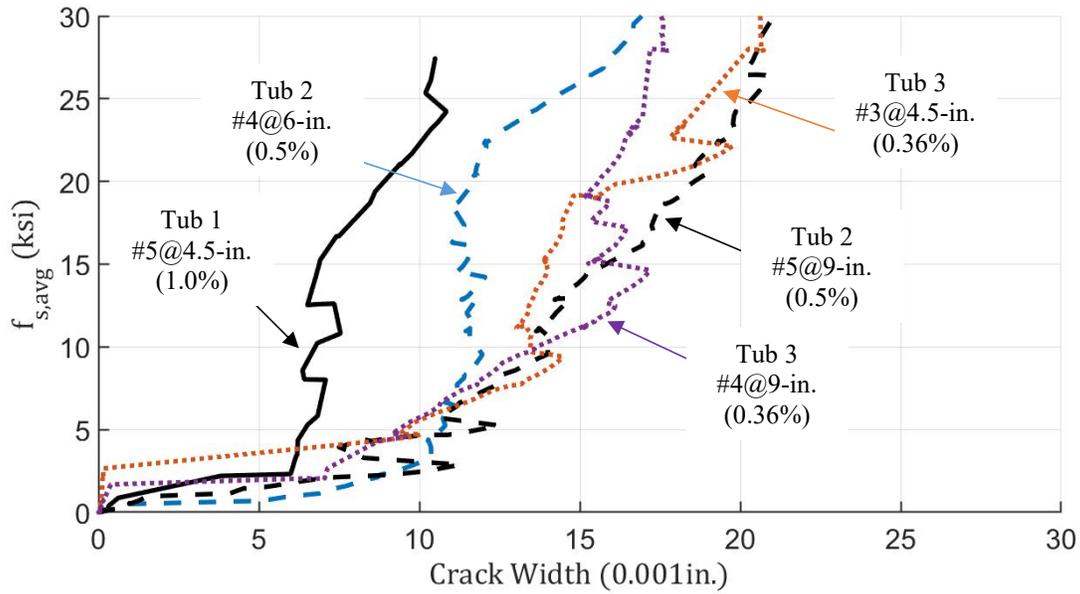
Figure 5- 30 Average Reinforcing Bar Stress Versus Crack Width

Since there were significant stress gradients in the reinforcing bars embedded in the cracked concrete, there is no reliable method to measure either the average reinforcing bar stress in the critical region or the maximum reinforcing bar stress at cracks. However, the average reinforcing bar stress can be obtained from the average deck strain measured by the DIC system, and the maximum reinforcing bar stress can be derived from the average reinforcing bar stress. This calculation is based upon the equilibrium principle that the tensile stress in the concrete between cracks all transferred to the reinforcing bar at cracks where concrete cannot carry any tensile loads. Therefore, the reinforcing bar stress at cracks is combined with the average reinforcing bar stress in the critical region and the additional reinforcing bar stress transferred from concrete. The tensile stress in the concrete between cracks can be estimated by the widely used concrete "tension stiffening" model. This method can be summarized in the following equations:

$$f_{s,max} = f_{s,avg} + \frac{f_{ct}}{\rho} \tag{5-1}$$

$$f_{s,avg} = \varepsilon_{avg} \times E_s \tag{5-2}$$

$$f_{ct} = \frac{f_t}{1 + \sqrt{500\varepsilon_{avg}}} \tag{5-3}$$

in which:

$f_{s,max}$ = maximum reinforcing bar stress at cracks (*ksi*)

$f_{s,avg}$ = average reinforcing bar stress in the critical region (*ksi*)

ε_{avg} = average strain measured by the DIC system

E_s = elastic modulus of reinforcing steel, $E_s = 29000 \ ksi$

f_{ct} = average tensile stress in cracked concrete, or named as the concrete "tension stiffening" effect (ksi)

f_t = deck concrete direct tensile strength (ksi)

ρ = deck reinforcement ratio

Figure 5-31 shows the relationship between the average reinforcing bar stress and the calculated maximum reinforcing bar stress at the crack locations. This calculation is based upon the concrete direct tensile stress estimated from the concrete compressive strength with the equation shown following:

$$f_t = 4\sqrt{f_c'} \qquad\qquad (5\text{-}4)$$

where:

f_c' : concrete compressive strength measured on the testing day

The reinforcement ratio has critical influences on the maximum reinforcing bar stresses. For Tub 3 specimen, whose reinforcement ratio is 0.36%, the calculated maximum reinforcing bar stresses are beyond 60-ksi immediately after deck cracking, which means the longitudinal reinforcing steel would already yield. The maximum reinforcing bar stresses in Tub 2, whose reinforcement ratio is 0.5%, are approximate 50-ksi when the average reinforcing bar stresses are under 15-ksi. Due to the variability in the concrete tensile strength, yielding of the reinforcing steel in Tub 2 probably occurred when the average reinforcing bar stresses are insignificant. Regarding Tub 1, whose deck reinforcement ratio is 1.0%, the maximum reinforcing bar stresses are between 30 to 40-ksi when the average reinforcing bar stresses between 10 to 20-ksi. As a result, the reinforcement ratio is the critical factor to the maximum reinforcing bar stress at cracks.
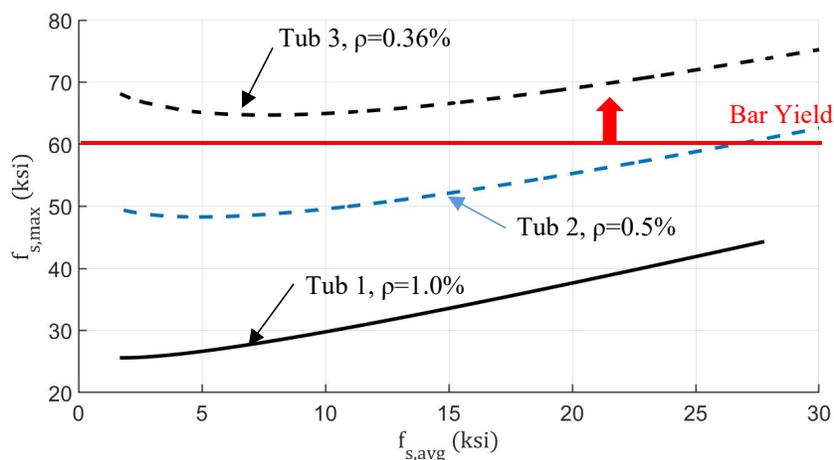
Figure 5- 31 Calculation Results of the Maximum Reinforcing Bar Stress

Figure 5-32 shows the relationship between the maximum reinforcing bar stress at cracks and the maximum crack width measured by the PI-gages in Tub 1 and Tub 2. Since the deck reinforcing steel in Tub 3 probable yielded soon after deck cracking, testing results from Tub 3 are not shown in Figure 5-32. The orange and yellow dash lines show the prediction of crack width based upon the Frosh equation (1999), which is currently adopted by AASHTO LRFD and will be shown in Chapter 6, corresponding to bar spacing as 4.5-inch and 9-inch, respectively. Generally, the crack width predictions and the measured results from Tub 1 and Tub 2 testings are at the same level.
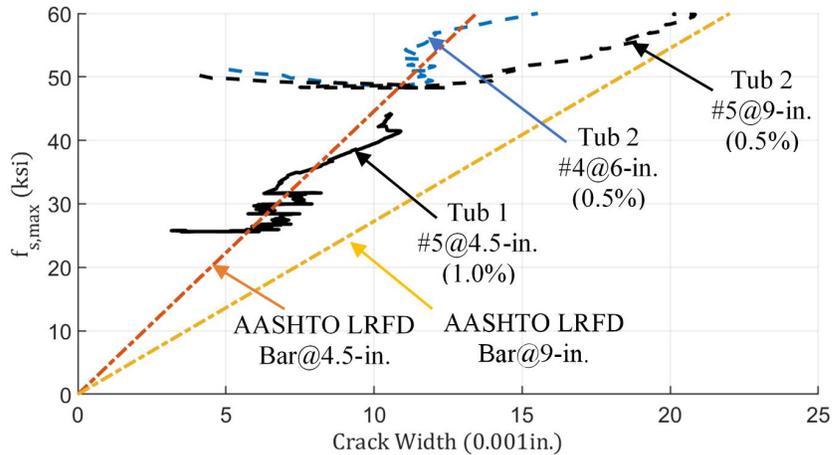
Figure 5- 32 Maximum Reinforcing Bar Stress at Cracks versus Crack Width
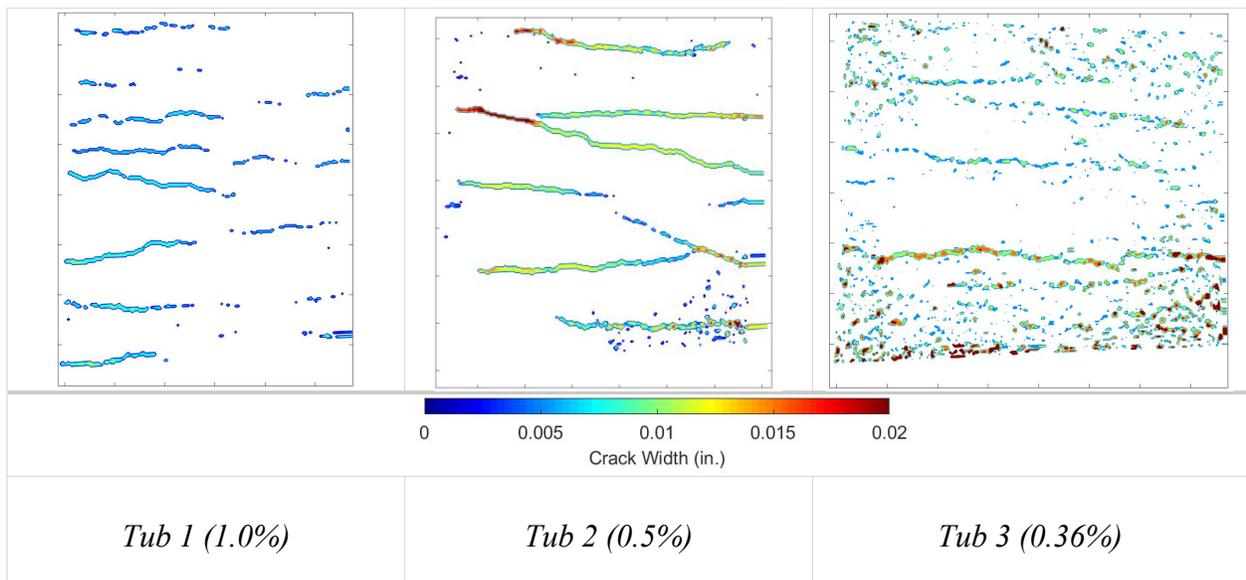
Figure 5- 33 Deck Cracking Distribution from DIC System ($f_{s,avg}$=20-ksi)
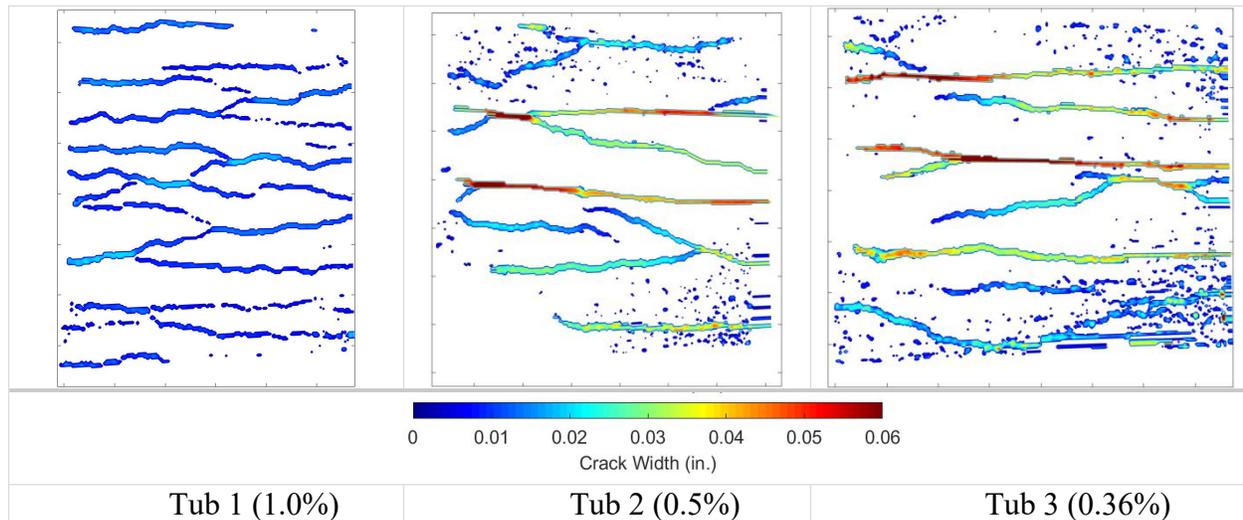
Figure 5- 34: Deck Cracking Distribution from DIC System (under ultimate bending moment)

Figure 5-33 and Figure 5-34 show the DIC measurements of deck cracking distribution in the negative moment region. Figure 5-33 selects the DIC results when the average reinforcing bar stresses approximate 20-ksi to represent the deck cracking behavior under service loading, while Figure 5-34 focuses on the deck cracking behavior under the ultimate negative bending moment of each test. The dimension of each plot is approximate 80-inch in the longitudinal direction.

As shown in Figure 5-33, the maximum crack width in Tub 1 is less than 0.01-inch, while the crack widths at several locations on the decks of Tub 2 and Tub 3 are approximate 0.02-inch. There are eight total transverse cracks observed in Tub 1, and the average crack spacing is approximately nine inches. Five transverse cracks were observed in Tub 2 and Tub 3, respectively, and the average crack spacing was approximately 14-inches. This difference is probably due to the different reinforcement ratio, and the longitudinal deck reinforcing steel at some locations may already yield in Tub 2 and Tub 3.

More transverse deck cracking occurred when specimens under the ultimate bending moment. Probably due to the local buckling at the internal diaphragm, the ultimate bending capacity of Tub 1 is no as significant as the other two specimens. As a result, the maximum crack widths in Tub 2 and Tub 3, which are up to 0.06-inch, can be three times larger than that of Tub 1. Even so, eleven total transverse deck cracking occurred in Tub 1, while seven total transverse deck cracking occurred in Tub 2 and Tub 3, respectively.

5.8 Summary

Negative bending tests were conducted on three composite tub girders with various deck longitudinal reinforcement details in the negative moment region. Several observation on the deck cracking behavior can be made from the experimental program:

- Utilizing more reinforcing steel shows benefits in reducing cracking widths and reducing crack spacing under a negative bending moment.
- With regard to Tub 1, whose reinforcement ratio is 1.0%, the deck crack width soon after cracking initiation is approximate 0.006-inch. The growing of crack width shows some correlations with the maximum reinforcing bar stress at cracks.
- With regard to Tub 2, whose reinforcement ratio is 0.5%, the deck crack width soon after cracking initiation is approximate 0.01-inch, and the calculated maximum reinforcing bar stress at cracks is approximate 50-ksi.
- With regard to Tub 3, whose reinforcement ratio is 0.36%, the deck crack width soon after cracking initiation is over 0.02-inch, and reinforcing bar yielding probably occurred at that condition.
- If the reinforcement ratio is very low, like that in Tub 2 (0.5%) and Tub 3 (0.36%), reducing bar spacing from 9-inch to 6-inch or 4.5-inch does not show significant benefit on reducing cracking widths.

Chapter 6. Direct Tension Tests on Reinforced Concrete Specimens

6.1 Overview

As described in the previous chapter, three large-scale laboratory tests on three continuous supported composite girders show some impact of the longitudinal reinforcing details on deck cracking control in the negative moment regions, and deck cracking widths show some correlation with the maximum reinforcing bar stresses at cracks. Because of the significant stress gradient in longitudinal reinforcing bar embedded in the cracked concrete, the maximum bar stresses at cracks cannot be measured but calculated based upon the model of concrete "tension stiffening" effect. With regard to uni-axial tensile tests on the reinforced concrete prism, the maximum reinforcing bar stress at cracks can be determined by the total external tensile loads. Therefore, member level laboratory tests on the reinforced concrete specimens under controlled uni-axial tensile loads are desirable. Since tests on member-level reinforce concrete specimens are more convenient compared with those three continuous supported composite girders, reinforced concrete specimens with a wider range of reinforcement ratio would be examined.

The purpose of these member level laboratory tests was to provide further insights into the influence of the reinforcing bar area on the concrete cracking behavior and to verify the concrete "tension stiffening" model. This chapter provides details on the description of the specimens, testing procedure, and results of the direct tension tests.

6.2 Experimental Specimens

Concrete specimens with one single reinforcing bar in the middle were cast in the Ferguson Laboratory. The concrete specimens were 30-inch long, with one #3, #4, #5, or #6 Grade 60 reinforcing bar in the middle. The bar extension at each end of specimens was eight inches. No transverse bars were utilized in the specimens. The reinforcement ratio varied between 0.5% to 2.2%. Figure 6-1 shows specimens during casting.

(a) Specimen casting-molds   (b) Specimens finishing

Figure 6- 1 Specimens Casting

Eight total types of specimens are listed in Table 3-1, and for each type, four specimens were fabricated in the laboratory. The differences between each specimen are among various sectional dimensions, concrete properties, and bar diameters. The specimen designations are according to the following convention: P(SP)X-#Y-Z, P represents a reinforced concrete prism with sectional dimension as 4.5″×4.5″, SP represents reinforced concrete prism with sectional dimension as 4.0″×4.0″, the number X defines the concrete casting batch, the number Y represents the bar diameter, and Z represents the concrete shrinkage effects in each specimen, while the letter "ns" (no shrinkage) means the specimen was cured in the water and "sh" (shrinkage) means shrinkage effect should be considered in the specimen.

Table 6- 1 Specimen Parameters

Specimen ID	Concrete Batch	Concrete Shrinkage	Dimension	Bar Diameter	Reinforcement Ratio (ρ)
P1-#4-ns				#4	1.0%
P1-#5-ns	1	-	30″×4.5″×4.5″	#5	1.5%
P1-#6-ns				#6	2.2%
P1-#4-sh				#4	1.0%
P1-#5-sh	1	180 με	30″×4.5″×4.5″	#5	1.5%
P1-#6-sh				#6	2.2%
P2-#4-ns				#4	1.0%
P2-#5-ns	2	-	30″×4.5″×4.5″	#5	1.5%
P2-#6-ns				#6	2.2%
P2-#4-sh				#4	1.0%
P2-#5-sh	2	250 με	30″×4.5″×4.5″	#5	1.5%
P2-#6-sh				#6	2.2%
P3-#3-ns	3	-	30″×4.5″×4.5″	#3	0.5%
SP3-#3-ns			30″×4.0″×4.0″	#3	0.7%

Table 6- 2 Concrete Material Properties

Concrete Batch	f'$_c$ (ksi)	E$_c$ (ksi)	f$_{sp}$ (psi)	Age (day)	ε_{sh} (με)
1	3630	5000	510	75	180
2	6140	5250	530	55	250
3	2640	3850	280	7	-

f'$_c$: Compressive Strength (psi)   E$_c$: Modulus of Elasticity (ksi)

f$_{sp}$: Splitting Tensile Strength (psi) ε_{sh}: Shrinkage Strain (με)

The concrete material properties of three concrete casting batches are listed in Table 6-2. The concrete compressive strength, modulus of elastic, and splitting tensile strength tests were conducted on 4-inch diameter concrete cylinders. For concrete batch 1 and batch 2, all specimens were removed from steel molds three days after casting. Then three specimens (Z=ns) were stored in the laboratory, and the shrinkage strains were monitored by the surface mounted Vibration Wire Gages (VWGs), as shown in Figure 6-2. To be compared, the other specimens

110

(Z=ns) were cured in the water to minimize concrete volume shrinkage. The measured shrinkage strains in specimens are shown in Figure 6-3. It shows that after approximate 50 days, the shrinkage strain readings are relatively stable. The shrinkage in specimens in Batch 1 specimens can be determined as approximate 180-$\mu\epsilon$ at the testing moment, while that in Batch 2 specimens can be determined as approximate 250-$\mu\epsilon$. Since the reinforcement ratios in Batch 3 specimens are less than 1%, and low tensile strength concrete is desirable to have concrete cracked before reinforcing bar yield, uni-axial tensile testing was conducted soon after concrete hardened. As a result, the shrinkage effect is not examined in the Batch 3 specimens.

Figure 6- 2 Specimen shrinkage measured by VWGs
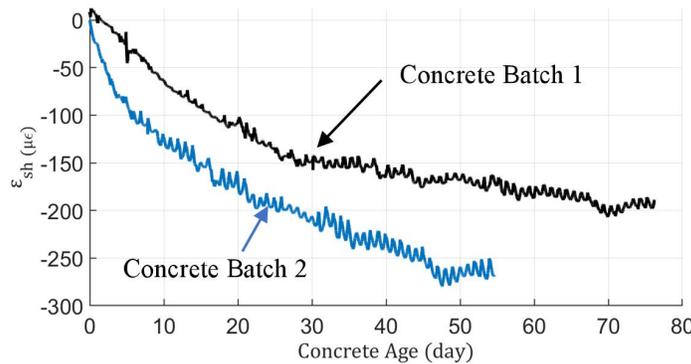
Figure 6- 3 Measured shrinkage strains in specimens

Uni-axial tension testing was conducted on short samples of reinforcing bars that were used in the specimens. Table 6-3 presents the measured yield stress and ultimate tensile strength values. The yield stresses from #4 and #5 bars are closed to 60-ksi, but that from #3 bars is approximately 70-ksi.

Table 6- 3 Characteristics of Reinforcing Bar

Bar Diameter	Yield Stress (ksi)	Yield Strain (1×10^{-3})	Ultimate Strength (ksi)	Ultimate Strain (1×10^{-3})
#3	70.6	2.49	107.4	95.7
#4	67.5	2.35	103.5	133.6
#5	63.5	2.28	102.9	134.7
#6	62.7	2.26	103.3	123.4

6.3 Testing Setup

The direct tension testing was conducted on a 220-kip MTS machine that could be operated in deformation or load control mode. As shown in Figure 6-4, the specimen was installed vertically in the setup, and the extending reinforcing bar at each end of specimens is restrained by the Vee-grips at the top and bottom of the MTS machine. The tensile loads from the MTS machine can be applied to the reinforced concrete specimens through the extending reinforcing bar.

Figure 6- 4 Uni-axial Tensile Test Setup

The maximum reinforcing bar stress ($f_{s,max}$) at cracks or in extending bars at the specimen ends was utilized to estimate the tensile load from MTS machine, as described in the following equation:

$$f_{s,max} = \frac{N}{A_s} \tag{6-1}$$

where:

N : Tensile load from MTS machine (kip)

A_s : Nominal area of reinforcing bar (inch^2)

The load testing is under load-controlled, with a rate of $f_{s,max}$ as 0.05-ksi/sec.

6.4 Instrumentation

The Digital Image Correlation (DIC) systems were the primary equipment used in the direct tension tests. The DIC system is a non-contact measurement solution for measuring field distribution of displacements and strains. Therefore, the local opening width of concrete cracking at random locations on the specimen surface can be obtained by the DIC system. To obtain complete surface displacements and strains on four total surfaces of specimens, two sets of DIC system were installed toward the corners of the reinforced concrete prism, as shown in Figure 6-5. For each DIC system set, there are a pair of 12.3-MegaPixel digital cameras mounted on an aluminum bar, which is supported by a tripod. Each camera takes one picture every 10-sec during tests.

Figure 6- 5 DIC System in the Direct Tension Tests

Since the DIC system is a relatively new measuring method in the laboratory, validation with a traditional deformation measurement method is necessary to make sure the DIC system is appropriately utilized. The specimen's global elongation under test was utilized to validate the DIC measurement.
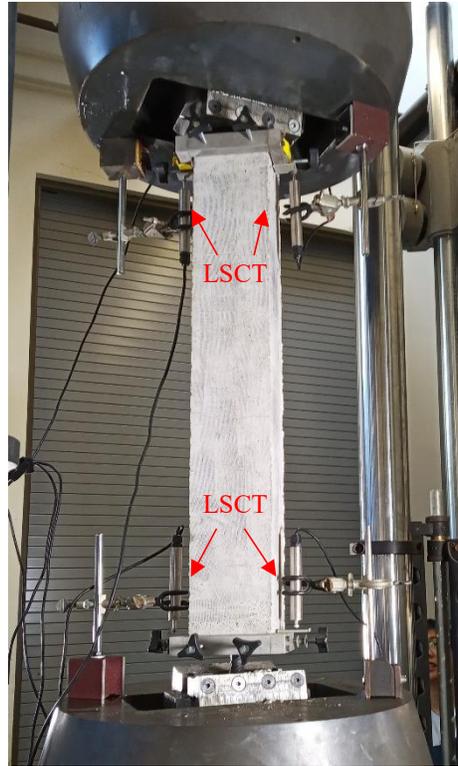
Figure 6- 6 Four LSCTs Mounted on the Specimen

The total displacement in the MTS machine includes the global elongation of the specimen under tensile load, elastic deformation at the extending bar, and the slips at top and bottom grips. Linear Strain Conversion Transducers (LSCT) are utilized to measure the slips at both ends. As shown in Figure 6-6, two LSCTs are mounted at the top head of the MTS machine to measure the slips in the top grip, while the other two LSCTs are mounted at the bottom head of the MTS machine to measure the slips in the bottom grip. The elongation of specimens can be computed as the following:

$$\Delta = \Delta_{MTS} - S_{top} - S_{bottom} \tag{6-2}$$

where:

Δ : Elongation of the specimen (inch)

Δ_{MTS} : Total displacement measured by the MTS machine (inch)

S_{top} : Bar deformation and slip in the grip measured by LSCTs at the top (inch)

S_{bottom} : Bar deformation and slip in the grip measured by LSCTs at the bottom (inch)

The average strains can be calculated based upon global specimen elongation as the following:

$$\mathcal{E}_{avg} = \frac{\Delta}{L_0} \qquad\qquad (6\text{-}3)$$

where:

L_0 : The length of the whole specimen (inch.).

$\mathcal{E}_{avg}$: Average strain of the whole specimen, and because the plane sections remain plane theory, the average strain in the concrete ($\mathcal{E}_{c,avg}$) and average strain in the reinforcing bar ($\mathcal{E}_{s,avg}$) are all equal to the average strain of the whole specimen ($\mathcal{E}_{avg}$), before and after concrete cracking. One example of the average strain measured by both the DIC system and LSCTs during a test is shown in Figure 6-7.
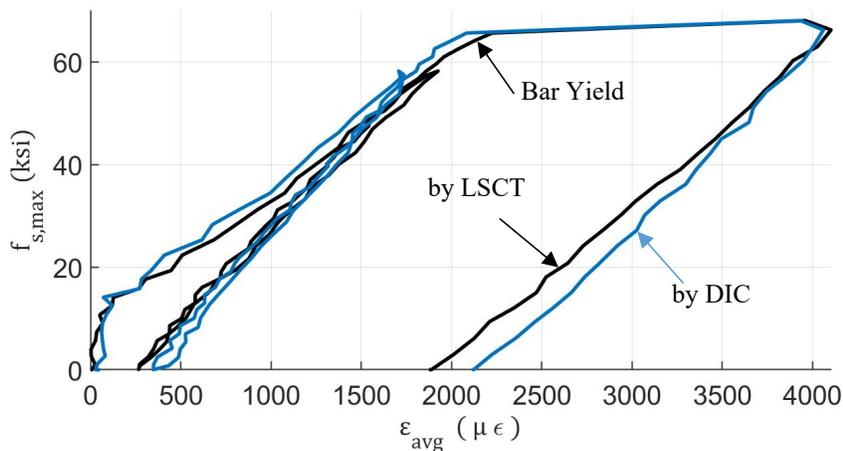
Figure 6- 7 Specimen Average Strain Measured by DIC and LSCT

As shown in Figure 6-7, those two plots of average strains, measured by DIC systems and LSCTs, respectively, match each other well in the loading and unloading procedures. However, the LSCTs mounted on the specimen surface will block some part of the specimen surface, which prevents the DIC systems obtains measurement on the whole surface field. Therefore, LSCTs were only utilized in the fist several testings to validate measurement from the DIC systems. After that, the LSCTs were removed from testing so that the DIC system can obtain measurement on the whole specimen surface.

6.5 Testing Result 1: Crack Initiation

Figure 6-8 shows the crack width measurement from P1-#6-sh as an example. For each crack, the opening width increases suddenly to approximately 0.0035-inch right after crack initiation, and then grows progressively with external force increasing. Therefore, the cracking process can be classified into two stages: crack initiation and crack developing. As the deck strains from field instrumentation in the bridge located in Round Rock, which is provided in Technical Memorandum No. 5, the crack opening right after crack initiation shares a majority part of the long-term crack width. Therefore, the crack initiation is highlighted in this subsection.
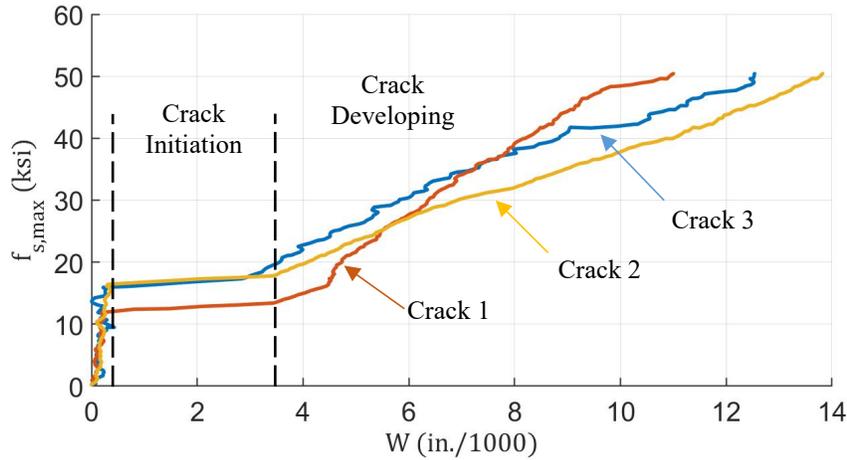
Figure 6- 8 Measured Crack Widths from P1-#6-sh

The reinforcing bar stress at cracks ($f_{s,max}$) when cracking occurred, and the crack width right after cracking initiation (W_i) of each specimen are summarized in Table 6-4. Generally, three cracks occurred in the specimens with #6 reinforcing bar, two or three cracks occurred in the specimens with #5 reinforcing bar, and two cracks occurred in the specimens with #4 or #3 reinforcing bar. The number of cracks in each specimen shows some correlation with the reinforcement ratio. The crack width right after cracking initiation (W_i) varies between 0.003-inch to 0.012-inch. All the W_i over 0.008-inch is marked as red in Table 6-4. Generally, these large crack widths are from specimens with #4 or #3 reinforcing bar. Increasing the reinforcement ratio show some benefits in controlling the crack width right after cracking.

Table 6- 4 Crack Initiation of Each Specimen

Specimen ID	Number of Cracks	Crack 1		Crack 3		Crack 3	
		$f_{s,max}$ (ksi)	W_i (in./1000)	$f_{s,max}$ (ksi)	W_i (in./1000)	$f_{s,max}$ (ksi)	W_i (in./1000)
P1-#4-ns	2	35.9	7.4	43.2	8.0	-	-
P1-#5-ns	3	19.7	3.7	24.2	4.7	38.9	3.9
P1-#6-ns	3	10.0	3.0	13.2	3.9	16.0	5.6
P1-#4-sh	2	32.2	9.3	34.9	8.7	-	-
P1-#5-sh	3	22.3	4.2	24.3	8.1	25.0	4.3
P1-#6-sh	3	11.7	3.5	16.1	3.0	16.1	3.5
P2-#4-ns	2	38.8	10.9	44.8	9.6	-	-
P2-#5-ns	2	24.4	4.5	27.6	5.7	-	-
P2-#6-ns	3	20.4	5.2	24.1	5.7	27.0	3.2
P2-#4-sh	2	34.8	7.0	36.6	8.1	-	-
P2-#5-sh	2	22.4	5.6	39.6	7.0	-	-
P2-#6-sh	3	15.2	4.2	18.1	4.8	25.2	2.0
P3-#3-ns	2	40.7	12.3	40.7	7.8	-	-
SP3-#3-ns	2	44.0	7.4	48.0	10.0	-	-

116

6.6 Testing Result 2: Crack Width verse Reinforcing Bar Stress

Currently, the crack width equation proposed by Frosh (1999) is commonly used in practice and adopted in the AASHTO LRFD (2017), which is expressed in the following:

$$W = 2\frac{f_s}{E_s}\beta\sqrt{d_c^2 + (\frac{s}{2})^2}$$
(6-4)

Where

W = most probable crack width (inch)

f_s = reinforcing bar stress under service loading (ksi)

E_s = elastic modulus of reinforcing bar (ksi)

d_c = thickness of cover from extreme tension fiber to the closed bar center (inch)

s = bar spacing (inch)

$\beta = 1.0 + 0.08 d_c$

However, reinforcing bar stress (f_s) utilized in the equation is not explicit, whether it should be the average or maximum reinforcing bar stress in the cracked region.

The relationship between crack width in each test and the maximum reinforcing bar stress is shown and compared in Figure 6-9. The color line plots are the average crack widths measured by the DIC systems, and the black dash line is the computed results from the crack equation utilized in the AASHTO LRFD. For reinforcement ratio (ρ) between 2.2% to 0.5%, the measurements of crack width after cracking initiation generally matches the trend of the calculation results. Soon after cracking occurred, the crack widths rapidly increase to approximate the predicted values. In addition, the relationship between maximum reinforcing bar stress and crack width is apparently independent of the reinforcement ratio. Lastly, the specimens with concrete shrinkage strains show a slight increase in the crack widths, compared with the other specimens cured in the water.
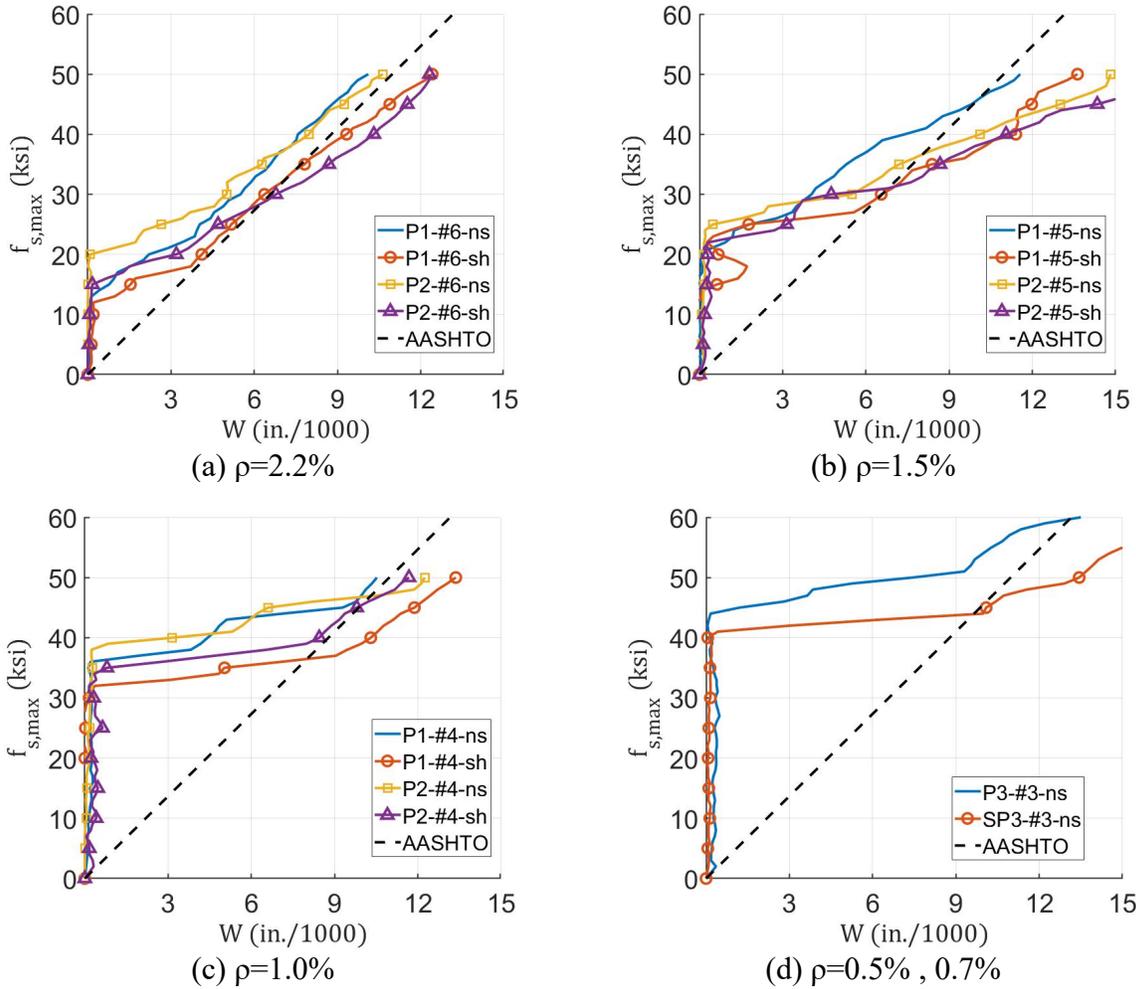
Figure 6- 9 Crack Widths verse Maximum Reinforcing Bar Stress

The relationship between crack width of each testing and the average reinforcing bar stress is shown and compared in Figure 6-10. The average reinforcing bar stress is derived from the average concrete surface strain measured by the DIC system. For the specimens with #6 reinforcing bar, the calculated crack widths based upon average reinforcing bar stress match well with measured crack widths. However, for the specimens with #5 reinforcing bar, the calculated crack widths are significantly smaller than the measurements, and for the specimens with #4 or #3 reinforcing bar, the calculated crack widths are approximated half of the testing results. Overall, the prediction of crack width based upon average reinforcing bar stress is dependent on the reinforcement ratio.
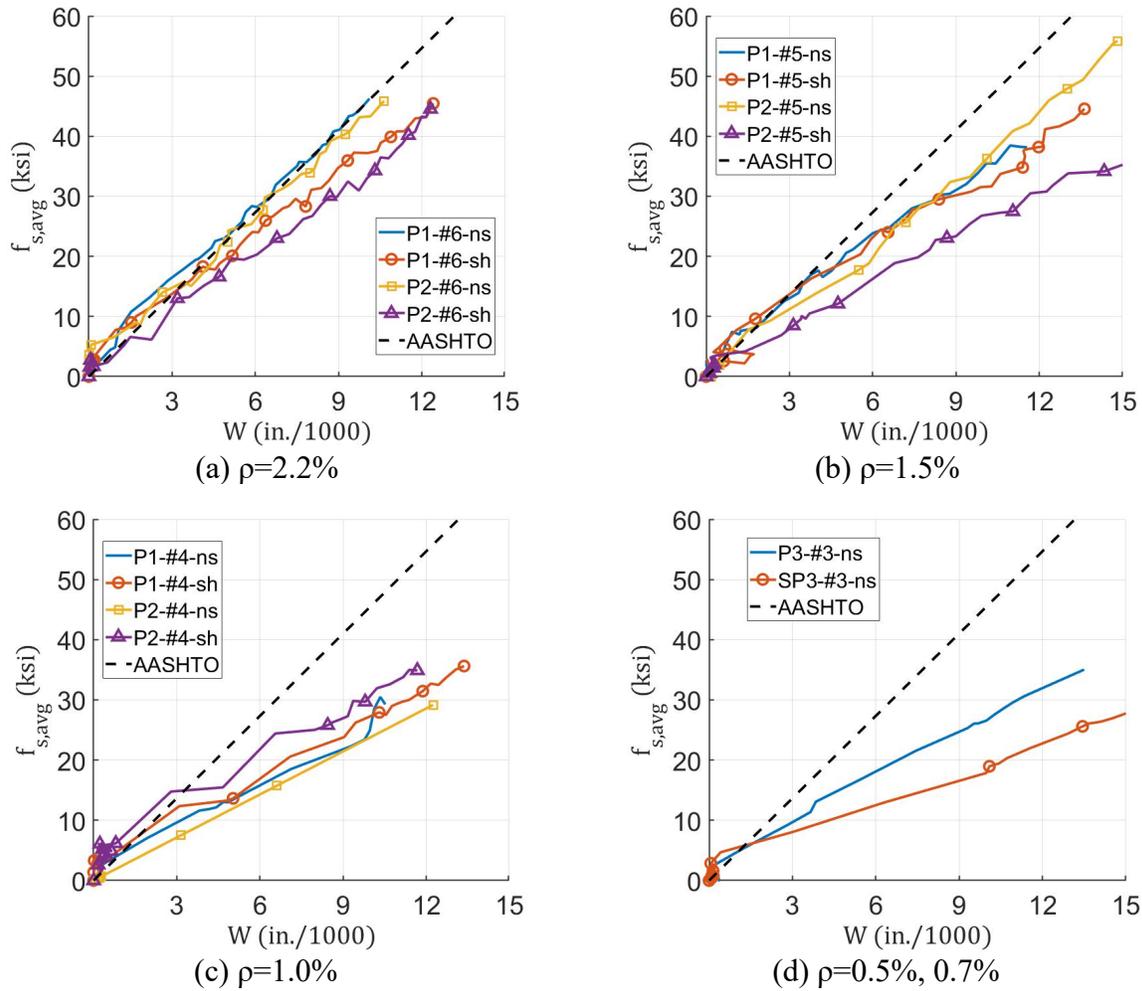
Figure 6- 10 Crack Widths verse Average Reinforcing Bar Stress

6.7 Testing Result 3: Concrete Tension Stiffening Effect

The tensile stress-strain response of concrete can be divided into two stages: pre-cracking and post-cracked. Generally, prior to cracking, the tensile response is assumed to be linear-elastic. For the concrete elastic-brittle model, the concrete tensile stresses diminish to zero after cracking, which is precisely for concrete at the cracked section. However, due to the bond action between the reinforcing bar and concrete, the tensile stresses still exist in the concrete between cracks. Therefore, the average tensile stress of cracked concrete should be existed but no larger than the concrete cracked strength.

One commonly used concrete tension stiffening model was developed by Collins and Mitchell in 1987, as shown in the following:

$$f_{ct} = E_c \times \varepsilon_{ct} \quad for \ 0 < \varepsilon_{ct} \leq \varepsilon_{cr} \qquad (6-5)$$

$$f_{ct} = \frac{f_{cr}}{1 + \sqrt{500 \times \varepsilon_{ct}}} \quad for \ \varepsilon_{cr} < \varepsilon_{ct} \tag{6-6}$$

Where

f_{ct} = concrete average tensile stress (psi)

ε_{ct} = concrete average tensile strain (in./in.)

f_{cr} = concrete cracking stress (psi)

ε_{cr} = concrete cracking strain (in./in.)

E_c = Modulus of elastic of concrete (psi)

The average concrete tensile stress in specimens is based upon the measured averaged strains of specimen and equilibrium theory. The calculation method is expressed in the following:

$$f_{ct} = \frac{N - \varepsilon_{avg}E_sA_s}{A_c} \tag{6-7}$$

Where

N = Total load in the MTS machine (kip)

ε_{avg} = Average strain of the specimen measured by the DIC system (in./in.)

E_s = Elastic modulus of reinforcing bar (ksi)

A_s = Area of the reinforcing bar (inch^2)

A_c = Area of concrete (inch^2)

The normalized tensile stress-strain responses of each testing are shown and compared in Figure 6-11. The black dash lines show the concrete tension stiffening behavior correlating with the Collins-Mitchell Model. Although the measured tensile stress-strain responses do not match the computed results very correctly, the tension stiffening effect is confirmed from specimens with the reinforcement ratio varies from 2.2% to 0.5%. When the average strain is five to ten times the concrete cracking strain, the average tensile stress in the concrete is approximately half of the concrete cracking stress.
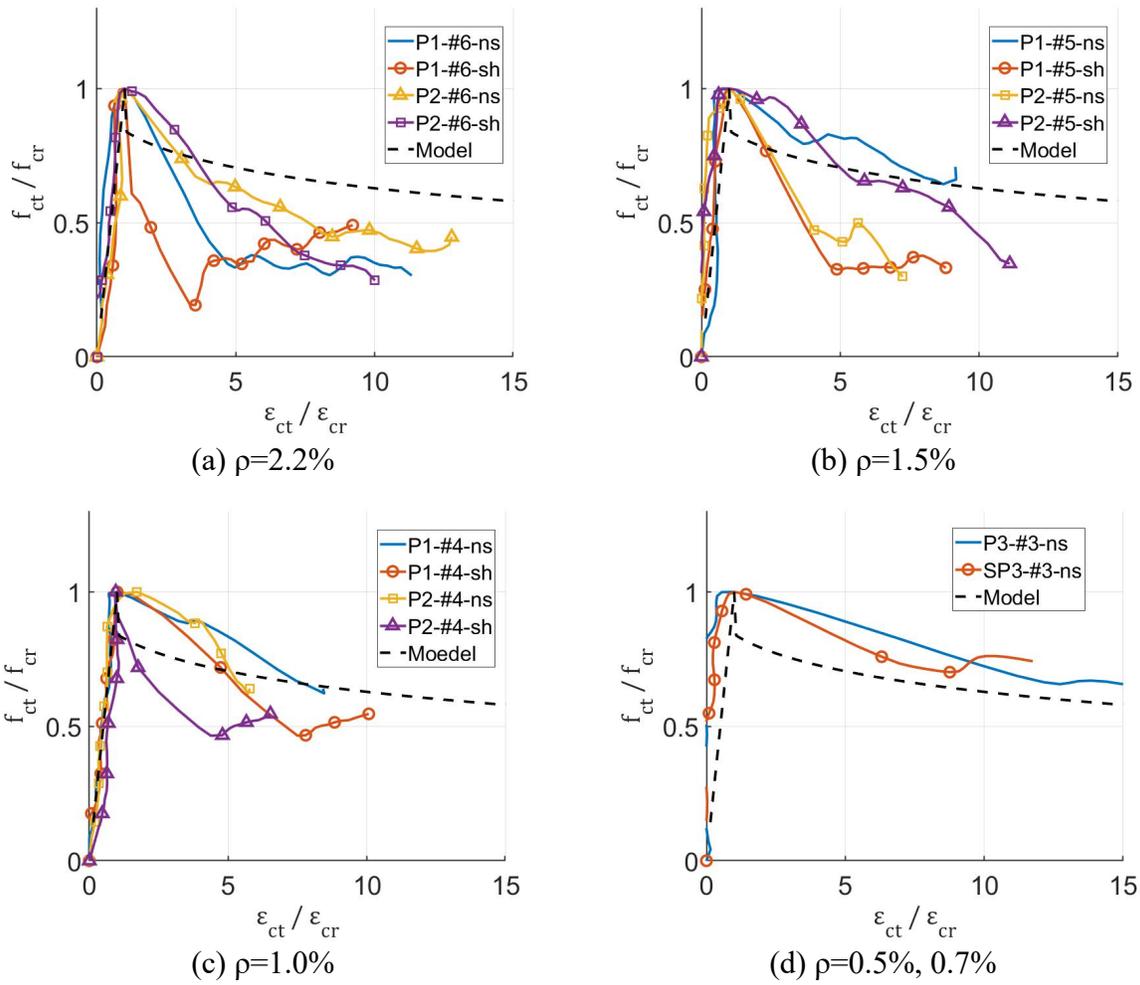
Figure 6- 11 Measured Concrete Tension Stiffening Effect

The probable reasons are listed in the following:

- The high inherent variability in the tensile behavior of cracked concrete.
- The specimens are 30-inch long, which might not be enough for the average strain measurement.
- The practical accuracy of the DIC system may not be accurate enough to measure the tension stiffening effect.

6.8 Summary

Direct tension tests were conducted on specimens with various concrete materials and reinforcing bar diameters. The reinforcement ratio of specimens under testing is between 0.5% to 2.2%. The following observation on the concrete cracking behavior can be made from the experimental program:

- Utilizing more reinforcing steel shows benefits in reducing cracking widths soon after crack initiation.
- The measured crack widths generally matched the predictions from the AASHTO crack width equation correlating with the maximum reinforcing bar stress.
- Concrete tension stiffening effect was observed in the cracked reinforced concrete specimens.

Chapter 7. Finite Element Modeling and Parametric Studies

7.1 Overview

According to the results of the large-scale laboratory testing and the AASHTO crack width equation, the maximum reinforcing bar stress is the most critical factor for the opening crack width. Factors that may have an influence on the maximum reinforcing bar stresses were considered in the parametric studies, such as the stiffness of the supporting girders, the deck reinforcement ratio, with or without PCPs as the form work for the CIP deck, and others.

Finite element models of continuous bridges with different span lengths and girder profiles were developed in Abaqus/CAE. To conduct a more extensive parametric study, the research team also developed a sectional analytical method based upon the concept of "plain sections remaining plain." The results from both methods were compared and verified by the field instrumentation results from two continuous concrete bridges in Round Rock, TX. For higher calculation efficiency, analytical modeling was selected as the primary method in the parametric studies.

7.2 General Assumption

Both steel and concrete girder systems were considered in the studies. For concrete girder systems, as typical representatives of continuous bridges, three-span continuous girder systems with TxDOT standard CIP-PCP concrete deck supported by precast concrete girders were the primary focus in the parametric studies. The length of mid-span (L) was varied between 130-ft to 320-feet, with 10-ft intervals. The exterior span lengths were symmetric with a length that was 1/1.3 of the mid-span, as depicted in Figure 7-1. According to the deck cracking behavior, the differences between continuous bridges supported by the concrete girders and steel girders are the girder stiffness and the AASHTO LRFD service load combination.
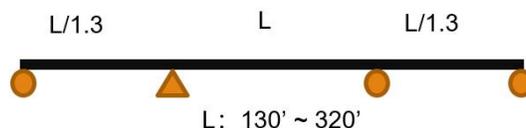
Figure 7- 1 Girder Layout of Three-span Continuous Bridge

Fully composite behavior was assumed between the supporting girder system and the concrete deck, which was comprised by 4-inch PCPs and a 4.5-inch CIP layer. Since these parametric studies focused on the concrete deck under service load, the supporting girders were assumed to remain elastic. However, based upon field observations, the concrete deck was assumed already cracked in the construction period.

Based on the TxDOT standard I-girder section and the girder details of the Round Rock Bridge, a series of simplified concrete I-girder were designed for the parametric studies. As shown in Figure 7-2, the girder depths varied between 60-inch to 200-inch, with identical dimensions in the top and bottom flanges, but variations in the web depth. The top flanges were

assumed as 42-inch wide and 5-inch thick, and the bottom flanges were assumed as 32-inch wide and 12-inch thick. The deck width over each supporting girder is considered as 90-inch.
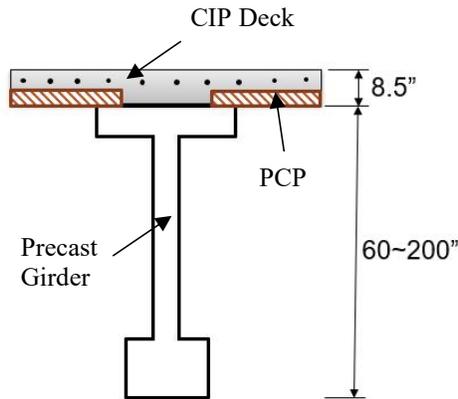
Figure 7- 2 Cross-section Utilized in the Parametric Studies

The compressive strength of the girder concrete was assumed as 6000-psi, meeting the material requirements of TxDOT. In the general analysis, the compressive strength of the CIP decks and the PCPs were assumed as 5000-psi. Since the reinforcing bar stresses might be sensitive to the deck concrete material properties, the strength of the deck concrete was considered as a critical variable in one of the parametric analysis.

Concrete decks supported by steel girders were also considered in the parametric studies. More information and analytical results for steel girders are provided in Section 7.3.

7.3 Service Load Combination

According to Section 3.4.1 of AASHTO LRFD (2017) design specification, the Service I load combination was applied on bridges with prestressed concrete girders, and the Service II load combination was applied on bridges with steel girders. These two service load combinations can be summarized as follows:

Service I = 1.0×(LL+IM)+0.5TG+TU+PS+SH +CR+SE   (7-1)

Service II = 1.3×(LL+IM)+TU+SH+SE   (7-2)

where:

LL+IM: live load effect and the dynamic allowance

TU: uniform thermal effect

TG: thermal gradient effect

PS: prestress forces in the precast girder

SH: concrete shrinkage effect

CR: concrete creep effect

SE: foundation differential settlements

The main differences between these two service load combinations are:

The "1.3" load factor for the *LL+IM* in *Service II* for steel girders

Considering 0.5TG for concrete girders but not for steel girders

Considering PS & CR for concrete girders only

More details about each term in the service load combination are described in the following subsections.

7.3.1 Live Load Effect

According to Section 3.6.1 of AASHTO LRFD (2017), the HL-93 design truck and design lane load were considered as the Vehicular Live Load. The total weight of one design truck is 72-kip, and one design lane load is 0.64-klf. For the critical negative moment over the interior piers, 90 percent of the effect of two design trucks spaced a minimum of 50-ft, combined with 90 percent of the effect of the design lane load. The two design trucks were placed in adjacent spans to produce the maximum force effects.

According to Section 3.6.2 of AASHTO LRFD (2017), the static effects of the design truck shall be increased with a dynamic allowance factor. For the service load combination, this factor is 33 percent. According to the influence line, the critical live load configuration for the negative moment region of the three-span bridge is shown in Figure 7-3.
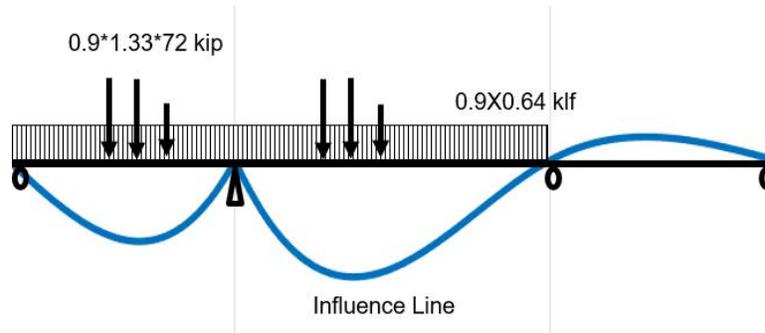
Figure 7- 3 Critical Live Load Configuration

According to Section 4.6.2.2 of AASHTO LRFD (2017), for the beam-slab bridges, the live-load distribution factor should also be applied to the live-load effects. For the bridges supported by I-shape girders, the critical case is for the moment in the external girder caused by one design lane. The "Lever Rule" should be used to calculate the distribution factor, and the 1.2 "multiple presence factors" shall also be included. The distribution factor was taken as 0.725 to simplify the analysis procedure.

7.3.2 Thermal Effects

For normal weight concrete and structural steel, the thermal coefficients of expansion were taken as 6.0 με/℉ and 6.5 με/℉ , respectively. With the assumption that the thermal coefficient for the concrete deck is the same as that of the precast girders, the uniform thermal

effect (TU) will not cause any restraint stress in the concrete deck. Therefore, TU was only considered in the steel girder systems. According to Section 3.12.2 of AASHTO LRFD (2017), the temperature range varies between 0 ℉ to 120 ℉ in the moderate climate region for steel girders would be applicable in Texas. A 60℉ rising temperature was considered as the uniform thermal effects in the concrete decks supported by steel girders.

The vertical temperature gradient (TG) in the concrete structures was also considered in the service limit combination. Following AASHTO LRFD Section 3.12.3, the temperature difference between the deck upper surface and the supporting girder was taken as 46℉. This temperature gradient effects causes compressive strains in the concrete decks, which is favorable for the deck cracking behavior. Therefore, the negative temperature gradient effects were applied in the analyses, with a factor as -0.3.

7.3.3 Concrete Shrinkage Effect

The magnitude of the concrete shrinkage strain depends on the environmental conditions, concrete material properties, specimen dimensions, and the concrete age. Based upon AASHTO LRFD Section 5.4.2.3.3, the volume shrinkage strains in the CIP concrete deck in Texas can vary between 400 με to 700 με, depending on the humidity condition. Detailed information in concrete shrinkage can be found in Chapter 2.

The differential shrinkage strains between the CIP concrete deck and the other precast concrete part or steel supporting girders can cause stresses related to the restraint from the concrete deck. For the parametric studies, a 500 με shrinkage strain was assumed in the CIP deck layer with no shrinkage in the PCPs or precast concrete girders.

7.3.4 Prestress Forces and Concrete Creep Effect

Due to the construction sequence, the concrete creep effect combined with post-tensioning forces in the precast girders might impact the behavior of the bridge decks. However, according to Section 5.9.2.3 of AASHTO LRFD, the maximum tensile stresses in the prestressed concrete should be no larger than 600-psi under Service I. The Service I is the combination of the live load effect and other permanent load effects, such as dead load, prestress forces, etc.

If the girder depth is between 1/20 to 1/25 of the span length, based upon elastic sectioning analysis, the calculated tensile stresses in the top flange of precast girder caused by the negative moment from the live load effect are no less than 1000-psi in tension. The stresses in the top flange caused by the permanent effects can be estimated as:

$$\sigma_{permanent} = \sigma_{Service\ I} - \sigma_{LL} \tag{7-3}$$

$$\sigma_{permanent} \leq 600\ psi - 1000psi \tag{7-4}$$

$$\sigma_{permanent} \leq -400psi \tag{7-5}$$

where:

$\sigma_{permanent}$: concrete stress in the top flange caused by the permanent effects

$\sigma_{Service\,I}$: concrete stress in the top flange caused by Service I load combination

σ_{LL}: concrete stress in the top flange caused by live load effects

Therefore, the top flanges of the precast girder should be under compression under the permanent effects. Consequently, the creep effect due to the permanent compressive stresses in the top flange will cause compressive strains in the concrete deck, which helps to reduce deck strains in the negative moment region. As a favorable effect combination to deck cracking behavior, the concrete creep effect, and prestressed forces in the precast girder can be assumed to compensate for each other. This conservative simplification effectively reduced the uncertainty from the design of the post-tensioning tendons.

7.3.5 Foundation Differential Settlement

For continuous bridges, differential settlement in the foundations can also cause negative moments in the critical regions. The magnitude of foundation settlements is generally dependent on the field geotechnical conditions, and the typical settlement value used in the bridge design practice is uncertain. To inspect a general influence of this effect , a one-inch foundation settlement was included in the load combination.

7.4 Reinforcing Bar Stress and Crack Width

As examined in the large scale laboratory tests, the maximum reinforcing bar stress at cracks can be derived from the average reinforcing bar stress in the cracked region, utilizing Equation 7-6:

$$f_{s,max} = f_{s,avg} + f_{ct}/\rho \qquad (7\text{-}6)$$

Where $f_{s,avg}$ is the average reinforcing bar stress, which can be calculated from finite element solutions or using an analytical solution; f_{ct} was the average tensile stress in the concrete after cracking, which can be determined by the concrete "Tension Stiffening Model;" ρ is the reinforcement ratio according to the CIP concrete area; and the term f_{ct}/ρ is the difference between the average reinforcing bar stress and maximum reinforcing bar stress, referred to as the additional reinforcing bar stress at cracks.

One commonly used concrete tension stiffening model was developed by Collins and Mitchell in 1987, as shown in the following:

$$f_{ct} = E_c \times \varepsilon_{ct} \quad for\ 0 < \varepsilon_{ct} \le \varepsilon_{cr} \qquad (7\text{-}7)$$

$$f_{ct} = \frac{f_{cr}}{1 + \sqrt{500 \times \varepsilon_{ct}}} \quad for\ \varepsilon_{cr} < \varepsilon_{ct} \qquad (7\text{-}8)$$

Where

ε_{ct} = concrete average tensile strain (in./in.)

f_{cr} = concrete cracking stress (psi), which

ε_{cr} = concrete cracking strain (in./in.)

E_c = Modulus of elastic of concrete (psi)

The crack width equation proposed by Frosh (1999) is broadly used in practice and adopted in the AASHTO LRFD (2017), which is expressed in the following:

$$W = 2\frac{f_{s,max}}{E_s}\beta\sqrt{d_c^2 + (\frac{s}{2})^2}$$

(7-9)

Where

W = most probable crack width (inch)

$f_{s,max}$ = the maximum reinforcing bar stress at cracks (ksi)

E_s = elastic modulus of reinforcing bar (ksi)

d_c = thickness of cover from extream tension fiber to the closed bar center (inch)

s = bar spacing (inch)

$\beta = 1.0 + 0.08d_c$

To examine factors that may influence the deck cracking behavior, a series of continuous bridges with various span lengths and girder depths were analyzed through analytical and finite element models.   An initial step in the procedure was the estimation of the average deck reinforcing bar stress under the service load combination. Next, the maximum reinforcing bar stress was obtained by the combination of the average reinforcing bar stress and the additional reinforcing bar stress at cracks. Finally, the probable crack width was predicted based upon the maximum reinforcing bar stress and the deck reinforcing layout.

Based upon existing equations, girder stiffness, deck concrete tensile stress, and deck reinforcing layout all influence the width of deck cracks. Therefore, these factors are examined in the following section.

7.5 Develop Finite Element Models

7.5.1 Develop Models for Prismatic Continuous Bridges

In order to verify the results from the analytical method, structural analyses were performed utilizing the general-purpose Finite Element Modeling Software Abaqus/CAE (2017). The overall geometry of the three-span continuous bridge model is depicted in Figure 7-4. Only one bay of the bridge has been modeled. The length of two side-span is 180-feet, and the mid-span length is 250-feet, with prismatic girder sections. Prismatic sections were implied in the previous modeling to minimize variables in the girder section. The girder depth "D" varied between 100 inches to 160 inches with an interval of 20 inches.
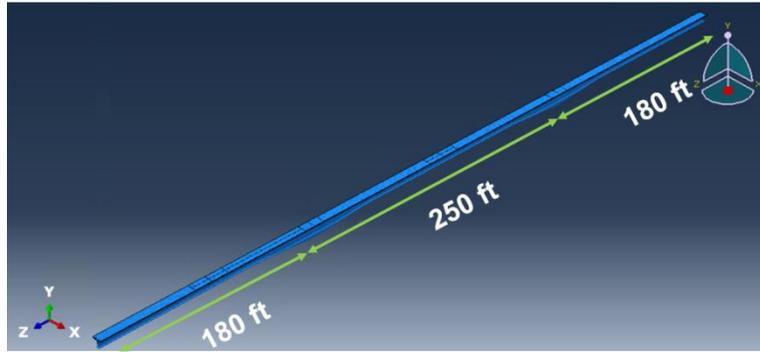
Figure 7- 4 Finite Element Model of Three-span Bridge

The model is assembled with five separate parts---the concrete girder with prismatic I-shape section, the CIP bridge deck, the two PCPs under the CIP deck, and the reinforcement bars. All components except the reinforcing steel were modeled with 3D solid element while the reinforcing bar was modeled with a 1D truss element. A total of 15 #6 reinforcing bars were created and embedded in the CIP deck with a total bar area of 1% of the CIP deck area. The compressive strength of the concrete in the supporting girders and the concrete decks were 6000-psi and 5000-psi, respectively.

Different parts of the model were assembled with certain constraints between their boundaries. For all concrete parts, tie constraint was used to attach each other together. The reinforcing bar was perfectly embedded in the concrete deck. Classic pinned and roller boundary conditions were used in this model.The loads acting on the FEA bridge model follow the AASHTO Service I load combination, and a shrinkage effect of 500-$\mu\varepsilon$ was imposed on all CIP concrete deck. All loads and shrinkage were introduced to the model instantly. The shrinkage is simulated by enforcing temperature change in the CIP deck.

7.5.2 Develop Models for the Round Rock Bridge

A two-dimensional finite element model for the instrumented bridge in Round Rock was also developed, as shown in Figure 7-5, to examine the influence of the non-prismatic girder sections. Detail information about this bridge can be found in Chapter 3. As depicted in Figure 7.5 (b), a haunched girder was utilized with a significantly deeper section in the negative moment region compared to the rest of the girder. In this region, a series of sections were implemented to model the various web depth and various bottom flange thickness.
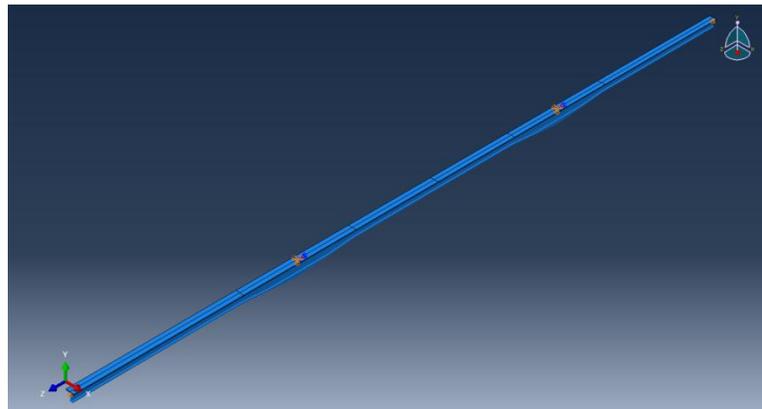
(a) Whole bridge
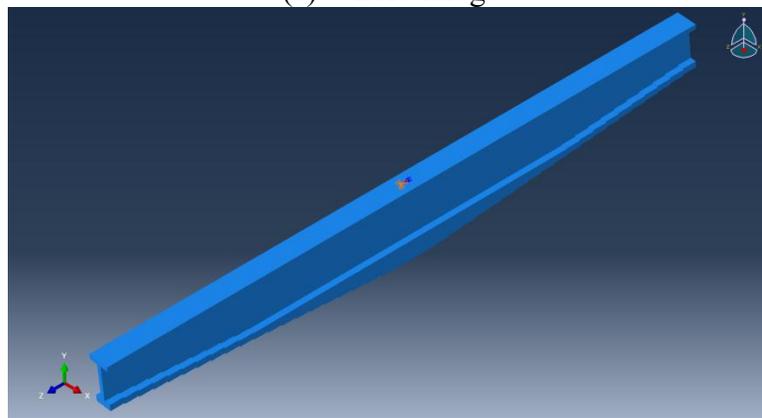
(b) Haunched girder

Figure 7- 5 Finite Element Model of the Round Rock Bridge

7.6 Validation of Parametric Modeling

7.6.1 Validation from Finite Element Modeling

Figure 7-6 shows a comparison of results of the maximum reinforcing bar stress calculated using Finite Element Models (black dots) and the analytical method (blue dots) when the deck reinforcement ratio is 1.0%. The parameter on the horizontal axis (L/D) is the length of the middle span over the girder depth and provides a measure of the stiffness of the supporting girder. It can be observed that the maximum reinforcing bar stresses from these two methods have a reasonable agreement.
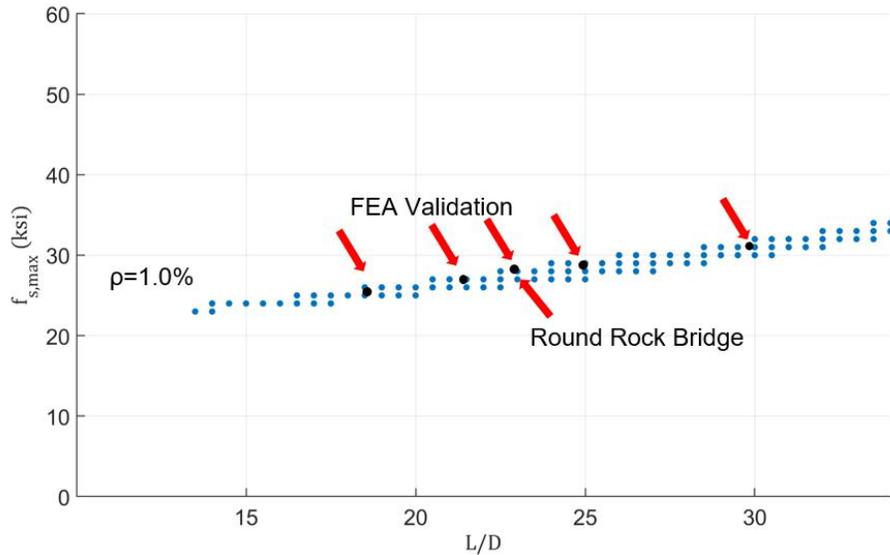
Figure 7- 6 Reinforcing Bar Stresses Comparison between FEA and Analytical Method

7.6.2 Validation from Field Instrumentation

The deck reinforcing bar stresses from the analytical method were also compared with the long-term monitoring record in the Round Rock bridges. The long-term changes in the average reinforcing bar stresses contributed to the deck shrinkage effects (SH); the differences between the maximum reinforcing bar stress and the average reinforcing bar stress were identified as the additional reinforcing bar stress at cracks (f_{ct}/ρ). The live load effects (LL) were recorded from the field load testing, which included four fully-loaded dump trucks. The daily fluctuation in the measured reinforcing bar stresses that were likely caused by the temperature changing, contributed to the thermal gradient effects (TG). Foundation settlements (SE) were not monitored in the field. More detail information related to the field instrumentation and field load testing in the continuous bridges is included in Chapters 3 & 4.

From the pie charts in Figure 7-7, with the reinforcement ratio varies from 2.2% to 0.8%, the predicted maximum reinforcing bar stresses are all slightly larger than the measured results. The average reinforcing bar stresses caused by SH, LL, and other effects do not change significantly with different reinforcement ratios. However, as the most significant proportion of the maximum reinforcing bar stresses, the additional reinforcing bar stresses caused by deck cracking increased with reductions in the reinforcement ratios.
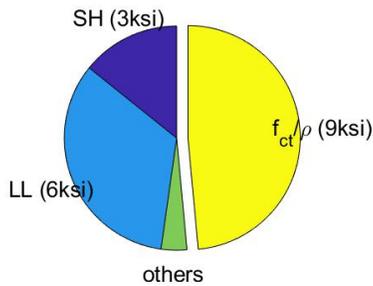
131
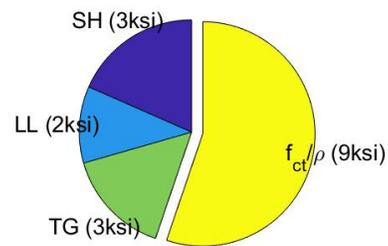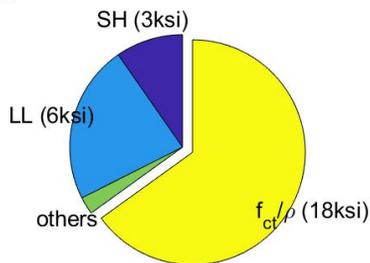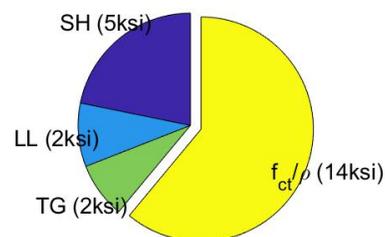
(a) Calculated, 2.2%
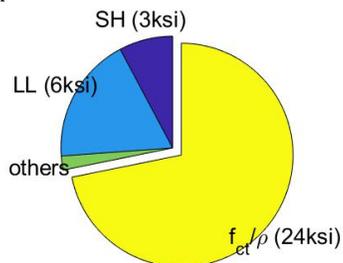
(b) Measured, 2.2%

(c) Calculated, 1.1%

(d) Measured, 1.1%

(e) Calculated, 0.8%
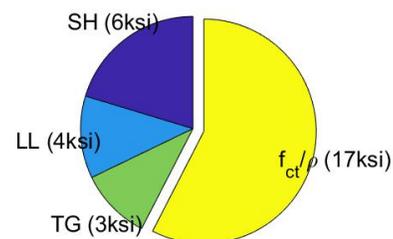
(f) Measured, 0.8%

Figure 7- 7 Reinforcing Bar Stresses Comparison between Field Instrumentation and Analytical Method

7.7 Results of Parametric Modeling

Through the analytical method, the maximum deck reinforcing bar stresses in the negative moment regions of three-span continuous bridges were calculated. As described in the previous section, the mid-span length varied between 130 and 320-feet, with an interval of 10-feet, and the lengths of the middle span and the side spans was maintained at a ratio of 1.3.

For each bridge with different span lengths, the girder cross-sectional was depth varied between 60-inches and 200-inches, with intervals of 10-inches. The ratio between span length and girder depth (L/D) provided an measure of the relative girder stiffness. In some cases, the

132

combination of span length and girder depth can result in an unfeasible L/D ratio. For example, The L/D ratio of a bridge with 320-feet span length and 60-inch girder depth is 64, and the deck reinforcing bar stress caused by service load combination can be higher than the acceptable stress level. Since the broadly used L/D ratios of the concrete bridges are between 20 to 25, the analytical results from bridges with L/D ratios are limited in this section to values between 10 and 35. Values outside this range are deemed unlikely and impractical.

7.7.1 Deck Reinforcement Ratio

The influence from the area of deck reinforcing steel is examined first. As shown in Figure 7-8, the maximum reinforcing bar stresses in the concrete deck with 0.5%, 1.0%, and 1.5% reinforcing steel inside are approximately 45-ksi, 30-ksi, and 25-ksi, respectively. Increasing the reinforcing steel from 0.5% of the deck area to 1.0% can significantly reduce the maximum reinforcing bar stress at cracks. Reductions in reinforcing bar stresses from increasing reinforcing steel from 1.0% to 1.5% of deck area did not show similar benefits.

Figure 7-8 also shows that the girder stiffness has a slight influence on the maximum stress of deck reinforcing steel when the girder stiffness is in a reasonable region. Compared to increasing girder depth, increasing the area of deck reinforcing steel will be more effective in reducing reinforcing bar stresses and deck surface crack widths.
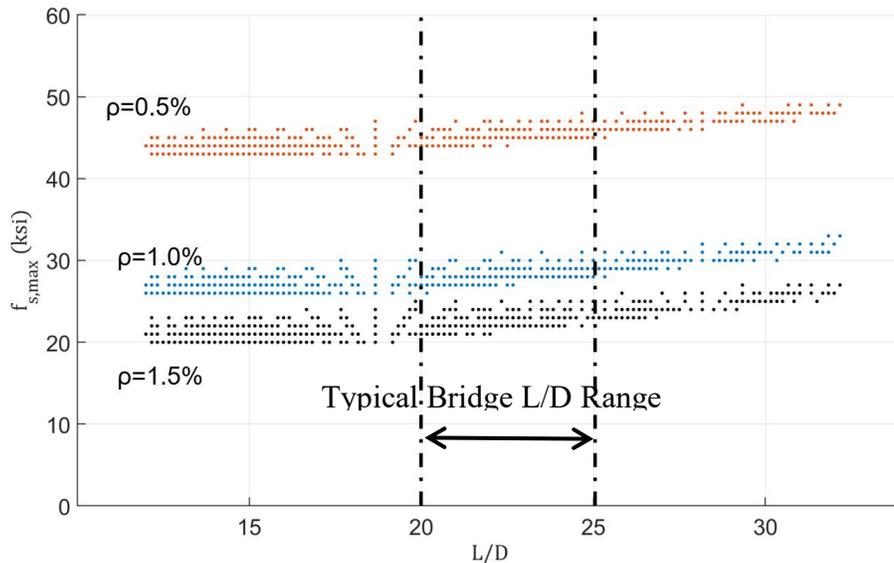
Figure 7- 8 Calculated Deck Reinforcing Bar Stresses While ρ Varies from 0.5% to 1.5%

7.7.2 The Influence of PCPs

As one of the TxDOT standard bridge design details, four-inch depth PCPs are utilized as the bottom layer of the 8.5-inch total depth concrete deck. However, an 8.5-inch full depth CIP concrete deck is also a feasible solution. To examine the influence of the PCPs, identical deck reinforcement details with #5 bars spaced at six-inches represented two different deck details since these cases provide a different reinforcement ratio. According to Equation 7-7, the maximum reinforcing bar stresses depend on the reinforcement ratio (ρ), which is defined as the ratio between the deck reinforcing bar area and the CIP concrete deck area. Because of the gap between each precast concrete panel in the longitudinal direction, the concrete deck in the

bottom layer can be assumed as already cracked. Therefore, no tensile force would be transferred from concrete to the reinforcing bar.

The analytical results of deck reinforcing bar stress in bridge decks with or without PCPs are shown in Figure 7-9. If the same reinforcement details are implemented, utilizing PCPs will have an insignificant influence on the average reinforcing bar stresses but can significantly reduce the maximum reinforcing bar stresses. As a result, from a deck shrinkage perspective, PCPs do not have a negative impact on the cracking behavior and actually reduce the reinforcing bar stress in the concrete deck over interior supports of continuously girders.
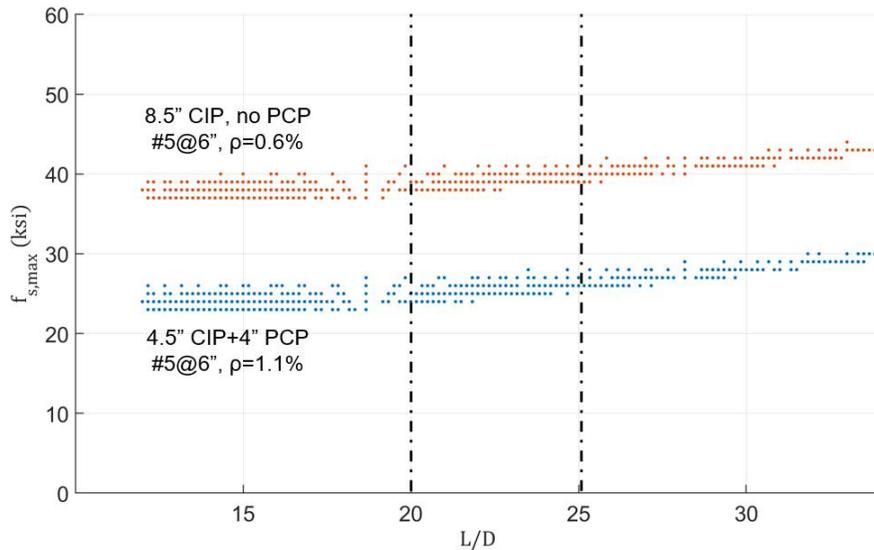
Figure 7- 9 Calculated Deck Reinforcing Bar Stresses in Bridge Deck with or without PCPs

7.7.3 Analytical Results of Steel Girders

Similar analytic studies were also conducted in the continuous bridges supported by steel plate girders. Since no standard section for steel plate girder is available from TxDOT, a simplified plate girder section was utilized to conduct the parametric study. As shown in Figure 7-10, the deck width over each girder is 90-inch, with the longitudinal reinforcing bar area as 1.0% of the CIP deck area. For different span length of bridges, the depths of prismatic girder varied between 60-inches and 100-inches, and the width of the top and bottom flanges were 30% of the girder depths. The flange thickness in the negative moment region was taken as three inches, and the web thickness was taken as one inch. The bridge layouts for the steel girder analysis are the same as the previous analysis of the concrete bridges, but the Service II load combination was applied.
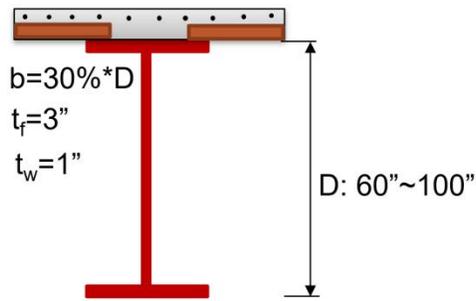
Figure 7- 10 Cross-section Utilized in the Steel Girder Analytical Studies

The maximum reinforcing bar stresses in the deck reinforcing bar over steel girders are shown in Figure 7-11. Not all the calculated results from the steel girders with one-inch flanges are shown in this figure, because their mid-span deflections were over L/800, not fulfilling the AASHTO LRFD design limit. The broadly used L/D for steel girders is between 25 and 30. If the reinforcement ratio is 1.0%, the maximum deck reinforcing bar stresses can be limited to approximately 30-ksi. A similar trend from steel girders and concrete girders in the maximum deck reinforcing bar stresses can be observed in Figure 7-8. The maximum deck reinforcing bar stresses mainly depend on the deck reinforcement ratio and slightly depend on the girder stiffness.
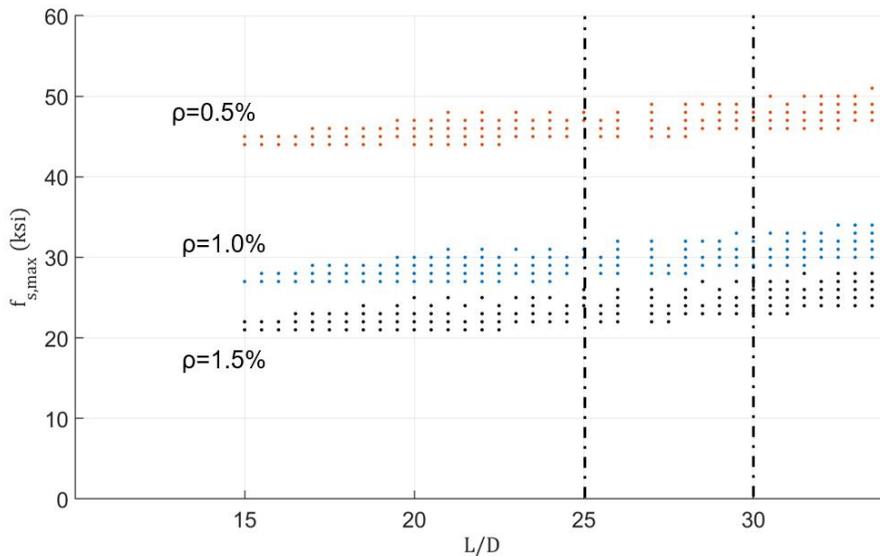
Figure 7- 11 Calculated Deck Reinforcing Bar Stresses in Bridge Deck with ρ Varying from 0.5% to 1.5%

The deck reinforcing bar stresses in the steel bridges are slightly larger than those in the concrete bridges. Part of this can be attributed to the 1.3 factor for the live load effect in the Service II combination, which makes the live load effects in steel bridges 30% larger than that in the concrete bridges.

7.8 Summary

For the parametric modeling of continuous bridge systems with PCPs, studies were carried out using both finite element method and analytical method are utilized in this task. The maximum deck reinforcing bar stresses are highlighted in the analysis. The reinforcing bar stresses from the two different methods generally had a well agreement, and also agreed well with the data obtained by the field instrumentation in the Round Rock bridges.

Based upon the parametric studies of the concrete deck in the native moment region of continuous bridges, the following conclusions can be made:

- The deck reinforcement ratio is the critical factor for the maximum reinforcing bar stress.
- If the longitudinal bar area can be 1.0% of the CIP deck area, the maximum reinforcing bar stresses can be limited to approximately 30-ksi under service load combination for both concrete and steel girder systems.
- Compared with the full depth CIP decks, utilizing PCPs in the bottom layer can significantly reduce the maximum reinforcing bar stresses, if the same deck reinforcement design is utilized.

Chapter 8. Design Methodology and Examples

8.1 Overview

Currently, most continuous girder systems in Texas have made use of steel girders since shorter segments can be shipped and bolted in the field. In recent years TxDOT has carried out research on spliced concrete girder systems, which are starting to be used in practice. However, the requirements in the negative moment region of continuous girders are unclear. Because of the composite action between the deck and its supporting girders, the longitudinal bars of the deck reinforcement participate in resisting negative moments.

Based upon the field monitoring, laboratory testing, analytical, and computational studies on the cracking behavior of bridge decks conducted in this project, the research team developed a design methodology and details for the deck reinforcement in continuous girder systems with PCPs.

8.2 Empirical Design Method for the Transverse Reinforcement

TxDOT has clear reinforcing guidelines and experiences for the concrete deck over simply supported girders. As shown in Section 2 of the TxDOT Bridge Manual-LRFD (2017), the Empirical Design Method is adopted for the concrete deck over I-girders, U-beams, steel plate girders, and steel tub girders. The concrete of the CIP deck should be Class S (f'c= 4.0 ksi), If the deck will be regularly subjected to de-icing agents, Class S (HPC) concrete should be used. "Use Grade 60 reinforcing steel. Use un-coated reinforcing steel unless the deck will be subjected regularly to de-icing agents based on district policy, in which case use epoxy-coated reinforcing steel." The standard top mat reinforcement design is #4 bars at 9-inch maximum spacing in both transverse and longitudinal directions, as shown in Figure 8-1. Place longitudinal bars closest to the top deck surface, with the clear cover as 2.5-inch. The reinforcement ratio in each direction is 0.5 percent of the cast-in-place portion of the deck (4.5-inches).
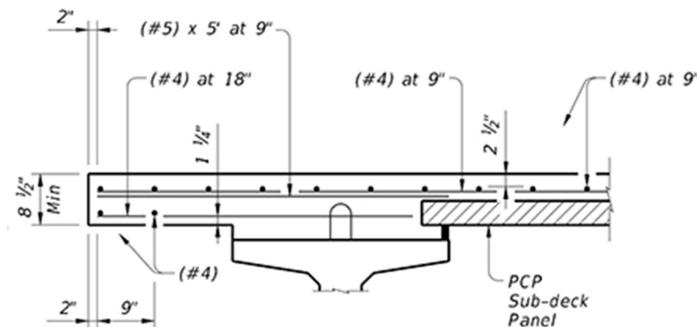
Figure 8- 1 TxDOT Deck Reinforcing Detail (Holt and Smith, 2014)

According to the Commentary 9.7.2.1 of AASHTO LRFD 2017, in the Empirical Design Method for concrete deck, " The additional longitudinal reinforcement provided for the slab in the negative moment region of continuous beams and girder-type bridges beyond that required for isotropic reinforcement according to the provisions of Article 9.7.2.5 (0.27 in^2/ft. of steel for each bottom layer and 0.18 in^2/ft. of steel for each top layer) need not be matched in the

perpendicular direction. Theoretically, this portion of the deck will be orthographically reinforced, but this does not weaken the deck." In other words, Empirical Design can still be utilized in the perpendicular direction, and the deck reinforcement detail in the transverse direction stays consistent in both positive and negative moment regions. The compressive strength of the girder concrete was assumed as 6000-psi, meeting the material requirements of TxDOT. In the general analysis, the compressive strength of the CIP decks and the PCPs were assumed as 5000-psi. Since the reinforcing bar stresses might be sensitive to the deck concrete material properties, the strength of the deck concrete was considered as a critical variable in one of the parametric analysis.

8.3 Proposed Design Method for the Longitudinal Reinforcement

As mentioned in the previous subsection, the longitudinal bars of the deck reinforcement participate in resisting negative moments in the negative moment regions of continuous bridge systems. A design procedure is proposed to estimate the maximum reinforcing bar stresses and deck surface crack widths under service load combination. The design procedure for the longitudinal deck reinforcement is outlined schematically in Figure 8-2.
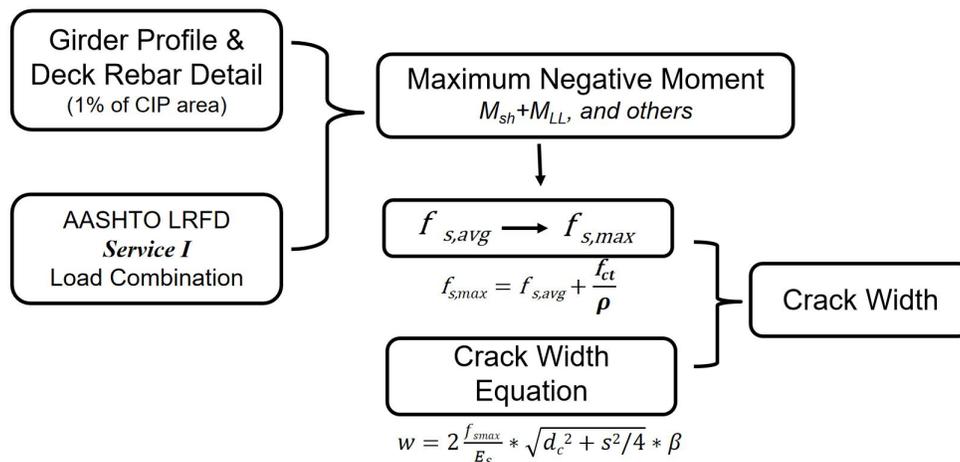
Figure 8- 2 Proposed Design Procedure for Longitudinal Deck Reinforcement in Negative Moment Regions

8.3.1 Step 1: Conditions for Deck Reinforcement Design

The maximum negative moment from gravity loads can be calculated through structural analysis based upon the girder profile and deck details. The TxDOT standard 4.5-inches CIP concrete deck over 4-inches PCPs deck design and 8.5-inches full depth CIP concrete deck are both applicable for the concrete deck in the negative moment region of continuous bridges.

According to Section 3.4.1 of the AASHTO LRFD (2017) Bridge Design Specifications, the Service I load combination should be applied on bridges with prestressed concrete girders, and the Service II load combination should be applied on bridges with steel girders. The effects considered in these service load combinations include effects from live loads, concrete shrinkage, changes in thermal environment (uniform and gradients), and foundation differential settlement effects.

One of the major differences between Service I and Service II is the load factor for the live load effects and the dynamic load allowance, with live load factors of 1.0 in Service I and 1.3 in Service II. Service II is applied primarily to control yielding of steel structures, but not to control crack widths in the reinforced concrete deck. The design limitations for bridge decks over precast concrete girders and steel girders are also different. According to the provisions for concrete structures in AASHTO LRFD Section 5.6.7, maximum steel stresses must not exceed 60 percent of the yield stress (0.6*fy=36-ksi) and the crack widths should be limited to acceptable levels (0.012-inch under humidity exposure conditions), under Service I. However, for steel structures in AASHTO LRFD Section 6.10.1.7, the design limitation in the area of reinforcement should be no less than one percent of the total cross-sectional area of the concrete deck. The provisions for steel structures are intended to ensure the nominal yielding of longitudinal reinforcement does not occur under the Service II load combination.

For the purposes of developing a design methodology, the research team does not believe there should be separate Service Level limits for the deck design in concrete girder bridges versus steel girder bridges. Therefore, a conservative approach is desirable. Based upon the numerical parametric studies in project 0-6909, with reasonable stiffness in the supporting girders, the maximum stresses in the longitudinal deck reinforcement caused by the Service I load combination should be limited to 36-ksi, with approximately 10-ksi of this stress caused by Live Load. Therefore, for concrete decks over either concrete girders or steel girders, using the Service I load combination and checking the corresponding crack widths will be a conservative approach. While typical analysis software can be used to evaluate the stresses from live load or temperature changes, commercial software that estimates the shrinkage moment is not available. Although general purpose finite element software can be used to obtain estimates of the shrinkage moment, such an approach is not practical for design. Therefore a simple method for evaluating shrinkage-induced stresses is necessary to avoid the need for general purpose finite element software. The following subsection outlines the simplified method that is proposed.

8.3.2 Step 2: Shrinkage Moment Calculation

Moments induced from free shrinkage occur in steel and precast concrete girder bridges and in both simply supported and continuous girder systems. This free shrinkage moment, caused by the different strain offsets between precast versus cast-in-place concrete decks, can be estimated by the following equation:

$$M_{fs} = E_{cip} A_{cip} \varepsilon_{sh}\, e \qquad\qquad (8\text{-}1)$$

where:

M_{fs} = free shrinkage moment

E_{cip} = elastic modulus of cast-in-place concrete deck

A_{cip} = area of cast-in-place concrete deck

ε_{sh} = free shrinkage strain per AASHTO LRFD Section 5.4.2.3

$e =$ distance between the center of cast-in-place concrete deck and the neutral axis of the composite girder section.

Although the concrete deck stiffness decreases after cracking, the elastic modulus of the uncracked concrete deck is conservatively utilized to estimate the free shrinkage moment here.

For statically-determinate structures such as simply-supported bridges, the free shrinkage moment is the only moment caused by concrete shrinkage. However, for indeterminate structural systems such as continuous bridges, the girder deflection caused by the effects of internal restraints induce a redistribution of vertical load resulting in changes in the support reactions. This redistribution of vertical reactions results in a component of the moment along the girder systems in the longitudinal direction. This mechanism is referred to as the secondary restraint effect or external restraint effect. The moment caused by the restraints from boundary conditions is the restrained shrinkage moment or secondary shrinkage moment. For example, for a three-span continuous bridge with CIP deck over steel girders, the secondary restraint effect due to deck shrinkage will increase the vertical reaction at the internal support, and reduce the vertical reactions at the end supports.

(a) Three-span Continuous Bridge

(b) Half Structure
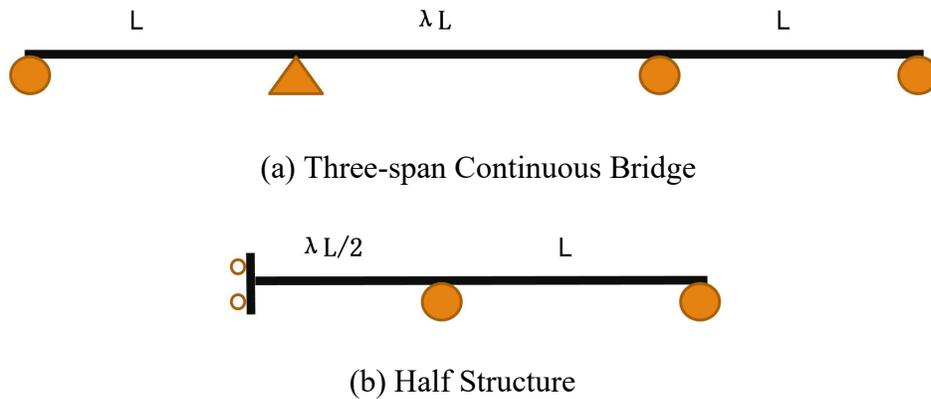
Figure 8- 3 Layout of The Design Example

A symmetric three-span continuous bridge is referenced as an example in Figure 8-3. The restrained shrinkage moment can be calculated through the principle of virtual work. Since the structure is symmetric, only half of the structure need be considered, as shown in Figure 8-4. The length of the middle span is represented as λL, where L is the length of the exterior spans. The general procedure consists of the following steps:

1. Remove the redundant vertical support at the end of the beam, and calculate the upward deformation caused by the free shrinkage moment, as described in Equation 8-2 and depicted in Figure 8-4.
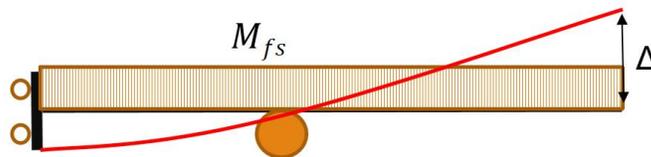
Figure 8- 4 Deformation Caused by the Free Shrinkage Moment

$$\Delta = \frac{M_{fs}(L^2 + \lambda L^2)}{2E_c I_c} \tag{8-2}$$

where:

Δ = the deformation at the bridge end

M_{fs} = free shrinkage moment

L = the length of the side span

λ = the ratio of the middle and side span length

E_c = effective elastic modulus of the composite girder section

I_c = effective moment of inertia of the composite girder section

2. Based upon the determinate structure without end support, calculate the relationship between the downward deformation at the end and the concentrated-force magnitude at that end, as described in Equation 8-2 and depicted in Figure 8-5.
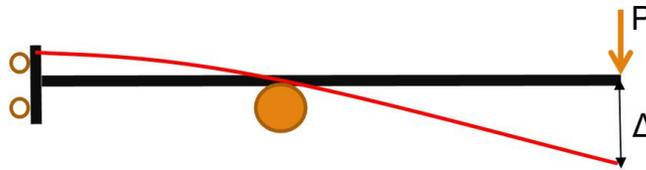
Figure 8- 5 Deformation Caused by the Restraint Force at Bridge End

$$\Delta = \frac{1}{2E_c I_c}\left(\frac{PL^3}{3} + \frac{\lambda PL^3}{2}\right) \tag{8-3}$$

where:

P = restraint force at the bridge end

3. Since there is no deformation caused by the shrinkage effect at the bridge ends, the upward deformation caused by the free shrinkage moment and the downward deformation caused by the point load should counteract each other. The amount of the restraint force at the bridge ends can be determined from this, as described in Equations 8-4 and 8-5.

$$\frac{M_{fs}(L^2+\lambda L^2)}{2E_c I_c} = \frac{1}{2E_c I_c}\left(\frac{PL^3}{3} + \frac{\lambda PL^3}{2}\right) \tag{8-4}$$

$$P = \frac{3 + 3\lambda}{2 + 3\lambda} \frac{M_{fs}}{L} \tag{8-5}$$

4, The restrained shrinkage moment in the continuous bridge can be computed using Equation 8-6.

$$M_{rs} = PL = \frac{3 + 3\lambda}{2 + 3\lambda} M_{fs}$$

<div align="right">(8-6)</div>

where:

M_{rs} = restrained shrinkage moment at the critical section

Equation 8-6 shows that the restrained shrinkage moment can be represented as a function of the factored free shrinkage moment, according to the ratio of the middle and side span length of a three-span continuous bridge. A common span ratio, λ, for three-span systems is between 1.0 to 1.5, which makes the factor $[(3+3\lambda)/(2+3\lambda)]$ approximately equal to 1.15 to 1.20. However, a two-span continuous bridge (with equal spans) can be treated as an extreme case of three-span continuous bridge with the span ratio as zero. Under this situation, this shrinkage moment factor $[(3+3\lambda)/(2+3\lambda)]$ can be up to 1.5.

While Equation 8-6 can be used to accommodate for differences in geometry of 3-span systems, practical values can be estimated as a factored free shrinkage moment, αM_{fs}. With the following recommended values:

$$M_{rs} = \alpha M_{fs}$$

Two-Span Bridge: $\alpha = 1.5$

Three-or-more span Bridge: $\alpha = 1.2$

After deck cracking, the free shrinkage moment located at the cracked section sharply drops due to the discontinuity of the concrete deck. Therefore, the shrinkage moment used to estimate the deck steel stress is the restrained shrinkage moment, rather than the combination of the free and restrained shrinkage moments.

8.3.3 FEA Analysis and Comparison

To validate the proposed method of estimating the shrinkage moments, comparisons were made between the proposed method and finite element analysis (FEA) results. Three-dimensional finite element models of two-span and three-span continuous bridges were developed in Abaqus. Solid elements were used to model the concrete deck, with embedded reinforcing bars, and shell elements were used to model steel supporting girders. The bridge layouts are shown in Figure 8-6 (a&b). The girder cross section and deck concrete strength of for a full-depth CIP deck were taken as those of the tested bridge located in Bastrop, TX, as shown in Figure 8-6(c). Detailed information of this bridge is described in Chapter 9. This bridge utilized PCP's with a CIP topping, so the concrete strength was taken from this bridge as a representative concrete strength. The area of longitudinal deck reinforcement is one percent of the area of the CIP deck. The free shrinkage strain of the CIP deck was assumed as -500 $\mu\varepsilon$.

Elastic behavior was assumed for the deck concrete, although the concrete deck would crack under shrinkage effects. To quantify the influence of concrete material nonlinearity, both linear and nonlinear material models were applied to the CIP deck. The nonlinear response of concrete under tension, considering the post-crack tension stiffening effect, is shown in Figure 8-6 (d).
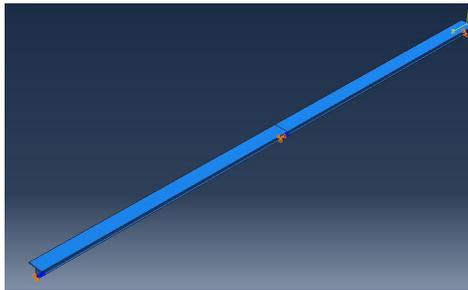
(a) 150-ft.+180-ft.
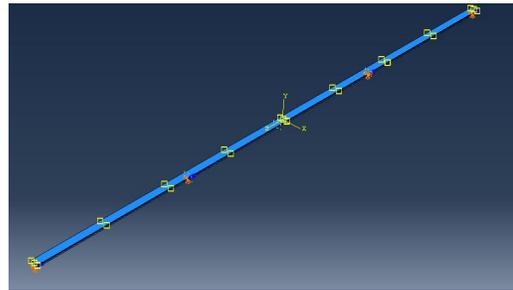
(b) 180-ft.+250-ft.+150-ft.
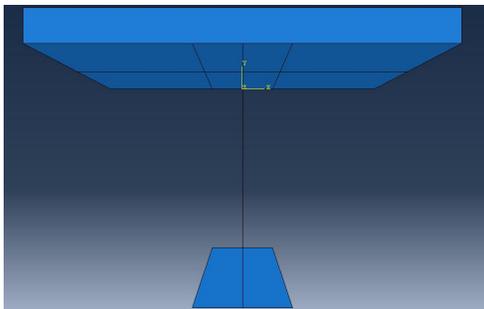
(c) CIP Deck over Steel Girder
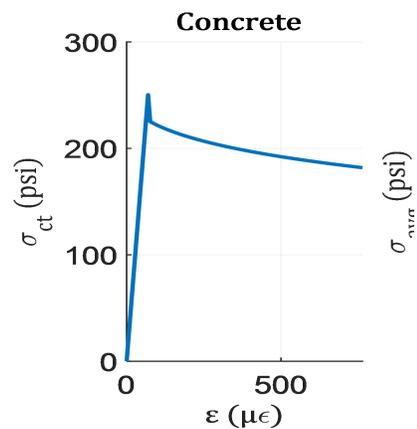
(d) Concrete Tension Stiffening Model

Figure 8- 6 FEA Models of Two-span and Three-span Bridges

The shrinkage moments estimated using each method at the section over an interior support, are shown in Table 8-1. For both two-span and three-span bridges, the shrinkage moment calculated by the proposed method and the linear FEA are close to each other, but significantly larger than that from the nonlinear FEA. Since the proposed method does not consider the post-crack nonlinearity in the deck concrete, the proposed method is valid in comparison with the linear FEA, and very conservative in comparison with the nonlinear FEA.

Table 8- 1 Comparison of Shrinkage Moment Estimation

	Proposed Method	Linear FEA	Nonlinear FEA
2-span Bridge	-4495 kft.	-4740 kft.	-1730 kft.
3-span Bridge	-3476 kft.	-3824 kft.	-1273 kft.

Therefore, a factor, k_e, is introduced to modify the modulus of elasticity of the deck concrete, to estimate the shrinkage moment caused by the cracked concrete deck. Under this scenario, Equation 8-1 is modified as follows:

$$M_{fs} = k_e E_{cip} A_{cip} \varepsilon_{sh} \, e' \qquad\qquad (8\text{-}7)$$

where:

M_{fs} = free shrinkage moment

k_e = factor for the effect of concrete cracking

E_{cip} = elastic modulus of cast-in-place concrete deck

A_{cip} = area of cast-in-place concrete deck

ε_{sh} = free shrinkage strain per AASHTO LRFD Section 5.4.2.3

e' = distance between the center of cast-in-place concrete deck and the neutral axis of the composite girder section, consider the factor for cracked concrete (k_e) in equivalent section.

Taking the two-span bridge as an example, the shrinkage moment, averaged deck bar stress, and maximum deck bar stress caused by shrinkage effects are shown in Table 8-2. Since the distance between the CIP deck and the neutral axis of the composite girder section is also changed, the influence of the k_e factor will be nonlinear for both shrinkage moment and rebar stresses caused by the shrinkage moment. As shown in Table 8-2, although the computed shrinkage moments vary significantly with changes in the k_e factor. However, the average and maximum deck reinforcement stresses are quite close to each other, as well as that from nonlinear FEA model. Consequently, the computed reinforcement stresses are quite insensitive to the k_e factor.

Table 8- 2 Influence of k_e Factor

	Nonlinear FEA	Proposed Method k_e=1.0	Proposed Method k_e=0.5	Proposed Method k_e=0.3
M_{rs}	-1730 kft.	-4495 kft.	-3070 kft.	-2158-kft.
$f_{s,avg}$	4.2 ksi	5.4 ksi	5.8 ksi	5.3 ksi
$f_{s,max}$	29.8 ksi	30.3 ksi	30.5 ksi	30.3 ksi

This section provides guidance on a simple method of evaluating the shrinkage moment for use in the proposed deck reinforcement design procedure. Key points from this report are as follows:

● Shrinkage moment is a part of the "Maximum Negative Moment", associated with live load effects, thermal gradients, and other service loads.

- For continuous bridges, the shrinkage moment consists of two parts: free shrinkage moment and restrained shrinkage moment.

- For the cracked section, the shrinkage moment used for deck steel stress is the restrained shrinkage moment, which can be estimated as a factored free shrinkage moment, αM_{fs}. With the following recommended values:

$$M_{rs} = \alpha M_{fs}$$

Two-Span Bridge: $\alpha = 1.5$

Three-or-More-Span Bridge: $\alpha = 1.2$

- The k_e factor is introduced to estimate shrinkage moment caused by the cracked concrete deck, but it has a minimum influence in deck steel stresses.

8.3.4 Step 3: Calculate Maximum Deck Reinforcing Bar Stress

The prestressed concrete girder or steel girder can be assumed elastic under service load combination. However, from the field instrumentation and numerical parametric analysis, the concrete deck can be assumed as already cracked. Therefore, the geometric property of the composite girder should be found on the cracked section. Only the longitudinal deck reinforcement but not the concrete deck should be considered in this sectioning analysis. The results from numerical parametric studies show that the average deck reinforcing bar stresses are not very sensitive to the reinforcement ratio, because the bending resistance caused by the deck reinforcement is insignificant compared with that from the supporting girder. The initial design value for the deck reinforcement can be taken as #5 bar at 6-inch spacing. Based upon "plane sections remain plane," the average longitudinal deck reinforcing bar stresses can be calculated as

$$f_{s,avg} = \frac{E_s M_{Service} \Delta}{E_{girder} I_{cr}}$$

(8-7)

Where:

$f_{s,avg}$ = Average deck reinforcing bar stress (ksi)

$M_{Service}$ = Total moment under service load combination (kip·inch)

I_{cr} = Moment of inertia of the cracked girder section (inch4)

Δ = Distance between the longitudinal deck reinforcement to the neutral axis (inch)

E_s = Elastic Modulus of reinforcing steel (ksi)

E_{girder} = Elastic Modulus of supporting girder (ksi)

The maximum reinforcing bar stress, which is corresponding to the concrete crack width, can be derived from the average reinforcing bar stress, as the following

$$f_{s,max} = f_{s,avg} + f_{ct}/\rho$$

(8-8)

Where:

145

$f_{s,max}$ = the maximum reinforcing bar stress at cracks;

f_{ct} = the average tensile stress in the concrete after cracking, which can be determined by the concrete "Tension Stiffening Model;"

ρ = reinforcement ratio determined by the area of longitudinal deck reinforcement and the area of the CIP concrete deck, which can be calculated as:

$$\rho = \frac{A_s}{s \times d_{cip}} \qquad (8\text{-}9)$$

Where:

A_s = nominal area of top-mat longitudinal bar (in^2);

s = bar spacing (in.);

d_{cip} = depth of CIP deck layer (4.5-inch);

One commonly used concrete tension stiffening model was developed by Collins and Mitchell in 1987, as shown in the following:

$$f_{ct} = \frac{f_{cr}}{1 + \sqrt{500 \times \varepsilon_{ct}}} \qquad (8\text{-}10)$$

Where

ε_{ct} = concrete average tensile strain (in./in.), which equals to the average tensile strain in the deck reinforcement as $f_{s,avg}/E_s$

f_{cr} = concrete direct tensile strength (psi), which can be taken as $4\sqrt{f'_c}$

f'_c = concrete compressive strength

Overall, the design equations in this subsection can be summarized as

$$f_{s,max} = f_{s,avg} + \frac{4\sqrt{f'_c}}{(1 + \sqrt{500 \times f_{s,avg}/E_s})\rho} \qquad (8\text{-}11)$$

8.3.5 Step 4: Deck Crack Width Prediction

The crack width equation proposed by Frosh (1999) is broadly used in practice and was adopted in the AASHTO LRFD (2017), which is given by the following expression:

$$W = 2\frac{f_{s,max}}{E_s}\beta\sqrt{d_c^2 + (\frac{s}{2})^2} \qquad (8\text{-}12)$$

Where

W = most probable crack width (inch)

$f_{s,max}$ = the maximum reinforcing bar stress at cracks (ksi)

E_s = elastic modulus of reinforcing bar as 29000 ksi

d_c = thickness of cover from deck surface to the closed bar center (2.5 in.)

s = bar spacing (inch)

$\beta = 1.0+0.08d_c$

The limitation of crack widths in bridge decks is dependent on the environmental condition of each individual project, and there is no universal conclusion on crack widths limitation from different design codes. ACI Committee 224 (2008) provides a "Guide for reasonable crack widths" in reinforced concrete under service load, as shown in Tab 8-3. The report also notes that "It should be expected that a portion of the cracks in the structure will exceed these values. With time, a significant portion can exceed these values. These are general guidelines for design to be used in conjunction with sound engineering judgment." Engineering experience on bridge deck cracking from bridges located in the adjacent area will be quite valuable. For bridge deck out of regions where deicing chemicals are utilized, 0.012-inch can be a reasonable crack width limitation. Otherwise, a stricter crack width requirement should be taken.

Table 8- 3 Reasonable Crack widths (ACI Committee 224, 2008)

Exposure condition	Crack widths	
	inch	mm
Dry air or protective membrane	0.016	0.41
Humidity, moist, soil	0.012	0.30
Deicing chemicals	0.007	0.18
Seawater and seawater spray, wetting, and drying	0.006	0.15
Water-retaining structures	0.004	0.10

If the predicted deck crack width is larger than the selected limit, the analysis for crack width is repreated with a new reinforcement detail. There are two options to reduce possible deck surface crack widths: increasing the diameter of the reinforcing bar and/or reducing the spacing between each bar. Since the average reinforcing bar stress is insensitive to the reinforcement ratio, the new maximum reinforcing bar stress can be derived from the existed average stress.

8.4 Design Example for Concrete Deck with PCPs

The girder cross-section used over the internal supports of the Bastrop steel girder bridge (see Chapter 9) will be used to illustrate the design procedure. This is a two-span continuous steel bridge, with TxDOT standard half-depth CIP concrete deck over PCPs. This bridge consists of two-span continuous girders with spans of 150-ft and 180-ft., and the depth of each steel girder is 5-ft, 3-inches, as shown in Figure 8-7. Detailed information about this bridge is provided in Chapter 9: Implementation Project: Field Instrumentation of Steel Girder Bridge with Partial Depth Precast Concrete Deck Panels.
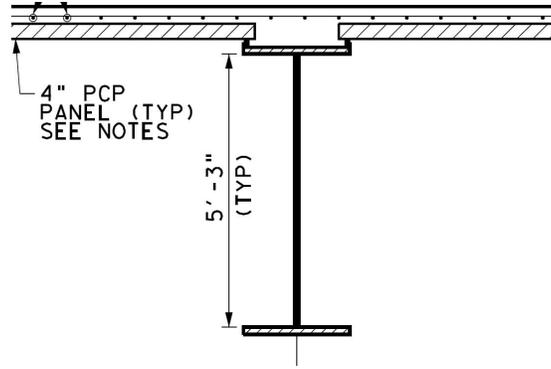
Figure 8- 7 Girder Cross-section of Design Example

Step 1: Conditions for Deck Reinforcement Design

Girder Sectional Properties (one girder):

Girder Spacing: 8.75-ft.

Girder Flange Width: 24-inch

Girder Flange Thickness: 1.75-inch

Girder Web Thickness: 5/8-inch

Moment of inertia of steel Girder: $I_g=1.01\times10^5$-$inch^4$

Steel Girder modulus of elastic: $E_s= 29000$-ksi

Concrete Deck Properties :

Deck depth: 4.5-inch CIP+4-inch PCP+2-inch haunch

Deck width: 89-inch over each girder

Longitudinal reinforcement design: #5 bars spaced at 6-inch in the CIP layer

Reinforcement yield strength: $f_y=60$-ksi

Elastic modulus of steel : $E_s=29000$-ksi

Clear cover: 2.5-inch

Deck concrete compressive strength: $f'_{cd}=5.0$-ksi

Deck concrete modulus of elastic: $E_{cip}=4030$-ksi

Moment of inertia of Composite Girder: $I_{tot}=1.89\times10^5$-$inch^4$

Distance between deck reinforcement to the neutral axis: $e = 19.4$-inch

Step 2: Shrinkage Moment Calculation

The free shrinkage strain (ε_{sh}) of the CIP deck was assumed as -500 µε, here. Shrinkage in PCPs is ignored.

Free shrinkage moment, per Equation 8-1:

$$M_{fs} = E_{cip}A_{cip}\varepsilon_{sh}\,e = 4030 * (4.5 * 89 + 6 * 24) * 500 * 10^{-6} * 19.4/12 = 1773\ kft.$$

Restrained Shrinkage Moment (two-span bridge so α = 1.5):

$$M_{rs} = \alpha M_{fs} = -1.5 M_{fs} = -\,2660\ kft.$$

Step 3: Calculate Maximum Deck Reinforcing Bar Stress

Service I Load Combination over interior support:

The moments from live load and thermal effects can be determine with commercial design software or other approaches. These moments are additive to the shrinkage effects.

Shrinkage Effect: $M_{rs}= -2660$-kft.

Live Load Effect: $M_{LL}= -4745$-kft. (Design Truck+Design Lane+Impact Allowance)

Thermal Effect and Foundation Settlement: $M_{etc}= -442$-kft

Total: $M_{Service}= -7847$-kft.

The average stress in the longitudinal deck reinforcement:

$$f_{s,avg} = \frac{E_s M_{Service}\,e}{E_{girder}I_{tot}} = \frac{29000 \times 7847 \times 12 \times 19.4}{29000 \times 1.89 \times 10^5} = 9.7\ ksi$$

The average tensile stress in the concrete after cracking:

$$f_{ct} = \frac{f_{cr}}{1 + \sqrt{500 \times \varepsilon_{ct}}} = \frac{4 \times \sqrt{5000}}{1 + \sqrt{500 \times \dfrac{9.7}{29000}}} = 201\ psi$$

The reinforcement ratio in the CIP deck layer:

$$\rho = \frac{A_s}{s \times d_{cip}} = \frac{0.31}{6 \times 4.5} = 1.1\%$$

The maximum stress in the longitudinal deck reinforcement:

$$f_{s,max} = f_{s,avg} + \frac{f_{ct}}{\rho} = 9.7 + \frac{0.201}{0.011} = 28.0\ ksi < 0.6 f_y$$

Step 4: Deck Crack Width Prediction

$$W = 2\frac{f_{s,max}}{E_s}\beta\sqrt{d_c{}^2 + (\frac{s}{2})^2} = 2\frac{28.0}{29000}(1 + 0.08 \times 2.5)\sqrt{2.5^2 + \left(\frac{6}{2}\right)^2} = 0.009 \; inch$$

If the bridge is not in a region where de-icing agents are regularly used, the exposure condition for the concrete deck falls into the category of "humidity, moist, soil" from Table 8-3 and the acceptable crack width can be taken as 0.012-inch. Therefore, the longitudinal deck reinforcement design #5 bars spaced at 6-inch is acceptable. The transverse deck reinforcement design and overhang reinforcement design both follow the current TxDOT standard design. The deck reinforcement detail is shown in Figure 8-8(a), and similar deck design details can be also utilized in the concrete deck over steel girders, as shown in Figure 8-8(b).
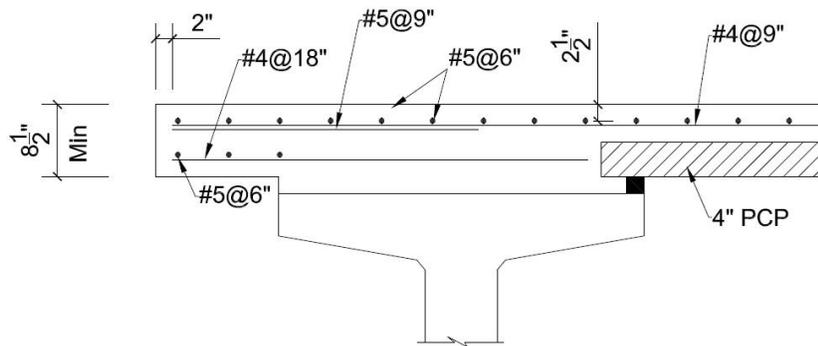
(a) Over Concrete Girder
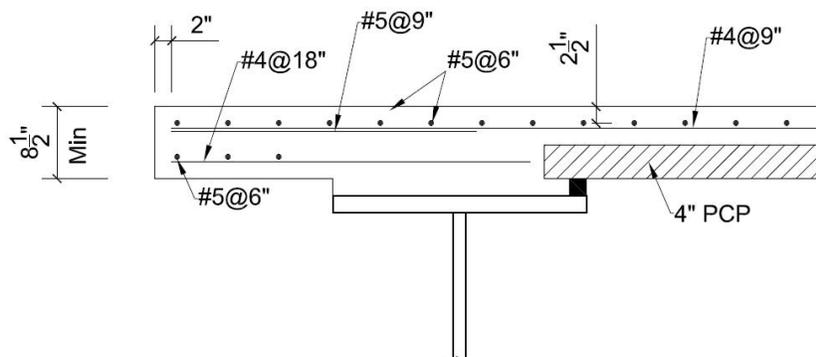
(b) Over Steel Plate Girder

Figure 8- 8 Deck Reinforcing Detail for Concrete Deck with PCPs

8.5 Relationship between Crack Width and Reinforcement Spacing

The spacing between longitudinal reinforcement is one of the critical parameters in the longitudinal deck reinforcement design. Increasing the bar spacing will increase the maximum bar stress and the crack width as well. If the bridge is located in the "dry air" area, where the crack width limitation can be taken as 0.016-inch, and #5 bars spaced at 9-inch reinforcement could be tried. The reinforcement ratio in the CIP deck layer:

$$\rho = \frac{A_s}{s \times d_{cip}} = \frac{0.31}{8 \times 4.5} = 0.76\%$$

The maximum stress in the longitudinal deck reinforcement:

$$f_{s,max} = f_{s,avg} + \frac{f_{ct}}{\rho} = 10.2 + \frac{0.182}{0.0076} = 34.2 \; ksi < 0.6 f_y$$

The calculated deck crack width:

$$W = 2 \frac{f_{s,max}}{E_s} \beta \sqrt{d_c^2 + (\frac{s}{2})^2} = 2 \frac{34.2}{29000} (1 + 0.08 \times 2.5) \sqrt{2.5^2 + \left(\frac{9}{2}\right)^2} = 0.015 \; inch$$
$$< 0.016 \; inch$$

The #5 bars spaced at 9-inch deck reinforcement design is acceptable in the "dry air" region.

In another case, if the bridge is located in the region subjected to de-icing chemicals, where the crack width limitation can be taken as 0.007-inch, #5 bars spaced at 4-inch reinforcement could be tried. The reinforcement ratio in the CIP deck layer:

$$\rho = \frac{A_s}{s \times d_{cip}} = \frac{0.31}{4 \times 4.5} = 1.7\%$$

The maximum stress in the longitudinal deck reinforcement:

$$f_{s,max} = f_{s,avg} + \frac{f_{ct}}{\rho} = 10.2 + \frac{0.182}{0.017} = 20.9 \; ksi < 0.6 f_y$$

The calculated deck crack width:

$$W = 2 \frac{f_{s,max}}{E_s} \beta \sqrt{d_c^2 + (\frac{s}{2})^2} = 2 \frac{20.9}{29000} (1 + 0.08 \times 2.5) \sqrt{2.5^2 + \left(\frac{4}{2}\right)^2} = 0.006 \; inch$$
$$< 0.007 \; inch$$

The #5 bars spaced at 4-inch deck reinforcement design is acceptable in the region subjected to de-icing chemicals. Overall, depending on different deck crack control performance requirements, changing the bar spacing can be an effective design option in practice.

8.6 Relationship between Crack Width and Deck Concrete Strength

As shown in Equation 8-7 and 8-8, the deck concrete strength has a direct connection with the maximum reinforcing bar stress and also has an influence on the deck crack width. According to the TxDOT Bridge Design Manual (2017), the design strength for the CIP deck layer should be 4.0-ksi. According to ACI-301R (2010), if 30 or more concrete cylinders were sampled, the standard deviation of concrete strength (std) could be determined, and the normal distribution curve of concrete strength can be determined as the plot in Figure 8-9. The relationship between characteristic strength (f'c) , required average strength (f'cr), and maximum possible strength (f'c,max) can be taken as:

$$f'_{cr} = f'_c + 1.34std \tag{8-13}$$

$$f'_{c,max} = f'_{cr} + 1.34std \tag{8-14}$$

When data is not available to establish standard deviation, the 1.34std can be taken as 1.2-ksi for concrete under 5.0-psi. Therefore, for the CIP concrete deck, whose f'c taken as 4.0-ksi, the average compressive strength can be taken as 5.2-ksi, and the maximum compressive strength can be taken as 6.4-ksi.
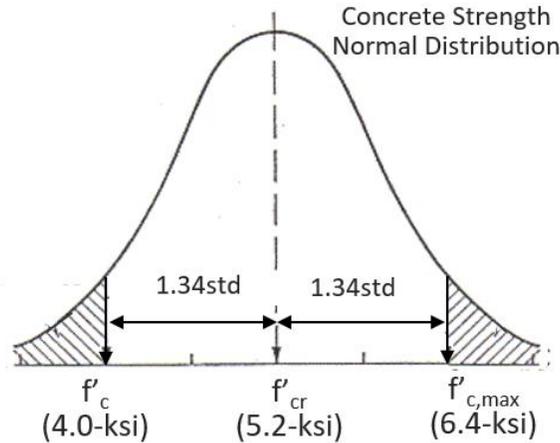
Figure 8- 9 Concrete Strength Normal Distribution

To accelerate the bridge construction process, and to make sure the measured material strength exceeds the specified strength, the deck concrete strengths are typically larger than 4.0-ksi. The compressive strength of concrete sampled in those four bridges from the field instrumentation are list in Table 8-4. The measured concrete strengths are between 4.8-ksi to 7.5-ksi.

Table 8- 4 Deck Concrete Compressive Strength

	San Marcos SH123	Bastrop SH71	Round Rock Ramp 20	Round Rock Ramp 21
f'_c *(ksi)*	7.5	5.1	4.8	5.4

The Round Rock Bridge in the previous subsection is still used as the design example to consider the influence of the deck concrete strength. With the deck concrete strength varying between 4.0-ksi to 6.4-ksi, and the deck reinforcement detail remains at #5 bars spaced at 6-inch, the results of the maximum reinforcing bar stresses and the calculated crack widths are summarized in Table 8-5.

Table 8- 5 Deck Concrete Strength v.s. Crack Width

f'_c	4.0 ksi	6.0 ksi	8.0 ksi
$f_{cr}=4\sqrt{f'_c}$	253-psi	310-psi	360-psi
Reinforcement Detail	#5@6-inch ($\rho = 1.1\%$)		
$f_{s,max}$	27-ksi	30-ksi	33-ksi
Crack Width	0.009-inch	0.011-inch	0.012-inch

These calculated results showed that the deck crack width could be 30% higher than the original estimation if the actual deck concrete strength is significantly higher than the 4.0-ksi design strength. A similar trend was also observed by Frosch et al. (2013) through field investigations on bridge deck cracks.

Because of the harmful influence from the high strength deck concrete, a design factor "k" can be applied to the concrete design strength, so that the additional reinforcing bar stress at cracks can be conservatively estimated in the deck reinforcement design procedure. The Design Equation 8-5 can be rewritten as:

$$f_{s,max} = f_{s,avg} + \frac{4\sqrt{kf'_c}}{(1 + \sqrt{500 \times f_{s,avg}/E_s})\rho} \tag{8-15}$$

Based upon ACI 301R (2010), if there is no specific information about the standard deviation of deck concrete strength, the design factor k can be taken as:

$$k = \frac{f'_{c,max}}{f'_c} = \frac{6.4\ ksi}{4.0\ ksi} = 1.6 \tag{8-16}$$

8.7 Design for Full-depth CIP Concrete Deck

While the focus of this investigation was primary considering PCPs in negative moment regions, the design procedure can also be utilized for full-depth CIP concrete decks over concrete or steel girders in negative moment regions. One major difference compared to the cases with the PCPs is that the full 8.5-inch deck depth should be considered to determine the deck reinforcement ratio, and bottom mat deck reinforcement will be necessary. According to the commentary in AASHTO LRFD 6.10.1.7, "where feasible, approximately two-thirds of the required reinforcement should be placed in the top layer." With reference to the design example in TxDOT Bridge Detailing Guide (2018), the longitudinal reinforcement detail in the top mat is one #4 bar and one #5 bar with spacing 4.5-inch placed next to each other, and #4 bar at 9-inch in the bottom mat. The reinforcement ratio is 0.93 percent of the total cross-sectional area of the concrete deck.

The average tensile stress in the concrete after cracking:

$$f_{ct} = \frac{f_{cr}}{1 + \sqrt{500 \times \varepsilon_{ct}}} = \frac{4 \times \sqrt{1.6 \times 4000}}{1 + \sqrt{500 \times \dfrac{10.2}{29000}}} = 230 \; psi$$

The reinforcement ratio in the CIP deck:

$$\rho = \frac{A_s}{A_{cip}} = \frac{0.31 + 0.2 + 0.2}{8.5 \times 9} = 0.93\%$$

The maximum stress in the longitudinal deck reinforcement:

$$f_{s,max} = f_{s,avg} + \frac{f_{ct}}{\rho} = 10.2 + \frac{0.23}{0.0093} = 34.9 \; ksi < 0.6 f_y$$

The crack width in the deck surface:

$$W = 2\frac{f_{s,max}}{E_s}\beta\sqrt{d_c{}^2 + (\frac{s}{2})^2} = 2\frac{34.9}{29000}(1 + 0.08 \times 2.5)\sqrt{2.5^2 + \left(\frac{4.5}{2}\right)^2} = 0.010 \; inch$$

Because reducing the spacing between the reinforcing bars has a positive influence on reducing deck crack width, this design detail, with bar spacing at 4.5-inch in the top mat, will be more conservative than using #5 bar spacing at 6-inch as the longitudinal reinforcement in both top mat and bottom mat. The deck reinforcement detail is shown in Figure 8-10.
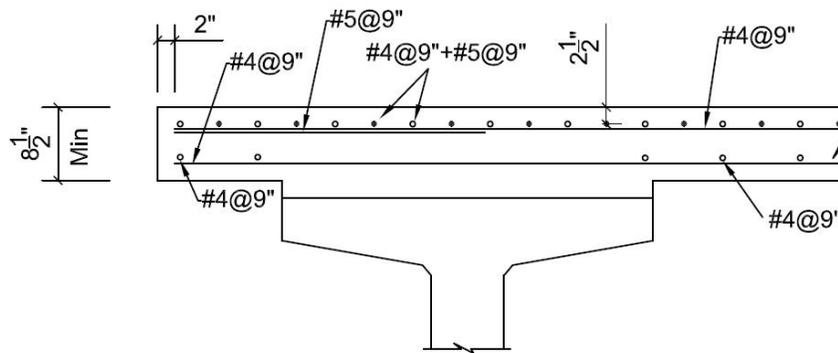
(a) Over Concrete Girder
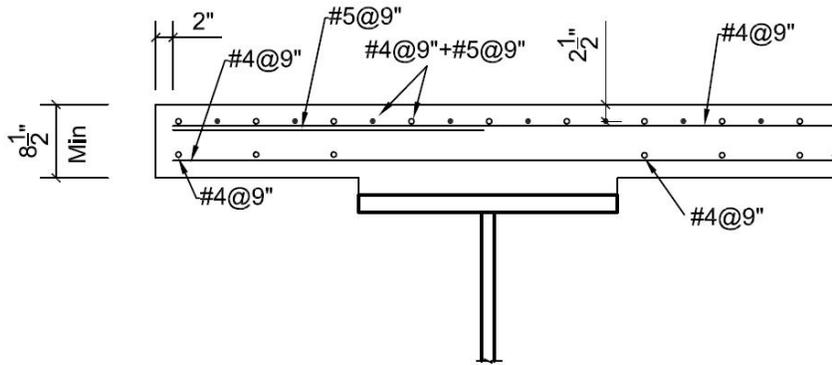
(b) Over Steel Girder

Figure 8- 10 Deck Reinforcing Detail for Concrete Deck without PCPs

8.8 Impact of Support Skew

Although the impact of support skew was not specifically investigated in Project 0-6909 or 5-6909, the first bridge instrumented in Project 0-6909, located on SH123 in San Marcos, TX, had a 45-degree skew. The girders were simply supported; however a poor-boy continuous deck was used with a crack initiator in the deck. Under long-term monitoring during construction and during field load testing, no significant differences in deck strains or deck surface crack widths were observed in this skewed bridge, compared with the results obtained from a similar bridge with normal supports and a poor-boy continuous deck that was instrumented on SH71 in Bastrop, TX. Several diagonal deck surface cracks were observed during the field load testing on the skewed bridge, as shown in Figure 8-11. Most crack origins started at the bent cap center-line at the girder locations. From there, the cracks typically propagated at a diagonal to the adjacent girder. The diagonal cracking pattern is believed to be due to the skew of the bridge. However, the cracks were too small to be read with the crack width indicator. The cracks were primarily visable when the four loaded dump trucks were on the bridge. All cracks closed after the trucks were removed.
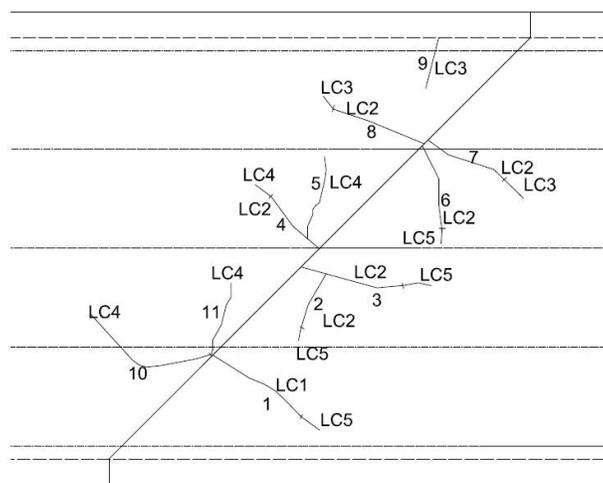
Figure 8- 11 Crack Diagram in San Marcos Bridge

Nouri and Ahmadi (2012) studied the influence of skew angle on continuous composite girder bridges. The general conclusion included:

- "An increase of skew angle causes a reduction in both the exterior and interior support moment girders. The reduction was about 10% for skew angles less than to 20° and it reached 33% for a skew angle of 45°."

- "With an increase of skew angle, the shear decreased significantly in the interior girders. It increased in the exterior girders at the pier support of continuous composite two-lane bridges."

The deck surface crack widths or stresses in deck reinforcement depends on the girder moments, instead of shear forces. In other words, support skew may be beneficial for deck cracking control. However, to control probable diagonal deck cracking, the details of deck transverse reinforcement over interior supports may need to be examined in future research.

8.9 Proposed Changes to AASHTO

The findings in this study can be used to propose changes or modifications to the AASHTO Specification and Commentary related to deck reinforcing details in the negative moment regions of continuous girders. The following subsections identify potential regions that changes can be made. In the recommendations summarized below, the current 9th edition provisions are presented as "Original" followed by draft changes presented as "Recommendation".

8.9.1 AASHTO LRFD Section 6: Steel Structures

Original: 6.10.1.7-Minimum Negative Flexure Concrete Deck Reinforcement

"Wherever the longitudinal tensile stress in the concrete deck due to either the factored construction loads or Load Combination Service II in Table 3.4.1-1 exceeds ϕ f_r, the total cross-sectional area of the longitudinal reinforcement shall not be less than one percent of the total cross-sectional area of the concrete deck."

The required reinforcement should be placed in two layers uniformly distributed across the deck width, and two-thirds should be placed in the top layer. The individual bars should be spaced at intervals not exceeding 12.0 in.

Recommendation:

Wherever the longitudinal tensile stress in the concrete deck due to either the factored construction loads or Load Combination Service II in Table 3.4.1-1 exceeds ϕ f_r, the total cross-sectional area of the longitudinal reinforcement shall not be less than one percent of the total cross-sectional area of the concrete deck. When partial-depth precast deck panels are used in conjunction with a cast-in-place topping slab, the total cross-sectional area of the longitudinal reinforcement in the cast-in-place layer shall not be less than one percent of the total cross-sectional area of the cast-in-place deck.

The required reinforcement should be placed in two layers uniformly distributed across the deck width, and two-thirds should be placed in the top layer. The individual bars should be spaced at intervals not exceeding 12.0 in. Smaller diameter reinforcement with closer spacing between individual bars are desired to control the width of deck cracks. When partial depth

precast deck panels are used as deck forms, it may not be possible to place the longitudinal reinforcement in two layers. In such cases, the reinforcement should be placed in a single layer.

8.9.2 AASHTO LRFD Section 9: Decks and Deck Systems

Original: 9.7.2-Empirical Design

9.7.2.6—Deck with Stay-in-Place Formwork

Stay-in-place concrete formwork shall not be permitted in conjunction with empirical design of concrete slabs.

Recommendation:

9.7.2.6—Deck with Stay-in-Place Formwork

Using partial depth Precast Concrete Panels (PCPs) as stay-in-place concrete formwork shall be permitted in conjunction with empirical design of concrete slabs.

New Section: 9.7.2.7—Minimum Deck Reinforcement in Negative Moment Region

In locations that the longitudinal tensile stress in the concrete deck due to either the factored construction loads or Load Combination Service I in Table 3.4.1-1 exceeds $\phi\, f_r$, the total cross-sectional area of the longitudinal reinforcement shall not be less than one percent of the total cross-sectional area of the concrete deck. When partial depth precast deck panels are used as deck forms, the total cross-sectional area of the longitudinal reinforcement shall not be less than one percent of the total cross-sectional area of the cast-in-place deck. ϕ shall be taken as 0.9 and f_r shall be taken as the modulus of rupture of the concrete determined as follows:

- For normal-weight concrete:

$$f_r = 0.24\, f'_c$$

- For lightweight concrete: f_r is calculated as specified in Article 5.4.2.6,

The reinforcement used to satisfy this requirement shall have a specified minimum yield strength not less than 60.0 ksi; the size of the reinforcement should not exceed No. 6 bars.

8.9.3 TxDOT Bridge Design Manual - LRFD

Chapter 3, Section 2: Concrete Deck Slabs on I-Girders, U-Beams, Spread Box Beams, Spread Slab Beams, Steel Plate Girders and Steel Tub Girders

Original:

Materials: Use Class S concrete (f'_c= 4.0 ksi). If the deck will be subjected regularly to de-icing agents based on district policy, use Class S (HPC) concrete.

Design Criteria: Top mat reinforcement is No. 4 bars at 9 in. maximum spacing (0.27 sq in/ft) in both transverse and longitudinal direction. Place longitudinal bars closest to the top slab surface. In the overhangs, place No. 5 bars extending 2 ft. minimum past fascia girder web centerline between each transverse No. 4 bar.

Recommendation:

Materials: Use Class S concrete (f'c= 4.0 ksi). If the deck will be subjected regularly to de-icing agents based on district policy, use Class S (HPC) concrete. Lower strength deck concrete is desired to minimize deck crack width.

Design Criteria: Top mat reinforcement is No. 4 bars at 9 in. maximum spacing (0.27 sq in/ft) in both transverse and longitudinal direction. Place longitudinal bars closest to the top slab surface. In the overhangs, place No. 5 bars extending 2 ft. minimum past fascia girder web centerline between each transverse No. 4 bar. In the negative moment region, there are two options depending on the designers preference. Option 1: place No. 5 bars at 6 in. maximum spacing (0.62 in^2/ft). Option 2: place No. 5 bars at 9 in. maximum spacing in addition to the No. 4 bars at 9 in. max. spacing (0.68 in^2/ft) in the longitudinal direction in top mat. All reinforcing steel should extend at least one development length (L$_d$) past the point of contraflexure. Option 1 provides the minimium recommended amount of reinforcing steel. Option 2 may lead to improved efficiency since the No. 5 bars at 9 in. spacing are easy to add to the No. 4 bars spaced at 9 in. from the positive moment region details.

8.10 Summary

A design methodology and several examples are provided in this Technical Memorandum. Several key points can be highlighted here.

- The design detail of transverse deck reinforcement in the negative moment region can follow the existing empirical design in the TxDOT design manual: using #4@9-inch plus #5@9-inch in the top mat and #4@9-inch in the bottom mat.
- For the cracked section, the shrinkage moment used for deck steel stress is the restrained shrinkage moment, which can be estimated as a factored free shrinkage moment, with a factor between 1.2 to 1.5 for continuous bridges, depending on the ratio of the middle and side span lengths.
- The k_e factor is introduced to estimate shrinkage moment caused by cracked concrete deck, but it has a minimum influence in deck steel stresses.
- The maximum reinforcing bar stress in the longitudinal deck reinforcement should be limited to 36-ksi under Service I load combination.
- If the area of deck longitudinal reinforcement is approximately one percent of the area of the CIP concrete deck area, the deck crack width can be limited to 0.012-inch.
- Reducing the spacing between longitudinal reinforcement is an effective method to reduce possible deck crack width.
- Support skew may be beneficial for deck cracking control. The details of deck transverse reinforcement over interior supports may need to be examined in future research.

Chapter 9. Implementation Project: Field Instrumentation of Steel Girder Bridge with Partial Depth Precast Concrete Deck Panels

9.1 Overview

The University of Texas at Austin completed TxDOT Research Project 0-6909 (Designing for Deck Stress over Precast Panels in Negative Moment Regions) in December of 2019. The investigation focused on the design for deck stresses over precast concrete panels (PCPs) in the negative moment regions of continuous concrete or steel girders. The study provided recommendations on the required deck reinforcing steel in the negative moment regions to control deck cracking resulting from a variety of sources. The sources leading to cracking include concrete shrinkage as well as strains introduced from temperature changes and in-service loading. Field monitoring from the original study focused on four bridges with concrete girders with PCPs including traditional applications on simply-supported prestressed concrete girders as well as two spliced prestressed concrete girders.

Although PCPs have long been used in Texas on precast prestressed concrete girders, there is significant interest in using PCPs on steel girder systems. The use of PCPs on steel girder systems has the potential to improve the economy and efficiency of steel girder bridges and provide contractors with alternatives on the deck construction. A continuous steel-girder bridge in Bastrop began construction in 2020, and the design included the use of PCPs. This bridge provided an opportunity to implement the findings from TxDOT Research Project 0-6909 as well as providing data on the performance of steel girder systems with PCPs. TxDOT Implementation Project 5-6909-01 is focused on the instrumentation and monitoring of the continuous steel bridge in Bastrop. The primary instrumentation consisted of vibrating wire gage that were installed next to the deck reinforcing steel above two of seven steel girders in the negative moment region prior to placement of the concrete deck. The two steel girders were also instrumented with strain gages on the flanges and webs. Following the placement of the concrete, the bridge was monitored to gather data on the strains induced from concrete shrinkage. The deck was monitored until late June of 2021. Prior to opening to traffic, researchers from Ferguson Structural Engineering Laboratory worked with TxDOT to carry out a live load test using four dump-trucks loaded with sand.

9.2 Review Bridge Plans

The instrumented bridge is a part of the west-bound frontage road (WBFR) over the Colorado River along State Highway 21 in the Bastrop County, TX. This bridge consists of two-span continuous girders with spans of 150-ft and 180-ft. The bridge width in this region varies between 53 ft. to 67 ft., as shown in Figure 9-1. The bridge deck is supported by seven steel girders, and the depth of each girder is 5-ft, 3-inches.
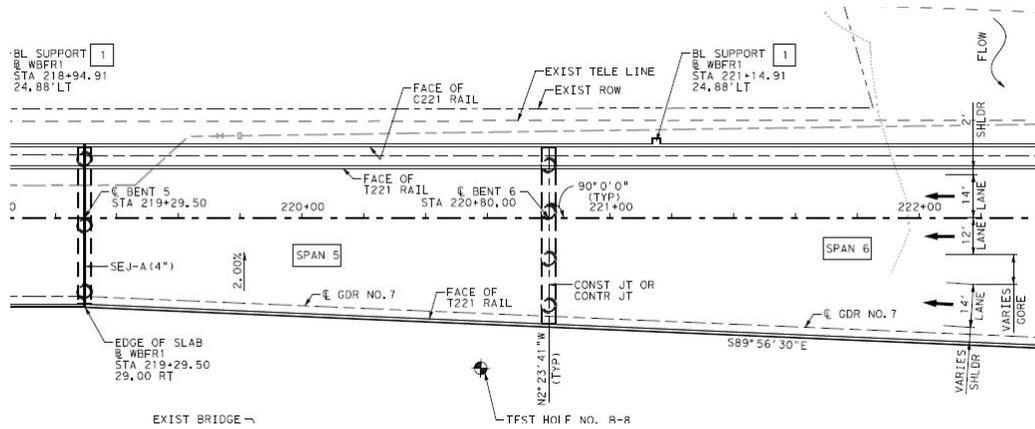
Figure 9- 1 Plan View of the Bastrop Bridge

The bridge deck includes 4-inch thick partial-depth prestressed precast concrete panels (PCPs) as the bottom layer and 4.5-inch thick cast-in-place concrete as the top layer. The original reinforcement design for the deck specified #6 bars spaced at 4.5 inches over the negative moment region in the longitudinal direction, with #5 bars spaced at 9 inches for transverse steel on top. Based upon the recommendations from the Project 0-6909, changes were proposed in the reinforcing steel over select girders. After approval of the engineer of record, TxDOT bridge division, and the contractor, the deck reinforcing steel details were changed in the negative moment region. The longitudinal reinforcement details consist of #6 bars spaced at 4.5 inches (reinforcement ratio of 2.2%, as per the original design) in the north half of the deck and #6 bars spaced at 9 inches (reinforcement ratio of 1.1%) in the south half of the deck, as shown in Figure 9-2. Following the findings from the original research study 0-6909, the reinforcement ratios listed here were based upon the reinforcing bar area divided by the cast-in-place concrete area.

160
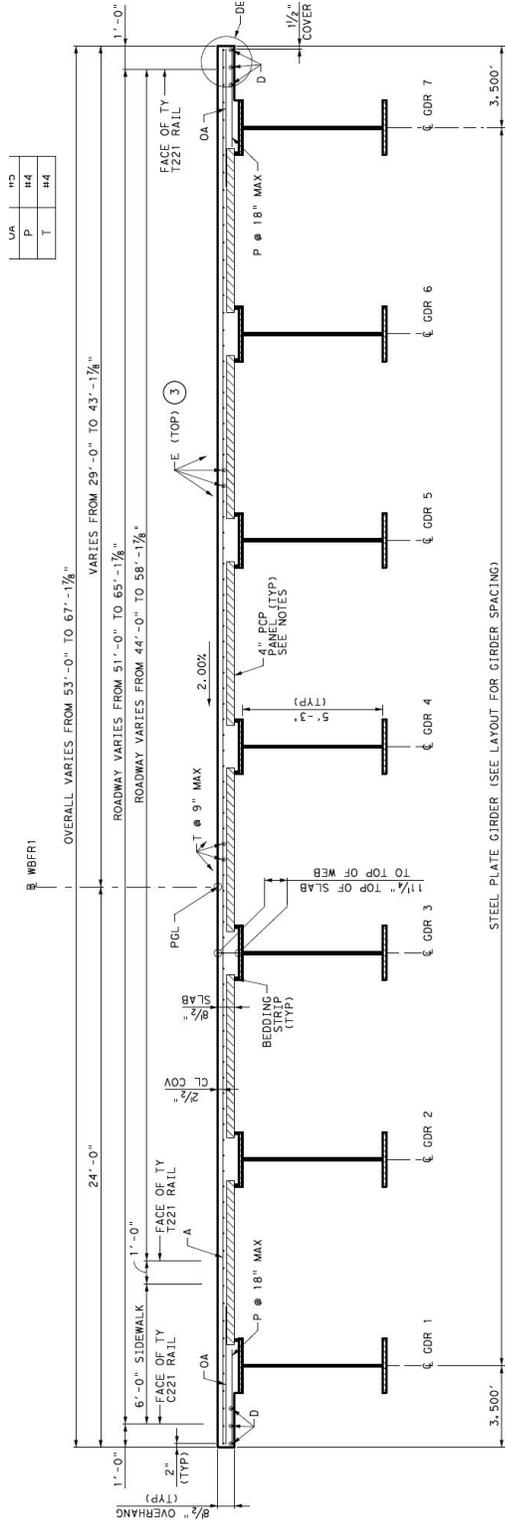
Figure 9- 2 Instrumented Cross-section of the Bastrop Bridge

161

9.2.1 Sensors and Equipment Used in Field Instrumentation

Following instrumentation of the girders and deck, the structural performance was monitored as the concrete cured and construction of the bridge was completed. The primary focus was on the concrete shrinkage strains in the deck. Prior to the bridge opening to traffic, the instrumentation was also used to gather data during a field load test using dump-trucks loaded with sand. Vibrating wire gages (VWGs), weldable strain gages, and data logging equipment, as shown in Figure 9.3 (a-c), were the primary tools used for measurements and data collection. The data logger equipment and batteries providing power were placed in housing boxes, as shown in Figure 9.3 (d-e). The length of time for monitoring was selected to ensure adequate and representative data could be collected to characterize bridge deck cracking behavior under shrinkage, thermal gradient, and live load effects.

(a) VWG   (b) Data-logging Equipment   (c) Weldable Strain Gauge

(d) Housing Box for Data logger   (e) Housing Box for Batteries

Figure 9- 3 Field Instrumentation Equipment

The primary objective of the instrumentation was to capture the behavior of the bridge deck cracking in the region of negative bending (tension region for the concrete deck). To study the global behavior and deck cracking at the critical section, both the steel girder and CIP deck in the negative moment region were instrumented. VWGs were embedded in the CIP portion of the concrete deck to measure the concrete strain, and weldable strain gages were attached on the surface of the steel girders to measure the girder strain profile, as shown in Figure 9-4.
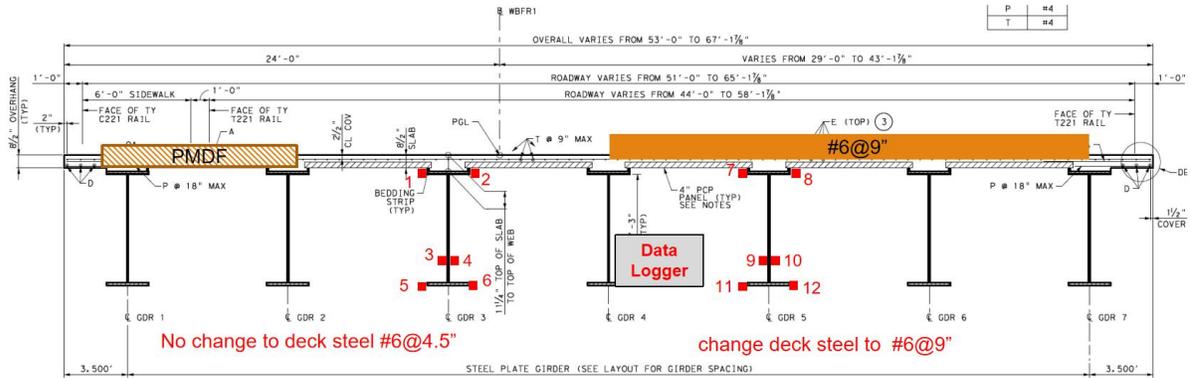
Figure 9- 4 Weldable Strain Gages on Steel Girders

9.2.2 Step 1: Field Instrumentation of Steel Girders

Monitoring the bending effects in the steel girders provides a measure of the shrinkage effects caused by the deck concrete during curing. The specific gage locations on the steel girder surface are shown in Figure 9-5. Six weldable strain gages were applied on each target steel girder, with two on the top flange, two on the web, and two on the bottom flange. The six gages on each girder allow considering effects of local plate bending as well as warping/lateral bending behavior in the flanges.
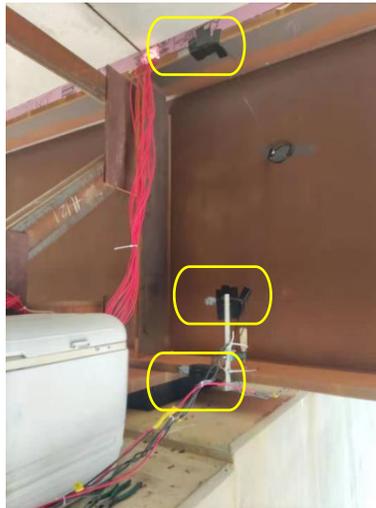
Figure 9- 5 Weldable Strain Gages on Steel Girders

9.2.3 Field Instrumentation in Concrete Deck

Similar to the previous work in Project 0-6909 on bridges in Round Rock that consisted of continuous spliced concrete girders, the objective of the field instrumentation at the Bastrop steel continuous bridge was to measure the impact of variations in the deck reinforcing steel at the critical sections of the concrete deck above the interior supports. A reduction in the concrete strain and crack width is expected to correlate with increasing the amount of steel. To measure the effect of changes in reinforcing steel, the research team monitored two different longitudinal reinforcement details over interior supports of two steel girders.

163

| (a) VWGs for #6@4.5-in. region | (b) VWGs for #6@9-in. region |
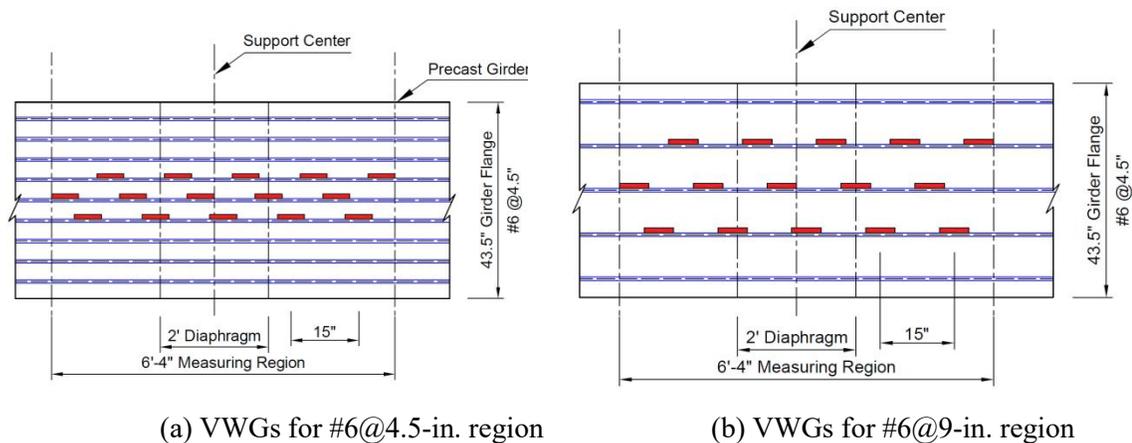
Figure 9- 6 Plan Views of Instrumentation in Concrete Deck

As noted earlier, the original design, consisting of #6 bars spaced at 4.5 inches in the longitudinal direction (2.2% of CIP area) were utilized in the north half of the instrumented cross-section. Fifteen VWGs were placed along reinforcing bars over one steel girder, as shown in Figure 9-6(a). To avoid affecting the connection between concrete and reinforcing steel, the research team placed VWGs on several reinforcing bars over the beamline. The net spacing between each VWG is approximately 8 inches. The modified detail consisting of #6 bars spaced at 9 inches (1.1% of CIP area) was used in the south half of the instrumented cross-section, as shown in Figure 9-6(b). Fifteen VWGs were placed along reinforcing bars over one steel girder as well, as shown in Figure 9-7.
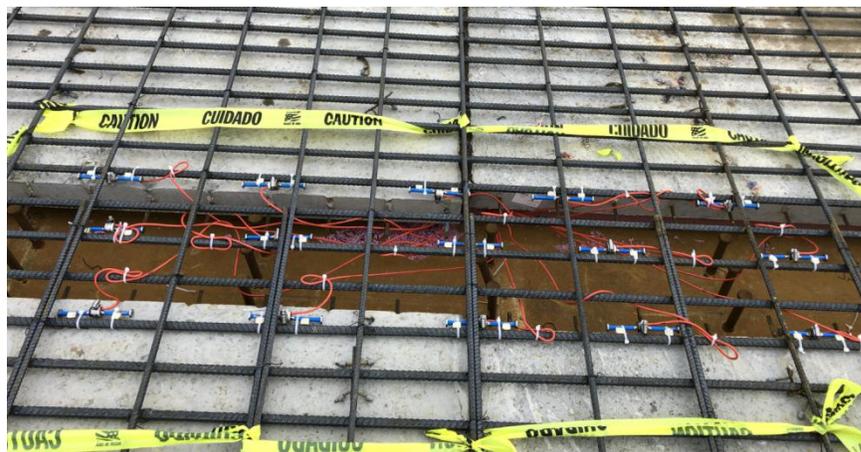
Figure 9- 7 VWGs Installed Besides Longitudinal Deck Steel

9.2.4 Deck Construction

The cast-in-place deck was placed during the evening of February 2, 2021, as shown in Figure 9-8. The VWGs installed beside the longitudinal reinforcement were carefully protected from damage during concrete placement. The gages were scanned every 15 minutes to track changes in the shrinkage strains. The VWGs also include a thermistor that tracks the temperature at the gage location. The instrumentation was

closely monitored during deck placement with frequent scans to track the behavior of the freshly-placed concrete. The scans immediately following the placement were closely monitored to capture shrinkage effects.

Figure 9- 8 Deck Casting on Feb. 2, 2021

Concrete samples were prepared during casting and tested after 28 days. The concrete strengths are listed in Table 9-1:

Table 9- 1 Concrete Material Properties

Compressive Strength	Elastic Modulus	Modulus of Rupture	Cracking Strain
6600 psi	4630 ksi	610 psi	132 με

9.3 Field Instrumentation During Construction - Results

9.3.1 Visual Observations

Surface cracks in the deck were inspected before and after the live load testing on June 16, 2021. One crack initiator, referred to as a "zip-strip", was applied in the Cast-In-Place concrete deck over the interior supports, as shown in Figure 9-9. Zip strips or other crack initiators are commonly used on simply supported concrete girders with TxDOT's "poor-boy continuous" detail to initiate the crack right at joint. The research team does not believe these strips would normally be used on continuous girders and were likely utilized since they are used on other sections of the bridge with simply supported girders. However, the zip-strips will not impact the long-term behavior of the deck and simply initiate a crack at that location. No other transverse deck crack could be observed in the deck region with the instrumentation region. At each side of the interior support, (outside of the instrumented region) one crack was observed 6-ft. away from the zip-strip in the reduced reinforced region (1.1%). No deck cracks were observed in the originally reinforced region (2.2%). Another deck crack was also observed close to the concrete rail, but did not propagate to the monitored region. Since the rail is constructed after the concrete deck has cured, this crack was likely initiated due to rail shrinkage, instead of

deck shrinkage effects. Widths of all these observed deck surface cracks were very small, less than 0.006 inch. The deck cracks were actually quite difficult to see.

(a) Deck Crack Initiator   (b) Transverse Deck Crack
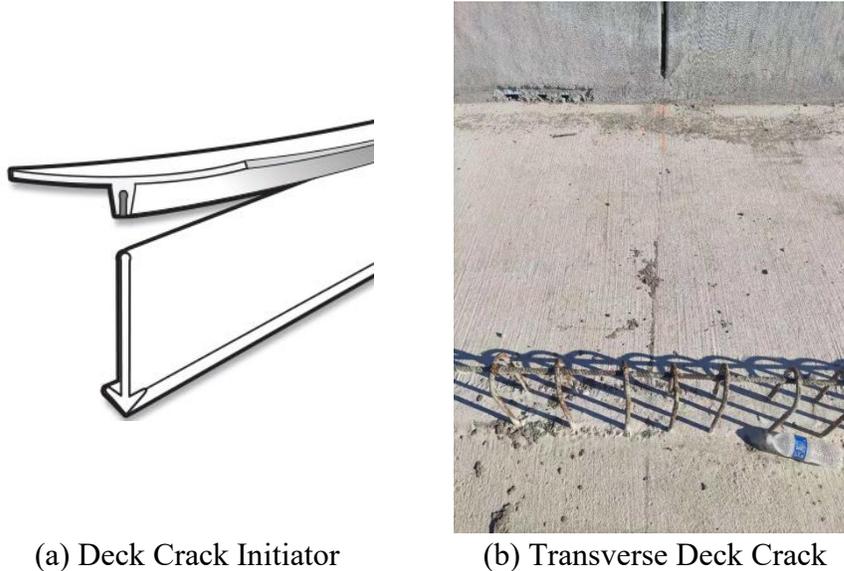
Figure 9- 9 Transverse Deck Crack in Deck Instrumentation Region

9.3.2 Long-term Field Monitoring

The long-term field monitoring lasted around 150 days, between February 2nd to June 28th. The VWGs and weldable strain gages were sampled every 15 minutes. However, to minimize the influence from thermal effects, only data between 2 AM and 4 AM are shown in the figures below. Temperature was monitored from both the thermistor embedded in concrete deck and the temperature sensor in the data-logger that was located on the interior bent, which is representative of the temperature of bridge deck and steel girders at the underside of the bridge. As indicated by the temperature measured during the long-term monitoring, shown in Figure 9-10, the thermal gradient effects are quite negligible during the nighttime hours.
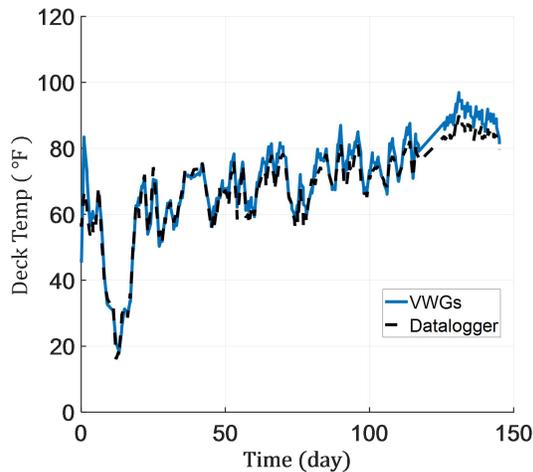
Figure 9- 10 Temperature Recorded during Long-term Monitoring

For both instrumentation regions with different longitudinal reinforcing bar details, deck cracking occurred after the concrete curing period at the location of the crack initiator. After that, readings from the VWGs across the crack initiator increased significantly in a short time, and with reinforcing bar stresses increasing simultaneously. Measured concrete strains exceeding 200 με, indicate that this VWG was located across a deck crack. In each region, two or three VWGs were across the concrete cracks. The measured concrete strains of deck regions with different reinforcement details are shown in Figure 9-11. After these significant crack initiations, the concrete strains increased over time. For the region with more reinforcing steel (#6 bars spaced at 4.5 inches), lower concrete strains were measured for the VWGs that crossed cracks. For the region with less reinforcing steel (#6 bars spaced at 9 inches), the concrete strain increased to approximately 400 με after crack initiation and then gradually grew to approximately 1000 με.

(a) #6 bars spaced at 4.5-in. (2.2%)   (b)#6 bars spaced at 9-in. (1.1%)
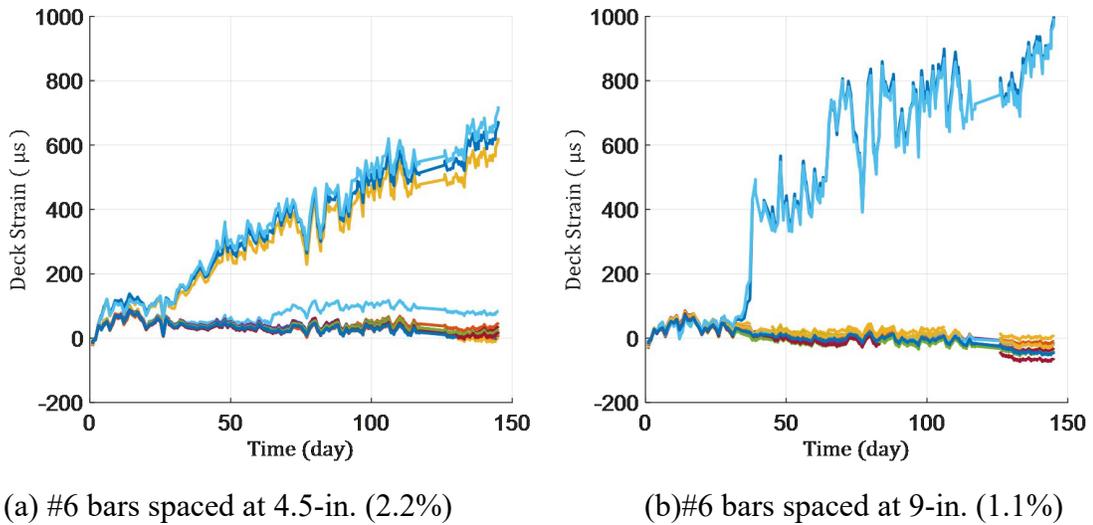
Figure 9- 11 Concrete Strains Measured by VWGs

The spatial distribution of concrete strains for each reinforcement detail is shown in Figure 9-12. Generally, only VWGs located in the middle of the instrumented regions are across the deck crack, which matches well with the location of crack initiator (zip-strip), and also matches well with the visual observations. The spatial distribution of deck strains also shows a comparison between the two different deck reinforcement details. The region with more deck reinforcement showed lower concrete deck strains. However, for the region with less reinforcing steel, based on visual observations of VWG measurements, deck crack widths were still within an acceptable range.
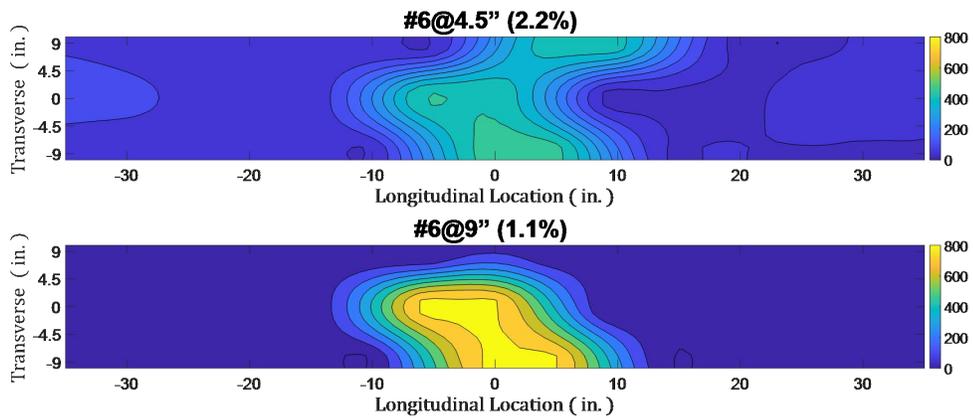
Figure 9- 12 Concrete Strains Spatial Distribution

The girder stresses near the interior support were monitored using weldable strain gages on the girder surface, as shown in Figure 9-13. Due to the dead load of the CIP concrete deck, the top flanges were under tension and bottom flanges were under compression after the CIP layer was cast. After that, insignificant changes occurred in girder stresses due to concrete shrinkage effects.
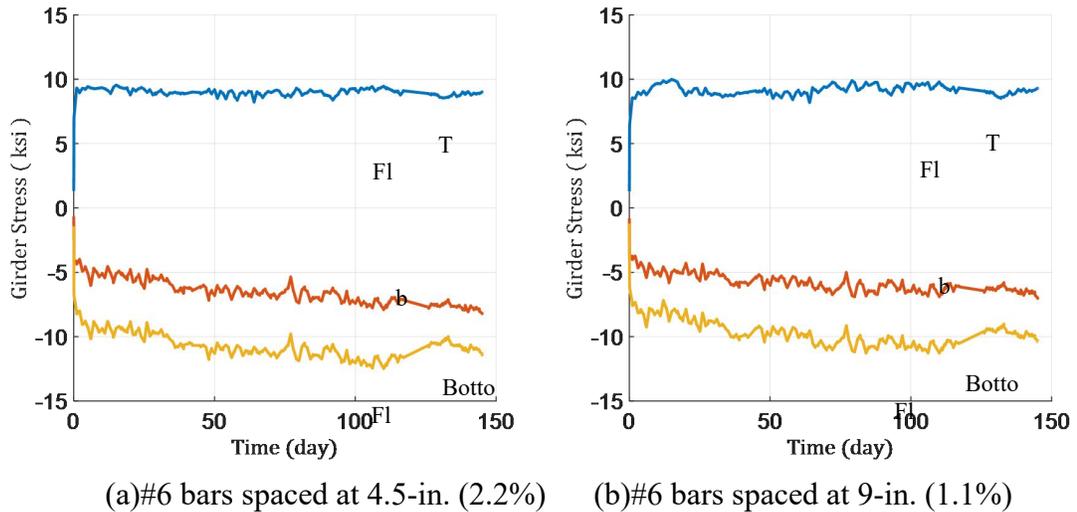
(a)#6 bars spaced at 4.5-in. (2.2%)   (b)#6 bars spaced at 9-in. (1.1%)

Figure 9- 13 Girder Stresses Measured by Weldable Strain Gages

9.3.3 Summary

A two-span continuous bridge in Bastrop County, TX was instrumented and monitored for approximately 150 days after the CIP portion of the deck was cast and before the bridge was opened to traffic. Different reinforcement details were compared, with reinforcement ratios of 1.1% and 2.2%, to examine crack widths due to concrete shrinkage effects. Based upon the field instrumentation measurements and visual observations, for the concrete deck in the negative moment region of this continuous bridge, the following observations were made:

- One transverse crack occurred at the crack initiator strip and was monitored by VWGs embedded in the CIP layer.

- The deck surface cracks were very small, and the crack widths were less than 0.006 inch.

- Measured deck shrinkage was approximately 400 to 800 $\mu\varepsilon$.

- The 2.2% reinforcement ratio resulted in somewhat smaller deck strains. However, the 1.1% reinforcement ratio controlled deck strain within acceptable tolerances.

- Stresses in the steel girders did not show significant change after the CIP layer was cured.

9.4 Live Load Testing - Results

The field live load testing on the Bastrop bridge was conducted on the morning of June 16, 2021. Four fully loaded dump trucks were provided by TxDOT for the testing. Five loading configurations were used with trucks positioned at different locations. Using the long-term field instrumentation described above, the bridge decks and steel girders over the interior support were monitored during the live load tests. Twelve Pi-gages were also installed on the deck surface to record the crack opening during field load testing, as shown in Figure 9-14(a). The vertical deflections of the two instrumented girders were also recorded by laser distance meters located under the bridge, as shown in Figure 9-14(b). Since the east span of this bridge is over the Colorado River, only the deflections in the middle of the west span were measured.

(a) Pi-gage on Deck Surface   (b) Laser Distance Meter

Figure 9- 14 Supplementary Instrumentation Used in Live Load Testing Summary

9.4.1 Loading Configurations

Four fully-loaded dump trucks were provided by TxDOT for the tests, as shown in Figure 9-15(a). The geometric configuration and gross weight of each truck are provided in Table 9-2. Five loading configurations were tested with trucks positioned at different locations, as shown in Figure 9-15(b). To maximize the girder moments over the interior support, trucks were located at the middle of each span. The location of each truck for a given load case is shown in Figure 9-16. Between each load case, the four dump trucks were relocated on the two tested spans, to permit readings before, during and after each test.
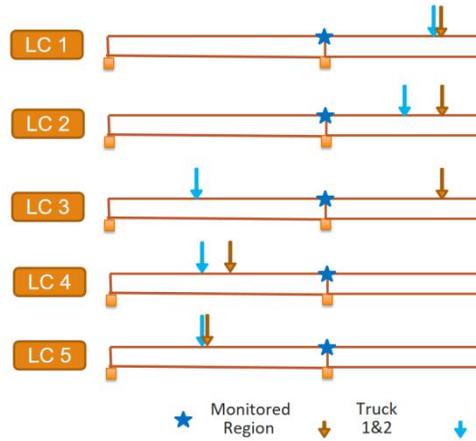
(a) Four Dump Trucks   (b) Five Load Cases

Figure 9-15 Supplementary Instrumentation Used in Field Load Testing

Table 9- 2 Truck Dimensions and Weights

	L (ft.)	W (ft.)	a (in.)	b (in.)	c (in.)	d (in.)	e (in.)	Gross Weight (kip)
Truck 1	24.7	7.9	80	39	168	55	34	49.5
Truck 2	23.8	8.2	83	30	168	55	32	51.0
Truck 3	23.5	8.2	83	33	164	53	32	50.6
Truck 4	24.3	8.1	83	30	168	54	40	52.2
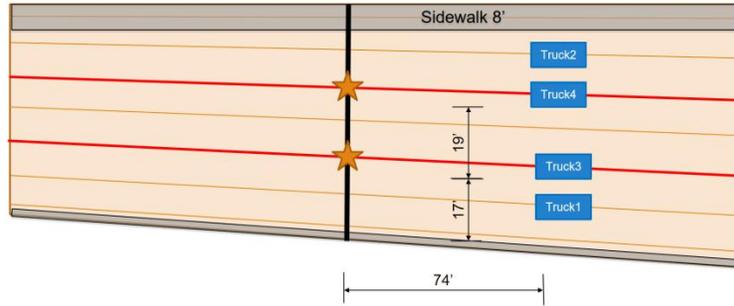
(a) Load Case 1

(b) Load Case 2

(c) Load Case 3

(d) Load Case 4

(e) Load Case 5

Figure 9-16 Truck Locations for Each Load Case

172

9.4.2 Temperature and Girder Deflections

The live load testing was conducted between 9:30 AM and 11:00 Am. Temperatures were recorded by the VWGs embedded in the concrete deck and by the data-logger located on top of the bent, directly under the bridge. The data logger temperatures are considered as representative of the steel girder temperatures. As shown in Figure 9-17(a), the temperature difference between concrete deck and steel girder changed little during the approximately 90-minute testing period, indicating that changes in thermal gradients were likely small during the load testing period. Since the data that was recorded focused on the strain changes and girder defections during a given load case (approximately 10-minute duration), the temperature effects during each test were insignificant.

Girder deflection readings were taken from the underside of the west-span. Two laser distance meters placed on tripods were used to measure distances between the girder bottom surfaces and the ground in the loaded and unloaded conditions. Three readings were taken per test. The difference between the unloaded and loaded distances was averaged to determine the deflection. As shown in Figure 9-17(b), the largest measured girder deflection of the west span was 0.5 inch during Load Case 5, around 1/3800 of the span length.
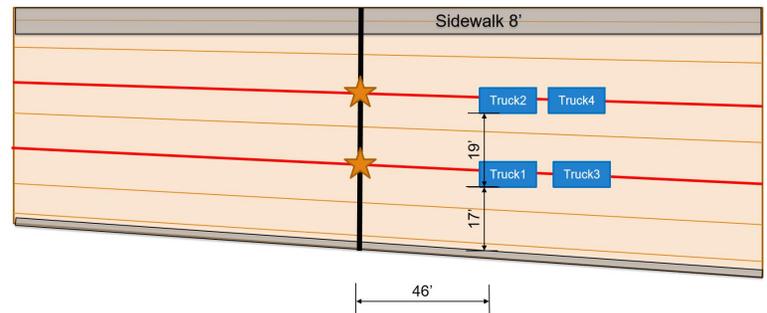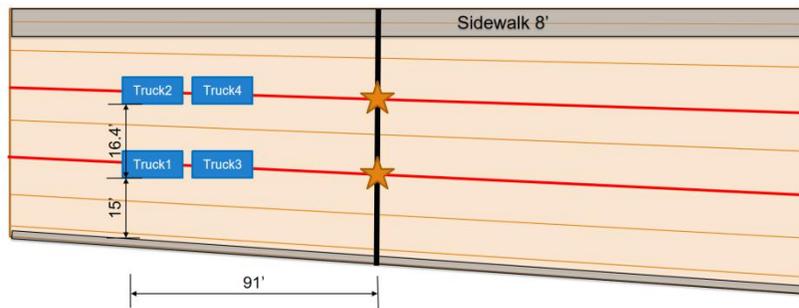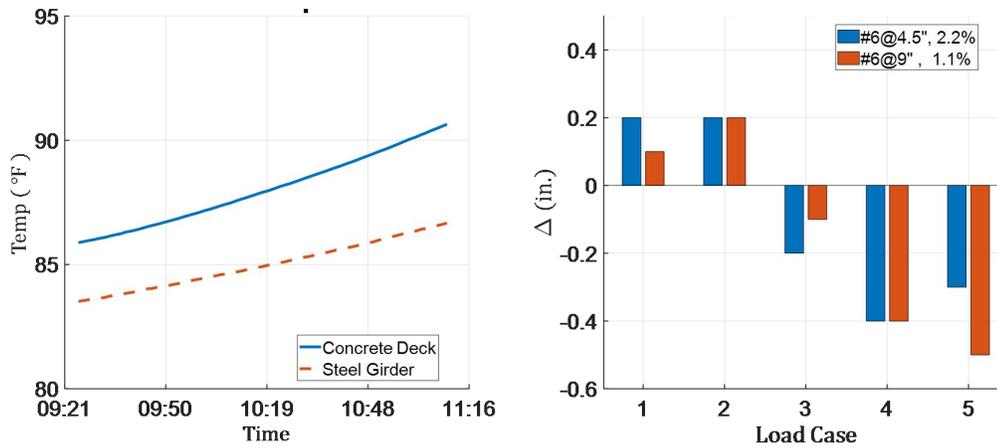

(a) Temperature during Testing   (b) Girder Deflections

Figure 9-17 Temperature Changing and Girder Deflections during Testing

9.4.3 Deck Strains and Crack Openings

The VWGs embedded in the concrete deck were used to record concrete strains during the load testing. According to the VWG readings, no new deck cracking occurred in the instrumented region. Thus, the only crack in the region with VWGs was at the crack initiator. The averaged change in the VWG readings across this deck crack is shown in Figure 9-18(a). The averaged strains in the deck region with the #6 bars spaced at 4.5 inches are around half of those in the deck region with the #6 bars spaced at 9 inches. The averaged deck crack openings measured by the Pi-gages at the crack initiator showed a similar pattern, as shown in Figure 9-18(b). Increasing the area of longitudinal reinforcing steel and decreasing the bar spacing showed some benefits in reducing deck

strains and crack openings. However, the maximum crack opening recorded during the live load test in the region with less deck reinforcement was no greater than 0.002 inch. This is quite small compared with the 0.012-inch acceptable crack width under the AASHTO LRFD Service Load Combination. This indicates that the contribution of live load to deck cracking is relatively small compared to the contribution from concrete shrinkage.

(a) Deck Strains   (b) Deck Crack Opening
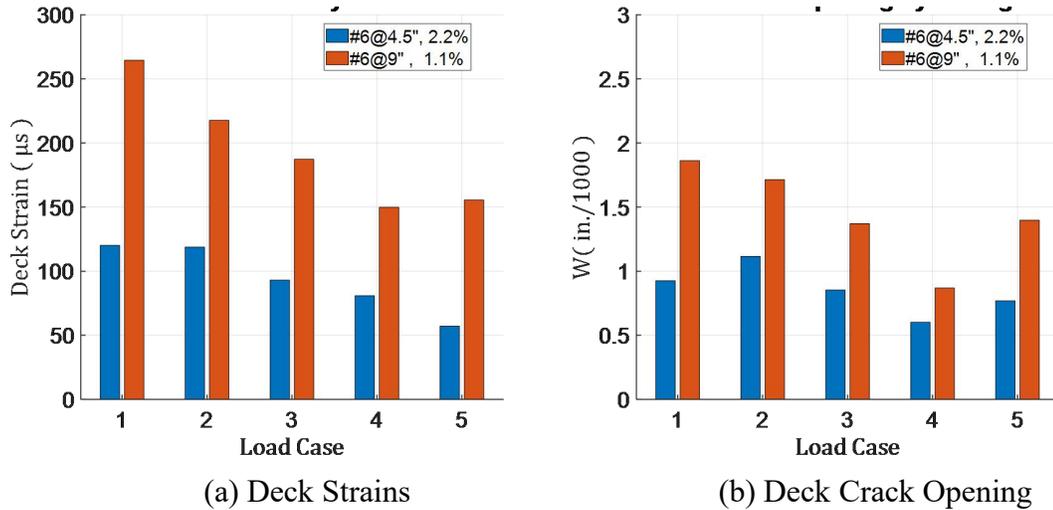
Figure 9-18 Deck Strains and Deck Crack Opening under Each Load Case

During live load testing, one crack was observed at each side of the interior support, 6-ft. away from the crack initiator in the reduced reinforced region (1.1%). No deck cracking was observed in the regions with the original reinforcing details (2.2%) other that at the crack initiator. Most likely, these two deck cracks were initiated before live load testing, but were too small to be observed. One of these cracks' surface opening was measured by Pi-gages during Load Case 3 to Load Case 5, as shown in Figure 9-19. The opening widths of this "natural crack" (i.e. compared to the crack at the zip strip crack initiator) was around half of that of the crack at the crack initiator.
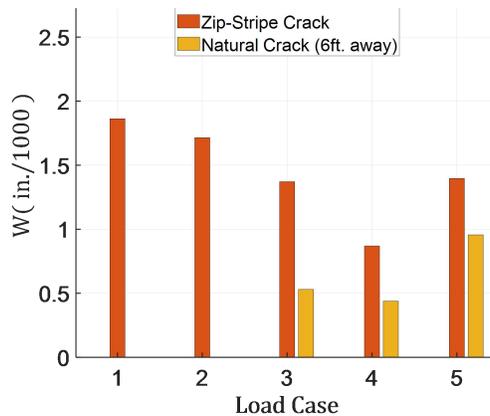
Figure 9-19 Crack Width Openings at the Crack Initiator Location and at Approximately 6-ft Away

9.4.4 Deck Strains and Crack Openings

The girder stresses near the interior support were monitored by weldable strain gages on the girder surface. Under each load case, the measured stress profile of the two girders under the CIP deck regions with different reinforcement details showed similar patterns. Generally, compared with long-term monitoring results, girder stresses caused by four fully loaded dump trucks are around 15% of those caused by dead load of CIP deck, as shown in Figure 9-20.
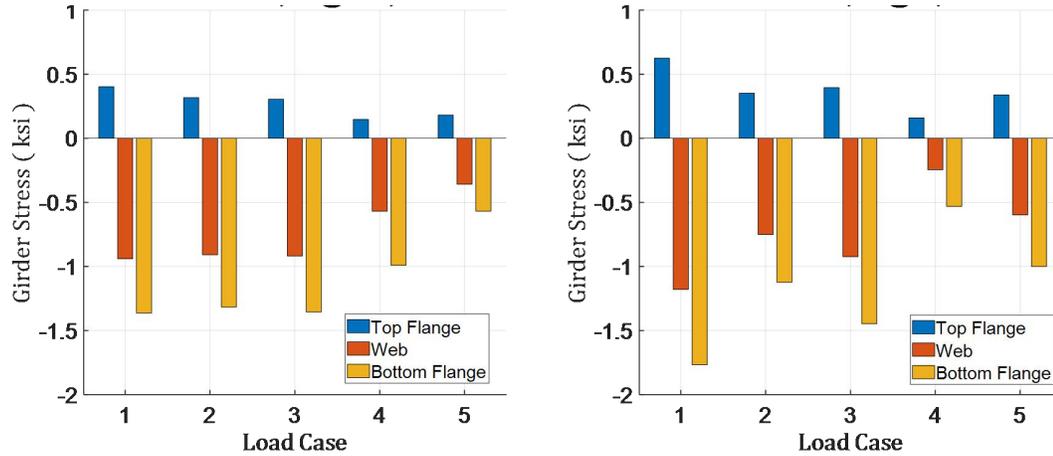
(a) Girder under #6@4.5 inches Deck Steel   (b) Girder under #6@9 inches Deck Steel

Figure 9-20 Girder Stresses under Each Load Case

One weldable strain gage was installed on each side of the web plate of each monitored steel girder. The measured stresses from these gages were examined, as shown in Figure 9-21. Generally, readings from the weldable gages at different sides of the web were quite closed to each other, indicating there was little out-of-plane bending of the web.
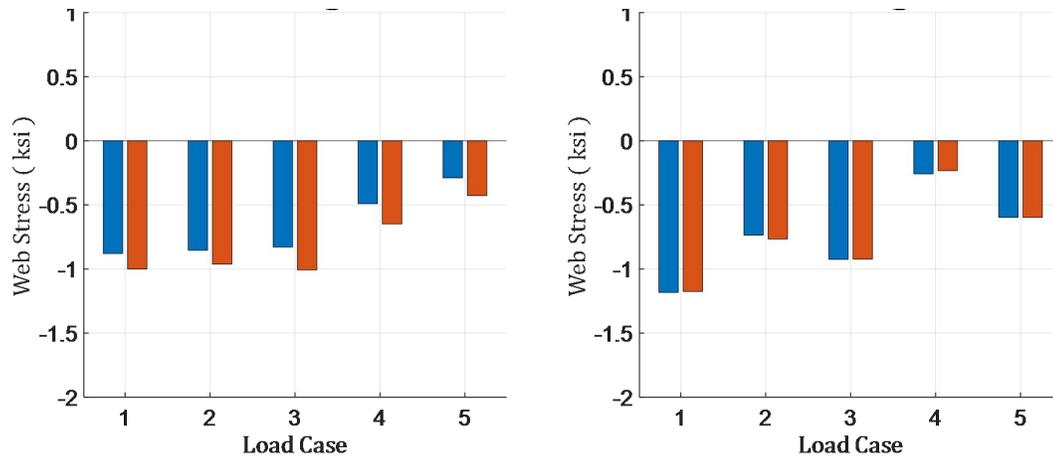
(a) Girder under #6@4.5 inches Deck Steel   (b) Girder under #6@9 inches Deck Steel

Figure 9-21 Web Stresses under Each Load Case

9.4.5 Summary

The live load testing on the Bastrop bridge was conducted on the morning of June 16, 2021. Four fully loaded dump trucks were provided by TxDOT for the testing, and five loading configurations were used with trucks positioned at different locations. The largest girder deflection measured during testing was 0.5 inch. The maximum crack opening width measured during testing was under 0.002 inch. The following observations can be made for the concrete deck in the negative moment region of continuous steel bridges :

● Deck strains and deck surface crack widths under controlled live loading were small compared with those due to concrete shrinkage effects.

● Increasing the area of longitudinal reinforcing steel and decreasing bar spacing showed some benefits in reducing deck strains and crack openings.

● Thermal gradient effects were small during the short testing time.

9.5 Project Summary

TxDOT Research Project 0-6909 developed a methodology for determining the amount of reinforcement needed in the CIP portion of the deck in the negative moment region of continuous girder bridges that use precast concrete deck panels (PCPs), to provide adequate control of deck cracking. The amount of deck reinforcing steel recommended in Project 0-6909 depends on the type of girder (steel girders versus spliced concrete girders), span arrangements and span lengths, and other factors. However, over a broad range of bridge types and configurations, the recommended amount of longitudinal steel reinforcement is approximately 1-percent of the area of the CIP layer. In Project 0-6909, the adequacy of this amount of reinforcing steel to provide satisfactory control of crack widths was verified by field testing and measurements on a continuous bridge constructed using spliced concrete girders in Round Rock, Texas.

However, there was no opportunity during Project 0-6909 to monitor a continuous steel girder bridge with PCPs, as there were none under construction at that time.

The continuous steel girder bridge with PCPs that was constructed on SH 21 over the Colorado River in Bastrop, Texas provided a unique opportunity to further evaluate deck reinforcement requirements. The instrumentation, monitoring, and live load testing of this bridge that was conducted as part of this implementation project provided further validation of the design recommendations developed in TxDOT Research Project 0-6909.

This two-span continuous bridge in Bastrop County, TX was instrumented and monitored for approximately 150 days during construction, starting with casting of the CIP deck layer. Two different reinforcement details were compared. One detail had #6 bars spaced at 4.5 inches (reinforcement ratio of 2.2%, as per the original design). The other detail had #6 bars spaced at 9 inches (reinforcement ratio of 1.1%). Following the placement of the CIP deck layer, the bridge was monitored to gather data on concrete shrinkage strains for approximately 150 days. The bridge was not open to traffic during this time. The deck was monitored until late June of 2021. Live load tests on this bridge were conducted on the morning of June 16, 2021. This was also before the bridge had ever been opened to traffic. Prior to the four dump trucks, the only traffic that was likely on the bridge were vehicles related to construction activity such as ready mix trucks casting the bridge rail. The four dump trucks each weighing approximately 50 kips were therefore, the most significant traffic on the bridge to date. The four fully loaded dump trucks were provided by TxDOT for the testing, and five loading configurations were used with trucks positioned at different locations.

Key observations from this bridge are as follows:

- One transverse crack made by the crack initiator was monitored by the field instrumentation.

- The deck surface cracks were relatively small, with crack widths no greater than 0.006 inch.

- Shrinkage is the dominant effect for deck cracking, which will cause 400 to 800 $\mu\varepsilon$ strain in the concrete.

- Increasing the deck reinforcement ratio and decreasing the bar spacing showed some benefits, but the 1.1% reinforcement controlled deck strain acceptably.

- Deck strains and deck surface crack widths under controlled live loading were small compared with those due to concrete shrinkage effects.

Chapter 10. Summary and Conclusions

A leading factor contributing to structural deficiency in the US bridge inventory is related to deterioration and durability issues with concrete bridge decks. The federal classification, structural deficient, has been replaced with the designation, Poor Condition. Bridges is "Poor Condition" are ones exhibiting signs of advanced structural deterioration and are not unsafe. The long-term costs associated with maintenance issues on bridges can quickly exceed the initial bridge cost. A primary factor that can affect the durability of the concrete deck is cracking that provides a direct conduit for moisture and other corrosive agents to penetrate the concrete and attack the reinforcing steel.

With increases in the use of PCPs in Texas bridges, ensuring acceptable deck cracking behavior is of paramount importance so as to avoid long-term maintenance problems. The purpose of this study is to understand the cracking behavior of reinforced concrete bridge decks with precast concrete panels in the negative moment regions of continuous girders (prestressed concrete and steel) under service loading and to develop comprehensive guidelines for reinforcing steel details in the bridge decks in the negative moment regions of bridges utilizing Precast Concrete Panels.

This project includes field monitoring, laboratory testing, and numerical parametric studies on the cracking behavior of bridge decks in the negative moment region, with and without PCPs. A major focus of the study is the influence of the reinforcing details on the control of deck crack width.

10.1 Field Instrumentation and Live Load Testing

Two "poor-boy" continuous bridges and two three-span spliced continuous prestressed concrete bridges were monitored during the construction period. Deck strain distribution, reinforcing steel stress distribution, and surface crack widths were measured during construction and in service. Different reinforcement details were compared, with reinforcement ratios from 0.5% to 2.2%, to control cracking widths under service loading conditions.

The results from the strain measurements during the early stages after bridge deck casting show the influences of additional reinforcement in the CIP portion of the "Poor-boy" continuous deck joints. Probably due to the crack former, only minor benefits on reducing deck strain were measured by using more reinforcing steel or reducing reinforcing bar spacing on "Poor-boy" joints, in some cases. The transverse distribution of concrete deck strain was measured at "Poor-boy" joints, as the concrete strain over bridge lines were always more significant than that measured over PCPs. From the field instrumentation and long-term monitoring of these two bridges, the research team got valuable experience on field instrumentation procedures and deck cracking behavior.

Four kinds of longitudinal deck reinforcement details were examined in the two spliced concrete bridges located in Round Rock. The reinforcement details are #6 bars spaced at 4.5-inch (2.2%), #6 bars spaced at 9-inch(1.1%), #5 bars spaced at 6-inch(1.1%), and #5 bars spaced at 9-inch(0.8%), respectively. Key observations from this bridge are as follows:

- With each reinforcement detail, early-age transverse deck cracking occurred in the construction period but did not increase significantly after live load testing or after the bridge was opened to traffic.

- All the observed surface cracks in the critical regions are less than 0.006-inch.

- Concrete early-age shrinkage is the dominant reason for deck cracking with concrete strains in the range of 500~1000με and maximum reinforcing bar stresses of 12~20 ksi.

- Increasing reinforcement ratio and decreasing reinforcing bar spacing showed some benefits.

- Four loaded dump trucks (~ 200 total kips) did not cause significant increases in deck strains or crack widths in the negative moment regions.

- Minor cracking occurred following bridges opening to traffic.

10.2 Large Scale Laboratory Testing

Negative bending tests were conducted on three composite tub girders with 6.5-inch Cast-In-Place concrete deck and various deck longitudinal reinforcement details in the negative moment region. Key observations from this testing are as follows:

- Utilizing more reinforcing steel shows benefits in reducing cracking widths and reducing crack spacing under a negative bending moment.

- With regard to Tub 1, whose reinforcement ratio is 1.0%, the deck crack width soon after cracking initiation is approximate 0.006-inch. The growing of crack width shows some correlations with the maximum reinforcing bar stress at cracks.

- With regard to Tub 2, whose reinforcement ratio is 0.5%, the deck crack width soon after cracking initiation is approximate 0.01-inch, and the calculated maximum reinforcing bar stress at cracks is approximate 50-ksi.

- With regard to Tub 3, whose reinforcement ratio is 0.36%, the deck crack width soon after cracking initiation is over 0.02-inch, and reinforcing bar yielding probably occurred at that condition.

- If the reinforcement ratio is very low, like that in Tub 2 (0.5%) and Tub 3 (0.36%), reducing bar spacing from 9-inch to 6-inch or 4.5-inch does not show significant benefit on reducing cracking widths.

To provide further insights into the influence of the reinforcing bar area on the concrete cracking behavior, concrete specimens with one single reinforcing bar in the middle were cast in the Ferguson Laboratory. The concrete specimens were 30-inch long, with one #3, #4, #5, or #6 Grade 60 reinforcing bar in the middle. No transverse bars were utilized in the specimens. The reinforcement ratio varied between 0.5% to 2.2%. Key observations from this testing are as follows:

- The cracking process can be classified into two stages: crack initiation and crack developing.

- Three cracks occurred in the specimens with #6 reinforcing bar (2.2%), two or three cracks occurred in the specimens with #5 reinforcing bar (1.5%), and two cracks occurred in the

specimens with #4 or #3 reinforcing bars (1% or less). The number of cracks in each specimen shows some correlation with the reinforcement ratio.

- Increasing the reinforcement ratio show some benefits in controlling the crack width right after cracking.

- The surface crack widths generally matched the predictions from the AASHTO crack width equation correlating with the maximum reinforcing bar stress

- Concrete tension stiffening effect was also observed in the cracked reinforced concrete specimens.

10.3 Numerical Parametric Studies

According to the results of the large-scale laboratory testing and the AASHTO crack width equation, the maximum reinforcing bar stress is the most critical factor for the opening crack width. Factors that may have an influence on the maximum reinforcing bar stresses were considered in the numerical parametric studies, such as the stiffness of the supporting girders, the deck reinforcement ratio, with or without PCPs as the form work for the CIP deck. Finite element models of continuous bridges with different span lengths and girder profiles were developed in Abaqus/CAE. To conduct a more extensive parametric study, the research team also developed a sectional analytical method based upon the concept of "plain sections remaining plain." The maximum deck reinforcing bar stresses are highlighted in the analysis. The reinforcing bar stresses from the two different methods generally had a well agreement and also agreed well with the data obtained by the field instrumentation in the Round Rock bridges.

Based upon the parametric studies of the concrete deck in the negative moment region of continuous bridges, the following conclusions can be made:

- The deck reinforcement ratio is the critical factor for the maximum reinforcing bar stress.

- If the longitudinal bar area is 1.0% of the CIP deck area, the maximum reinforcing bar stresses can be limited to approximately 30-ksi under service load combination for both concrete and steel girder systems.

- Compared with the full depth CIP decks, utilizing PCPs in the bottom layer can significantly reduce the maximum reinforcing bar stresses, if the same deck reinforcement design is utilized.

10.4 Conclusions and Design Recommendation

Based upon the field monitoring, laboratory testing, analytical, and computational studies on the cracking behavior of bridge decks conducted in this project, the research team developed a design methodology and details for the longitudinal deck reinforcement in continuous girder systems with PCPs, as shown in Figure 10-1.
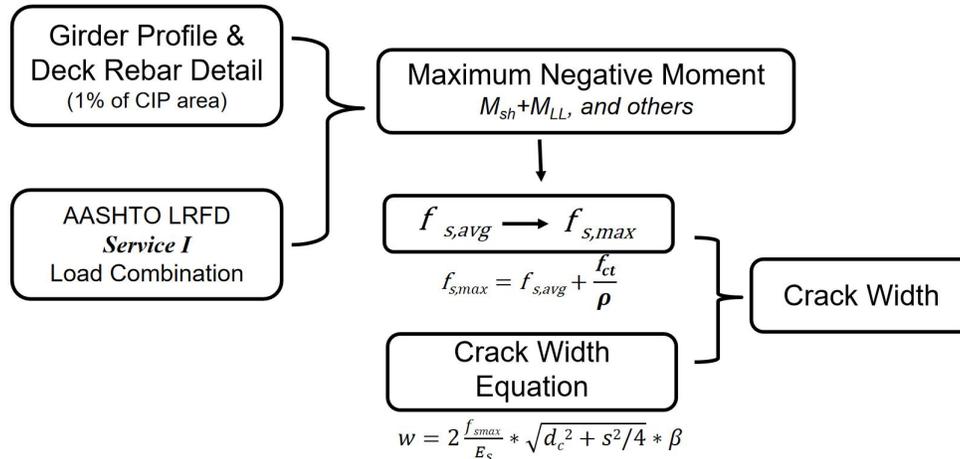
Figure 10- 1 Proposed Design Procedure for Longitudinal Deck Reinforcement

where:

M_{sh} = restraint shrinkage moment at the critical section

M_{LL} = moment caused by live load effect and dynamic allowance

$f_{s,avg}$= Average deck reinforcing bar stress (ksi)

f_{ct} = the average tensile stress in the concrete after cracking, which can be determined by the concrete "Tension Stiffening Model"

ρ = reinforcement ratio determined by the area of longitudinal deck reinforcement and the area of the CIP concrete deck

$f_{s,max}$ = the maximum reinforcing bar stress at cracks (ksi)

W = most probable crack width (inch)

E_s = elastic modulus of reinforcing bar as 29000 ksi

d_c = thickness of cover from deck surface to the closed bar center (2.5 in.)

s = bar spacing (inch)

β = 1.0+0.08d_c

The average reinforcing bar stress under *Service I* load combination can be obtained through compatibility sectional analysis (plan sections remain plan). In the next step, the maximum reinforcing bar stress can be derived from the average reinforcing bar stress and concrete tension stiffening effect. The maximum reinforcing bar stress in the longitudinal deck reinforcement should be limited to 36-ksi under Service I load combination. Finally, the deck crack widths can be checked based upon the maximum reinforcing bar stress.

If the area of deck longitudinal reinforcement is approximately one percent of the area of the CIP concrete deck area, the deck crack width can be limited to 0.012-inch. #4 bars spaced at

9-inch plus #5 bars spaced at 9-inch (1.3% total) or #5 bars spaced at 6-inch (1.1%) can be an appropriate longitudinal deck reinforcement design choice for the concrete deck with PCPs as stay-in-place form, as shown in Figure 10-2.
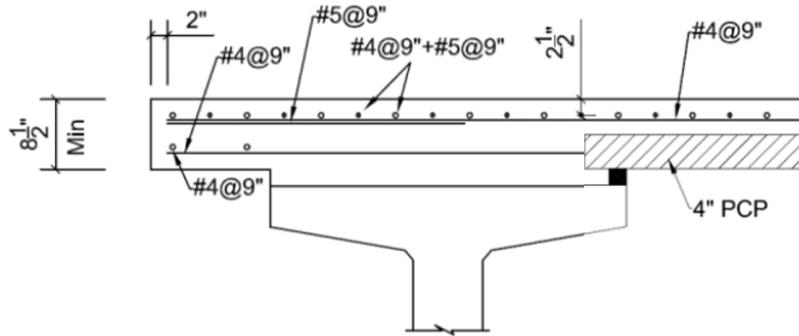
(a) #4 bars @9-inch+#5 bars @9-inch
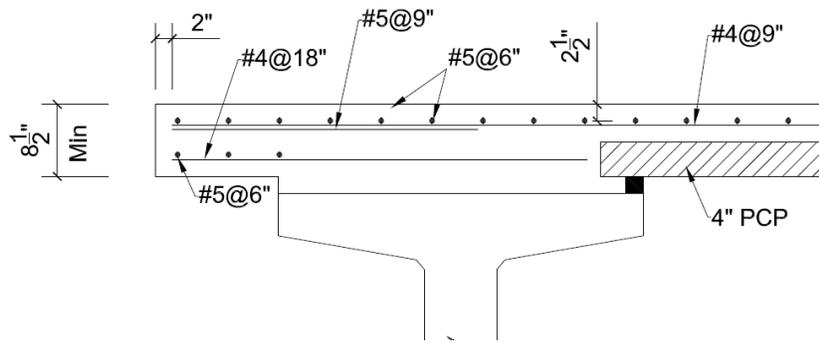
(b) #5 bars @6-inch
Figure 10-2 Proposed Deck Reinforcement Detail over Concrete Girder

The deck concrete strength has a direct connection with the maximum reinforcing bar stress and higher CIP concrete strength adversely affects crack widths. The upper strength of the CIP deck concrete should be considered in the concrete mixture design. If the acceptable of deck crack width is smaller than 0.012-inch, reducing the spacing between longitudinal reinforcement is an effective method to reduce possible deck crack width.

10.5 Implementation Project: Field Instrumentation of Steel Girder Bridge with Partial Depth Precast Concrete Deck Panels

Texas Department of Transportation provided a unique opportunity to further evaluate deck reinforcement requirements, with one continuous steel girder bridge with PCPs constructed on SH 21 over the Colorado River in Bastrop, The instrumentation, monitoring, and live load testing of this bridge that was conducted as part of TxDOT 5-6909-01 Implementation Project provided further validation of the design recommendations developed in TxDOT Research Project 0-6909. Two different reinforcement details were compared. One detail had #6 bars spaced at 4.5 inches (reinforcement ratio of 2.2%, as per the original design). The other detail had #6 bars spaced at 9 inches (reinforcement ratio of 1.1%). Following the placement of the CIP deck layer, the bridge

was monitored to gather data on concrete shrinkage strains for approximately 150 days. The deck was monitored until late June of 2021. Four loaded dump trucks were used for live load testing. Key observations from this bridge are as follows:

- The deck surface cracks were relatively small, with crack widths not greater than 0.006 inch;

- Concrete early-age shrinkage is the dominant effect for deck cracking, with measured strains in the range of 400 to 800 $\mu\varepsilon$.

- Increasing the deck reinforcement ratio and decreasing the bar spacing showed some benefits, but the 1.1% reinforcement controlled deck strain acceptably;

- Deck strains and deck surface crack widths under controlled live loading were small compared with those due to concrete shrinkage effects.

References

AASHTO, L. (2017). AASHTO LRFD bridge design specifications. American Association of State Highway and Transportation Officials, Washington, DC.

ACI Committee 209. (2008). Guide for modeling and calculating shrinkage and creep in hardened concrete. American Concrete Institute (ACI) 209.2 R-08.

ACI Committee 222. (2001). Protection of Metals in Concrete Against Corrosion. American Concrete Institute (ACI) 222R-01.

ACI Committee 224. (2007). Causes, evaluation, and repair of cracks in concrete structures. American Concrete Institute (ACI) 224.1 R-07

ACI Committee 224. (2008). Control of Cracking in Concrete Structures. American Concrete Institute (ACI) 224R-08.

ACI Commite 301. (2010). Specifications for Structural Concrete for Buildings. American Concrete Institute International (2010):15.

ACI Committee 318. (1995). Building Code Requirements for Structural Concrete:(ACI 318-95); and Commentary (ACI 318R-95). American Concrete Institute.

ACI Committee 318. (2014). Building Code Requirements for Structural Concrete (ACI 318-14): Commentary on Building Code Requirements for Structural Concrete (ACI 318R-14): an ACI Report. American Concrete Institute. ACI.

Agnew, L. S. (2007). "Evaluation of the Fatigue Behavior of Bridge Decks with Precast Panels at Expansion Joints", MS Thesis, Dept. of Civil Engineering, Univ. of Texas at Austin.

Armijos-Moya, S., Wang, Y., Helwig, T., Engelhardt, M., Clayton, P., and Williamson, E., "Improved Tub Girder Details: Final Report," Research Report No. FHWA/TX-19/0-6862-1, Center for Transportation Research, University of Texas at Austin, Austin, Texas, 2019.

Association, P. C. . (1979). Durability of concrete bridge decks. Final Report Transportation Research Board Washington Dc.

Atimtay, E., & Ferguson, P. M. (1974). Early Chloride Corrosion of Reinforced Concrete Test Report. Materials Performance, 13(12), 18-21.

Barker, J. M. (1975). "Research, Application, and Experience with Precast Prestressed Bridge Deck Panels," PCI Journal, 20, 66-85.

Bayrak, O., Deschenes, D., and Dunkman, D. (2009), Performance of the 'Poor-Boy' Continuous Deck Detail. Research presentation to TxDOT.

Beeby, A. W. (1979). The prediction of crack widths in hardened concrete. The Structural Engineer, 57(1), 9-17.

Beverly, P. (Ed.). (2013). fib model code for concrete structures 2010. Ernst & Sohn.

Boswell, C. A. (2008). Simple Design Details using Precast Concrete Panels at Skewed Expansion Joints (Doctoral dissertation, Univ. of Texas at Austin).

Brown, M., Sellers, G., Folliard, K. J., & Fowler, D. W. (2001). Restrained shrinkage cracking of concrete bridge decks: State-of-the-Art Review (No. FHWA/TX-0-4098-1).

Buth, E., H. L. Furr & H. L. Jones (1972). "Evaluation of a Prestressed Panel, Cast-in-Place Concrete Bridge," Research Report 145-3, Texas Transportation Institute, College Station, Texas.

Ceb-Fip Mode Code. (1990). Comite Euro International du Beton, 51-59.

Clark, A. P. (1956). Cracking in reinforced concrete flexural members. In Journal Proceedings (Vol. 52, No. 4, pp. 851-862).

Collins, M. P., & Mitchell,D. (1997). Prestressed concrete structures. Response Publications.

Coselli, C. J. (2004). "Behavior of Bridge Decks with Precast Panels at Expansion Joints", MS Thesis, Dept. of Civil Engineering, Univ. of Texas at Austin.

Dowell, R. K., and Smith, J. W. (2006). Structural Tests of Precast, Prestressed Concrete Deck Panels for California Freeway Bridges. PCI Journal, March-April, 2-13.

Folliard, K., Smith, C., Sellers, G., Brown, M., & Breen, J. E. (2003). Evaluation of Alternative Materials to Control Drying-Shrinkage Cracking in Concrete Bridge Decks (No. FHWA/TX-04/0-4098-4,).

Foster, S. W. (2010). Reducing top mat reinforcement in bridge decks (Master Thesis, Univ. of Texas at Austin).

Frosch, R. J. (1999). Another look at cracking and crack control in reinforced concrete. Structural Journal, 96(3), 437-442.

Frosch, R. J., Blackman, D. T., & Radabaugh, R. D. (2003). *Investigation of bridge deck cracking in various bridge superstructure systems* (No. FHWA/IN/JTRP-2002/25,).

Gergely, P., & Lutz, L. A. (1968). Maximum crack width in reinforced concrete flexural members. Special Publication, 20, 87-117.

Hadidi, R., & Saadeghvaziri, M. A. (2005). Transverse cracking of concrete bridge decks State-of-the-art. Journal of Bridge Engineering, 10(5), 503-510.

Hognestad, E. (1962). High-strength bars as concrete reinforcement, Part 2: Control of flexural cracking. Journal of the PCA Research and Development Laboratories, 46-63.

Holt, John and Smith, Amy, "Reducing Steel in Bridge Decks" Concrete Bridge Views, Issue 78, Sept/Oct 2014.

Kaar, P. (1963). High-strength bars as concrete reinforcement, Part 4: Control of cracking. Journal of the PCA Research and Development Laboratories, 15-38.

Kaar, P. H., & Hognestad, E. (1965). High strength bars as concrete reinforcement, part 7: control of cracking in T-beam flanges. Journal of the PCA Research and Development Laboratories.

Martin, H., & Schiessl, P. (1969). The Influence of Cracks on the Corrosion of Steel in Concrete. In International Symposium on the Durability of Concrete.

Merrill, B. D.(2002), "Texas' Use of Precast Concrete Stay-In-Place Forms for Bridge Decks," Proceedings, Concrete Bridge Conference, National Concrete Bridge Council, Skokie, IL.

Nouri, G., & Ahmadi, Z. (2012). Influence of skew angle on continuous composite girder bridge. Journal of Bridge Engineering, 17(4), 617-623.

Jones, H. L., & Furr, H. L. (1970). Study of In-Service Bridges Constructed with Prestressed Panel Sub-Decks. Texas Transportation Institute, Research Report 145-1.

Raphael, M., & Shalon, R. (1971). A study of the influence of climate on corrosion and reinforced concrete. In Proceedings, RILEM Symposium on Concrete and Reinforced Concrete in Hot Climates (pp. 77-96).

Rüsch, H., and Rehm, G. (1963), "Versuche mit Betonformstahlen," Deutscher Ausschuss für Stahlbeton, Bulletins, No. 140, Part 1, 1963; No.160, Part 2, 1963; and No. 165, Part 3, 1964. (in German)

Russell, H.G.(2014), NCHRP Synthesis of Highway Practice 333: Concrete Bridge Deck Performance, Transportation Research Board of the National Academies, Washington, D.C., 2004, 101 pp.

Russell, H.G. (2013), NCHRP Synthesis of Highway Practice 441: High-Performance Concrete Specifications and Practices for Bridges, Transportation Research Board of the National Academies, Washington, D.C., 2013, 73 pp.

Russell, H.G. (2017). NCHRP Synthesis of Highway Practice 500: Control of concrete cracking in Bridges. *Transportation Research Board, Washington, DC*, *188 pp*.

Sansalone, M. J., & Streett, W. B. (1997). Impact-echo. Nondestructive evaluation of concrete and masonry.

Sneed, L., A. Belarbi & Y. M. You. (2010). "Spalling Solution of Precast-Prestressed Bridge Deck Panels," Report TRyy0912, Missouri Department of Transportation.

Tsui, C. K., Burns, N. H., & Klingner, R. E. (1986). Behavior of Ontario-type bridge deck on steel girders: Negative moment region and load capacity.

Tremper, B. (1947). The corrosion of reinforcing steel in cracked concrete. In Journal Proceedings (Vol. 43, No. 6, pp. 1137-1144).

TxDOT Bridge Design Manual, T. B. D. (2015). Texas Department of Transportation.

TxDOT Bridge Detailing Guide (2018). Texas Department of Transportation.